HAL
open science

Cours Master 2 : Hybrid Integrated Photonics and Nanophotonics Devices

Bruno Bêche

▶ **To cite this version:**

Bruno Bêche. Cours Master 2 : Hybrid Integrated Photonics and Nanophotonics Devices. Master. France. 2021, pp.0-218. hal-03291856v2

HAL Id: hal-03291856

https://cel.hal.science/hal-03291856v2

Submitted on 7 Sep 2023

HAL is a multi-disciplinary open access archive for the deposit and dissemination of scientific research documents, whether they are published or not. The documents may come from teaching and research institutions in France or abroad, or from public or private research centers.

L'archive ouverte pluridisciplinaire **HAL**, est destinée au dépôt et à la diffusion de documents scientifiques de niveau recherche, publiés ou non, émanant des établissements d'enseignement et de recherche français ou étrangers, des laboratoires publics ou privés.

MODULE: Hybrid integrated photonics & Nanophotonics devices [12h]

- B. Bêche, Pr. Univ. Rennes IETR CNRS / Elements of course -

- CONTENTS -

Chapter I). Introduction to integrated photonics, overview

▪ Materials and technologies, thin-layer processes for the fabrication of such devices, packaging and miniaturization. Examples of thin layers processes for waveguides and structures.

Chapter II). Theory of electromagnetic waveguides, photonic's propagation, quantification of the optical modes

▪ Notion of guided modes / radiation modes; geometrical approach of the propagation of guided modes; ray optics and phase shift; Goos-Hänschen shift; effective guide thicknesses.

▪ Fundamentals on the electromagnetic theory of dielectric waveguide (Maxwell's approach); dispersion relations and calculus of photonic's modes (eigenvalues and eigenvectors); channel optical waveguides and geometries; dispersion phenomena and pulse's spread; optical guides with various graded-index profiles; stored energy and power flow; historic methods on the calculus of effective indices (the effective index method, separation of variables and method of field shadows, the Marcatili's method); extended approaches to another waveguides structures; multilayer slab waveguides and global matrix formalism; finite difference spatial methods (semi-vectorial and vectorial); spectral methods; modes expansion and normalization; finite difference time domain (FDTD); numerical analysis; curved waveguides formalism and S-bend propagation; circular waveguides (optical fibres and tubular structures); waveguide transitions; tapers and junctions.

▪ Resonant cavity or micro-resonators (ring, disk, sphere); quality factor and energy-management.

▪ Coupled-mode theory representation; differential form of coupled amplitude equations; notion of supermodes.

▪ Energy formulation of equations and their resolution.

Chapter III). Microphotonic components

▪ Applications to MOEMS (sensors, optical telecommunication); generic devices for photonic measurements (physical, chemical, biologic measurements); characterisations of photonic structures.

Chapter IV). Nanophotonic, sub-wavelength photonics, nano-components

▪ Electron-photon analogies, development of the basics on photonic crystals (PC); wave equation and eigenvalues; one-dimensional model (PC-1D or Bragg mirror); Bloch's theorem and Fourier expansion of dielectric functions; plane waves method decomposition; spatial periodicities and photonics band gap; two- and three-dimensional crystals cases (PC-2D and -3D); photonic band calculation; phase velocity, group velocity and density of states; cavity and decay time of a mode; bands engineering and control of the photonic dispersion curves; localized defect modes; cavity; photonic structures based on photonic crystals (PC-waveguides, resonators, couplers, filters, mirrors, lasers); 2.5D-PC-components examples; technical characterisations of structures; mapping of CP-research in France and LEOM-INL / ECL Lyon example.

▪ Near field optical; introduction to the main concepts; presentation of specific probes, and near optical field microscopy (STOM, SNOM).

▪ Biomimetic and auto-assembled molecular nano-materials for photonics; nano- wires and tubes; nano-connexions and networks; bio-nanophotonic.

▪ Plasmonic photonics; surface plasmon; electromagnetic modes localized at interface; evanescent waves; excitation of plasmon.

References. • A. Yariv, ' Quantum electronics ', Ed. John Wiley & Sons, 1989. • M. J. Adams, ' An introduction to optical waveguide ', Ed. John Wiley & Sons, 1981. • A. W. Snyder, J. D. Love, ' Optical waveguide theory ', Ed Chapman and Hall, 1983. • D. Marcuse, 'Theory of dielectric optical waveguides', ed. Academic Press, 1974. • T. Tamir, ' Guided-wave optoelectronics ', Ed. Springer-Verlag, 1990. • J. D. Joannopoulos, 'Photonic crystals : molding the flow of light', Ed. Princeton University Press, 1995. • K. Sakoda, 'Optical properties of photonic crystals', Ed. Springer-Verlag, (2005). • D. Courjon, C. Bainier, 'Le champ proche optique : théorie et applications', Ed. Springer, 2001.

Chapter I). Introduction to integrated photonics, overview

▪ I.1 Introduction (english):

As a concept described at the end of sixties, Integrated Photonics rely on the use of photons instead of electrons so as to design integrated optical circuits whose functions and performances proved to be increasingly enhanced along the recent years. In such a remarkable technological context, numerous telecommunication devices together with metrological systems and specific sensors, have been developed and arranged upon a great variety of materials and substrates, such as silicon, glass, lithium niobate, polymers and specific semiconductors. As the concept was particularly appealing to the early investigators, current research has been aimed at reducing the size of the devices while increasing their performance. More recently, as near field optics, nano-photonic structures and applications were devised, the development of new devices has increased dramatically whereas specifications were more and more stringent. Furthermore, environmental issues regarding a sustainable development hindered the use of hazardous materials and their related processes. Among the most interesting recent structures, photonics crystals proved to allow the control of optical dispersion curves, making possible to handle in many ways the flow of light. Then, nano-plasmonic and nano-wire structures proved to enable a sub-wavelength propagation mechanism: as a result, research in information technology crucially depends on a continuously demanding miniaturization policy.

▪ I.1-bis Introduction (français): ‘ Vers l’intégration des systèmes …’

L’optique intégrée est un concept qui s’est développé à partir de la fin des années soixante. Le terme ‘optique intégrée’ a été introduit pour la première fois dans une publication par Miller en 1969. L’idée originelle est d’utiliser les photons au lieu des électrons pour concevoir des ‘circuits optiques intégrés’. Pour ce type de circuits intégrés, il est nécessaire de réaliser sur un matériau de base un guide d’onde dans lequel la lumière se propage et d’intégrer sur ce matériau des structures réalisant des fonctions identiques aux composants optiques massifs : lentilles, interféromètres, modulateurs électro-optiques et acousto-optiques, sources, détecteurs, filtres, capteurs, etc. En traversant ces différentes micro- et nano-structures qui agissent sur l’onde guidée, le guide d’onde apparaît comme l’élément de base dans tous ces dispositifs. Une étude approfondie de la propagation guidée des ondes dans les différentes structures guidantes (composants passifs) sera donc présentée.

L’intégration est l’une des voies permettant de réaliser des systèmes optiques à hauts débits, à faibles tensions de commandes, sous une forme très compacte pour des applications dans les domaines des télécommunications et des capteurs (MOEMS), c’est-à-dire respectivement relatifs à la transmission d’une information, puis à la mesure. Ces composants actifs utilisent les propriétés de la lumière : la vitesse de propagation, la direction de propagation, la longueur d’onde, l’état de polarisation, la phase, la cohérence. Ces systèmes ou composants actifs sont généralement basés sur une modulation (pour des applications télécom) ou mesure (pour des applications capteurs) de variables physiques (ou attributs attachés à l’onde optique), à savoir l’amplitude de l’onde optique (intensité), sa direction de propagation (vecteur d ’onde), sa polarisation, sa phase et sa cohérence temporelle (retard optique, et interférence).

Les avantages majeurs de telles configurations utilisant la micro-optique (ou optique intégrée), résident aussi d'une part dans la très haute sensibilité de mesure de celles-ci, et d'autre part dans une isolation électromagnétique totale (CEM) par rapport à leur environnement, très recherchée à l'heure actuelle dans de nombreux domaines (par exemple dans le cas des milieux sensibles gazeux potentiellement explosifs, sécurité intrinsèque, etc).

Plus récemment, le développement de l'optique en champ proche puis de la nano-photonique intégrée (plasmonique, nano-élements, cristaux photoniques), objets de différents concepts innovants (contrôle des courbes de dispersion du photon depuis les travaux pionniers de E. Yablonovitch et J.D. Joannopoulos en cristaux photoniques, propagation photonique dans les nanostructures à grand facteur de forme avec les travaux récents sur nanofils, nanotubes et nano-sphères) se sont accentués dans le but de concevoir des composants intégrés photoniques à dimensions extrêmement réduites, compatibles avec celles de la nano-électronique, présentant de nouvelles fonctionnalités. Diverses solutions de couplage vers une photonique sub-micronique se développent d'ailleurs actuellement sur structures mésoscopiques.

Integrated photonics is based on confined electromagnetism propagation

↓

Optical waveguides

▪ I.2 Waveguides structures - examples of opto-geometries:

[optical wavelength, permittivities or indices, dimensions]

▪ **Plane and rectangular waveguides**

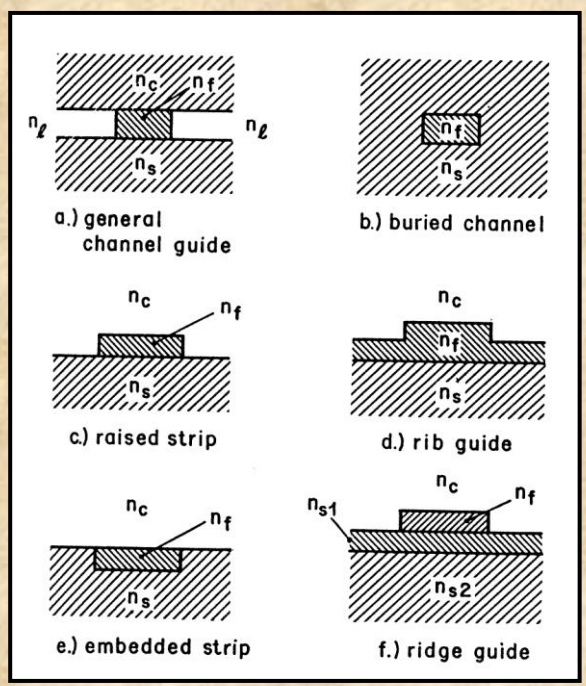

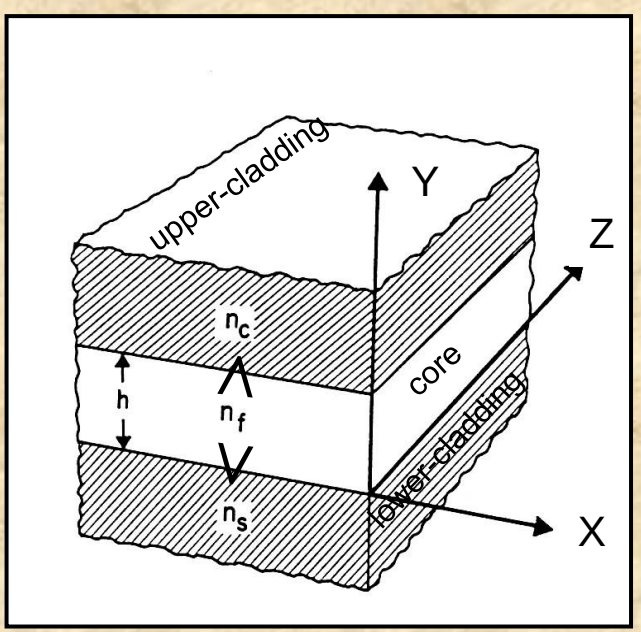

Z-axis : direction of effective propagation

▪ **Circular geometries (fibers, tubular structures)**

▪ **Various multi-forms and complex geometries (curved structures, V-cones, …)**

▪ **With in each case : possibilities of multilayers structures (*n* layers) with Totale Internal Reflection (TIR), and indices gradient laws (Eikonal or Iconale equation) with notions of caustic points.**

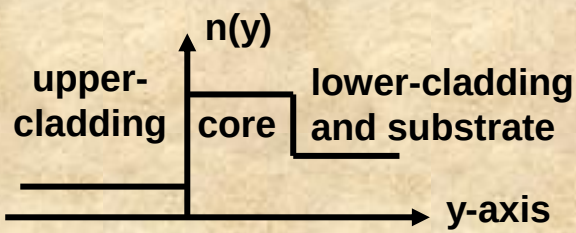

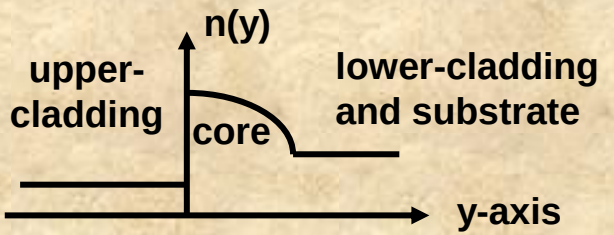

▪ I-3- Various materials and thin layers processes in integrated photonics:

- Glass
- Silicone
- III-V semiconductors (GaAs, AlAs, AlP, GaP, InP, AlN, GaN, InN, + ternary and quaternary compounds)
- II-VI semiconductors (MgS, MgSe, ZnSe, ZnS, CdSe)
- Lithium niobate($LiNbO_3$)
- Polymers
- Metals (Al, Au, …) + adhesion layers (Ti, Cr)

Different technical and thin layers ⬇ processes adapt to each material

- Clean room processes (drop-, spin-coating, classical UV-lithography, lift-off, development processes, step baking, chemical etch, …)
- Plasmas deposition and processes (reactive ion etching, functionalization,…)
- Sputtering, evaporation (electrodes)
- Chemical vapor deposition (CVD, PECVD)
- Molecular beam epitaxy

and so on…

Substrate materials	Characteristic material properties	Waveguide technologies	Advantages/ restrictions	Typical components
Glass	Inexpensive fabrication Very low losses	Ion exchange thermal or field assisted	Only passive components Monomode and multimode components Extremly low losses	Passive branches
Lithium niobate	Electro-optic and piezoelectric effects	Indiffusion of titanium, Proton exchange	Only monomode components Polarization dependent Optical damage Various demonstrated components	Phase modulators Coupler Switches Frequency modulator
Silicon	Electronics may be integrated Combination with micromechanics	Deposition techniques for silicon oxy-nitride Phosphorus silicate glasses	Only passive Monomode and multimode Integration of detector CMOS electronic and micromechanics Fiber adjustment via V-grooves	IO circuits with integrated detectors and CMOS circuits Micromechanics
III-V compounds	Electrooptic Light source, detectors and electronics may be integrated	Epitaxy (MBE. LPE, CVD, LPCVD, MOCVD)	High potential for application in the near future	
Polymers	Electrooptic Piezoelectric Sensor relevant changes of optical properties	Deposition from liquids Spin coating Dip coating	High potential for chemical, biological and medical sensors Embosssing techniques Multimode components	IO components with measurand-specific optical changes

- **Some examples:**
  - **i) Clean room processes**

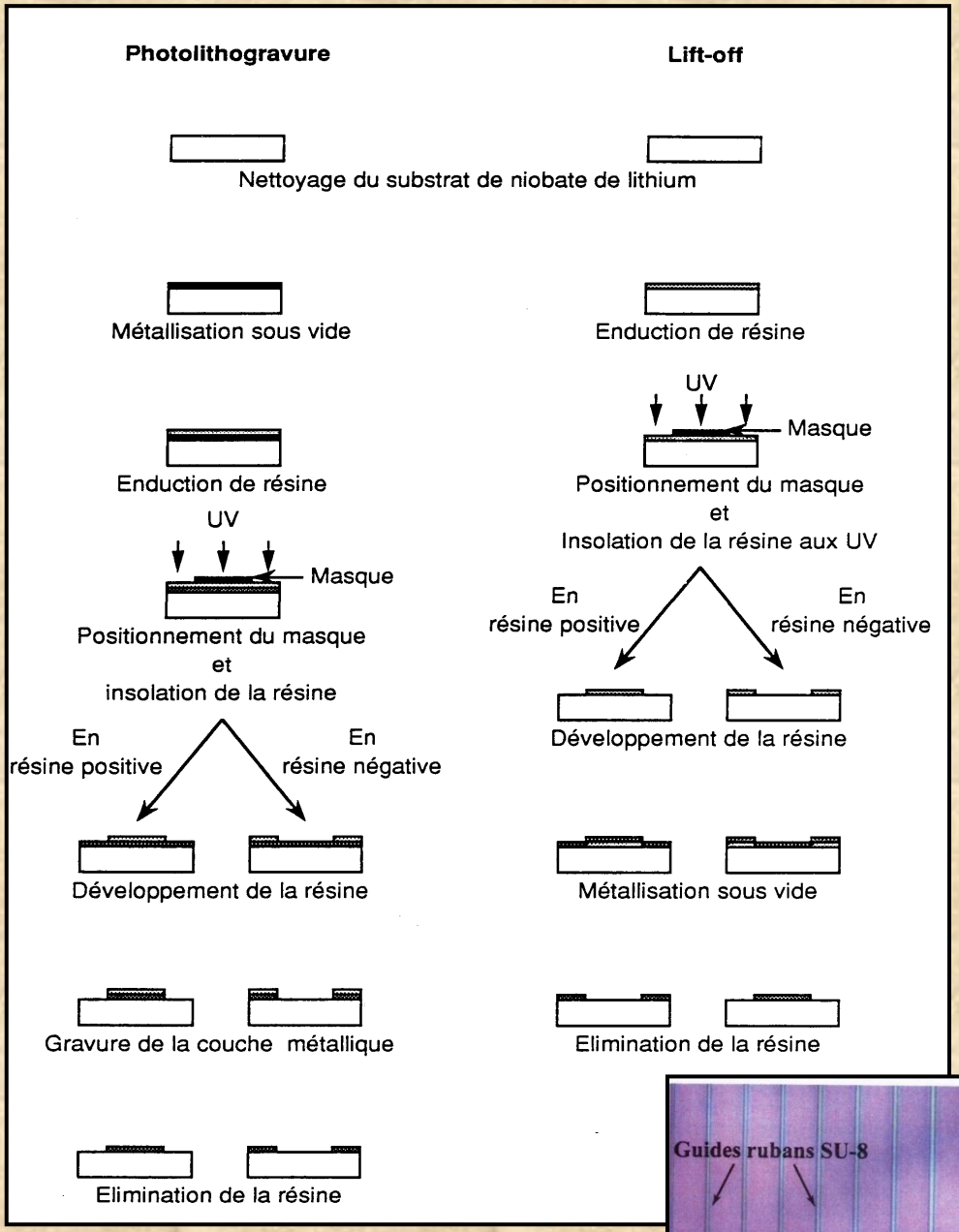

Polymer rib waveguides →

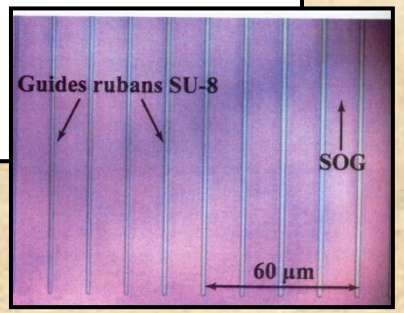

▪ ii) Waveguide realization with diffusion processes ($LiNbO_3$)

Ti diffusion on $LiNbO_3$ at high temperature (>1000°C) ; backing [200-400°C] after proton exchange ('PE'=substitution of Li^+ by H^+ from acid solution at the $LiNbO_3$ surface, implantation of $H_xLi_{1-x}NbO_3$ that present a higher n_e index) ; mixed previous methods.

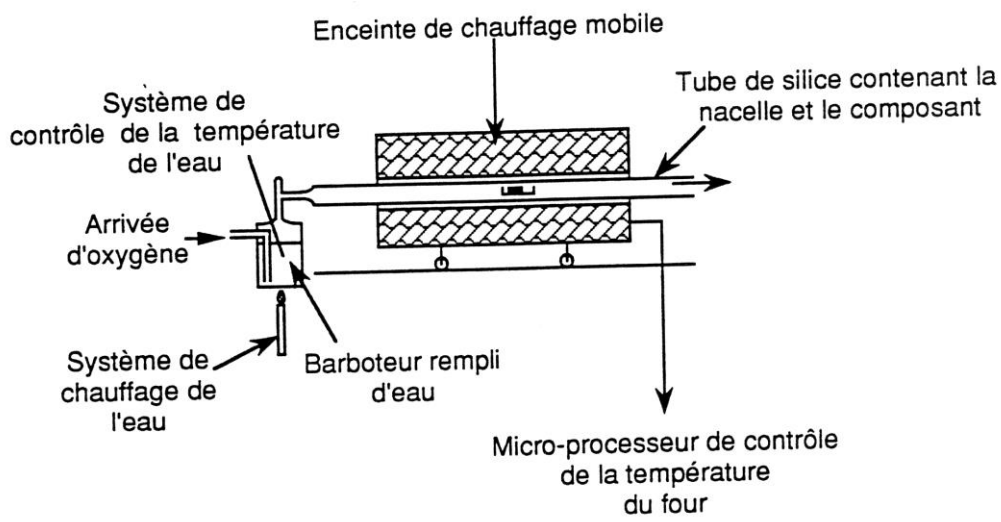

Figure : Représentation schématique du four à diffusion.

PE - process :

H^+ change the spontaneous polarization $\Delta P_s = p.\Delta N$

$$\Delta n_e \propto -\frac{r_{33}.n_e^3.p.\Delta N}{2\varepsilon_0(\varepsilon_{33}-1)}$$

with,

p : dipolar moment

ΔN : proton concentration into free Li^+ sites.

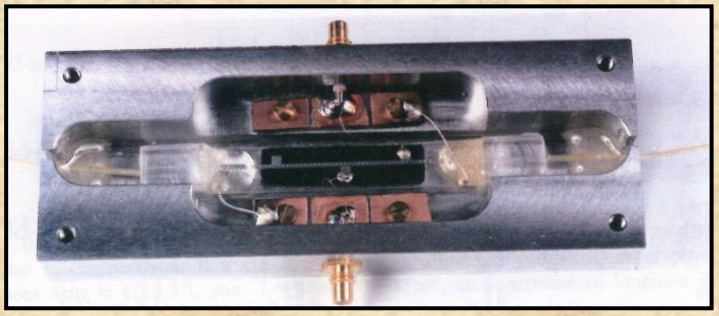

CNET France Telecom

Packaging-$LiNbO_3$-optical component

▪ iii) III-V semiconductors growth by MOCVD reactor : GaAs/AlAs or GaN cavities and waveguides, lasers applications

GaN on Sa or SiC substrate

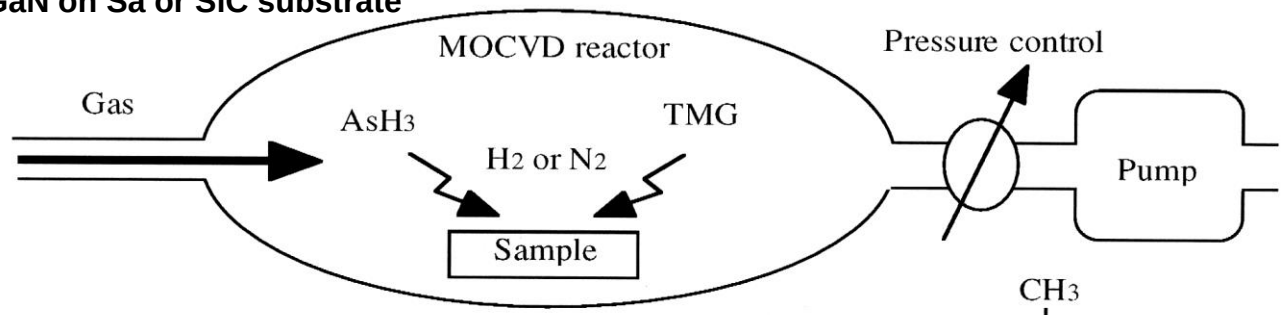

Nucleation or anomorphous layer necessary due to the high lattice mismatch between the substrate and GaN (dislocations)

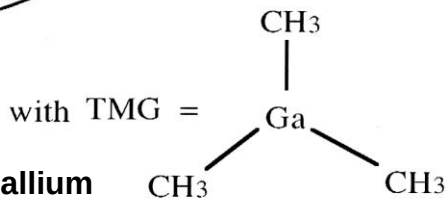

Trimethyl Gallium

TMG molecules are broken by the speed of gas molecules (H_2) ; CH_3 and CH_4 can be evacuated by the pump.

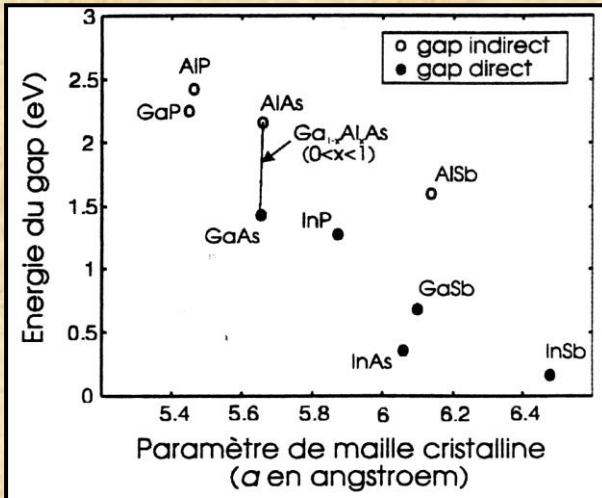

Fig. Energie de gap ou largeur de bande interdite (eV) des semi-conducteurs III-V (symétrie cubique) en fonction de leur paramètre de maille cristallin 'a'.

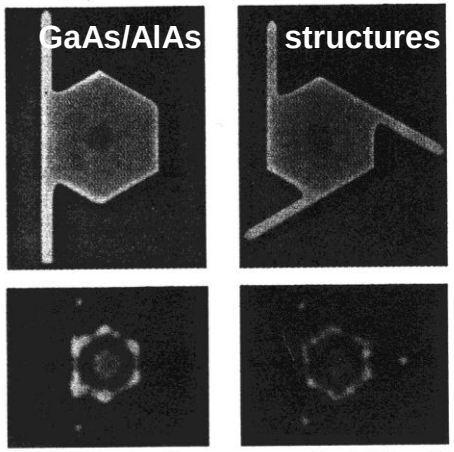

Fig. Two micro-laser structures (top), 12 µm in size, fabricated by selective-area crystal growth of GaAs/AlGaAs.

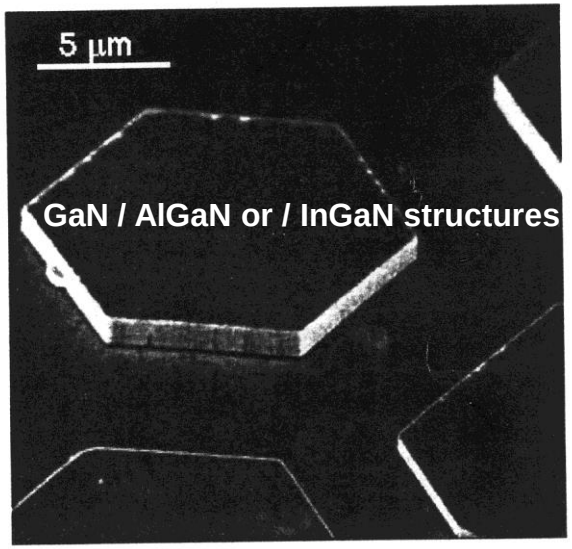

Nitride Semiconductor Facet lasers

▪ iv) GaAs/AlAs multilayers waveguides growth by MBE (or heteroepitaxy)

De telles hétérostructures peuvent être élaborées par des techniques de croissance épitaxiale. Celles-ci peuvent être classées en diverses familles : l'épitaxie en phase liquide (EPL, LPE 'Liquid Phase Epitaxy'), l'épitaxie en phase vapeur (EPV, VPE 'Vapor Phase Epitaxy'), et l'épitaxie par jets moléculaires (EJM, MBE 'Molecular Beam Epitaxy'). Cette dernière méthode d'épitaxie est particulièrement intéressante concernant différents paramètres: état de surface (rugosité inférieure à 1 nm), contrôle de la vitesse de croissance dans une large gamme (0.1 à 5 mm/h), obtention de grandes variations de dopage et de composition, température du substrat relativement faible permettant d'éviter des phénomènes de diffusion couche-substrat (de l'ordre de 500°C pour GaAs), et enfin grande pureté des dépôts due à la technique d'ultravide (pression proche de 10^{-11} Torr). Le principe consiste en l'interaction dans une enceinte sous ultravide de flux moléculaires (ou atomiques) et leur condensation sur un substrat monocristallin. Les flux utilisés sont typiquement de 10^{16} molécules/cm^2/s pour le groupe V, de 10^{15} molécules/cm^2/s pour les éléments du groupe III, et de l'ordre de 10^{10} molécules/cm^2/s pour les éléments dopants.

Un spectromètre d'électrons Auger permet l'analyse chimique des surfaces. Dans la chambre de croissance sous ultravide refroidie par circulation d'azote liquide, les cellules contiennent dans des creusets munis de caches, les éléments à épitaxier (Al, Ga, As, etc) et les dopants à incorporer si besoin (Si, Be). Plusieurs moyens d'analyse au cours de l'épitaxie existent. Un spectromètre de masse contrôle la qualité du vide. Enfin, la qualité cristalline des couches déposées est analysée par diffraction d'électrons de haute énergie (RHEED).

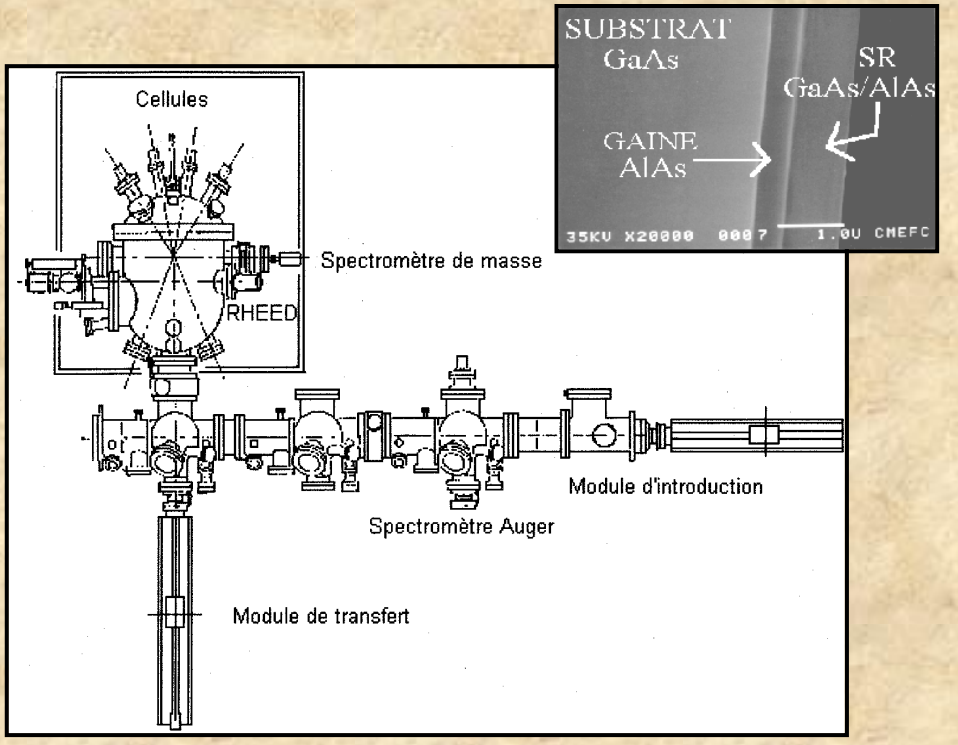

▪ v) Piezoelectric layer deposited by CVD, PECVD for transductors applications

De nos jours, il existe de nombreuses techniques pour déposer des couches minces très utilisées pour fabriquer des micro-composants. Parmi celles-ci, nous pouvons citer l'évaporation, la pulvérisation ('sputtering'), le dépôt chimique en phase vapeur classique ('Chemical Vapor Deposition' ou 'CVD') ou assisté plasma ('PECVD') .

La pulvérisation permet l'obtention de couches minces sur le substrat par éjection des atomes par un faisceau d'ions de haute énergie en présence ou non d'un gaz réactif. L'évaporation permet d'obtenir des dépôts par sublimation du matériau en le chauffant ou en le bombardant ('electron beam evaporation'). Dans les deux cas, ces dépôts sont obtenus par PVD ('Physical Vapor Deposition') par utilisation d'un faisceau électronique. Ces deux techniques sont fortement employées en optique, mais la CVD et la PECVD connaissent un développement important. Elles jouent maintenant un rôle primordial dans l'élaboration de couches minces pour la micro-électronique sur substrat Si, Ge, et GaAs, etc.

Pour le dépôt chimique en phase vapeur classique (c'est-à-dire thermique), les réactifs introduits dans le réacteur fonctionnant à pression réduite (quelques Torrs) sont pyrolysés thermiquement (500°C<T<1000°C) et le mélange chimique est transporté par convection et diffusion à la surface du substrat. Le dépôt chimique en phase vapeur assisté plasma (PECVD) se produit dans un réacteur chauffé à température réduite inférieure à la précédente technique et maintenu à basse pression constante. Une décharge électrique permet d'ioniser le mélange et de créer un plasma. L'excitation de la décharge peut être continue, ou comprise entre quelques kHz et plusieurs GHz (conditionne le déplacement des ions et des électrons).

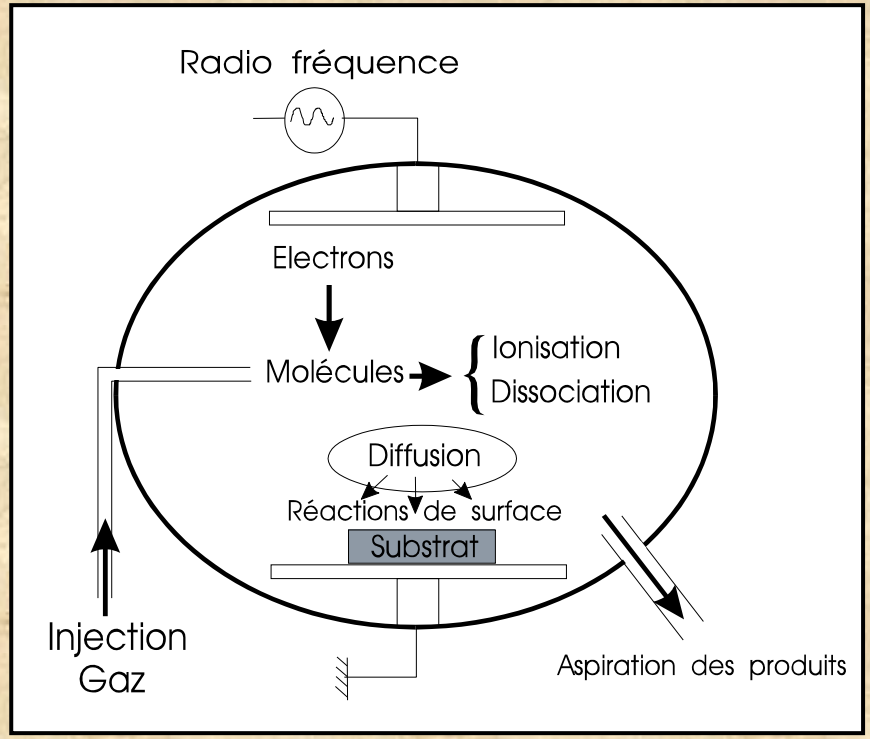

L'originalité de la PECVD par rapport à la CVD est donc la création d'un plasma, c'est-à-dire d'une multitude d'espèces. Les proportions, les énergies, et les mouvements des différentes espèces présentes (particules chargées), définiront le plasma. D'une manière générale, une bonne reproductibilité en épaisseur et en composition de la couche nécessite une maîtrise de certains paramètres expérimentaux (fréquence, pression et débit des flux gazeux, concentrations en espèces réactives,...). Ces deux dernières méthodes conduisent à l'obtention de matériaux déposés en couches minces de grande pureté et ayant de bonnes propriétés d'adhérence. Ces couches minces (<10 mm) résistent à de fortes déformations sans que celles-ci ne s'écaillent, même si le matériau de revêtement présente une grande fragilité sous forme massique. Dans certains cas, la CVD et la PECVD offre la possibilité de déposer les mêmes couches minces qu'en utilisant la PVD, mais avec une orientation des axes cristallographiques différentes (➔ exemple couches piézoélectriques ZnO, AlN ➔ applications transducteurs acoustiques).

- **Notation for next chapters :**

✎ **: Analytical demonstration and calculus to be done...**

Chapter II). Theory of electromagnetic waveguides, photonic's propagation, quantification of the optical modes

- **II.1 : Notion of guided modes / radiation modes; geometrical approach of the propagation of guided modes (zig-zag); ray optics and phase shift; first quantification along one direction; Goos-Hänschen shift; effective guide thicknesses**

- **II.1.1 Geometrical approach ('zig-zag'), scalar theory of waveguide - conditions for propagation**

- **Hypothesis**
  - **Symmetrical plane waveguide with permittivity discontinuities**
  - **Symmetrical potential barrier '$\varepsilon_2/\varepsilon_1/\varepsilon_2$'**
  - **Infinity lateral dimension (along x-axis)**
  - **Propagation along z-axis**
  - **Propagation TIR $n_1>n_2$**

- **Goal : Calculate and define such a modal quantification (eigenvectors) and determinate the equations of eigenvalues into this type of opto-geometric structures confined along one dimension (x-direction). Use only classical and basic notions of geometrical optics and wave-optics like phase shift.**

Remarque: On démontra ensuite dans ce chapitre que la résolution de ce même problème de confinement 1D par le formalisme de Maxwell (c'est-à-dire avec les notions de champs é-m-) nous fixe strictement le même résultat en terme d'équation aux valeurs propres et donc de première quantification des niveaux d'énergies.

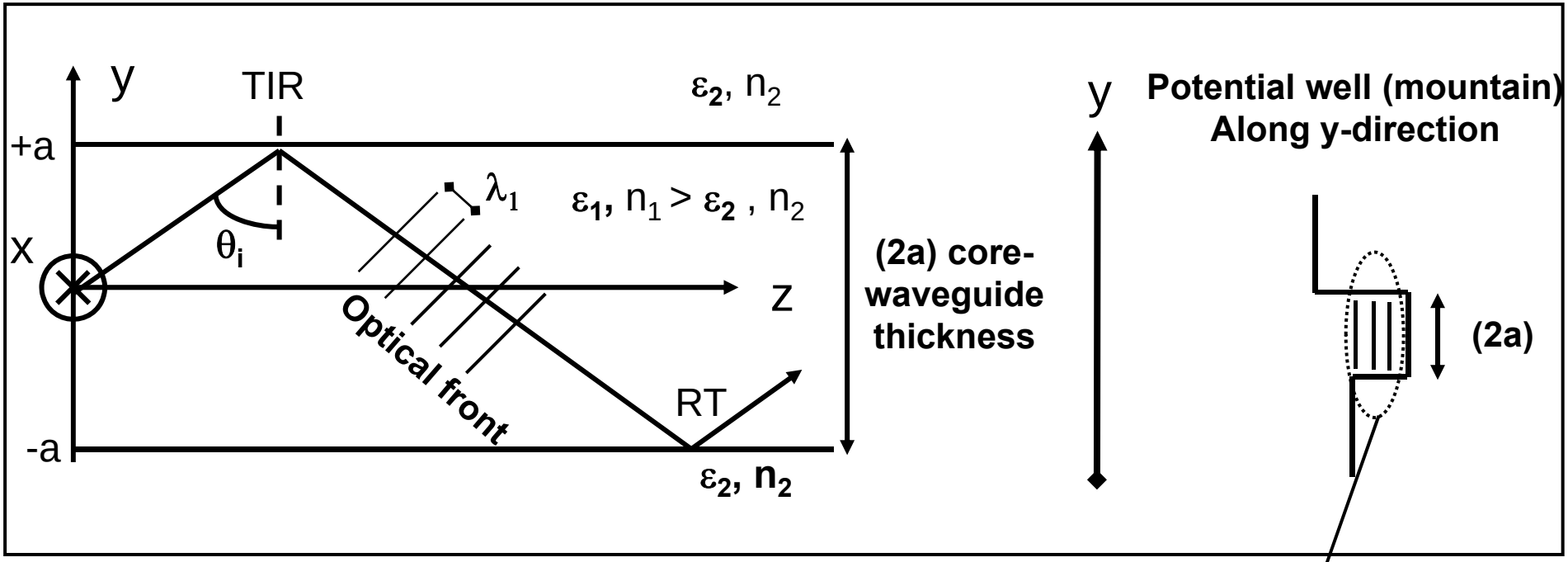

Conditions for propagation of the optical wave

Succession of TIR

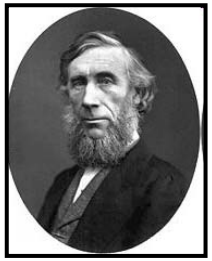

John Tyndal (1820-1893)

Condition of the accord of phase between the various front of wave

- **Confinement of the light into the heterostructure (or potential) along the y-direction (possibility of photon-propagation into such a channel along z-direction)**
  ➔ quantification of the energy of the light (photon)

At fixed thicknesses (2a), and fixed λ_1 (wave-front), $\exists\, \theta_i$ solutions / accord of phase = constructive interferences = propagation

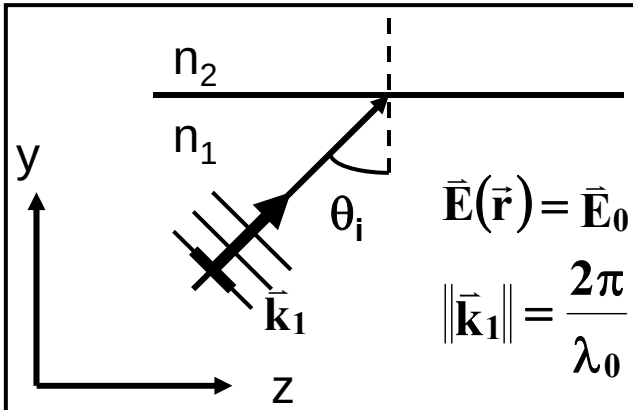

$$\vec{E}(\vec{r}) = \vec{E}_0 \exp j(\omega t - \vec{k}_1.\vec{r})$$

$$\|\vec{k}_1\| = \frac{2\pi}{\lambda_0} n_1 = \|\vec{k}_0\| n_1 = \frac{2\pi}{\lambda_{1(coeur)}}$$

λ_0 = wavelength relative to the wave in the air (n=1)

λ_1 = wavelength relative to the wave into the core material (n_1 index)

Decomposition of the problem along twice axes (➔ separation of variables)

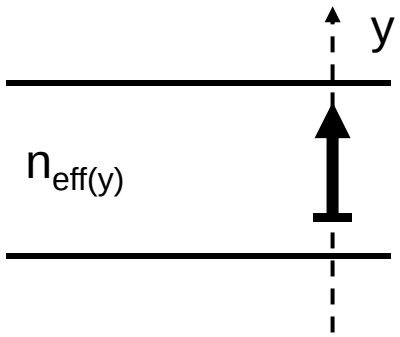

$$n_{eff(y)} = n_1 \cos\theta_i$$

$$\beta_y = k_0 n_{eff(y)} = \frac{2\pi}{\lambda_{eff(y)}}$$
$(k_\perp)$

$$\lambda_{eff(y)} = \frac{\lambda_0}{n_1 \cos\theta_i}$$

- Stationary phenomenon along y-axis, no propagation but confinement of the light, discretization and quantification of energy $E=hc/\lambda_{eff(y)}$

Condition of resonance :
(m integer=quantification)

[II-1]

$$\cos\theta_m = \frac{(m\pi + \varphi_r)}{4\pi a n_1}\lambda_0$$

'Schematic equivalent along z' : The wave propages along the z-direction into an effective material that present an effective index $n_{eff(z)}$ with a propagation effective constant $\beta_{eff(z)}$

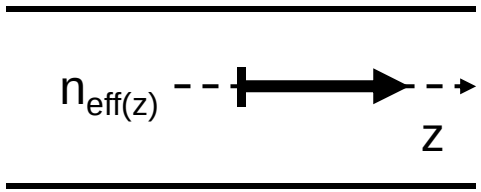

[II-2]

$$n_{eff(z)} = n_1 \sin\theta_i$$

$$\beta_z = k_0 n_{eff(z)} = \frac{2\pi}{\lambda_{eff(z)}}$$
$(k_{//})$

- According to the condition of resonance :
m = quantification of the possible ray optics,
➔ notion of confined and selective modes

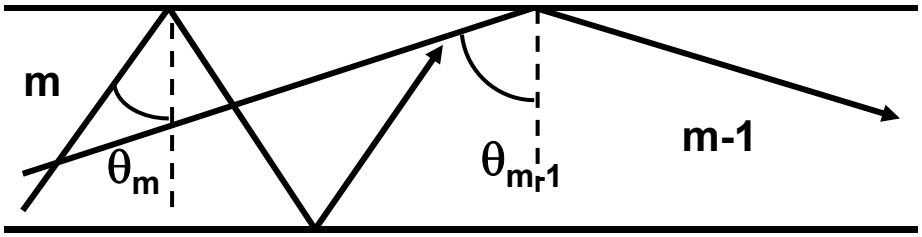

- m decrease ⇔ θ_m increase
- First optical mode m=0 ⇔ $\theta_0 \longrightarrow \pi/2$

- Expression of optical phase shift φ_r due to reflection (TIR) ; such expressions can be defined as the imaginary part of Fresnel coefficients written in complex form.

$$\varphi_{rTE} = 2\,\mathrm{arctg}\left(\sqrt{\frac{n_{eff}^2 - n_2^2}{n_1^2 - n_{eff}^2}}\right) \text{ and } \varphi_{rTM} = 2\,\mathrm{arctg}\left(\frac{n_1}{n_2}\right)^2\left(\sqrt{\frac{n_{eff}^2 - n_2^2}{n_1^2 - n_{eff}^2}}\right) \quad \text{[II-3]}$$

$$\text{with } n_{eff} \equiv n_{eff(z)} = n_1 \sin\theta_i$$

<u>Remarque et sens physique :</u> *même si coefficients appelés en 'réflexion', ce déphasage dépend du milieu (n_2) de l'autre côté du milieu n_1! Ainsi, l'onde a bien pénétré dans l'autre milieu et s'est donc réfléchit au-delà de l'interface n_1/n_2 ➔ notion géométrique de profondeur de pénétration (ou d'onde évanescente en vision modale).*

- **Interpretation**

- In the limit where cut is verified $\sin^2\theta_c = (n_2/n_1)^2$ ➔ $\boxed{\varphi_{rTE} = \varphi_{rTM} = 0}$ no phase at reflection.
- When $\theta_{i=m} \rightarrow \pi/2$ (case monomode m=0) ➔ $\boxed{\varphi_{rTE} = \varphi_{rTM} = \pi}$
- Maximum mode's number *m* that propagate : TIR impose $\theta_m > \theta_c$ that is $\cos\theta_m < \cos\theta_c$

$$\boxed{m \le \frac{2d}{\lambda_0}\sqrt{n_1^2 - n_2^2} \quad \text{or} \quad m \le \frac{2V}{\pi} \quad \text{with, } V = \frac{k_0 d}{2}\sqrt{n_1^2 - n_2^2} \text{ normalized frequency}}$$

▪ II.1.2 First quantification along one direction, eingenvalues equations of the optical modes

▪ **Determination of the optical modes proper to such planes structures**

If optical propagation mode existence is valid in such structures, then the condition of previous resonance must be verified.

PROBLEM

$$\cos\theta_m = \frac{(m\pi + \varphi_r)}{2\pi d\, n_1}\lambda_0$$

$$\begin{cases} \varphi_{rTE} = 2\,\mathrm{arctg}\left(\dfrac{\sqrt{n_{eff}^2 - n_2^2}}{\sqrt{n_1^2 - n_{eff}^2}}\right) \\ \varphi_{rTM} = 2\,\mathrm{arctg}\left(\dfrac{n_1}{n_2}\right)^2\left(\dfrac{\sqrt{n_{eff}^2 - n_2^2}}{\sqrt{n_1^2 - n_{eff}^2}}\right) \end{cases}$$

$$n_{eff} = n_1 \sin\theta_m$$

θ_m ?

Quantification and notions of optical modes

▪ Resolution for TE_m optical modes:

Change of variables ➔ u and v new eigenvalues of the modes :

$$u = k_0 a \sqrt{n_1^2 - n_{eff}^2} > 0 \quad \text{and} \quad v = k_0 a \sqrt{n_{eff}^2 - n_2^2} > 0$$

$$\text{Normalized frequency of waveguide} \Rightarrow V^2 = u^2 + v^2 = k_0^2 a^2 \left(n_1^2 - n_2^2\right) = \text{cste}$$

[II-4]

$$\rightarrow \varphi_{rTE\ et\ TM} = 2\,\text{arctg}\left[\left(\eta_{12}\right)^2 \frac{v}{u}\right], \text{ with } \eta_{12} = \begin{cases} 1 & \text{for TE modes} \\ \left(\dfrac{n_1}{n_2}\right) & \text{for TM modes} \end{cases}$$

New expression of the resonance condition for TE_m optical modes :

$$u = m\frac{\pi}{2} + \text{arctg}\left[\frac{v}{u}\right]$$

$$\begin{cases} \text{if m even}: \ v = u\,\text{tg}(u) \\ \text{if m odd}: v = -u\,\text{cotg}(u) \end{cases} \quad \text{with} \quad V^2 = u^2 + v^2 = \text{cste}$$

[II-5]

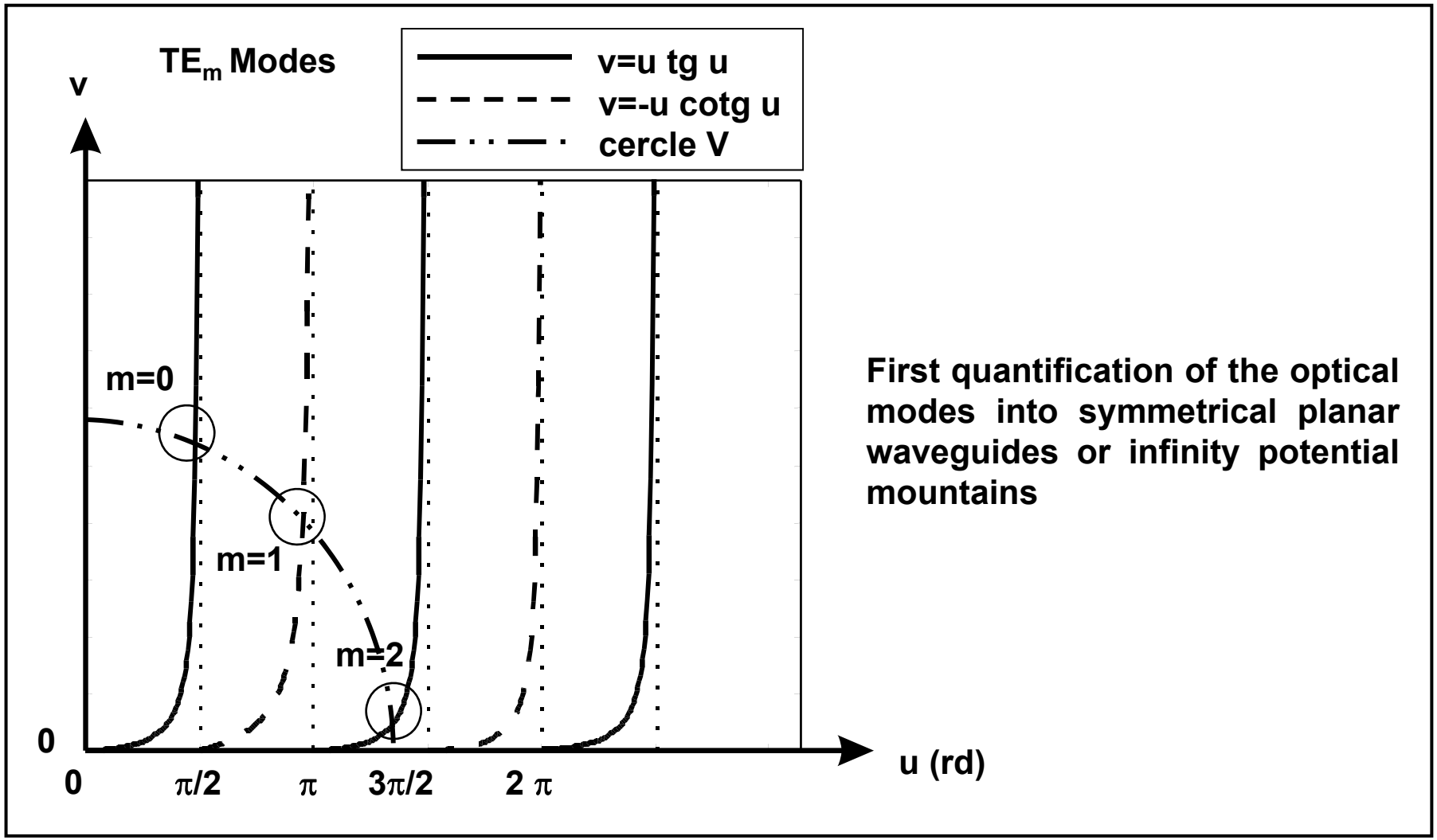

First quantification of the optical modes into symmetrical planar waveguides or infinity potential mountains

- **Interpretation**

- **Graphically, u and v ➔ n_{eff} ➔ β ➔ θ_m.**

- **We see that m=0 ➔ $\theta \rightarrow \pi/2$; then $n_{eff} \rightarrow n_1$ and $u \rightarrow 0$ (that is the first intersection point near lower u is the monomode or single mode TE_0).**

- **Into symmetrical waveguide, there is always existence of an optical mode ; that is no frequency-cut for m=0.**

- **More the normalized frequency V increase [that is λ_0 wavelength decrease, (n_1-n_2) increase, or d-thickness of waveguide increase] more the waveguide present many optical modes (multi-modal aspect).**

- **Graphically, $V \leq \pi/2$ define the cut-wavelength λ_c of the monomode waveguide (m<1) as**

$$\lambda_c \geq 2d\sqrt{n_1^2 - n_2^2}$$

Question : Quel est l'ordre de grandeur de l'épaisseur d'un guide plan monomode en verre (n_1=1.5, n_2=1.48) pour des applications télécom (λ_0=1550 nm) ?

Question : Soit un guide d'onde plan symétrique en verre d'indices n_1=1.46 et n_2=1.45, d'épaisseur d=4 µm. Combien de modes TE_m se propagent dans ce guide à une longueur d'onde λ_0=500 nm ?

- II.1.3 Determination of the repartition of the optical field in transversal y-direction (section of the waveguide)

- **Calculus of the variation of amplitude E(y) of the optical field**

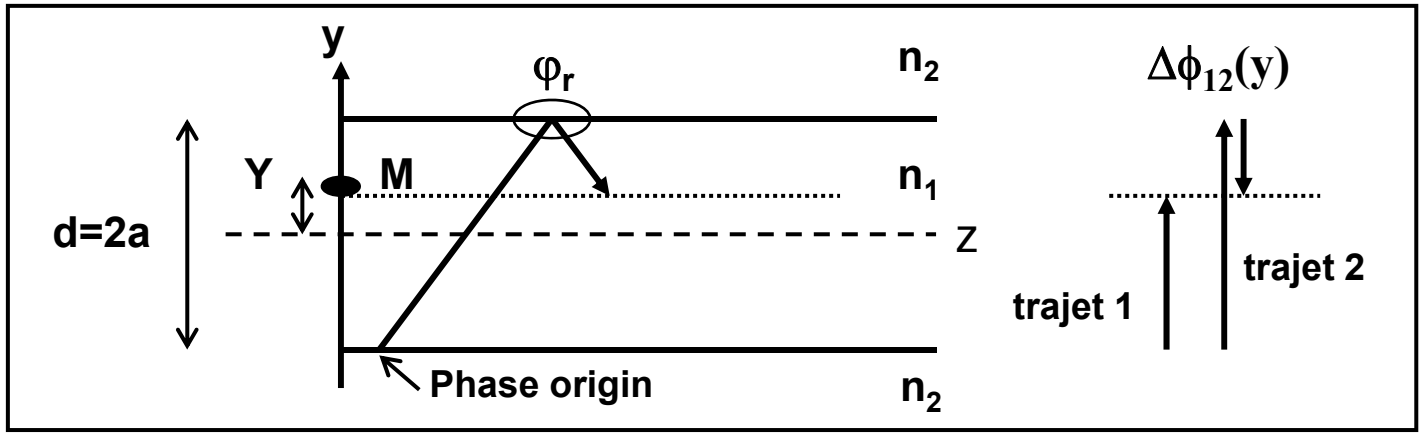

- **Calculus of the phase-shift at M point and global amplitude $E(M)_y$**

$$\Delta\phi_{12}(y) = \left|\frac{2\pi}{\lambda_y}(2Y - d) + \varphi_r\right| \rightarrow \sum_i E_i \rightarrow E(M) = E_0\cos(\omega t) + E_0\cos(\omega t - \Delta\phi_{12}(y))$$

$$E(M) = E(y)\cos\left(\omega t - \frac{\Delta\phi_{12}(y)}{2}\right) \quad \text{with} \quad E(y) = 2E_0\cos\left(\frac{\Delta\phi_{12}(y)}{2}\right)$$

- **Global amplitude of optical field in cases of single-mode and bi-modes waveguides**

- single-mode (or monomode) waveguide : m=0 and $\varphi_r \rightarrow \pi$

Expression of $\Delta\phi(y)$

$$\lambda_y = \frac{\lambda_0}{n_1\cos\theta_0} = 2d$$

+

Condition of resonance $\cos\theta_{m=0}$ [II-1]

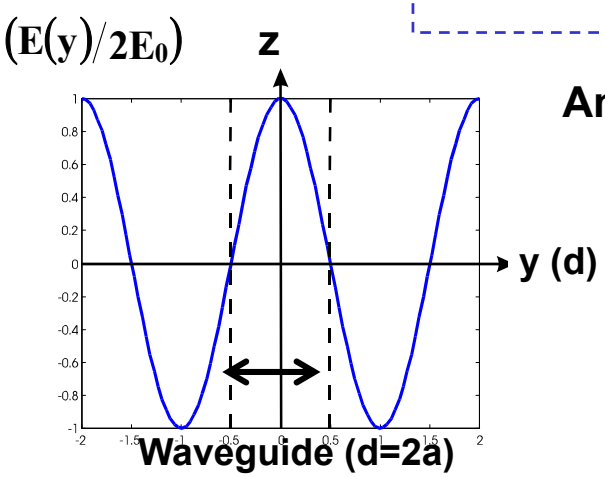

Amplitude

$$E(y) = 2E_0\cos\left(\frac{\pi y}{d}\right)$$

Period 2*d*

E(y) max at y=0

Intensity $E.E^*$ into planar monomode waveguide → z

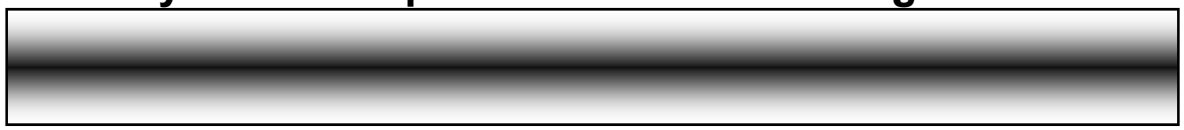

- Bi-mode waveguide : m=1 and $\varphi_r=\pi \rightarrow \lambda_y=d$

Amplitude $\Downarrow$ $E(y) = 2E_0 \sin\left(\frac{2\pi y}{d}\right)$

Period *d*

Opposition of phase at +/- *d/2*

Intensity $E.E^*$ into planar bi-mode waveguide $\longrightarrow$ z

▪ II.1.4 Goos-Hänschen shift ; notion of effective waveguide thicknesses

▪ Determination of the y_g and z_g parameters that characterize the Goos-Hänschen shift

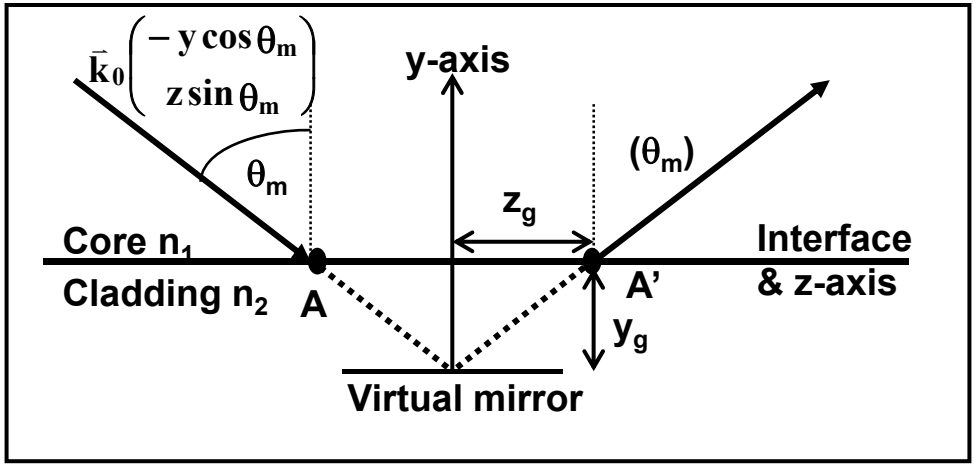

Method for the demonstration : Write the incident field ξ_i around A-point by the sum of twice waves with lower angular gap (θ_m-$\Delta\theta_m$) and (θ_m+$\Delta\theta_m$) (+ approx. tilted optical ray / surface-normal). Develop the reflected field ξ_r (at A'-point) as $\xi_i.e^{j\varphi_r(\theta m)}$. Use a Taylor development on (θ_m-/+$\Delta\theta_m$) to expressed ξ_r at A'-point.

$$\varphi_r(\theta_m \pm \Delta\theta_m) = \varphi_r(\theta_m) \pm \Delta\theta_m \cdot \frac{\partial \varphi_r}{\partial \theta_m}$$

$$\xi_i = E_1 \cdot e^{j\omega t} \cdot \exp[jk_0 n_1(-y\cos\theta_m + z\sin\theta_m)] \times 2\cos(k_0 n_1 z \Delta\theta_m \cos\theta_m)$$

$\rightarrow$ At z=0, ξ at A-point can be expressed

$$\xi_r = E_1 \cdot e^{j\omega t} \cdot e^{j\varphi_r(\theta_m)} \cdot \exp[jk_0 n_1(-y\cos\theta_m + z\sin\theta_m)] \times 2\cos\left(k_0 n_1 z \Delta\theta_m \cos\theta_m - \Delta\theta_m \frac{\partial \varphi_r}{\partial \theta_m}\right)$$

$$2\cos\left(k\,n_1 z\Delta\theta_m\cos\theta_m - \Delta\theta_m\frac{\partial\varphi_r}{\partial\theta_m}\right)=1 \quad \rightarrow \quad \boxed{z_g=\frac{1}{2k_0 n_1\cos\theta_m}\cdot\frac{\partial\varphi_r}{\partial\theta_m}=\frac{1}{2}\cdot\frac{\partial\varphi_r}{\partial\beta_{(z)}}}$$

moreover $\boxed{y_g=\frac{z_g}{\mathrm{tg}\,\theta_m}}$

▪ **Determination of the y_g and z_g parameters functions of global opto-geometrics parameters of such waveguides**

By using previous results of Fresnel $\varphi_{r(TE\text{ and }TM)}$ expressions of phases, we obtain :

$$\boxed{\begin{aligned} z_{gTE} &= \left[\frac{\mathrm{tg}\,\theta_m}{k_0\left(n_1^2\sin^2\theta_m - n_2^2\right)^{1/2}}\right] \\ z_{gTM} &= \left[\frac{n_2^2\,\mathrm{tg}\,\theta_m}{k_0\left(n_1^2\sin^2\theta_m - n_2^2\right)^{1/2}\left(n_1^2\sin^2\theta_m - n_2^2\cos^2\theta_m\right)}\right] \\ y_{gTE-TM} &= \frac{z_{gTE-TM}}{\mathrm{tg}\,\theta_m} \end{aligned}}$$ [II-6]

The parameter y_g represent the geometrical prenetration of the optical ray into the cladding (n_2) of such waveguide, this correspond to the notion of evanescent wave in wave-optics.

- **Notion of effective thickness of waveguide W_{eff}**

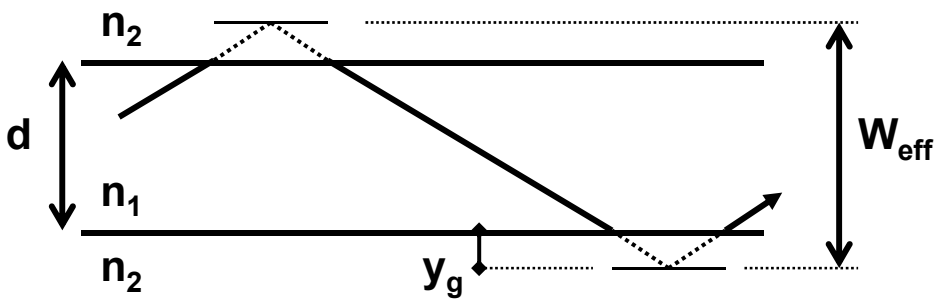

$$W_{eff\,(TE\ et\ TM)} = d + 2\,y_{g(TE\ et\ TM)}$$

Question : Calculer l'angle particulier θ_p tel que le glissement de Goos-Hänschen soit égal pour le deux polarisation TE et TM, c'est-à-dire $z_{gTE}=z_{gTM}$.

- II.2 : Fundamentals on the electromagnetic theory of dielectric waveguide (Maxwell's approach) ; dispersion relations and calculus of photonic's modes (eigenvalues and eigenvectors) into planar waveguide ; channel optical waveguides and geometries; dispersion phenomena and pulse's spread

- II.2.1 Some dates of electromagnetism history, Maxwell's approach for the planar waveguide, determination of the eigenvalues and eigenvectors, analytical expressions of the optical modes

- **Electromagnetism history, to optics at electromagnetism to quantum electrodynamics**

OPTIQUE: **1637 : Dioptrique de Descartes / 1665 : Grimaldi observe la diffraction / 1666 : Roemer découvre que la lumière a une vitesse finie / 1672 : *Newton* décompose la lumière blanche / 1679 : Principe de *Fermat* / 1690 : Théorie ondulatoire de la lumière par Huygens / 1704 : Traité d'optique de *Newton* (théorie corpusculaire) / 1800 : Malus trouve la polarisation par réflexion / 1803 : Young effectue les premières expériences de diffraction / 1814 : *Fresnel* développe la théorie ondulatoire de la lumière (diffraction et interférences) / 1819 : Arago et *Fresnel* prouve la nature transverse de la lumière / 1829 : Fizeau mesure la vitesse de la lumière / 1846 : Faraday montre l'effet d'un champ magnétique sur la lumière.**

ELECTRICITE ET MAGNETISME, ELECTROMAGNETISME, ELECTRODYNAMIQUE QUANTIQUE : **1731 : Gray : différence entre conducteurs et isolants / 1746 : Van Musshen Brock invente la bouteille de Leyde / 1750 : Francklin : deux types de charges / 1785 : Loi de Coulomb / 1800 : Volta invente la pile et Nicholson électrolyse l'eau / 1820 : Oersted crée un champ magnétique par un courant, Arago magnétise du fer et de l'acier, Loi de Biot et Savart, Ampère étudie la force entre deux courants / 1826 : Loi d'Ohm / 1831 : Etude du magnétisme terrestre par Gauss et Weber , Faraday découvre l'induction / 1834 : Loi de Lenz pour l'induction , Loi de Faraday pour l'électrolyse / 1835 : Henry et Faraday découvrent la self-induction / 1838 : Faraday découvre le condensateur / 1841 : Gauss effectue des mesures électriques et magnétiques dans les mêmes unités / 1842 : Henry étudie les circuits oscillants / 1865 : *Mawxell* propose les lois de 'l'électromagnétisme' / 1887-1893 : Hertz découvre les ondes radioélectriques qui confirment expérimentalement les équations de Maxwell / 1887 : Expérience de Michelson / 1905 : *Einstein* crée la relativité restreinte qui unifie la mécanique et l'électromagnétisme / 1949 : *Feynman* (diagrammes), Schwinger … unifient la mécanique quantique et l'électromagnétisme, c'est l'électrodynamique quantique => seconde quantification, choix et changements des jauges (invariance des champs et potentiels), description Lagrangienne, Hamiltonienne.**

Fresnel :

Maxwell :

- **Maxwell's approach for the planar waveguide, determination of the eigenvalues and eigenvectors, analytical expressions of the optical modes : infinite potential mountain $\varepsilon_2/\varepsilon_1/\varepsilon_2$**

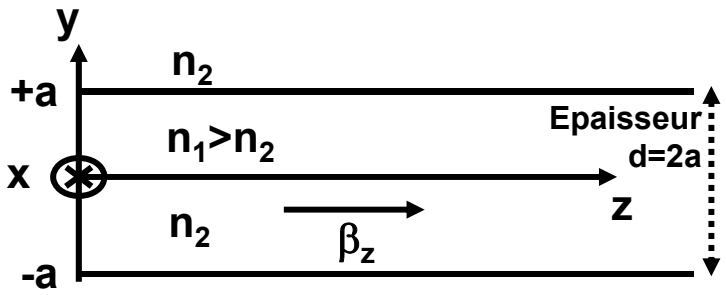

- **Hypothesis : Is there a wave that propagates along z-direction with an effective propagation constant β_z?**
- **Idea : If such a wave exists, then this one must verify the Maxwell equations.**
- **Goal : Find such an expression of optical wave and determinate the quantification of the optical modes**

$$\begin{cases} \overrightarrow{\mathrm{rot}}\,\vec{E} = \vec{\nabla} \wedge \vec{E} = -\dfrac{\partial \vec{B}}{\partial t} \\ \mathrm{div}\,\vec{B} = \vec{\nabla}.\vec{B} = 0 \end{cases} \qquad \begin{cases} \overrightarrow{\mathrm{rot}}\,\vec{H} = \vec{\nabla} \wedge \vec{H} = \cancel{\vec{j}} + \dfrac{\partial \vec{D}}{\partial t} \\ \mathrm{div}\,\vec{D} = \vec{\nabla}.\vec{D} = \cancel{\rho} = 0 \end{cases}$$ [II-7]

→ **Physical meaning…**

$$\begin{cases} \vec{\nabla}^2.\vec{E} - \mu_0 \varepsilon \dfrac{\partial^2 \vec{E}}{\partial t^2} = \cancel{\dfrac{1}{\varepsilon}\overrightarrow{\mathrm{grad}}\,\rho} + \mu_0 \dfrac{\partial \vec{j}}{\partial t} \\ \vec{\nabla}^2.\vec{B} - \mu_0 \varepsilon \dfrac{\partial^2 \vec{B}}{\partial t^2} = \cancel{-\mu_0 \overrightarrow{\mathrm{rot}}\,\vec{j}} \end{cases}$$ [II-8]

Vectorial-equations of propagation, Helmholtz equations, Alembert-type equation…

- **Hypothesis : no optical losses (ε real), no conductors, resolution for the TE case, that is →** $\vec{E}(E_x, 0, 0)$

$$\vec{E}_x(y,z,t) = \vec{i}\,\xi(y)\exp j(\omega t - \beta z)$$ [II-9] **?**

Change of amplitude along y-direction (≠ of a plane wave) , propagation of the wave along z-direction ($\beta = \beta_z$)
Phase celerity : $v_\varphi = \omega/\beta$

- **Determination of the magnetic field components** $\vec{H}$ **relative to TE optical polarization**

$$\overrightarrow{\mathrm{rot}}\,\vec{E} = -\mu_0 \partial \vec{H}/\partial t \longrightarrow \vec{H}\left(H_x = 0 \quad H_y = \frac{\beta}{\omega \mu_0} E_x \quad H_z = -\frac{j}{\omega \mu_0}\frac{\partial E_x}{\partial y} \right)$$ [II-10]

[II-9 & 10] → **Obtaining of equivalent 'zig-zag' model !**

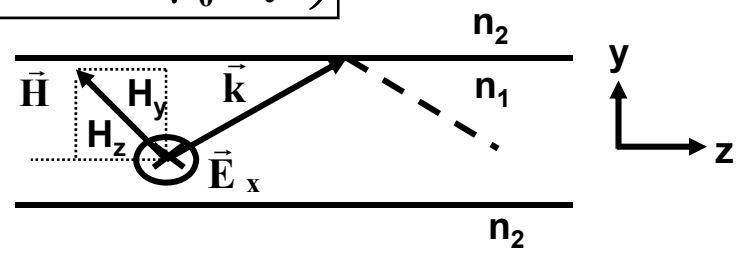

▪ Resolution and determination of the optical modes

[II-8 & 9] → $$\boxed{\frac{\partial^2 E_x}{\partial y^2} + \left(k_0^2 n_i^2 - \beta^2\right) E_x = 0 \qquad (i = 1, 2)}$$ [II-11] → always with [II.9]

$$\rightarrow \begin{cases} \dfrac{\partial^2 \xi(y)}{\partial y^2} + \dfrac{u^2}{a^2}\xi(y) = 0 & n_1 \text{ area} \\ \dfrac{\partial^2 \xi(y)}{\partial y^2} - \dfrac{v^2}{a^2}\xi(y) = 0 & n_2 \text{ area} \end{cases} \rightarrow \begin{cases} \xi(y) = A\cos\left(\dfrac{u}{a}y\right) + B\sin\left(\dfrac{u}{a}y\right) \\ \xi(y) = C\exp\left(\dfrac{v}{a}y\right) + D\exp\left(-\dfrac{v}{a}y\right) \end{cases}$$

with, A, B, C and D integration constants

Notion of evanescent wave in n_2 area : y<-a and y>a
➔ Telecom and sensors applications…

TE case : eigenvectors

[II-12]

n_1 area : core waveguide

$$\vec{E}(E_x,0,0) \quad \begin{cases} E_x = A\cos\left(\dfrac{u}{a}y\right)\exp j[\omega t - \beta z] & \text{symmetrical TE mode} \\ E_x = B\sin\left(\dfrac{u}{a}y\right)\exp j[\omega t - \beta z] & \text{anti-symmetrical TE mode} \end{cases}$$

identical

n_2 area : cladding layers

$$\begin{cases} E_x = C\exp\left(-\dfrac{v}{a}y\right)\exp j[\omega t - \beta z] & \text{for } y > a \\ E_x = D\exp\left(\dfrac{v}{a}y\right)\exp j[\omega t - \beta z] & \text{for } y < -a \end{cases}$$

Then, according to Maxwell approach, such an optical mode β_z exist !

▪ Resolution and determination of the effective indices or eigenvalues of the system

By using the continuities of (anti-) symmetrical E_x and H_z components respectively at y=+/-a with [II.12 & 10], we can obtain by Maxwell approach previous [II.5] as TE_m modes quantification

$$\boxed{\frac{C}{A} = \frac{\cos u}{e^{-v}} \quad \text{and} \quad \frac{D}{B} = \frac{\sin u}{e^{-v}}} \qquad \boxed{\frac{C}{A} = \frac{u \sin u}{v\, e^{-v}} \quad \text{and} \quad \frac{D}{B} = \frac{u \cos u}{v\, e^{-v}}}$$

$$\boxed{\begin{cases} \text{if m even}: \ v = u\, tg(u) \\ \text{if m odd}: v = -u \cot g(u) \end{cases} \quad \text{with} \quad V^2 = u^2 + v^2 = cste}$$

Remarques :

- Un raisonnement permettrait d 'obtenir les équations aux modes propres optiques TM.

- Le modèle géométrique des rayons et la théorie de Maxwell ondulatoire permettent de décrire le guidage optique tout en expliquant différemment la propagation guidée dans une structure (ici guide plan symétrique). Dans la suite, nous utiliserons la théorie de Maxwell pour l'étude du guidage optique dans l'ensemble des autres structures guidantes, à savoir : guide plan dissymétrique, guide multicouches (3, 4, 'n'), guide rectangulaire, guide à gradient d'indice, et guide circulaire (fibre optique)…

▪ Conclusion, analytical expressions of the TE optical modes

Core waveguide –a<y<a

Symmetrical TE modes	Anti-symmetrical TE modes
$E_x = A\cos\left(\frac{u}{a}y\right)\exp j(\omega t - \beta z)$	$E_x = B\sin\left(\frac{u}{a}y\right)\exp j(\omega t - \beta z)$
$H_y = \frac{\beta}{\omega\mu_0}E_x$	$H_y = \frac{\beta}{\omega\mu_0}E_x$
$H_z = \frac{j\,u}{\omega\mu_0 a}\mathrm{tg}\left(\frac{u}{a}y\right)E_x$	$H_z = \frac{j\,u}{\omega\mu_0 a}\mathrm{cotg}\left(\frac{u}{a}y\right)E_x$
$E_y = E_z = H_x = 0$	$E_y = E_z = H_x = 0$
$v = u\,\mathrm{tg}\,u$	$v = -u\,\mathrm{cotg}\,u$

$\beta = \sqrt{k_0^2 n_1^2 - \frac{u^2}{a^2}}$ and u, v defined in [II.4]

Cladding layers |y|>a

Symmetrical TE modes	Anti-symmetrical TE modes
$E_x = A\cos u\; e^{v}\; e^{-\frac{v}{a}\lvert y\rvert}\exp j(\omega t - \beta z)$	$E_x = \varepsilon B\sin u\; e^{-\frac{v}{a}\lvert y\rvert}\exp j(\omega t - \beta z)$
$H_y = \frac{\beta}{\omega\mu_0}E_x$	$H_y = \frac{\beta}{\omega\mu_0}E_x$
$H_z = \frac{j\,v}{\omega\mu_0 a}E_x$ for $y \geq a$	$H_z = \frac{j\,v}{\omega\mu_0 a}E_x$ for $y \geq a$
$H_z = -\frac{j\,v}{\omega\mu_0 a}E_x$ for $y \leq -a$	$H_z = -\frac{j\,v}{\omega\mu_0 a}E_x$ for $y \leq -a$
$E_y = E_z = H_x = 0$	$E_y = E_z = H_x = 0$

▪ II.2.2 dispersion phenomena and pulse's spread

▪ **Materials dispersion** ➔ Cauchy $\varepsilon(\omega)$ and $n(\omega)$ equivalent to transfert functions of the system ➔ causality (Hilbert type relations, Kramers-Krönig relations, Bode relations, …)

$$v_\varphi = \frac{\omega}{k(\omega)} = \frac{\omega}{k_0 n(\omega)} \quad \text{et} \quad v_g = \left(\frac{dk(\omega)}{d\omega}\right)^{-1} = \left(\frac{k_0 dn(\omega)}{d\omega}\right)^{-1} \qquad \text{[II-13]}$$

inverse slope of dispersion curves

$$k(\omega) = \frac{\omega}{c} n(\omega)$$

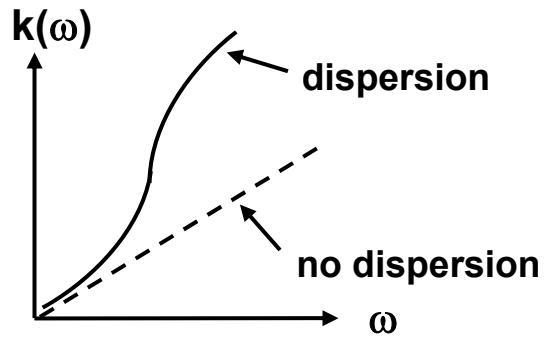

▪ **Modal dispersion phenomena in integrated photonics**

TE_m (n_{effTE} or β_{TE}) and TM_m quantifications are different (modal aspect due to the confinement and to the E and D continuities at interfaces, that is due to the propagation by TIR !) ➔ existence of pulse's spread

▪ **Interpretation** of the previous TE_m quantification (modal dispersion curves, see [II.5])

Intersections 'curves-circle V' = discretization and quantification, according to the expressions of u and v [II.4] :

$$\beta^2 = k_0^2 n_1^2 - \frac{u^2}{a^2} = k_0^2 n_2^2 + \frac{v^2}{a^2}$$

As an example in TE_0 case, graphically :

- We see that $\omega \to 0$ when [circle $V \to 0$, with $u \to 0$ and $v \xrightarrow[\text{faster than u}]{} 0$] :

$$\boxed{\beta_{TE0} \xrightarrow[\omega \to 0]{} k_0 n_2 \to 0}$$

- Moreover, $\omega \to +\infty$ when [circle $V \to +\infty$, with $u \to \pi/2$ and $v \to +\infty$] :

$$\boxed{\beta_{TE0} \xrightarrow[\omega \to +\infty]{} k_0 n_1 \to +\infty}$$

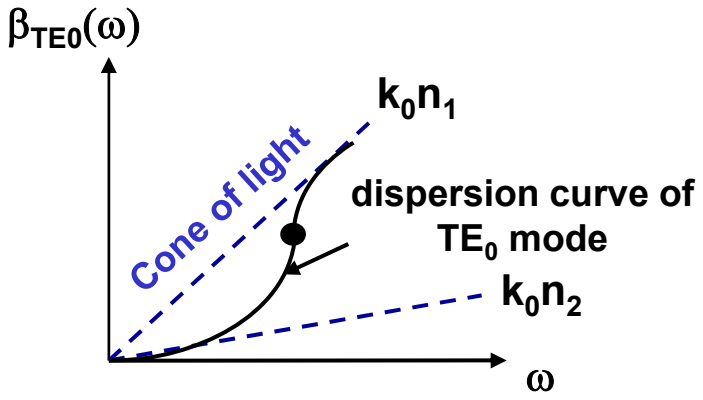

- No cut-frequency (ω_c or ν_c) into such symmetrical wave-guide for single mode TE_0 (and TM_0)

- There is an inflexion point corresponding to lower pulse's spread

$$\boxed{k_0 n_2 \le \beta_{eff(z)} = k_0 n_{eff(z)} \le k_0 n_1}$$

Propagation condition of guided modes

- **Pulse's spread due to the modal dispersion**

- Hypothesis : TE_0 single-mode waveguide, by considering the pulse $E_{L=0}(t)$ and $b(\nu)$ its associated spectral information

$$\boxed{E_{L=0}(t) = TF^{-1}[b(\omega)] = \frac{1}{2\pi}\int b(\omega)\exp[j\omega t]d\omega}$$

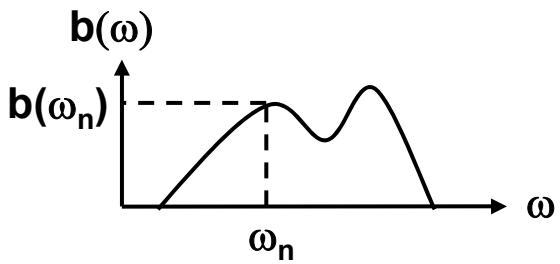

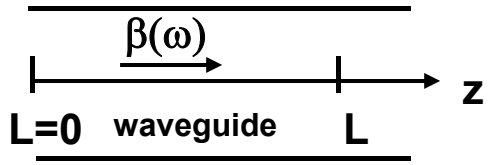

▪ By developing the wave vector around ω_0-pulsation, the phase-shift due to the propagation can be expressed as :

$$\beta(\omega) = \beta_0 + (\omega - \omega_0)\beta_0^{'} + \frac{(\omega-\omega_0)^2}{2}\beta_0^{''}$$

$$\text{with} \quad \beta_0^{'} = \left(\frac{d\beta}{d\omega}\right)_{|\omega=\omega_0} = \frac{1}{v_g}$$

$$\beta(\omega).L = a_0 + a_1\omega + a_2\omega^2 \quad \text{avec} \quad \begin{cases} a_0 = \left[\beta_0 - \omega_0\beta_0^{'} + \frac{\omega_0^2}{2}\beta_0^{''}\right]L \\ a_1 = \left[\beta_0^{'} - \omega_0\beta_0^{''}\right]L \\ a_2 = \left[\frac{\beta_0^{''}}{2}\right]L \end{cases}$$

[II-14]

▪ By writing the expression of the field at a L-distance, we found :

$$E_L(t) == \frac{1}{2\pi}\int b(\omega)\exp j\left[\omega t - \beta(\omega)L\right]d\omega$$

[II-15]

[II-14 & 15] ⟶

$$E_L(t) = \frac{e^{-ja_0}}{2\pi}TF^{-1}\left[b(\omega)\,e^{-ja_1\omega}\,e^{-ja_2\omega^2}\right]$$

$$\text{with} \quad \begin{cases} TF^{-1}\left[b(\omega)\right] = E_{L=0}(t) \\ TF^{-1}\left[e^{-ja_1\omega}\right] = \delta(t - a_1) \\ TF^{-1}\left[\exp\left(-\frac{\alpha^2}{16\pi^2}\omega^2\right)\right] = \frac{1}{2\pi^{3/2}\alpha}\exp\left(-\frac{t^2}{\alpha^2}\right) \end{cases}$$

[II-16]

- This can be shaped in the global form

$$E_L(t) = \frac{\sqrt{2}e^{-j(a_0+\pi/4)}}{16\pi^{7/2}\sqrt{L}} \cdot E_{L=0}(t) * \delta\left(t-\beta_0^{'}L\right) * \frac{1}{\sqrt{\beta_0^{''}}}\exp\left[\frac{j}{8\pi^2\beta_0^{''}L}\left(t+\omega_0\beta_0^{''}L\right)^2\right] \quad \text{[II-17]}$$

Term relative to the original signal with the delay $t=\beta'_0L$

Impulsion's spread due to β''_0

- The Green function (or percussional response, or propagator) of such waveguide can be expressed as :

$$G(t) = \delta\left(t-\beta_0^{'}L\right) * \Re\left\{\frac{1}{\sqrt{\beta_0^{''}}}\exp\left[\frac{j}{8\pi^2\beta_0^{''}L}\left(t+\omega_0\beta_0^{''}L-\frac{\pi}{4}-a_0\right)^2\right]\right\}$$

- **II.3 : Symmetrical planar waveguide with heterostructured-core or graded indices laws (parabolic, hyperbolic, and another power), analytical global methods to determinate all the overall physical parameters as the geometrical and optical paths, the trajectory, the caustics, the transit delay…**

- **II.3.1 Introduction, 'eikonale' or 'iconale' equation and procedure**

▪ Propagation in graded indices profiles is fashion by the locale relation called 'eikonale' or 'iconale' according to the origin (ikona in russian or eikona in byzantine greek).

$$\boxed{\frac{d\left[n(M).\vec{u}(M)\right]}{ds} = \overrightarrow{\text{grad}}\, n(M)} \quad \text{[II-18]}$$

with, $\overrightarrow{\text{grad}}\, n$ the gradient orthogonal to the interface 'n|n+Δn' along the increase indices, ds the curvilinear abscissa (trajectory), and $\vec{u}$ the known original ray optic.

▪ Implementation of such calculus

$$(n+\Delta n).\vec{u}(M_1) = n(M_0).\vec{u}(M_0) + \overrightarrow{\text{grad}}\, n(M_0).ds$$

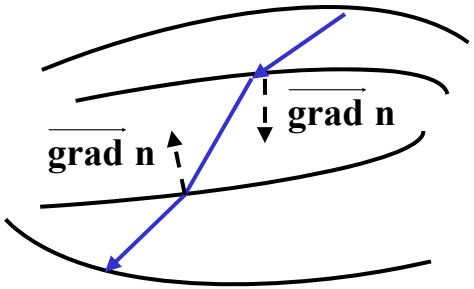

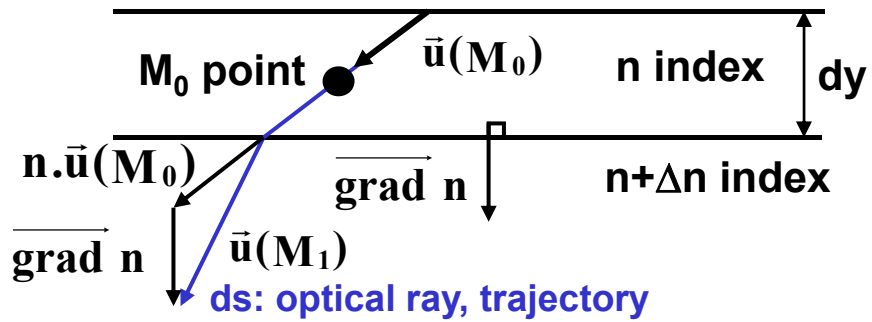

▪ Constant index ➔ rectilinear trajectory $\quad \dfrac{d\left[n(M).\vec{u}(M)\right]}{ds} = \vec{0} \;\Rightarrow\; n(M).\vec{u}(M) = cste$

▪ Possibility to obtain the optical propagation into various graded waveguides structures with no TIR on the claddings with surface defects ➔ lower optical losses, notion of optical caustic (for example, see first chapter and Ti-diffusion at high temperature for $LiNbO_3$ waveguides).

▪ II.3.2 Symmetrical planar waveguide based on heterostructured-core with a parabolic graded index law, analytical global methods to determinate all the overall physical parameters as the geometrical and optical paths, the trajectory, the transit delay.

▪ Study of the optical rays trajectory, method of calculus, notion of caustics

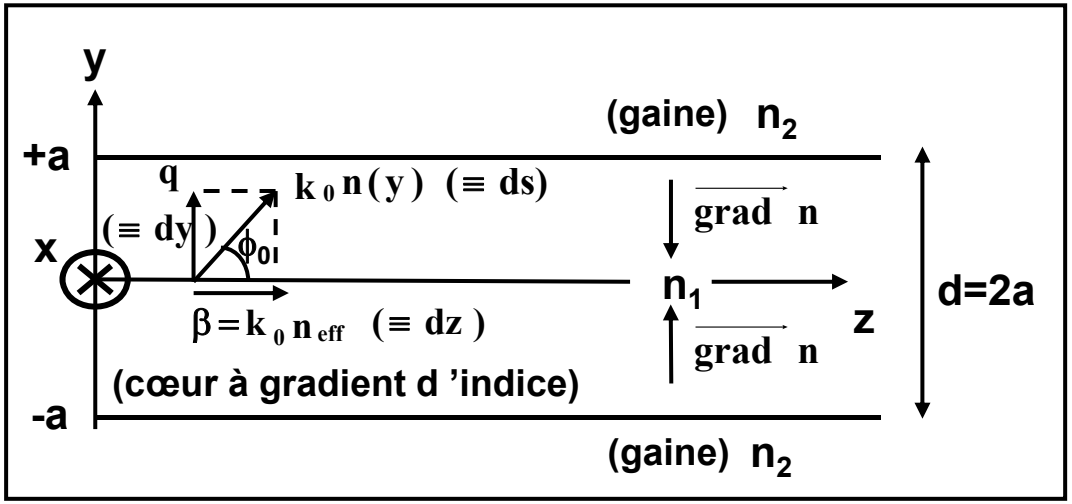

$$q = \left(k_0^2 n^2(y) - \beta^2\right)^{1/2} \quad \text{[II-19]}$$

$$n^2(y) = n_1^2\left[1 - 2\Delta\left(\frac{y}{a}\right)^2\right] \quad \text{[II-20]}$$

$$\text{avec } 2\Delta = \frac{n_1^2 - n_2^2}{n_1^2}$$

$$\frac{ds}{dy} = \frac{k_0 n(y)}{q} \quad \text{and} \quad \frac{dz}{dy} = \frac{\beta}{q} \quad \text{[II-21]}$$

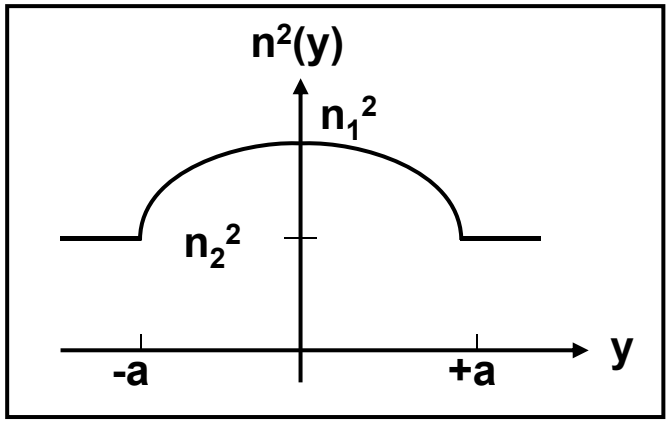

▪ Note :Weakly propagation case ($n_1 \approx n_2$) :

$$\Delta \approx \frac{n_1 - n_2}{n_1}$$

▪ **Hypothesis : For an elementary *ds*, the index is constant ; *n(y)* function slowly changes (flat parabola).**

▪ **Goal : Determinate the analytical expression of such optical ray trajectory.**

▪ **Method : Infer from [II.21] (*dz/dy*) plus the parabolic index profil case [II.20] the normalized expression (with *u* and *V* definitions [II.4]) of the z(y) trajectory. Then, with the initial conditions, bring forth the *y(z)* trajectory.**

$$\frac{dz}{dy} = \frac{\beta}{q} = \frac{\beta}{\left(k_0^{\,2} n^2(y) - \beta^2\right)^{1/2}} \quad \text{with} \quad n^2(y) = n_1^2\left[1 - 2\Delta\left(\frac{y}{a}\right)^2\right] \qquad \text{[II-22]}$$

$$\begin{cases} u^2 = a^2 q^2 = a^2 k_0^{\,2}\left(n_1^2 - n_{eff}^2\right) \\ V^2 = a^2 k_0^{\,2}\left(n_1^2 - n_2^2\right) = 2\, a^2 k_0^{\,2} n_1^2 \Delta \end{cases} \qquad \text{[II-23]}$$

$$\frac{dz}{dy} = \frac{a\beta}{\left(u^2 - V^2\left(\frac{y}{a}\right)^2\right)^{1/2}} \qquad \text{[II-24]}$$

▪ **Caustics or turning points notions : dy → 0**

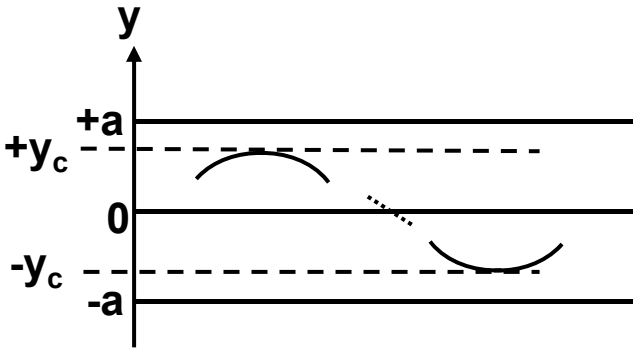

$$y_c = \pm\frac{u\,a}{V} \qquad \text{[II-25]}$$

▪ According to the initial conditions y_0 at the beginning of the waveguide $z_0=0$:

$$z(y)=\int_{y_0}^{y}\frac{a^2\beta}{V}\frac{dy}{\left(\frac{u^2a^2}{V^2}-y^2\right)^{1/2}}$$ [II-26]

$$\xrightarrow[y=\frac{u\,a}{V}\sin\theta]{\text{Variable change}}$$

$$z(y)=\frac{a^2\beta}{V}\left[\arcsin\left(\frac{V}{u\,a}y\right)-\arcsin\left(\frac{V}{u\,a}y_0\right)\right]$$ [II-27]

⟶ verification of y_c caustic

⟶ Maximum amplitude of trajectory : (2ua/V)

▪ Determination of the global *z(y)* trajectory according to initial conditions :

[II-27] ⟶ $$y(z)=\frac{u\,a}{V}\cos\left[\arcsin\left(\frac{V\,y_0}{u\,a}\right)\right]\sin\left(\frac{V}{a^2\beta}z\right)+y_0\cos\left(\frac{V}{a^2\beta}z\right)$$ [II-28]

Initial conditions $\left(\frac{dy}{dz}\right)_{|y=y_0}=\mathrm{tg}\,\phi_0$ with [II.24] and previous variable change

[II-24] ↓ $y=\frac{u\,a}{V}\sin\theta$

[II-29]

$$\mathrm{tg}\,\phi_0=\frac{u}{a\,\beta}\cos\left[\arcsin\left(\frac{V\,y_0}{u\,a}\right)\right]$$

⟵

[II-30] Final expression with CI (that is ϕ_0 and y_0)

$$y(z)=\frac{a^2\beta}{V}\mathrm{tg}(\phi_0)\sin\left(\frac{V}{a^2\beta}z\right)+y_0\cos\left(\frac{V}{a^2\beta}z\right)$$

Period of such trajectory function of β

- **Paraxial hypothesis (or lower tilt optical ray / z-axis), far from cut-off**

$q \rightarrow 0$ when $\beta \rightarrow k_0 n_1$ with lower ϕ_0 ➔ $V = \sqrt{2\Delta}\, a\, k_0 n_1$ and $\boxed{\left(V/a^2\beta\right) = \left(\sqrt{2\Delta}/a\right)}$ [II-31]

$$T = \frac{2\pi a}{\sqrt{2\Delta}}$$

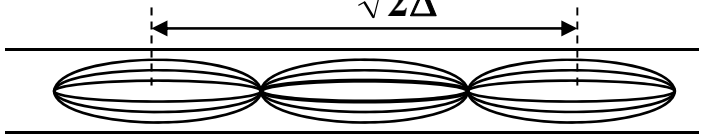

$$\boxed{y(z) = \frac{a\phi_0}{\sqrt{2\Delta}} \sin\left(\frac{\sqrt{2\Delta}}{a} z\right) + y_0 \cos\left(\frac{\sqrt{2\Delta}}{a} z\right)}$$ [II-32]

Period of such trajectory independent of β

- **Transit time τ , geometrical and optical paths (L_g and L_o)**
- **Transit time τ is defined as the integral optical path along the previous trajectory (L=waveguide length, $\int_{-y_c}^{+y_c} dz$ length along z-direction of trajectory between unitary period of caustic, then such a quotient ($L/\int_{-y_c}^{+y_c} dz$) represents the number of 'unitary length caustic' along z-axis projection ; then $\int_{-y_c}^{+y_c} n(y)ds/c$ is defined as the elementary time transit of one curvilinear element of trajectory between two successives caustics) :**

$$\boxed{\int_{traj} dz} \longleftarrow \boxed{\tau = \frac{L}{c} \frac{\int_{traj} n(y)ds}{\int_{traj} dz}} \longrightarrow \boxed{\int_{traj} n(y)ds}$$ [II-33]

[II-26 & 25] $\longrightarrow$ $$\int_{traj} dz = \int_{y_{c-} = \frac{-ua}{V}}^{y_{c+} = \frac{+ua}{V}} \frac{a^2\beta}{V} \frac{dy}{\left(\frac{u^2a^2}{V^2} - y^2\right)^{1/2}} = \frac{a^2\beta}{V}\left[\arcsin\left[\frac{y}{\left(\frac{ua}{V}\right)}\right]\right]_{-\frac{ua}{V}}^{+\frac{ua}{V}} = \frac{\pi a^2\beta}{V}$$

[II-21 & 20], with [II.24 & 22] $\frac{1}{q} = \frac{a}{\left(u^2 - V^2\left(\frac{y}{a}\right)^2\right)^{1/2}}$

$$\longrightarrow \int_{traj} n(y)ds = \int_{y_{c-}=\frac{-ua}{V}}^{y_{c+}=\frac{+ua}{V}} \frac{a k_0 n_1^2\left[1 - 2\Delta\left(\frac{y}{a}\right)^2\right]dy}{\left(u^2 - V^2\left(\frac{y}{a}\right)^2\right)^{1/2}} = \frac{a^2 k_0 n_1^2}{V} \int_{y_{c-}=\frac{-ua}{V}}^{y_{c+}=\frac{+ua}{V}} \frac{\left[1 - 2\Delta\left(\frac{y}{a}\right)^2\right]dy}{\left(\frac{u^2 a^2}{V^2} - y^2\right)^{1/2}}$$

Variable change

$$y = \frac{u\,a}{V}\sin\theta$$

$$\int_{traj} n(y)ds = \frac{a^2 k_0 n_1^2}{V}\left(\pi - \pi\Delta\frac{u^2}{V^2}\right)$$

- Transit time τ for the trajectory along L distance on z-axis

$$\boxed{\tau = \frac{L}{c}\frac{k_0 n_1^2}{\beta}\left(1 - \Delta\frac{u^2}{V^2}\right)}$$ [II-34]

- Weakly propagation conditions : $\beta \approx k_0 n_1$ and $u = a^2\left(k_0^2 n_1^2 - \beta^2\right) \approx 0 \longrightarrow \boxed{\tau \approx \frac{L}{c} n_1}$

τ is independent of β, each optical modes have the same transit time

- **Geometrical and optical paths (L_g and L_o), ray-half-period z_g**

According to [II.21 & 20], L_g, L_o and z_g can be explained

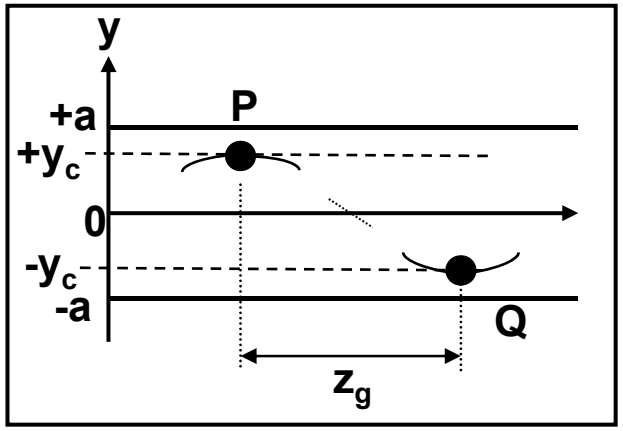

$$z_g = \int_P^Q dz = \int_{y_{c-}}^{y_{c+}} \frac{n_{eff}\, dy}{\left(n^2(y) - n_{eff}^2\right)^{1/2}} \quad \text{[II-35]}$$

$$L_g = \int_P^Q ds = \int_{y_{c-}}^{y_{c+}} \frac{n(y)\, dy}{\left(n^2(y) - n_{eff}^2\right)^{1/2}} \quad \text{and} \quad L_0 = \int_P^Q n(y)\, ds = \int_{y_{c-}}^{y_{c+}} \frac{n^2(y)\, dy}{\left(n^2(y) - n_{eff}^2\right)^{1/2}} \quad \text{[II-36]}$$

- **Note : The z_g expression is close to L_g, n(y) have to be substituted by n_{eff}.**

▪ II.3.3 Symmetrical planar waveguide based on heterostructured-core with another graded index law.

- **Such method can be can be used for another non-linear profiles related to :**

$$n^2(y) = n_1^2\left[1 - 2\Delta f(y)\right] \text{ with step index } 2\Delta = \frac{n_1^2 - n_2^2}{n_1^2}$$

$$\text{and } f(y) \text{ non negative function}$$

	profil $n^2(y)$	y_c	z_g
Parabolic (y^2)	$n_1^2\left[1-2\Delta\left(\frac{y}{a}\right)^2\right]$	$\pm\frac{a\left(n_1^2-n_{eff}^2\right)^{1/2}}{\sqrt{2\Delta}\,n_1}$	$\frac{\pi a\, n_{eff}}{\sqrt{2\Delta}\,n_1}$
Another exposant (y^q) (with q>0)	$n_1^2\left[1-2\Delta\left\lvert\frac{y}{a}\right\rvert^q\right]$	$\pm a\left(\frac{n_1^2-n_{eff}^2}{2\Delta n_1^2}\right)^{1/q}$	$\frac{\sqrt{2\pi}\,n_{eff}\,y_c}{\sqrt{\Delta}\,q\,n_1}\left(\frac{a}{y_c}\right)^{q/2}\frac{\Gamma\left(\frac{1}{q}\right)}{\Gamma\left(\frac{1}{q}+\frac{1}{2}\right)}$
Hyperbolic secant	$n_1^2\,\mathrm{sech}^2\left[\sqrt{2\Delta}\left(\frac{y}{a}\right)\right]$	$\pm\frac{a}{\sqrt{2\Delta}}\cosh^{-1}\left(\frac{n_1}{n_{eff}}\right)$	$\frac{\pi a}{\sqrt{2\Delta}}$

L_g	L_0
$a\left(\frac{2}{\Delta}\right)^{1/2}E\left(2\Delta\frac{y_c^2}{a^2}\right) \approx \frac{z_g}{4}\left(\frac{3n_1}{n_{eff}}+\frac{n_{eff}}{n_1}\right)$ si $\Delta<<1$	$z_g\left(\frac{n_1^2+n_{eff}^2}{2n_{eff}^2}\right)$
$\approx \frac{z_g}{q+2}\left(\frac{n_{eff}}{n_1}+(q+1)\frac{n_1}{n_{eff}}\right)$ si $\Delta<<1$	$\frac{z_g}{q+2}\left(q\frac{n_1^2}{n_{eff}}+2n_{eff}\right)$
$\frac{2z_g}{\pi}K\left(\frac{n_1^2-n_{eff}^2}{n_1^2}\right) \approx z_g\left(\frac{n_1+n_{eff}}{2n_{eff1}}\right)$ si $\Delta<<1$	$n_1 z_g$

with Gamma and elliptic mathematical functions :

$$\Gamma(z)=\int_0^{+\infty} t^{z-1}e^{-t}dt\,,\quad K(x)=\int_0^{\pi/2}\frac{d\theta}{\left(1-x\sin^2(\theta)\right)^{1/2}}\,,\text{ and } E(x)=\int_0^{\pi/2}\left(1-x\sin^2(\theta)\right)^{1/2}d\theta$$

▪ II.4 : Dissymmetrical multilayer slab waveguide-structures : formalism for 3, 4 and n-planar-layers

▪ II.4.1 Comprehensive analytical approach for dissymmetrical 3-layers slab waveguides, optical modes and electromagnetic energy distribution through the multilayer

▪ **Hypothesis**

- Dissymmetrical 3-layers planar waveguide with permittivity discontinuities (dissymmetrical potential barrier '$\varepsilon_3/\varepsilon_1/\varepsilon_4$')
- Infinity lateral dimension (along x_2-axis)
- Propagation along x_3-axis
- Propagation TIR $n_1 > n_3$ and n_4

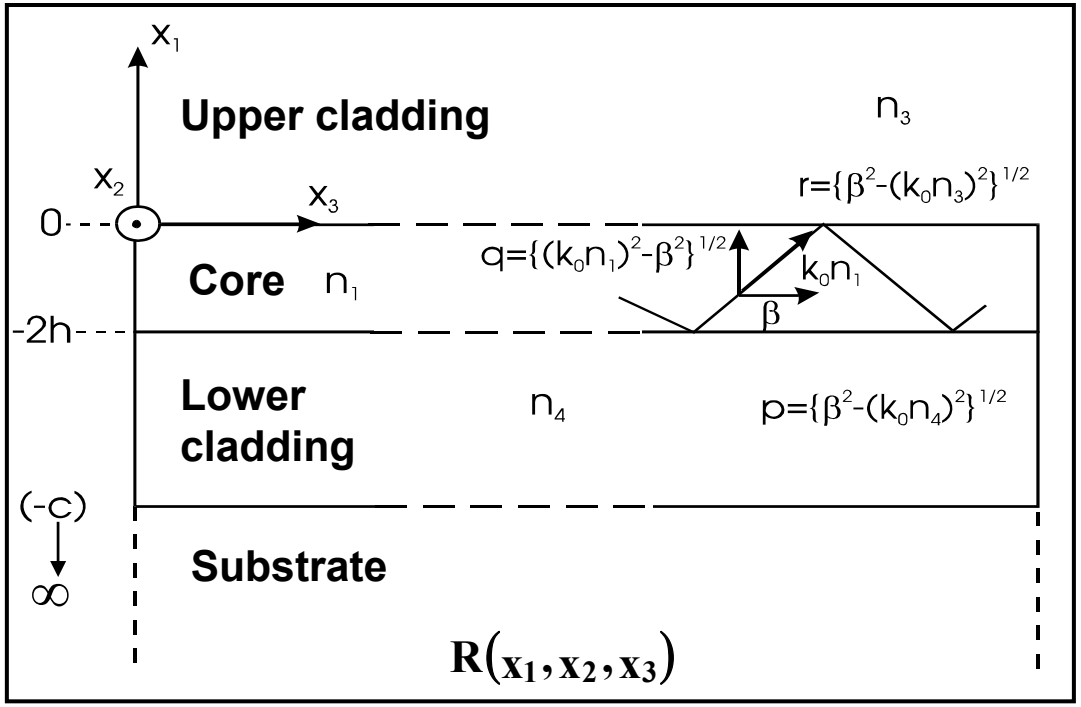

$$\nabla^2 \vec{A} = \mu_0 \varepsilon_0 \varepsilon_{ij} \frac{\partial^2 \vec{A}}{\partial t^2} \quad \text{[II-37]}$$

$$\vec{A} \equiv \vec{E} \text{ ou } \vec{H}$$

- 2h thickness of the core
- $k_0 = 2\pi/\lambda_0$, $\beta = k_0 n_{eff} = \beta_{x3}$
- q, r and p quantities are positives

$$q = \sqrt{(k_0 n_1)^2 - \beta^2}$$
$$r = \sqrt{\beta^2 - (k_0 n_3)^2}$$
$$p = \sqrt{\beta^2 - (k_0 n_4)^2} \quad \text{[II-38]}$$

- **Goal : Calculate and define such a modal quantification (eigenvectors) and determinate the equations of eigenvalues into this three-slab structures**

- **Propagation condition for guided optical modes**

$$\boxed{k_0^2 n_1^2 \geq \beta^2 = k_0^2 n_{eff}^2 \geq k_0^2 n_4^2 \geq k_0^2 n_3^2} \quad \text{[II-39]}$$

- **Study of the TE_m propagation modes**

$$\boxed{\vec{E}\left(0, E_{x2}(x_1) e^{j(\omega t - \beta x_3)}, 0\right)} \xrightarrow{\text{[II-7]}} \boxed{\vec{H}\left(H_{x1}(x_1) e^{j(\omega t - \beta x_3)}, 0, H_{x3}(x_1) e^{j(\omega t - \beta x_3)}\right)}$$

- **Invariance hypothesis along x_2-direction and resolution of [II.37] allow to defined in each area (i=1,3,4) :**

[II-40]

$$\boxed{\frac{\partial^2}{\partial x_1^2} E_{x2}(x_1) + \left(k_0^2 n_i^2 - \beta^2\right) E_{x2}(x_1) = 0} \longrightarrow \begin{cases} \frac{\partial^2}{\partial x_1^2} E_{x2}(x_1) - r^2 E_{x2}(x_1) = 0 & x_1 \geq 0 \text{ upper cladding} \\ \frac{\partial^2}{\partial x_1^2} E_{x2}(x_1) + q^2 E_{x2}(x_1) = 0 & 0 \geq x_1 \geq -2h \text{ core} \\ \frac{\partial^2}{\partial x_1^2} E_{x2}(x_1) - p^2 E_{x2}(x_1) = & x_1 \leq -2h \text{ lower cladding} \end{cases}$$

- **Continuities at respectively x_1=0 and -2h impose :**

$$\boxed{E_{x2}(x_1) \begin{cases} C \exp[-r\, x_1], & x_1 \geq 0 \text{ (upper clad.)} \\ C \cos(q\, x_1) + K \sin(q\, x_1), & 0 \geq x_1 \geq -2h \text{ (core)} \\ \left[C \cos(2h\, q) - K \sin(2h\, q)\right] \times \exp[p(x_1 + 2h)], & x_1 \leq -2h \text{ (lower clad.)} \end{cases}} \quad \text{[II-41]}$$

▪ **Moreover Maxwell equation [II.7] fixes :**

$$H_{x3}(x_1)\begin{cases} \dfrac{jCr}{\mu_0\omega}\exp[-r\,x_1], & x_1 \geq 0 \\ \dfrac{j}{\mu_0\omega}q\left[C\sin(q\;x_1)-K\cos(q\;x_1)\right], & 0 \geq x_1 \geq -2h \\ \dfrac{-j}{\mu_0\omega}p\left[C\cos(2h\,q\;)-K\sin(2h\,q\;)\right]\times\exp[p(x_1+2h)], & x_1 \leq -2h \end{cases} \quad \text{[II-42]}$$

▪ **Determination of the eigenvalues equation of such 3-layers slab waveguides**

According to the x_1=0 and -2h continuities of previous H_{x3} component, it can be shaped the global eigenvalues equation for the TE_m modes (*m* integer):

$$\boxed{tg(2h\,q\;-m\pi)=\frac{q\;(p+r)}{q^2-pr}} \quad \text{or} \quad \boxed{2h\,q\;-\mathrm{arctg}\left[\frac{p}{q}\right]-\mathrm{arctg}\left[\frac{r}{q}\right]=m\pi} \quad \text{[II-43]}$$

with, q, r, p defined previously in [II.38].

▪ An identical development on the TM-polarization $\vec{H}\left(0, H_{x2}(x_1)e^{j(\omega t-\beta x_3)}, 0\right)$ allows to shaped the general eigenvalues equation for the TM_m optical modes (*m* integer):

$$\boxed{tg\left(2hq + m\pi\right) = \frac{n_1^2 q\left(n_3^2 p + n_4^2 r\right)}{n_3^2 n_4^2 q^2 - n_1^4 pr}} \quad \text{or} \quad \boxed{2hq - arctg\left[\left(\frac{n_1}{n_4}\right)^2 \frac{p}{q}\right] - arctg\left[\left(\frac{n_1}{n_3}\right)^2 \frac{r}{q}\right] = m\pi} \qquad \text{[II-44]}$$

▪ Determination of the minimum of the core thickness, notion of cut-thickness

Such a cut is characterizes by the leaky modes or the 'radiation' of the modes into the cladding layer that present the upper index ($n_{eff}=n_4$ or p=0) :

$$\boxed{\left(2h_c\right) = \frac{\lambda_0}{2\pi\left(n_1^2 - n_4^2\right)^{1/2}}\left\{arctg\left[\eta_{13}\left(\frac{n_4^2 - n_3^2}{n_1^2 - n_4^2}\right)^{1/2}\right] + m\pi\right\}} \qquad \text{[II-45]}$$

with, $\eta_{13} = \left(\frac{n_1}{n_3}\right)^2$ ou 1 respectively for the TM_m and TE_m optical modes $(n_4 > n_3)$.

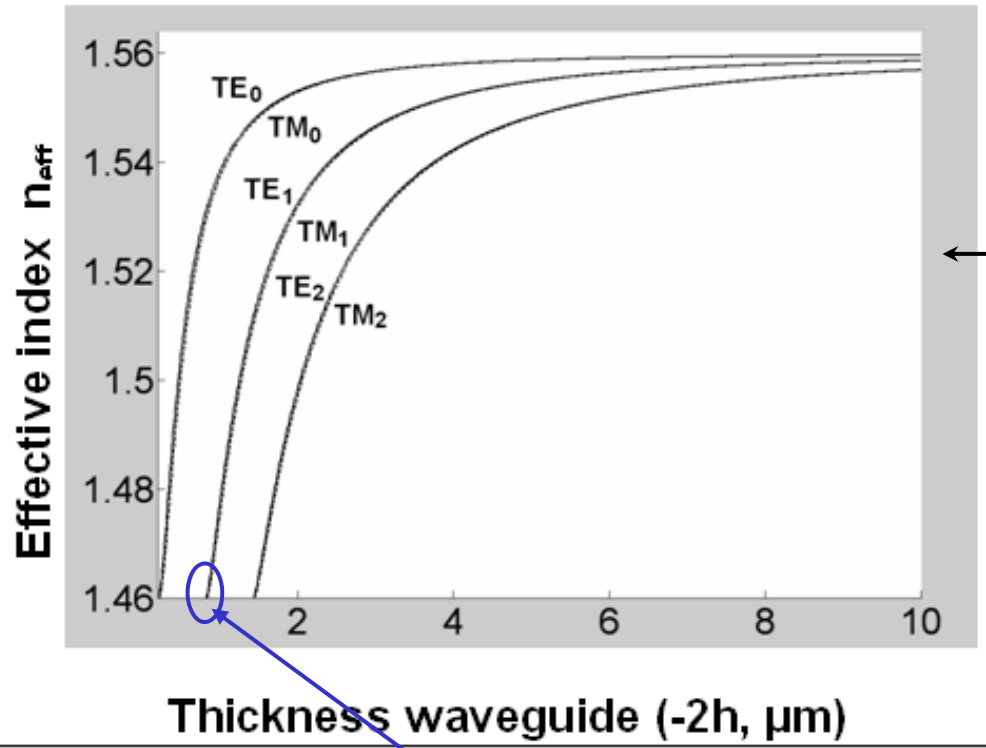

Variation of the effective indices function of the core-thickness waveguide at λ_0=670nm the TE-TM_m optical modes ($m = 0, 1, 2$).

Cut-thickness	**TE_0 : 0.225 µm** **TM_0 : 0.235 µm**	**TE_1 : 0.831 µm** **TM_1 : 0.841 µm**

Cut-thicknesses at λ_0=670 nm for $m = 0$ and $m = 1$.

3-layers slab waveguides with polymer core (n_1=1.56 at λ_0=670 nm) and claddings n_3=1 (air) and n_4 =1.45.

[II-43 & 44]

Good agreement between the numerical simulation of the eigenvalues equations and the analytical expression of the cut-thicknesses.

[II-45]

▪ Determination of the electromagnetic energy distribution through the 3-multilayer slab waveguide, confinement factor γ

▪ **Goal : Study the repartition or the fraction of the optical power in each layer, function of analytical and physical parameters of such family slab structures**

Energy that propagates along x_3-direction as a flux through the (x_1,x_2)-section of the x_3 Poynting-vector component

$$\frac{1}{2}\Re\left(E\wedge H^*\right)_{x3} = \begin{cases} \dfrac{\beta}{2\omega\mu_0}\left|E_{x2}\right|^2 & \text{(TE case)} \\ \dfrac{\beta}{2\omega n_j \varepsilon_0}\left|H_{x2}\right|^2 \quad j=1,3,\text{et } 4 & \text{(TM case)} \end{cases} \qquad \text{[II-46]}$$

Such energy expressions are deduce from the modal expressions [II.41 & 42] plus the eigenvalues equations [II.43 & 44].

▪ TE case :

- Into upper cladding :

$$P_{3(TE)} = \frac{\beta}{2\omega\mu_0}\int_0^{+\infty} C^2 e^{-2r x_1} d x_1 = \frac{\beta}{2\omega\mu_0}\frac{C^2}{2r} \qquad \text{[II-47]}$$

- Into lower cladding :

$$P_{4(TE)} = \frac{\beta}{2\omega\mu_0} Q^2 \int_{-\infty}^{-2h} e^{-2p(x_1+2h)} d x_1 = \frac{\beta}{2\omega\mu_0}\frac{Q^2}{2p}$$

with, $Q = \left[C\cos(2hq) - K\sin(2hq)\right] = C\cos(2hq)\left[1+\frac{r}{q}tg(2hq)\right]$

By using the TE eigenvalues equation [II.43] plus adapted trigonometric relations infra, we can defined :

$$\cos^2(2hq) = \frac{1+\cos(4hq)}{2} \quad \text{and} \quad \cos(4hq) = \frac{1-tg^2(2hq)}{1+tg^2(2hq)}$$

$$\boxed{P_{4(TE)} = \frac{\beta}{2\omega\mu_0}\frac{C^2}{2p}\left(\frac{q^2+r^2}{p^2+q^2}\right)} \quad \text{[II-48]}$$

- Into the core : $\boxed{P_{1(TE)}} = \frac{\beta}{2\omega\mu_0}\int_{-2h}^{0}\left[C\cos(q\ x_1) + K\sin(q\ x_1)\right]^2 d\,x_1$

$$\sin(4hq) = \frac{2\,tg(2hq)}{1+tg^2(2hq)} \quad \text{and} \quad \cos(4hq) = \frac{1-tg^2(2hq)}{1+tg^2(2hq)}$$

$$\boxed{P_{1(TE)} = \frac{\beta}{2\omega\mu_0}\frac{C^2}{2}\left(\frac{q^2+r^2}{q^2}\right)\left(2h + \frac{r}{q^2+p^2} + \frac{r}{q^2+r^2}\right)} \quad \text{[II-49]}$$

Evanescent physical sense

- Global power $\sum_i P_i$:

[II-50]

$$\boxed{\overline{P}_{(TE)} = \sum_{i=1,3,4} P_{i(TE)} = \frac{\beta}{2\omega\mu_0}\frac{C^2}{2}\left(\frac{q^2+r^2}{q^2}\right)W_{TE} \ \text{with effective thickness}\ W_{TE} = \left(2h + \frac{1}{p} + \frac{1}{r}\right)}$$

Analytical power expressions

TE case	TM case	Integration along x_1
$P_3^{TE} = \frac{F^{TE}}{r}$	$P_3^{TM} = \frac{F_1^{TM}}{r}$	$[0,+\infty[$
$P_1^{TE} = F^{TE}\left(\frac{\left(q^{TE}\right)^2 + r^2}{\left(q^{TE}\right)^2}\right) \times \left(2h + \frac{p}{\left(q^{TE}\right)^2 + p^2} + \frac{r}{\left(q^{TE}\right)^2 + r^2}\right)$	$P_1^{TM} = F^{TM}\left(\frac{n_3^4\left(q^{TM}\right)^2 + \left(n_1^{TM}\right)^4 r^2}{n_3^4\left(q^{TM}\right)^2}\right) \times \left(2h + \frac{\left(n_1^{TM} n_4\right)^2 p}{n_4^4\left(q^{TM}\right)^2 + \left(n_1^{TM}\right)^4 r^2} + \frac{\left(n_1^{TM} n_3\right)^2 r}{n_3^4\left(q^{TM}\right)^2 + \left(n_1^{TM}\right)^4 r^2}\right)$	$[-2h,0]$
$P_4^{TE} = \frac{F_4^{TE}}{p}\left(\frac{\left(q^{TE}\right)^2 + r^2}{p^2 + \left(q^{TE}\right)^2}\right)$	$P_4^{TM} = \frac{F_4^{TM}}{p}\left(\frac{n_4}{n_3}\right)^4\left(\frac{n_3^4\left(q^{TM}\right)^2 + \left(n_1^{TM}\right)^4 r^2}{\left(n_1^{TM}\right)^4 p^2 + n_4^4\left(q^{TM}\right)^2}\right)$	$]-\infty,-2h]$

with, $F^{TE} = \frac{\beta C^2}{4\omega\mu_0}$, $F_j^{TM} = \frac{\beta C^2}{4\omega\left(n_j^{TM}\right)^2\varepsilon_0}$ (*j=3, 1, 4*), and *C* integration constante

Confinement $\gamma = P_1/P_{total}$

	TE case	TM case
$\gamma =$	$\frac{\left(2h + \frac{p}{\left(q^{TE}\right)^2 + p^2} + \frac{r}{\left(q^{TE}\right)^2 + r^2}\right)}{W_{eff}^{TE}}$	$\frac{\left(2h + \frac{\left(n_1^{TM} n_4\right)^2 p}{n_4^4\left(q^{TM}\right)^2 + \left(n_1^{TM}\right)^4 p^2} + \frac{\left(n_1^{TM} n_3\right)^2 r}{n_3^4\left(q^{TM}\right)^2 + \left(n_1^{TM}\right)^4 r^2}\right)}{W_{eff}^{TM}}$

with,
$$\begin{cases} W_{eff}^{TE} = 2h + \frac{1}{p} + \frac{1}{r} \\ W_{eff}^{TM} = 2h + \frac{\left(n_1 n_4\right)^2\left(p^2 + \left(q\right)^2\right)}{p\left(\left(n_1\right)^4 p^2 + n_4^4\left(q\right)^2\right)} + \frac{\left(n_1 n_3\right)^2\left(r^2 + \left(q\right)^2\right)}{r\left(\left(n_1\right)^4 r^2 + n_3^4\left(q\right)^2\right)} \end{cases}$$

▪ II.4.2 Comprehensive analytical approach for dissymmetrical 4-layers slab waveguides, optical modes and electromagnetic energy distribution through the multilayer

▪ **lecture and study of the reference (2009, to be published):**

ARTICLE IN PRESS

Available online at www.sciencedirect.com

ScienceDirect

ELSEVIER

Optik ▮ (▮▮▮▮) ▮▮▮–▮▮▮

Optik Optics

www.elsevier.de/ijleo

Another way to shape the comprehensive analytical approach describing electromagnetic energy distribution through four-slab-layer structures

B. Bêche[a,*], E. Gaviot[b], A. Renault[a], J. Zyss[c], F. Artzner[a]

[a] *Institut de Physique de Rennes, IPR Université de Rennes I, IPR UMR CNRS 6251, 35042 Rennes, France*
[b] *Laboratoire d'Acoustique de l'Université du Maine, Micro_Cap_Ouest, LAUM-UMR CNRS 6613, 72000 Le Mans, France*
[c] *Laboratoire de Photonique Quantique et Moléculaire, IFR d'Alembert, ENS Cachan, LPQM-UMR CNRS 8537, 94235 Cachan, France*

Received 11 February 2008; accepted 15 June 2008

Abstract

Starting from the generalised four-slab layer in electromagnetic theory and photonics, this paper introduces a convenient method and a new proper change of variables in order to obtain the global analytical expressions of the power flows in such multilayer structures for the TE_m and TM_m optical modes. These proper changes of variables and relevant definitions of apt new parameters (Θ, W, Y and ξ) allow us to derive and shape new general analytical formulations and normalizations in terms of power flows. According to such specific parameters, it can be noted that such a comprehensive result brings in an effective criteria form of the classical results ascribed to three-slab problems. Moreover, we have verified with specific cases regarding three-slab problems the validity of our new global frame for analysing power flows. It clearly appears that classical three-slab-waveguide expressions directly stem from our formulation. Naturally, this global four-slab-waveguides approach can be used directly to the analytical calculus of corresponding ratios of power between the different layers, such as the core compared with buffer layers as upper and lower claddings.

© 2008 Elsevier GmbH. All rights reserved.

▪ II.4.3 Comprehensive analytical approach for global *n*-layers slab waveguides, generalization of optical modes into multilayer heterostructures, matrix method, multilayer stack theory

▪ Introduction :

The global heterostructure encompasses *n*-various layers (n>4) that includes for example the two cladding and the core shaped as (n-2)-stratum-layers (core thickness =h). The goal is to shaped the eigenvalues equations of TE_m and TM_m in such general multilayer case. By carried out a change of variable *U* et *V* on [II.10] $H_{x3} = (j/\omega\mu_0).(\partial E_{x2}/\partial x1)$ we can fixed $U=E_{x2}$ and $V=\omega\mu_0 H_{x3}= j(\partial U/\partial x1)$ for the TE case, and $U=H_{x2}$ and $V=\omega\varepsilon_0 E_{x3}= j(\partial U/\partial x1)$ for the TM case (equivalent notations for both polarizations). Then we don't have to write the ($\omega\mu_0$) or ($\omega\varepsilon_0$) terms at each iteration *and crossing to successive layer (implementation of such n-layers model). Then, U and* V are the couple of variable of the *n*-layer problem. The method is based on the determination of the optical field *U* and *V* by the initial field condition U_0 and V_0 at $x_1=0$, and on the matrix-crossing formalism from a layer to another one.

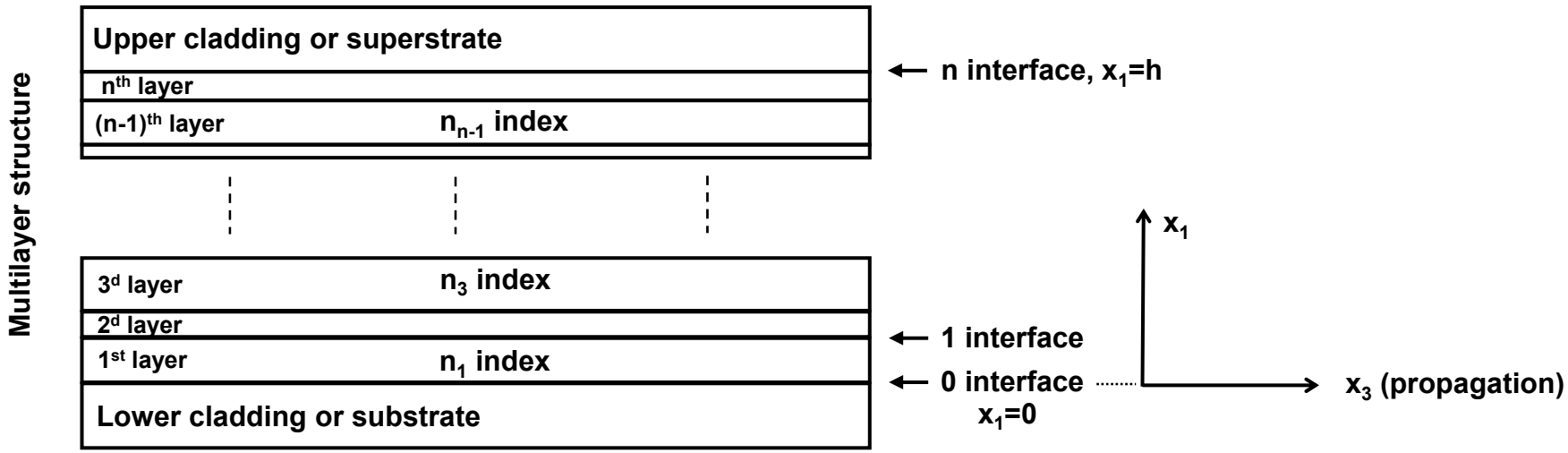

▪ Matrix method for TEm optical modes :

Propagation equation of U (that is E_{TE}) into a layer of n-index

$$\frac{\partial^2}{\partial x_1^2} U(x_1) = \left(\beta^2 - k_0^2 n^2\right) U(x_1) = -\kappa^2 U(x_1), \text{ that is : } U''(x_1) = -\kappa^2 U(x_1)$$

[II-50]

with solutions

$$\begin{cases} U(x_1) = A e^{-j\kappa x_1} + B e^{j\kappa x_1} \\ V(x_1) = \kappa\left(A e^{-j\kappa x_1} - B e^{j\kappa x_1}\right) \end{cases}$$

[II-51]

▪ Relation between the optical field at one interface

By considering the initials conditions on [II.51], $U_0=U(x_1=0)$ and $V_0=V(x_1=0)$, we deduce :

$$A = \frac{1}{2}\left(U_0 + \frac{V_0}{\kappa}\right) \text{ and } B = \frac{1}{2}\left(U_0 - \frac{V_0}{\kappa}\right)$$

[II-52]

By inserting [II.52] into [II.51], we can shaped the crossing-matrix related to an interface or from a layer to another one :

$$\begin{pmatrix} U_0 \\ V_0 \end{pmatrix} = M \begin{pmatrix} U(x_1) \\ V(x_1) \end{pmatrix} \text{ with } M = \frac{1}{2}\begin{pmatrix} e^{j\kappa x_1} + e^{-j\kappa x_1} & \frac{1}{\kappa}\left(e^{j\kappa x_1} - e^{-j\kappa x_1}\right) \\ \kappa\left(e^{j\kappa x_1} - e^{-j\kappa x_1}\right) & e^{j\kappa x_1} + e^{-j\kappa x_1} \end{pmatrix}$$

[II-53] ← crossing-matrix

$$\begin{pmatrix} U_1 \\ V_1 \end{pmatrix}$$

[II-53 too]

$$\begin{pmatrix} U_{i-1} \\ V_{i-1} \end{pmatrix} = M_i \begin{pmatrix} U_i \\ V_i \end{pmatrix} \text{ with } M_i \text{ associated matrix to the } i^{th}\text{-layer}$$

▪ Relation overall the global multilayer, extension and definition of such M_i matrix

$$\begin{pmatrix} U_0 \\ V_0 \end{pmatrix} = \overline{M} \begin{pmatrix} U_n \\ V_n \end{pmatrix} \quad \text{with} \quad \overline{M} = M_1 \times \ldots \times M_n \qquad \text{[II-54]}$$

← Stack matrix

According to [II.50] the expression of the normal wave vector κ_i in to the ith-layer of n_i index and l_i thickness can be expressed as :

$$\kappa_i^2 = \left(k_0^2 n_i^2 - \beta^2\right) = \left(n_i^2 - n_{eff}^2\right) k_0^2 \qquad \text{[II-55]}$$

Two cases must be considered on the nature of crossing matrix M_i (according to the [II.55] definition :

$n_{eff} < n_i$, κ_i is real and the optical field is oscillating into the ith-layer

$$M_i = \begin{pmatrix} \cos(\kappa_i l_i) & \frac{j}{\kappa_i}\sin(\kappa_i l_i) \\ j\kappa_i \sin(\kappa_i l_i) & \cos(\kappa_i l_i) \end{pmatrix} \qquad \text{[II-56]}$$

$n_{eff} > n_i$, κ_i is imaginary and the optical field is exponentially decreasing into the ith-layer

$$M_i = \begin{pmatrix} \cosh(\vartheta_i l_i) & \frac{j}{\vartheta_i}\sinh(\vartheta_i l_i) \\ -j\vartheta_i \sinh(\vartheta_i l_i) & \cosh(\vartheta_i l_i) \end{pmatrix}$$

$$\text{with} \quad \vartheta_i = j\kappa_i = \sqrt{\left(\beta^2 - k_0^2 n_i^2\right)}$$

▪ Expression of the optical field in the lower and upper cladding (noted L-clad, U-clad)

Lower cladding

$$\begin{cases} U(x_1) = A_{L-clad}\, e^{p x_1} \\ V(x_1) = jpA_{L-clad}\, e^{p x_1} \end{cases} \quad x_1 < 0 \quad \text{and} \quad \begin{cases} U(x_1) = B_{U-clad}\, e^{-r(x_1 - h)} \\ V(x_1) = -jrB_{U-clad}\, e^{-r(x_1 - h)} \end{cases} \quad x_1 > h$$

Upper cladding

with $A_{L\text{-}clad}$ and $B_{U\text{-}clad}$ the evanescent amplitude of the optical field into the cladding and r and $p \equiv \left(\beta^2 - k_0^2 n_{cladding}^2\right)^{1/2}$

By considering the continuity conditions at x_1=0 and h we obtain relations between optical fields adjacent to the upper and lower claddings (that the first layer *0*, and the final layer *n* :

$$\begin{cases} U_0 = A_{L.clad} \\ V_0 = jp\,A_{L.clad} \end{cases} \quad \text{and} \quad \begin{cases} U_n = B_{U.clad} \\ V_n = -jr\,B_{U.clad} \end{cases} \qquad \text{[II-57]}$$

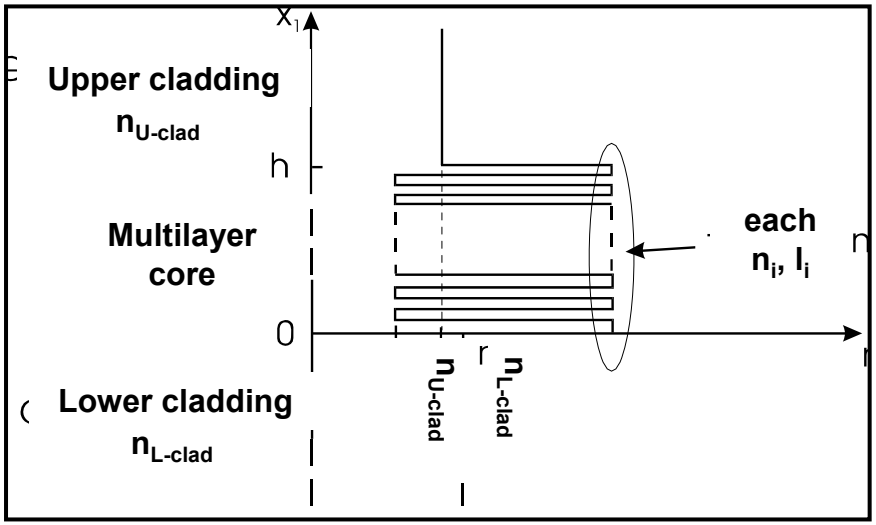

By successive crossing [II.54 & 57], knowing the initial amplitude, we can develop the final amplitude :

[II-58]

$$\begin{pmatrix} U_0 \\ V_0 \end{pmatrix} = \begin{pmatrix} A_{L.clad} \\ jp\,A_{L.clad} \end{pmatrix} = \overline{M} \begin{pmatrix} B_{U.clad} \\ -jr\,B_{U.clad} \end{pmatrix} = \overline{M} \begin{pmatrix} U_n \\ V_n \end{pmatrix}$$

$$\text{avec toujours } \overline{M} = M_1 \times \ldots \times M_n$$

▪ Eigenvalues equation for the TE_m optical modes in such multilayer

By using the condition to obtain no field at the infinite and replacing (U_0,V_0) (U_n,V_n) in [II.58], a TE_m eigenvalues equation can be considered :

$$\overline{m}_{11} - jr\,\overline{m}_{12} + \frac{j}{p}\overline{m}_{21} + \frac{r}{p}\overline{m}_{22} = 0 \qquad \text{[II-59]}$$

with $\overline{m}_{ij}$ the components of the product-matrix $\overline{M}$

▪ Eigenvalues equation for the TM_m optical modes in such multilayer

By using an equivalent reasoning, a TM_m eigenvalues equation can be expressed as,

$$\boxed{\frac{p}{n_{L-clad}^2}\,\overline{m}_{11} - j\frac{r}{n_{U-clad}^2}\frac{p}{n_{L-clad}^2}\,\overline{m}_{12} - j\overline{m}_{21} + \frac{r}{n_{U-clad}^2}\,\overline{m}_{22} = 0} \quad \text{[II-60]}$$

Note : Such expression can be obtained by change of variable $z \longrightarrow -\frac{z}{n^2}$ *for the normalized wave vectors* $z=\kappa$ *and* ϑ *into [II.56] expressions of* M_i.

▪ Eigenvectors : amplitudes of TE_m-TM_m optical modes in such multilayer

U_O (at interface i=0) must be fixed, successive reasoning applied,

$$\boxed{\begin{pmatrix} U_{i+1} \\ V_{i+1} \end{pmatrix} = M^{-1}\begin{pmatrix} U_i \\ V_i \end{pmatrix}} \quad \text{[II-61]}$$

with the possibility to normalize the global curve of the amplitude or intensity comparatively to the maximum.

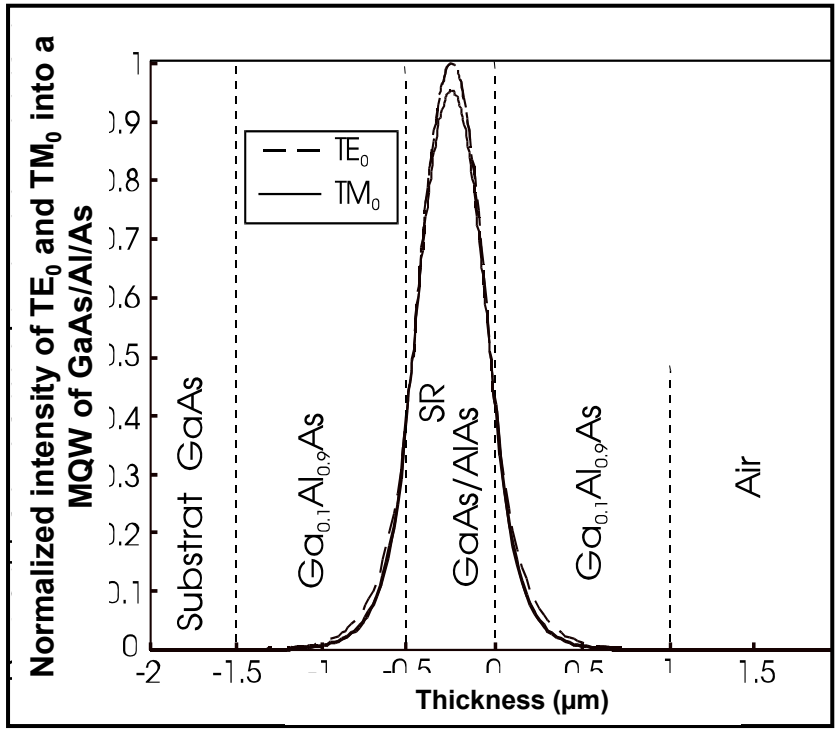

▪ II.5 : Lateral optical confinement, 2D-waveguide-structures, TE_{mn} and TM_{mn} quantifications of the optical modes

▪ II.5.1 Effective index method for rib waveguide-structures, determination of the width W of such waveguide, eigenvalues equations

Idea : Reduce such 2D-problem to a effective two 1D problem along each direction.

➔Calculus of n_{eff} of the optical modes TE-TM_m slab waveguides called n_α et n_β for respective thicknesses h_g and (h_g-d), with d the etching deep.

➔ Determination of the quantification along the second direction ($neff_{TEnm}$ and $neff_{TMnm}$) by considering the rib waveguide as a symmetrical slab waveguide $n_\beta|n_\alpha|n_\beta$ with TE←➔TM polarizations !

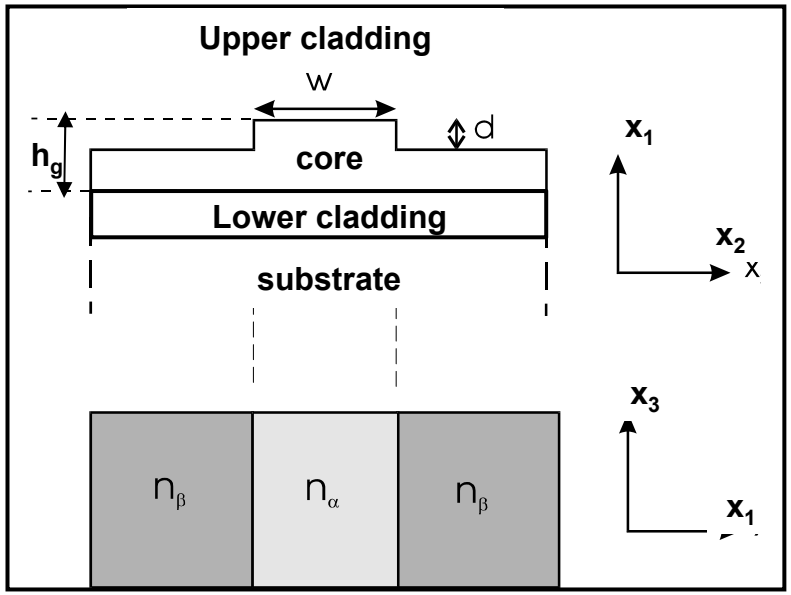

[II-44] ⟶

$$\boxed{w\,q^{(TE_{00}\text{ or }TM_{00})} - 2\,\mathrm{arctg}\left[\eta\left(\frac{p}{q^{(TE_{00}\text{ or }TM_{00})}}\right)\right] = 0} \quad \text{[II-62]}$$

$$\text{with, } \eta = \begin{cases} 1 \text{ for the } TM_{00} \\ \left(\dfrac{n_\alpha^{TE00}}{n_\beta}\right)^2 \text{ for the } TE_{00} \end{cases} \qquad q_{TE00} = \left\{\left(k_0 n_\alpha^{TE00}\right)^2 - \beta^2\right\}^{1/2} \qquad q_{TM00} = \left\{\left(k_0 n_\alpha^{TM00}\right)^2 - \beta^2\right\}^{1/2}$$

Example : AlGaAS / $SR_{period\text{-}20nm}$ GaAs/AlAs / Air structure at λ_0=1300 nm

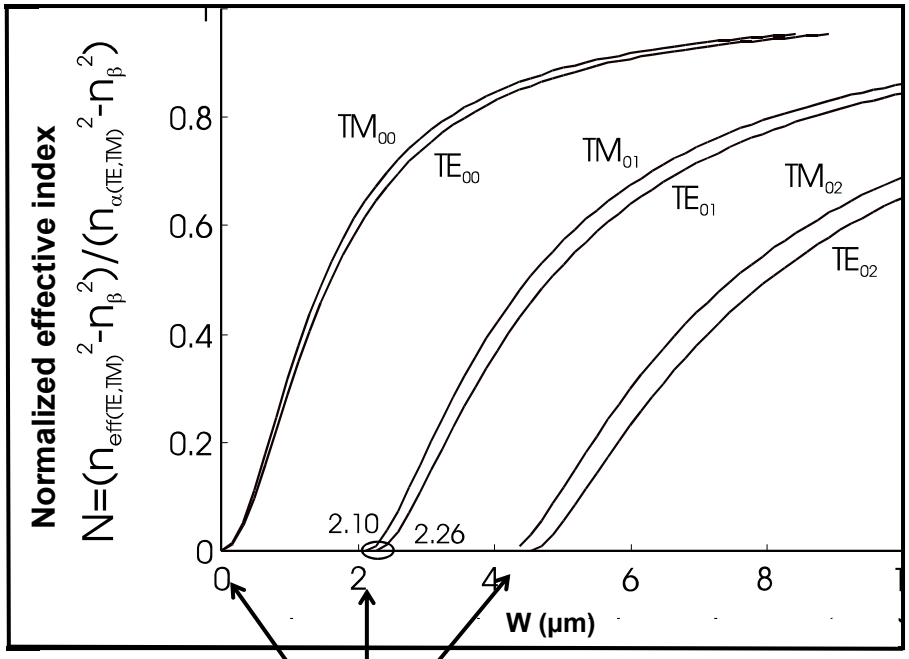

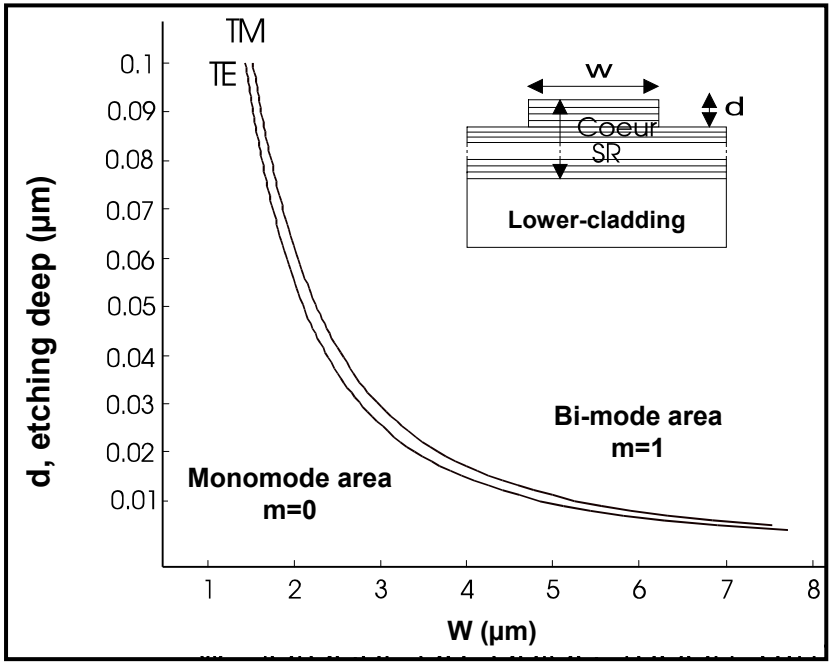

Cut-off thicknesses

$$w_c^{TE0m} = w_c^{TM0m} = \frac{m\lambda}{2\left(n_\alpha^2 - n_\beta^2\right)^{1/2}}$$ **[II-63]**

▪ II.5.2 Marcatili's method, shadow areas and buried waveguides

Method based on a separation of the two directions (x_1 and x_2) and an equivalent separation of variables. This one is useful for a range of channel guides or many cases. The method works well as long as the fields are well confined in the region of high index. Near cut-off the method is not applicable, because the fields penetrate into the shadow regions.

Cross-sections of six channel guide structures

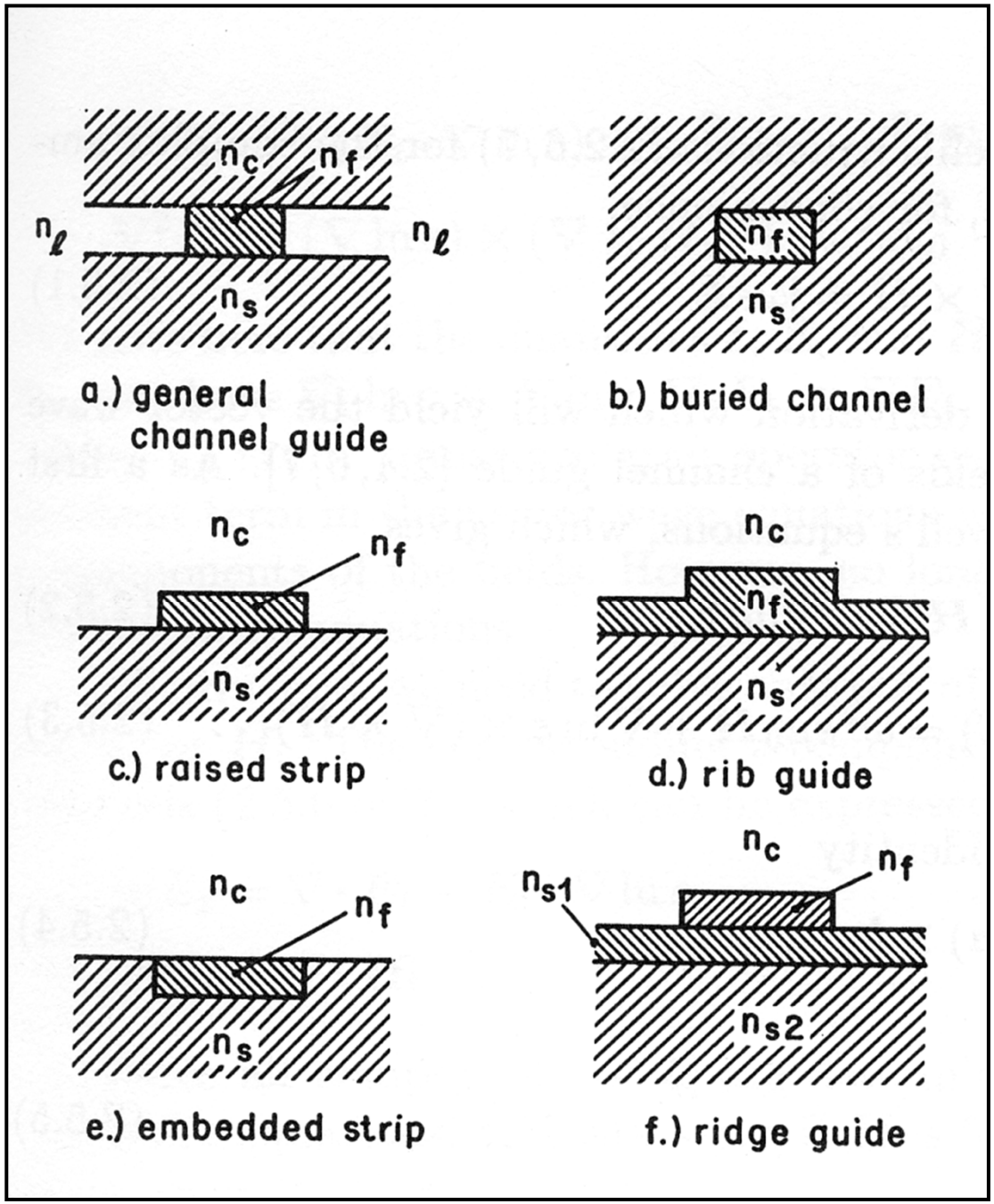

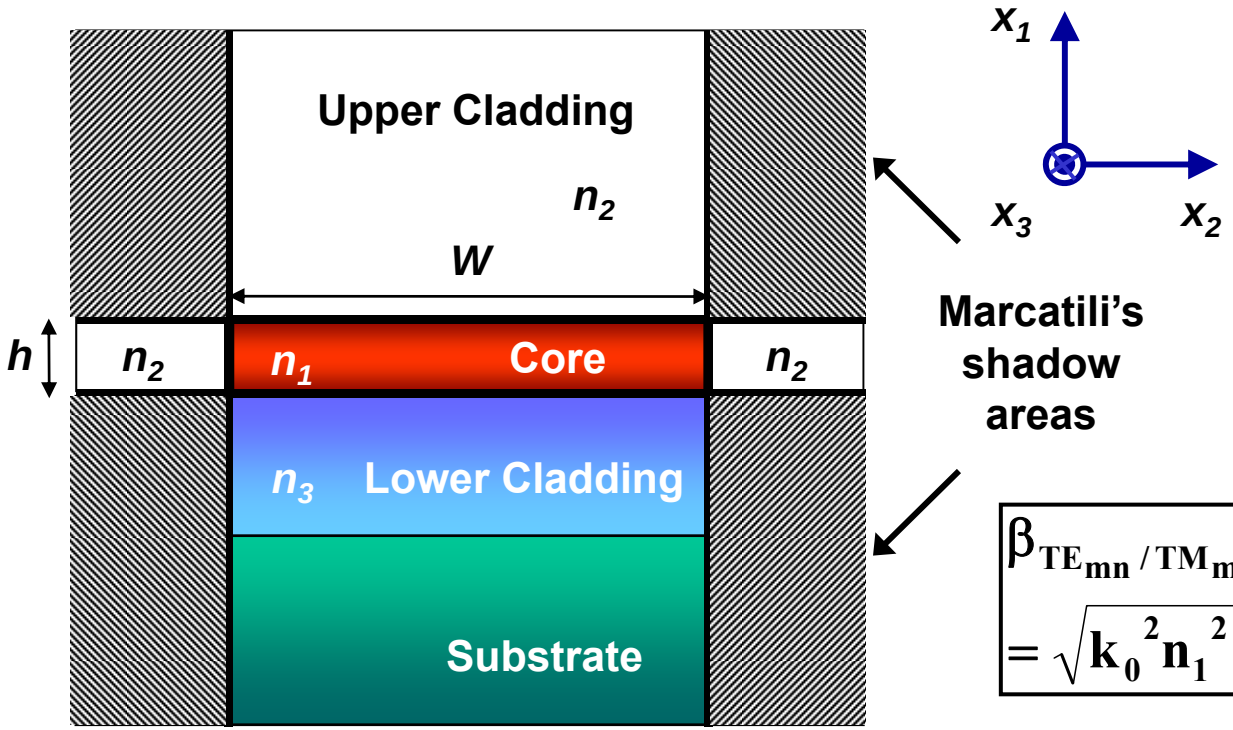

$$\beta_{TE_{mn}/TM_{mn}} = k_0 n_{effTE_{mn}/TM_{mn}} = \sqrt{k_0^2 n_1^2 - \beta_{x2}^2 - \beta_{x1}^2}$$ [II-64]

with, $$\beta_{x2} = \frac{(m+1)\pi}{W}\left(1 + 2\eta_{(x2)}\frac{A_2}{\pi W}\right)^{-1} \quad \begin{cases} \eta_{(x2)} = \left(\frac{n_2}{n_1}\right)^2 & TE_{mn} \text{ modes} \\ \eta_{(x2)} = 1 & TM_{mn} \text{ modes} \end{cases}$$

$$\beta_{x1} = \frac{(n+1)\pi}{h}\left(1 + \frac{\eta_{(x1)2}A_2 + \eta_{(x1)3}A_3}{\pi h}\right)^{-1} \quad \begin{cases} \eta_{(x1)i} = 1 & TE_{mn} \text{ modes} \\ \eta_{(x1)i} = \left(\frac{n_i}{n_1}\right)^2 & TM_{mn} \text{ modes} \end{cases}$$

$$A_i = \frac{\pi}{k_0}\sqrt{\frac{1}{n_1^2 - n_i^2}} \quad \text{and} \quad k_0 = \frac{2\pi}{\lambda_0}$$

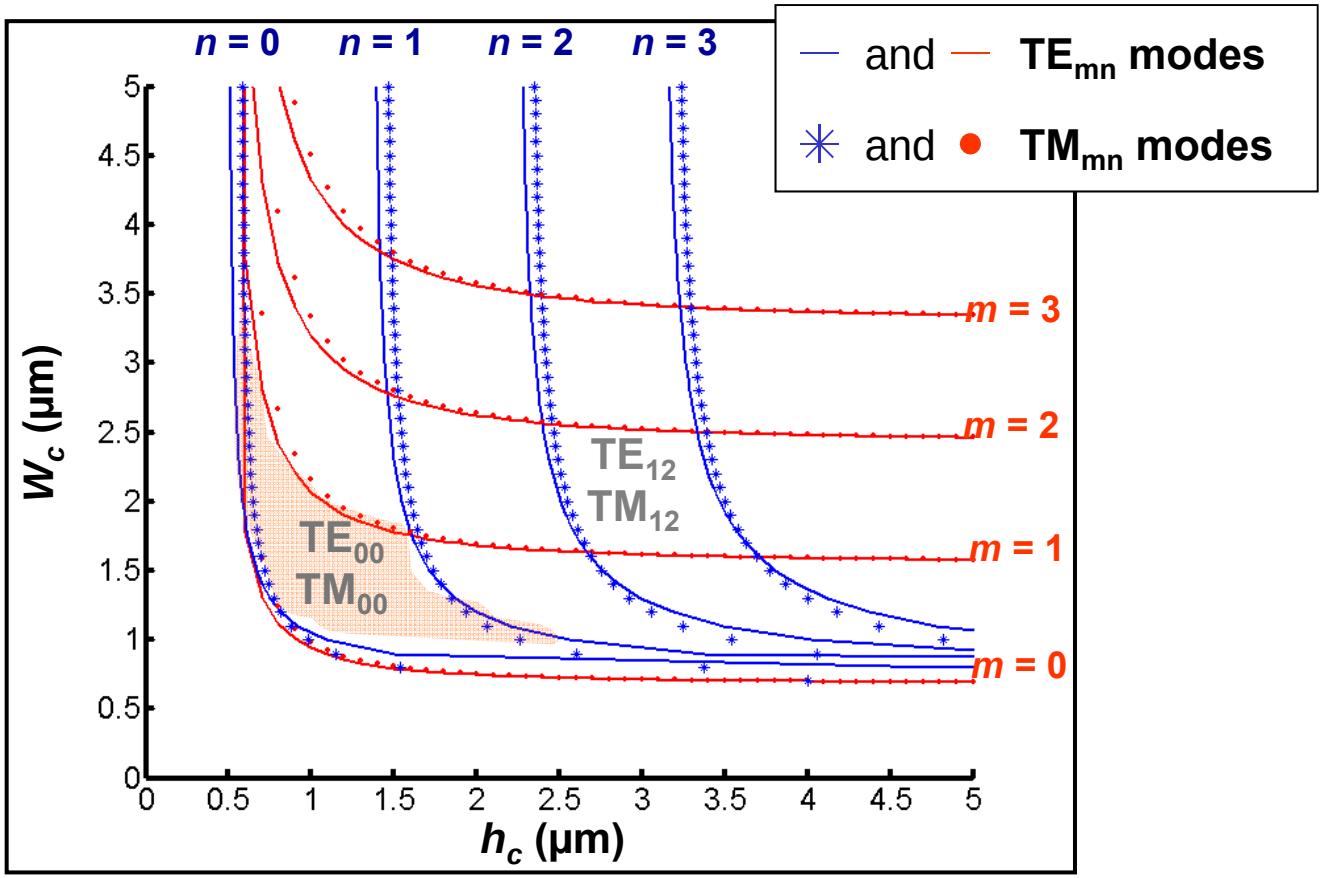

Monomode cut-off dimensions (TE_{00}/TM_{00}): $0.8\ \mu m < W_c < 1.8\ \mu m$

$0.5\ \mu m < h_c < 1.5\ \mu m$

- **In conclusion, global opto-geometries of many rectangular waveguides can be design by such classical theories and methods into various components (telecoms, sensors, and another devices)**

▪ II.5.3 Curved waveguides cases, curved radius R, conformal transformation

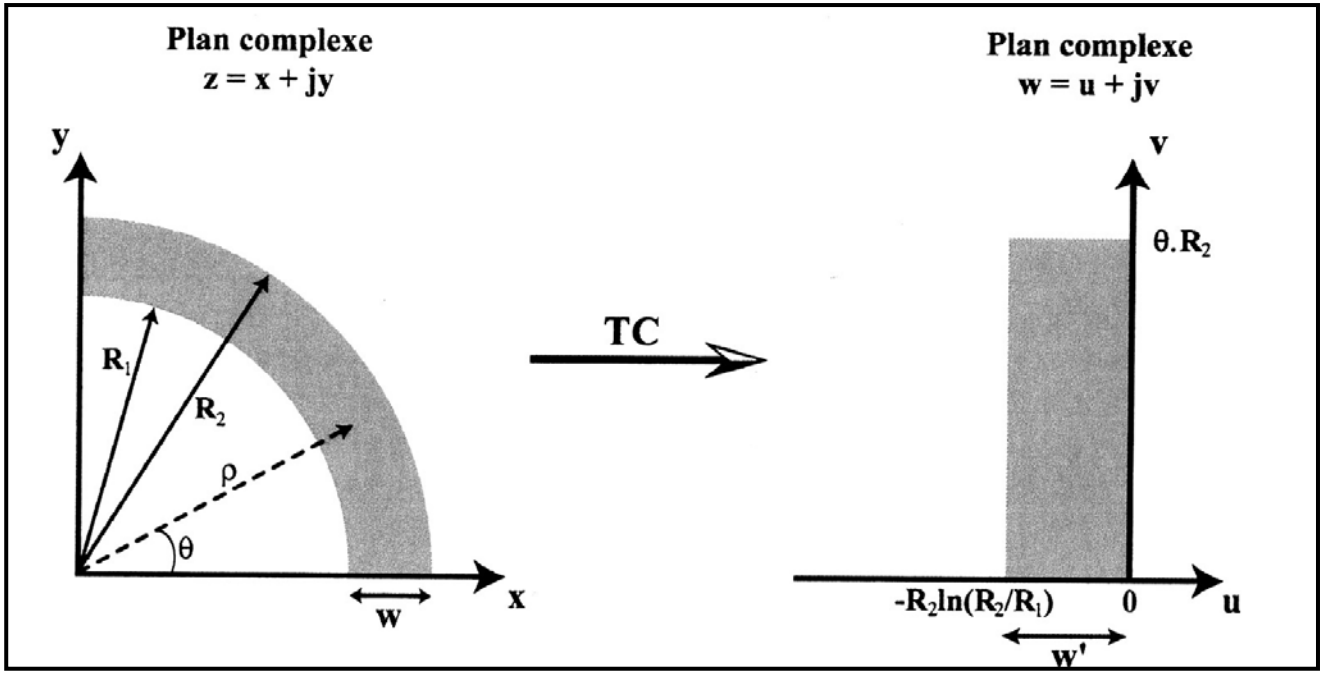

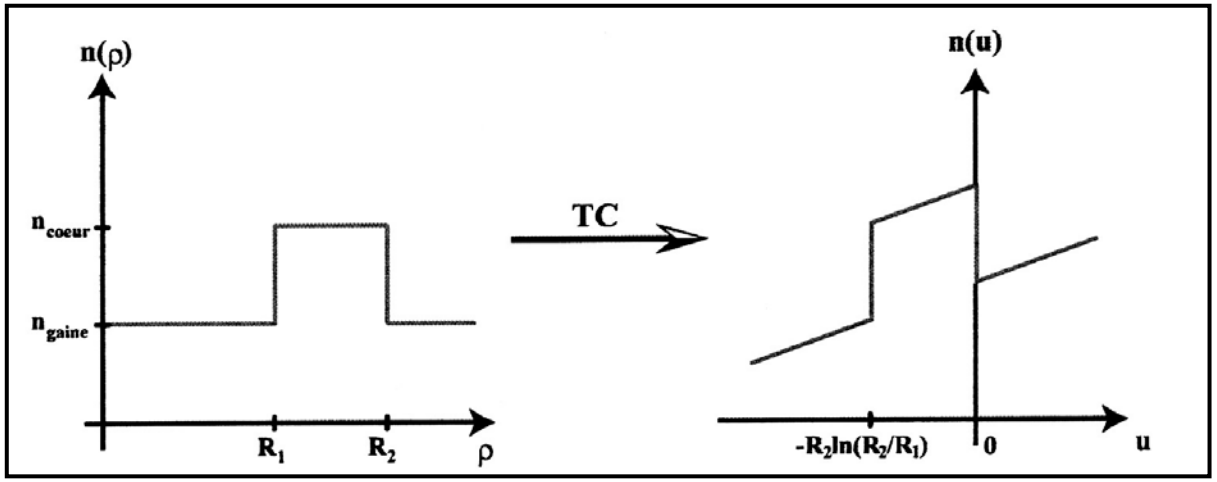

Equivalent index

$$n(u) = n(\rho).\left(1 + \frac{u}{R_2}\right)$$ [II-65]

- **II.5.4 Advanced numerical methods, Semi-Vectorial Difference Finite method, spectral method (Galerkin, and so on)**

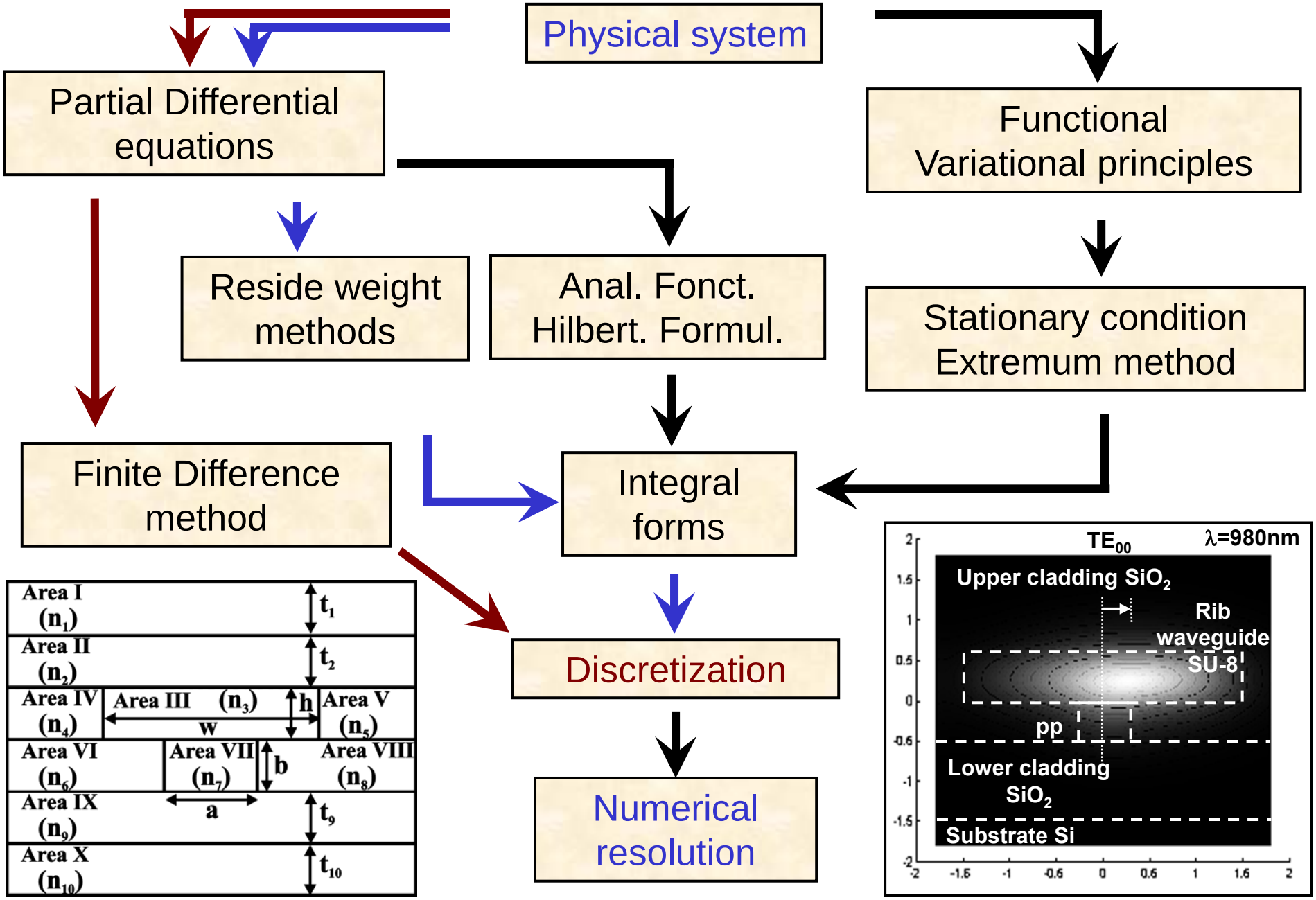

- Synoptic of SVFD-TC method

$\{\text{Propagation equation}\}: \vec{E}_t$

$t(x_1,x_2)$ transversal directions

x_2-direction TE

x_1-direction TM

SVFD

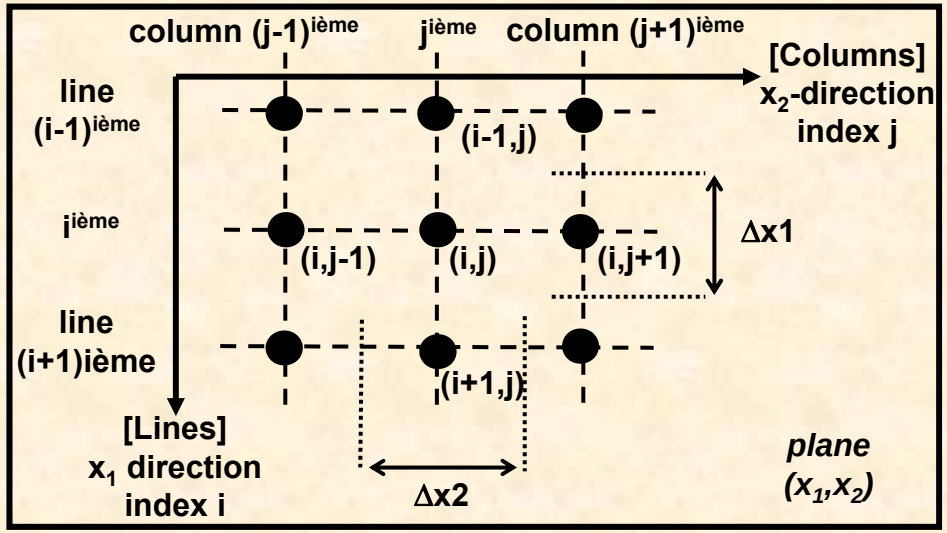

Change of variables

Matrix ➔ Vector

u=N(i-1)+j

➔ u=1 à N²

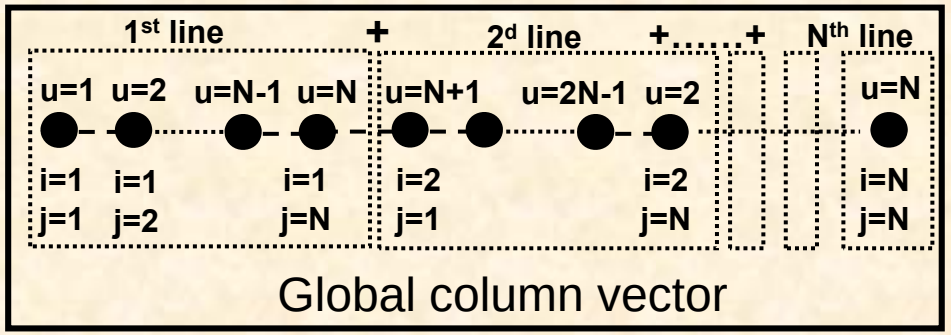

Global column vector

Effectives propagation constantes

➔ β_{eff} *et* n_{eff}

Amplitudes of the optical modes

➔ $E(TM_{uv}\text{-}TE_{uv})$

Eigenvalues problem

$$\left[\Lambda-\beta^2 Id\right].E = 0$$

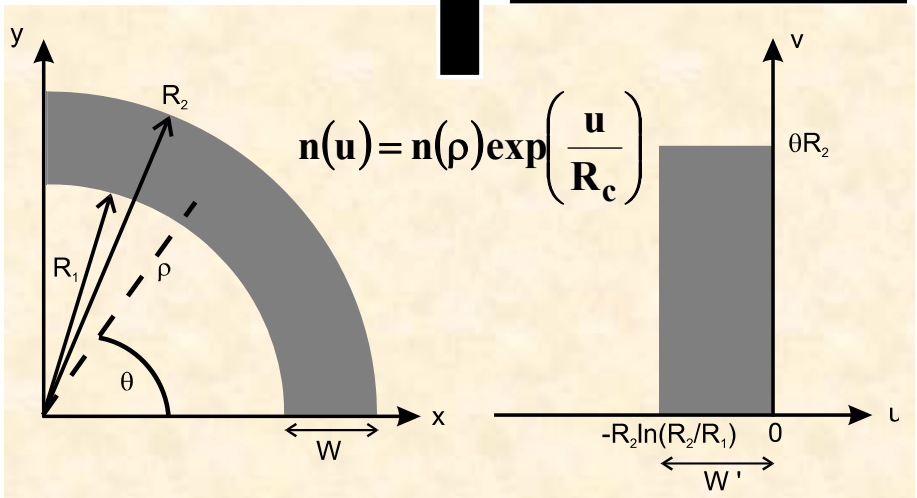

$$n(u) = n(\rho)\exp\left(\frac{u}{R_c}\right)$$

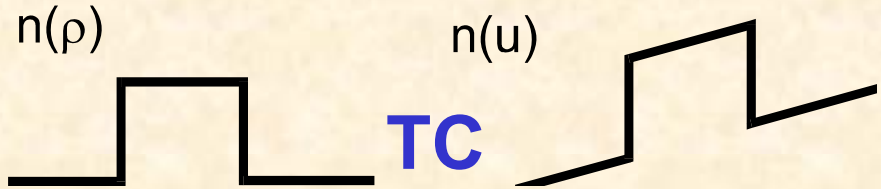

TC

Index profil (curved guide)

Index profil (rect. Equiv. guide)

- Synoptic spectral Galerkin method

$$\begin{cases} L(u) = f \ \text{ dans } \Omega \\ C(u) = g \ \text{ sur } \partial\Omega \end{cases}$$

Propagation eq.

➔ u_0 exact solution, we 'approximate' u_0 by :

$$\tilde{u} = \sum_{i=1}^{n} \tilde{u}_i = \sum_{i=1}^{n} \alpha_i \cdot \phi_i$$

with, ϕ_i trial functions (functions of approximations)

[residue weight method]

➔ Residues $R \equiv L(\tilde{u}) - f$ ➔ try to minimize these ones (average sense), or scalar product meaning.

$$\int_\Omega R \cdot w_i \, d\Omega = 0$$

➔ for Galerkin, weighting functions $w_i = \phi_i$

$$\int_\Omega \left[L\left(\sum_{k=1}^{n} \alpha_k \cdot \phi_k \right) - f \right] \cdot \phi_i \, d\Omega = 0$$

[II-66]

$$\phi_{mn}(x_1, x_2) = \frac{2}{\sqrt{cd}} \sin\left(\frac{m\pi}{c} x_1\right) \sin\left(\frac{n\pi}{d} x_2\right)$$

$$\langle \phi_{mn} | \phi_{pq} \rangle = \delta_{mp} \delta_{nq}$$

Eigenvalues and eignevectors problem

$$\sum_{m,n}\left(T^{TE,TM}_{pqmn} + jY^{TE,TM}_{pqmn}\right)\tilde{\alpha}^{TE,TM}_{mn} = \tilde{\beta}^{2}_{TE,TM}\,\tilde{\alpha}^{TE,TM}_{pq}$$

$T^{TE,TM}_{pqmn}$ $Y^{TE,TM}_{pqmn}$: Terms of surface integral on $d\Omega$ domains

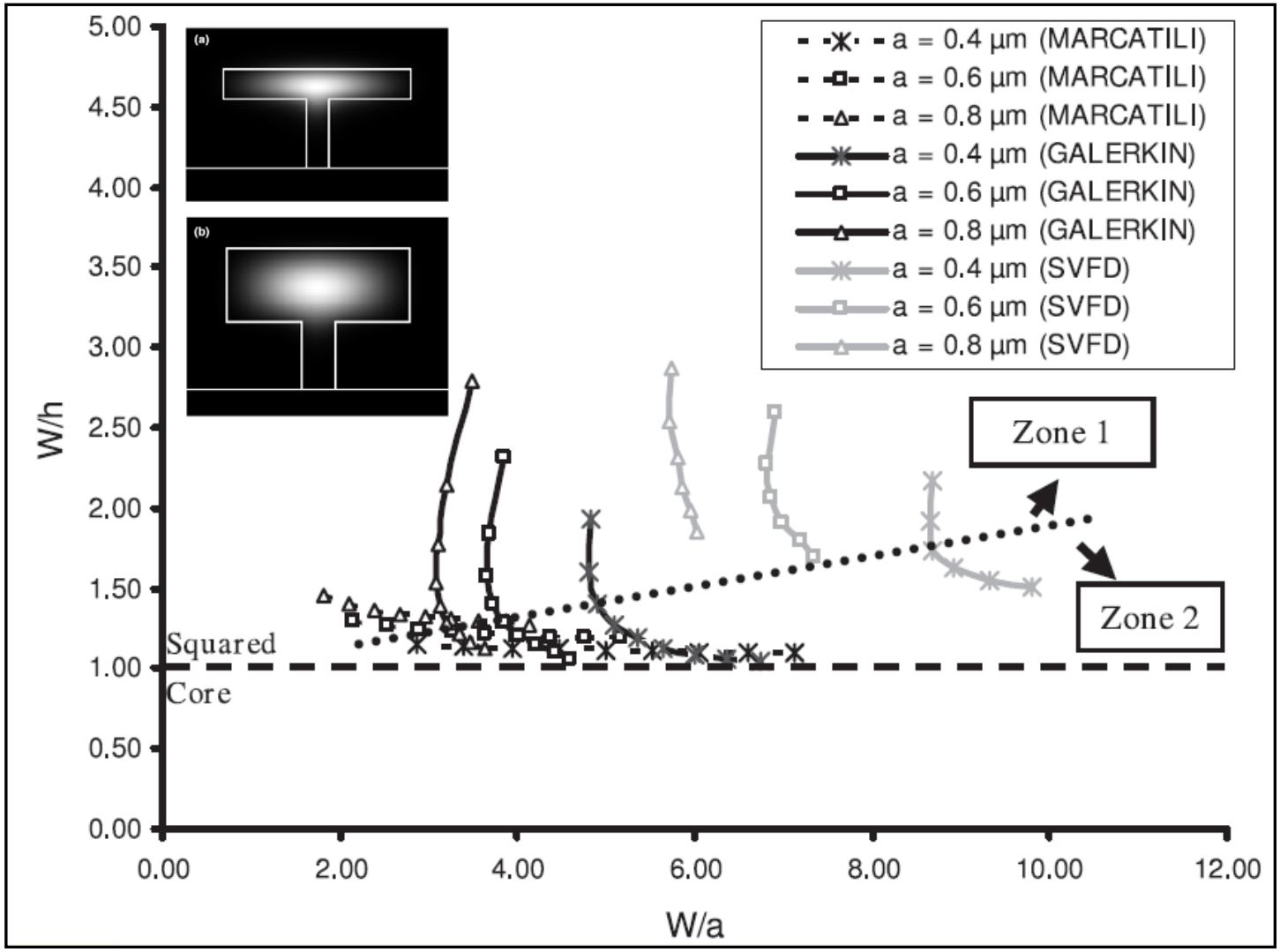

- **lecture and study of the references :**

Available online at www.sciencedirect.com
SCIENCE DIRECT®
ELSEVIER
Sensors and Actuators A 114 (2004) 59–64
SENSORS AND ACTUATORS A PHYSICAL
www.elsevier.com/locate/sna

PC software for analysis of versatile integrated optical waveguides by polarised semi-vectorial finite difference method

B. Bêche [a,*], J.F. Jouin [a], N. Grossard [b], E. Gaviot [a], E. Toussaere [c], J. Zyss [c]

[a] *Laboratoire d'Acoustique de l'Université du Maine, LAUM, UMR CNRS 6613, Micro_Cap_Ouest, 72000 Le Mans, France*
[b] *Photline Technologies, 16 Route de Gray, Batiment DF, BP 71025, 25001 Besançon Cedex 3, France*
[c] *Laboratoire de Photonique Quantique et Moléculaire, LPQM, UMR CNRS 8537, ENS Cachan, 94235 Cachan, France*

Received 1 July 2003; received in revised form 1 March 2004; accepted 4 March 2004

Available online 30 April 2004

Abstract

In this paper, a generic software package that provides an interactive and graphical environment for analysis by polarised semi-vectorial finite difference (SVFD) method of all kinds of integrated optical waveguides, such as buried channel, raised strip, rib, embedded, or ridge waveguides, is described. A coherent design rationale is formulated that takes into account the terms due to the interface between each layer as the basis of modal birefringence in integrated optics. Then, according to the opto-geometric parameters of a given waveguide, the modal propagation constants and the spatial fields patterns are calculated. Three examples regarding typical rib waveguides are dealt with, allowing to discuss the results (effective index values) compared with that of the Galerkin method. As fitted for personal computers, this software should be most useful for designing integrated optics components.
© 2004 Elsevier B.V. All rights reserved.

Keywords: PC software for integrated optics; Optical waveguides; Semi-vectorial finite difference method

IOP Publishing Journal of Optics A: Pure and Applied Optics
J. Opt. A: Pure Appl. Opt. **10** (2008) 055310 (9pp) doi:10.1088/1464-4258/10/5/055310

Marcatili's extended approach: comparison to semi-vectorial methods applied to pedestal waveguide design

T Begou[1,2], B Bêche[2], N Grossard[3], J Zyss[4], A Goullet[1], G Jézéquel[2] and E Gaviot[5]

[1] Institut des Matériaux Jean Rouxel, Université de Nantes, IMN-PCM UMR CNRS 6502, 44322 Nantes, France
[2] Institut de Physique, Université de Rennes I, IPR UMR CNRS 6251, 35042 Rennes, France
[3] Photline Technologies S.A., Z.I. Les Tilleroyes-Trépillot, 16 rue Auguste Jouchoux, 25000 Besançon, France
[4] IFR d'Alembert, Laboratoire de Photonique Quantique et Moléculaire, ENS Cachan, LPQM-UMR CNRS 8537, 94235 Cachan, France
[5] Laboratoire d'Acoustique de l'Université du Maine, Micro_Cap_Ouest, LAUM-UMR CNRS 6613, 72000 Le Mans, France

E-mail: thomas.begou@cnrs-imn.fr

Received 20 December 2007, accepted for publication 26 March 2008
Published 30 April 2008
Online at stacks.iop.org/JOptA/10/055310

Abstract
This paper deals with a theoretical study of pedestal waveguides. An extension of the Marcatili method has been developed in order to adapt this analytical method to pedestal structures. Simulations are performed for two different T-pedestal waveguide (T-PW) configurations corresponding respectively to a high and a lower core to pedestal widths ratio (T-PW I and T-PW II). Each configuration is simulated considering two core widths (2 and 4 μm) and a core height ranging from 1 to 2 μm at a 670 nm wavelength. Then, this extended Marcatili method has been compared with a semi-vectorial finite difference method (SVFD) and a spectral method developed by Galerkin, both based on a numerical approach. The simulation of the T-PW structure with these three methods shows a good congruence since the relative differences between Marcatili's method and the numerical methods remain below 6%.

Then, the three approaches are applied to study the modal birefringence minimization in the case of pedestal structures. Simulations are typically performed for waveguide height and width values ranging, respectively, around (1.6–2.6) μm and (1.8–6) μm, with pedestal widths ranging around (0.4–0.8) μm, at a 670 nm wavelength. The authors stress a specific property of pedestal configurations: by judiciously adjusting the dimensional parameters (core and pedestal width and core height), the birefringence can be completely screened out.

Keywords: pedestal optical waveguides, Marcatili's method, semi-vectorial finite difference (SVFD) method, Galerkin's method and modal birefringence minimization

Contents lists available at ScienceDirect

Optik

journal homepage: www.elsevier.de/ijleo

Short note

Hybrid composed method associating conformal transformation with matrix formulation for computing eigenvalues and eigenvectors in bended optical waveguides

L. Garnier[a], C. Saavedra[b], R. Castro-Beltrán[b], J.L. Lucio M.[b], E. Gaviot[c], B. Bêche[a,*]

[a] Institut de Physique de Rennes – IPR UMR CNRS 6251, Université de Rennes 1, 35042 Rennes, France
[b] Universidad de Guanajuato, División de Ciencias e Ingenierías-León, Guanajuato, Mexico
[c] Laboratoire d'Acoustique de l'Université du Maine – LAUM UMR CNRS 6613, Université du Maine, 72000 Le Mans, France

ARTICLE INFO

Article history:
Received 12 March 2017
Accepted 7 June 2017

Keywords:
Integrated optics
Hybrid composed method
Mathematic conformal transformation with multilayer formalism methods

ABSTRACT

A fast hybrid composed and numerical method for the calculation of eigenvalues (effective indices) and eigenvectors (optical modes) of a slab waveguide presenting a radius of curvature is presented in this letter. This compound method combines a conformal transformation of the complex plane plus a multilayer matrix formalism addressing directly the modified index profile obtained by the conformal transformation; the matrix formalism is then applied in second step so as to discretize and slice the profile in a virtual multilayer structure. This method being conveniently operable on a personal computer in a short amount of time and is easy to implement. Its results are then compared to values afforded with the commercial vectorial software COMSOL 3D so as to discuss their accuracy.
© 2017 Elsevier GmbH. All rights reserved.

Eur. Phys. J. Appl. Phys. **87**, 10501 (2019)
© L. Garnier et al., EDP Sciences, 2019
https://doi.org/10.1051/epjap/2019190092

THE EUROPEAN PHYSICAL JOURNAL APPLIED PHYSICS

Regular Article

Temporal derivation operator applied on the historic and school case of slab waveguides families eigenvalue equations: another method for computation of variational expressions

Lucas Garnier[1], Arthur Doliveira[2], Fabrice Mahé[2], Etienne Gaviot[3], and Bruno Bêche[1,4,*]

[1] Université de Rennes, CNRS, Institut de Physique de Rennes – UMR 6251, 35000 Rennes, France
[2] Université de Rennes, CNRS, IRMAR – UMR 6625, 35000 Rennes, France
[3] Université du Maine, CNRS, Laboratoire d'acoustique de l'Université du Maine – UMR 6613, 72000 Le Mans, France
[4] Université de Rennes, CNRS, Institut d'Électronique et de Télécommunications de Rennes – UMR S 6164, 35000 Rennes, France

Received: 19 March 2019 / Received in final form: 1 July 2019 /Accepted: 15 July 2019

Abstract. Starting from the well-known and historic eigenvalue equations describing the behavior of 3-layer and 4-layer slab waveguides, this paper presents another specific analytical framework providing time-laws of evolution of the effective propagation constant associated to such structures, in case of temporal variation of its various geometrical features. So as to develop such kind of time-propagator formulation and related principles, a temporal derivation operator is applied on the studied school case equations, considering then time varying values of all the geometrical characteristics together with the effective propagation constant. Relevant calculations are performed on three different cases. For example, we first investigate the variation of the height of the guiding layer for the family of 3-layer slab waveguides: then, considering the 4-layer slab waveguide's family, we successively address the variation of its guiding layer and of its first upper cladding. As regards the family of 4-layer waveguides, calculations are performed for two different families of guided modes and light cones. Such another approach yields rigorous new generic analytical relations, easily implementable and highly valuable to obtain and trace all the family of dispersion curves by one single time-integration and one way.

▪ II.6 : Circular waveguides, fiber optics, ray optics approach, resolution and quantification of the electromagnetic step-fiber modes TE, TM, HE, EH modes, weakly guiding fiber and LP-modes

▪ Origine…

À l'époque des Grecs anciens, le phénomène du transport de la lumière dans des cylindres de verre était déjà connu. Il était, semble-t-il, mis à profit par les artisans du verre pour créer des pièces décoratives. Plus tard, les techniques de fabrication utilisées par les artisans vénitines de la Renaissance pour fabriquer les « *millefiori* » ressembleraient beaucoup aux techniques actuelles de fabrication de la fibre optique. La première démonstration scientifique du principe de la RT fut faite par le physicien Irlandais John Tyndal devant la Société Royale britannique en 1854. À l´époque, l'idée de courber la trajectoire de la lumière, de quelque façon que ce soit, était révolutionnaire puisque les scientifiques considéraient que la lumière voyageait uniquement en ligne droite. Sa démonstration consistait à guider la lumière dans un jet d'eau déversé d'un trou à la base d'un réservoir. En injectant de la lumière dans ce jet, celle-ci suivait bien la courbure du jet d'eau, démontrant ainsi qu'elle pouvait être déviée de sa trajectoire rectiligne. Il put de cette manière démontrer le principe qui est à la base de la fibre optique. Par la suite, de nombreuses inventions utilisant le principe de la réflexion totale interne virent le jour ; comme les fontaines lumineuses ou des dispositifs permettant de transporter la lumière dans des cavités du corps humain. On doit la première tentative de communication optique à Alexander Graham Bell, connu pour l'invention du téléphone. En effet, il mit au point, au cours des années 1880, le photophone. Cet appareil permettait de transmettre la lumière sur une distance de 200 mètres. La voix, amplifiée par un microphone, faisait vibrer un miroir qui réfléchissait la lumière du soleil. Quelque 200 mètres plus loin, un second miroir captait cette lumière pour activer un cristal de sélénium et reproduire le son voulu. Le récepteur de cet appareil était presque identique à celui du premier téléphone. Bien qu'opérationnelle en terrain découvert, cette méthode s'avéra peu utilisée. La pluie, la neige et les obstacles qui empêchaient la transmission du signal condamnèrent cette invention, bien qu'il considérait lui-même que le photophone était sa plus grande invention, puisqu'elle permettait une communication sans fil.

▪ Fibre optique pour réseaux métropolitains…

La possibilité de transporter de la lumière le long de fines fibres de verres fut exploitée au cours de la première moitié du XXème siècle En 1927, Baird et Hansell tentèrent de mettre au point un dispositif d'images de télévision à l'aide de fibres. Hansell put faire breveter son invention, mais elle ne fut jamais vraiment utilisée. Quelques années plus tard, en 1930, Heinrich Lamm réussit à transmettre l'image d'un filament de lampe électrique grâce à un assemblage rudimentaire de fibres de quartz. Cependant, il était encore difficile à cette époque de concevoir que ces fibres de verre puissent trouver une application.

La première application fructueuse de la fibre optique eut lieu au début des années 1950, lorsque le fibroscope flexible fut inventé par van Heel et Hopkins. Cet appareil permettait la transmission d'une image le long de fibres en verre. Il fut particulièrement utilisé en endoscopie, pour observer l'intérieur du corps humain, et pour inspecter des soudures dans des réacteurs d'avion. Malheureusement, la transmission ne pouvait pas être faite sur une grande distance étant donnée la piètre qualité des fibres utilisées. En 1957, le fibroscope (endoscope flexible médical) est inventé par Basil Hirschowitz aux Etats-Unis. Les télécommunications par fibre optique restèrent impossibles jusqu'à l'invention du laser en 1960. Le laser offrit en effet l'occasion de transmettre un signal avec assez de puissance sur une grande distance. Dans sa publication de 1964, Charles Kao, des Standard Telecommunications Laboratories, décrivit un système de communication à longue distance et à faible perte en mettant à profit l'utilisation conjointe du laser et de la fibre optique. Peu après, soit en 1966, il démontra expérimentalement, avec la collaboration de Georges Hockman, qu'il était possible de transporter de l'information sur une grande distance sous forme de lumière grâce à la fibre optique. Cette expérience est souvent considérée comme la première transmission de données par fibre optique. Cependant, les pertes dans une fibre optique étaient telles que le signal disparaissait au bout de quelques centimètres, non par perte de lumière, mais parce que les différents chemins de réflexion du signal contre les parois finissaient par en faire perdre la phase. Cela la rendait peu avantageuse par rapport au fil de cuivre traditionnel. Les pertes de phase entraînées par l'usage d'une fibre de verre homogène constituaient le principal obstacle à l'utilisation courante de la fibre optique.

En 1970, trois scientifiques de la compagnie Corning Glass Works de New-York, Robert Maurer, Peter Schultz et Donald Keck, produisirent la première fibre optique avec des pertes de phase suffisamment faibles pour être utilisée dans les réseaux de télécommunications (20 décibels par kilomètre ; aujourd'hui la fibre conventionnelle affiche des pertes de moins de 0,25 décibel par kilomètre pour la longueur d'onde 1550 nm. utilisée dans les télécommunications). Leur fibre optique était en mesure de transporter 65 000 fois plus d'informations qu'un simple câble de cuivre, ce qui correspondait au rapport des longueurs d'onde utilisées. Le premier système de communication téléphonique optique fut installé au centre-ville de Chicagoen 1977. En France, la DGT a installé la première liaison optique à Paris entre les centraux téléphoniques des Tuileries et Philippe-Auguste. On estime qu'aujourd'hui plus de 85 % des communications à longue distance sont transportées le long de plus de 25 millions de kilomètres de câbles à fibres optiques partout dans le monde. La fibre optique s'est, dans une première phase (1984 à 2000), limitée à l'interconnexion des centraux téléphoniques, eux seuls nécessitant de forts débits. Cependant, avec la baisse des coûts entraînée par sa fabrication en masse et les besoins croissants des particuliers en très haut débit, on envisage depuis 2005 son arrivée même chez les particuliers : FTTH ((en)*Fiber To The Home*), FTTB ((en)*Fiber To The Building*), FTTC ((en)*Fiber To The Curb*), etc.

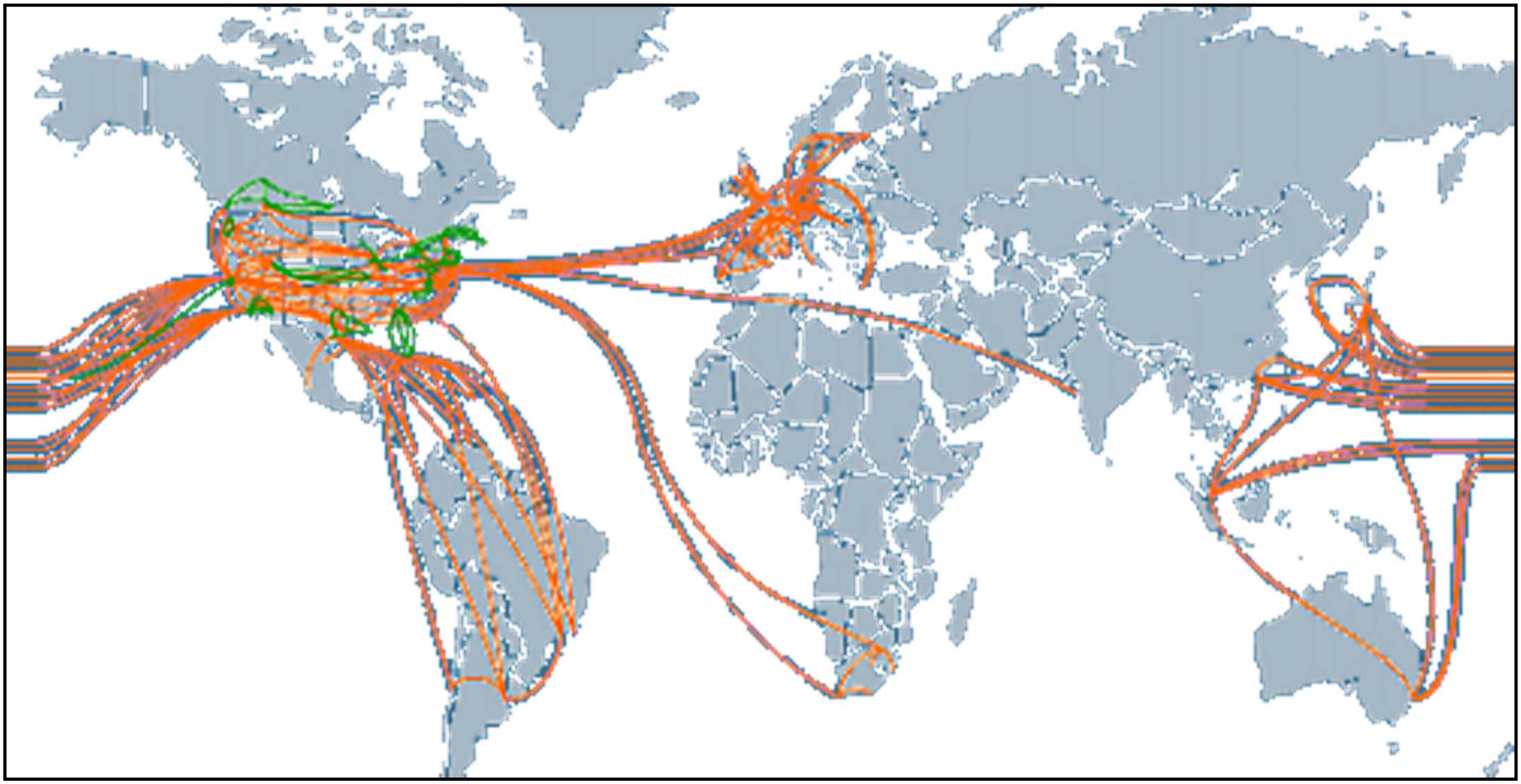

▪ II.6.1 Introduction, generalities

▪ Optical fiber = cylindrical dielectric waveguide TIR propagation ($n_c > n_g$), step index-profiles or gradient laws fibers, '2a/2b'-fibers (as 5/125 µm, 50/125 µm, 100/140 µm, …).

▪ **Materials** (core/cladding) :

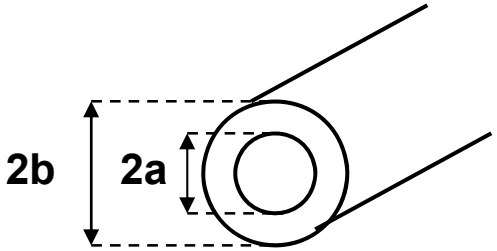

- Polymers (Polystyren, PMMA, Plastic Coated Silica or PCS,…)
- Borosilicates $SiO_2/B_2O_3:SiO_2$
- Germanosilicates $GeO_2:SiO_2/SiO_2$
+ with, fluorated glass doped GdF_3, BaF_2, ZnF_4, AlF_3, …
- Exotic fibers… (➔ lecture and study of the conference from IRCOM)

▪ **Attenuation and losses into fibers**

$$10 \log\left(\frac{P_{exit}}{P_{entrance}}\right)$$

- Optical power exponential decreasing
- On account of the material absorption (atomic structures ➔ lower than 0.1dB/cm at [0.8-1.6] µm, due to the impureties, or to the process of fabrication ➔ OH^- hydroxid at 0.93, 1.25 and 1.39 µm).

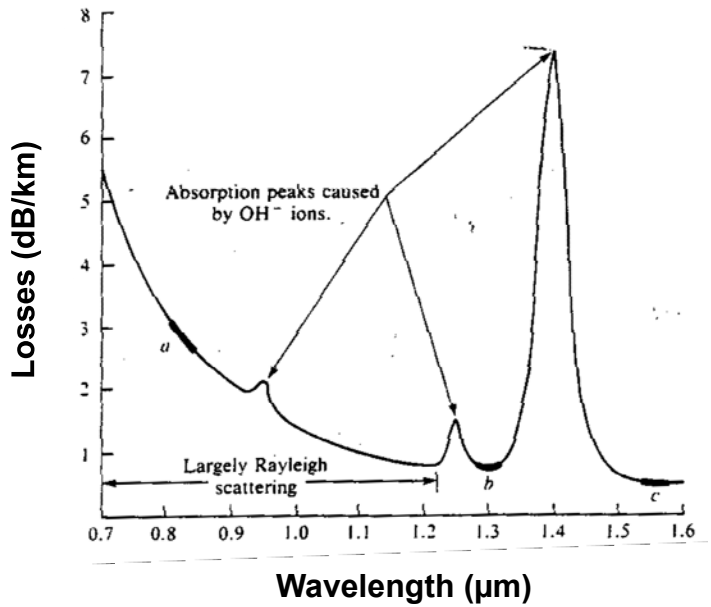

a, b, c, d telecoms windows

a – first window (at 0.8 μm)

b – second window (at 1.3 μm)

c - third (at 1.55 μm)

d - fourth (at 2.5 μm)

→ d

2.5 μm

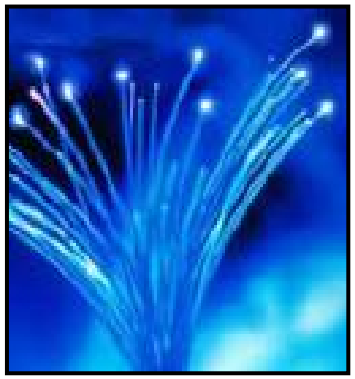

- On account of the diffusion of light (when default have molecular sizes ➔ Rayleigh diffusion ($\propto 1/\lambda^4$), with E_i incident field, α the average polarizability; such an diffused intensity is proportional to the square of dipole μ_i :

$$I_d = \frac{16\pi^4}{3c^3}\nu_i^4\overline{\mu_i^2} = \frac{8\pi^4 c}{3}\left(\frac{1}{\lambda^4}\right)E_i^2\alpha^2$$ **[II-67]**

- On account of the propagation-curved losses : structural variation of the fiber geometry, deformations, curves, …

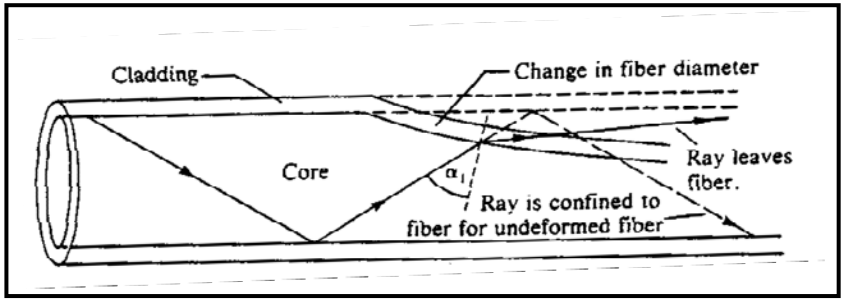

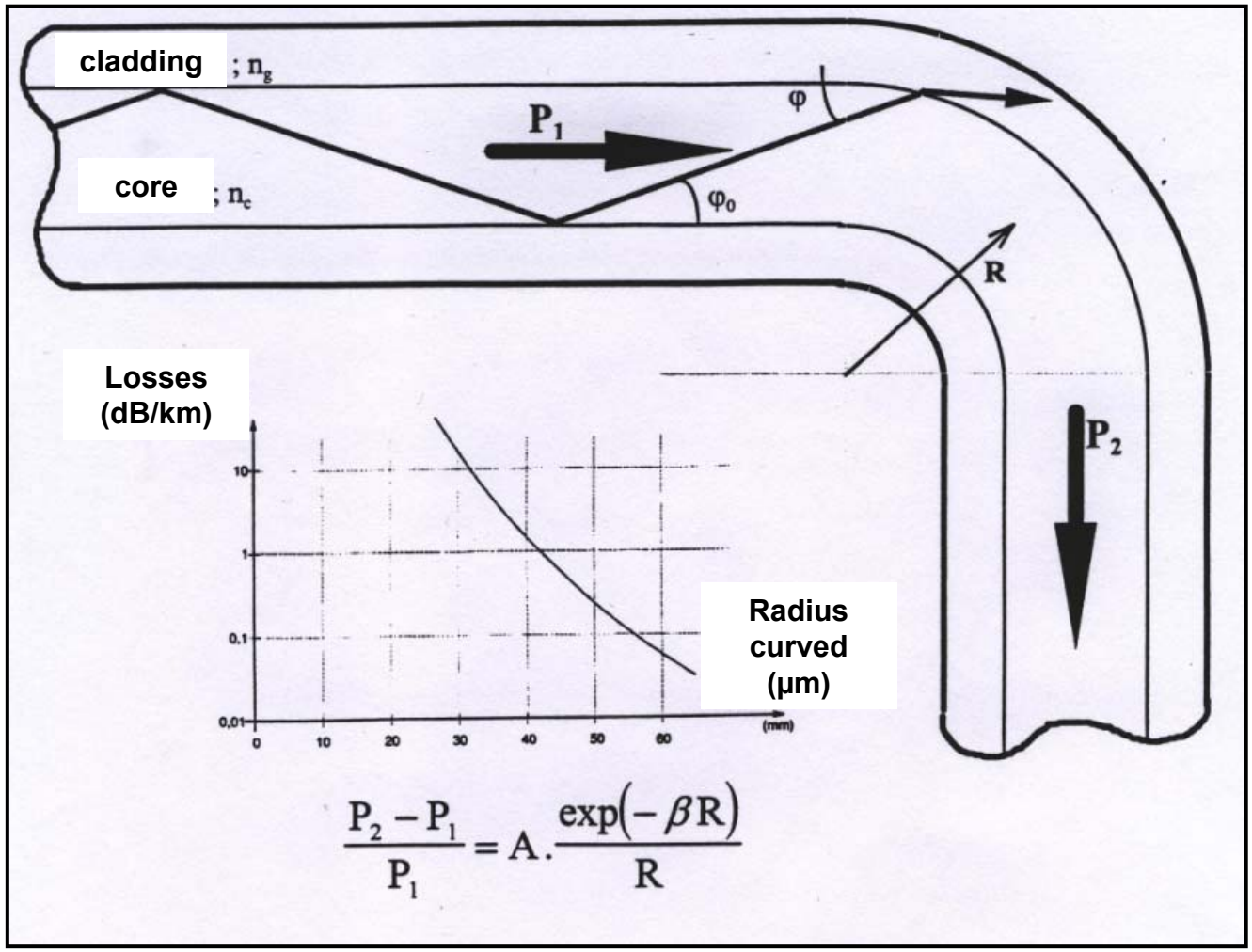

$$\frac{P_2 - P_1}{P_1} = A.\frac{\exp(-\beta R)}{R}$$

- Radiation modes into the cladding if $\varphi > \varphi_{limit}$; if high φ_0 (higher optical modes) ➔ leaky modes.
- No curved effect (losses) when $R >> R_c$ ($NA = \sqrt{n_c^2 - n_g^2}$)

[II-68]

Multimode fiber	$R_c = \left(\frac{2a.n_c^2}{(NA)^2}\right)$	Singlemode fiber	$R_c \approx 20.\frac{\lambda}{(n_c - n_g)^{3/2}}\left(2.75.\frac{\lambda}{\lambda_c}\right)^{-3}$

- Connectors losses (axial and angular displacement)

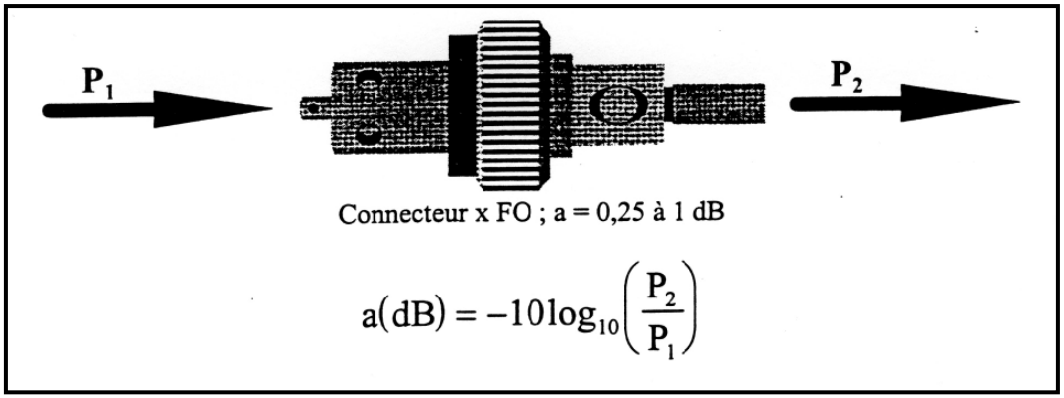

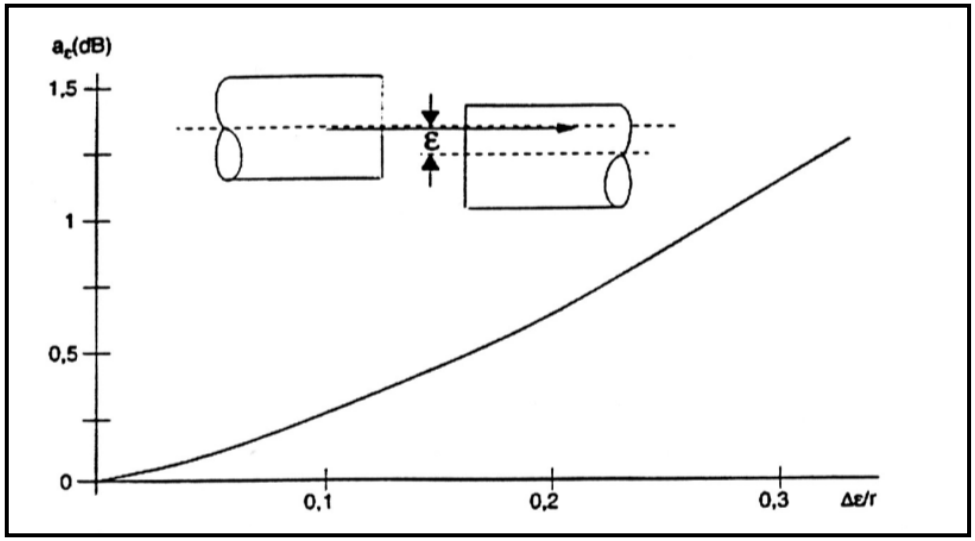

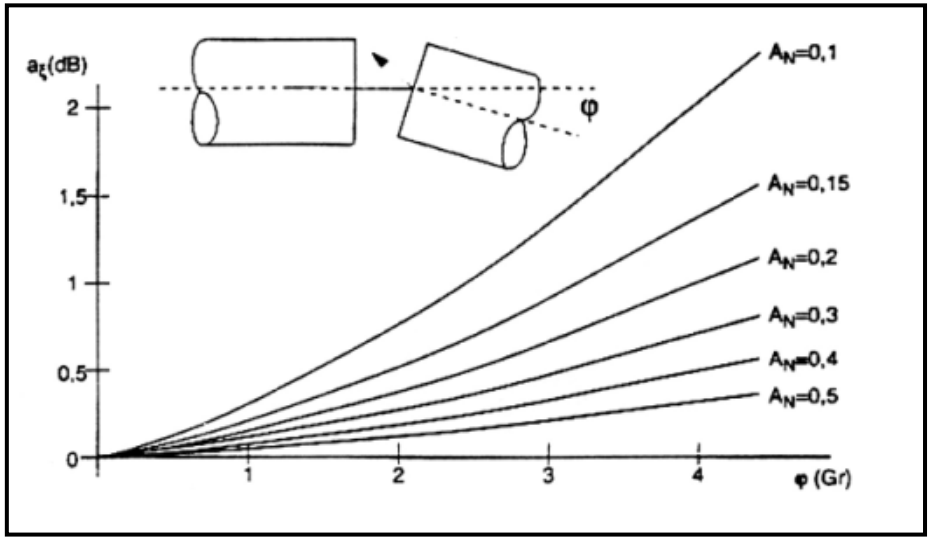

Possible excitation of optical modes in the cladding area (high axial displacement)

Losses are proportional to the angle and inverse-proportional to the NA (Numerical Aperture)

▪ **Dispersion of the signal** (inter-modal and intra-modal) :

- Inter-modal dispersion (D_{mod}, unity : MHz.km, only for multimode propagation!), propagation celerity is proper to the optical mode (temporal pulse's spread)

$$\boxed{D_{mod} \approx \frac{c}{\Delta n_{eff}}} \quad \text{[II-69]}$$

- Intra-modal dispersion (chromatic effect) (D_{chrom}, unity : ps/nm.km), celerity of an impulsion is function to the wavelength (due to the material dispersion and the modal dispersion too).

$$v_g = \frac{d\omega}{d\beta} = -\frac{2\pi c}{\lambda^2}\left(\frac{d\lambda}{d\beta}\right) \longrightarrow t_g = \frac{L}{v_g} = -\frac{\lambda^2 L}{2\pi c}\left(\frac{d\beta}{d\lambda}\right)$$

time of a λ-propagation for a λ-spectral-component

$$\boxed{D_{chrom} = \frac{1}{L}\frac{d\,t_g}{d\lambda}} \quad \text{[II-70]}$$

$$\longrightarrow (/\,km) \quad \boxed{D_{total}^2 = \left(\frac{1}{D_{mod}}\right)^2 + \left(D_{chrom}.\Delta\lambda\right)^2}$$

▪ II.6.2 Ray-geometrical approach and classification, numerical aperture (NA)

▪ **Introduction,** rays-classification, meridian, oblique

θ angle represent the incidence of the meridian-rays on the core/cladding interface; θ_z angle between rays and the z-axe revolution (direction of propagation).

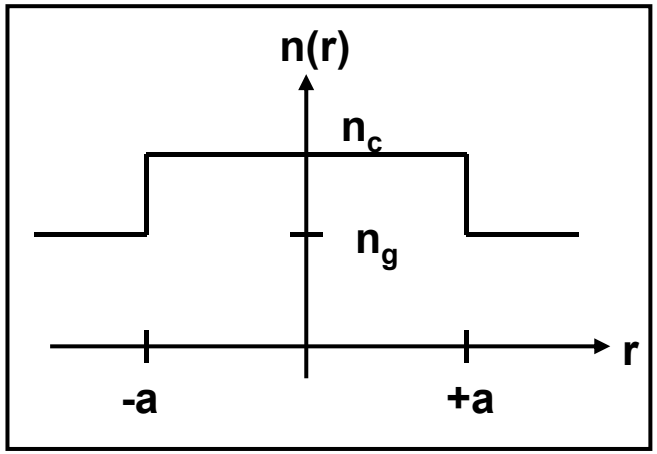

▪ **Trajectory of the meridian-rays and NA :**

They stay in the same plane after successive-TIR) ➔ TE and TM modes in electromagnetic approach

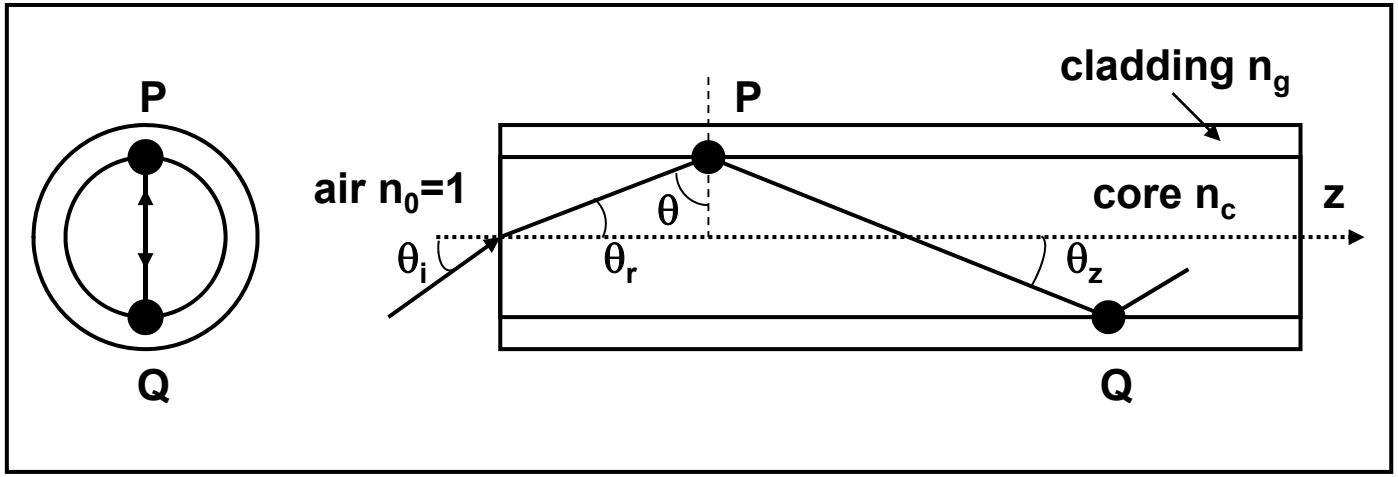

(θ_i defines a fiber-entrance-cone)

TIR ⟶ $$\sin\theta_i \le \frac{n_c}{n_0}\sqrt{1-\left(\frac{n_g}{n_c}\right)^2}$$ ⟶ $$n_0 \sin\theta_i \le \sqrt{n_c^2 - n_g^2} = \text{NA of fiber}$$ [II-71]

▪ Trajectory of the oblique-rays :

TIR propagation, but changes of planes at each reflection, helicoid by straight segments (such polygons defined are not necessary close) ➔ notion of caustic (r_c)

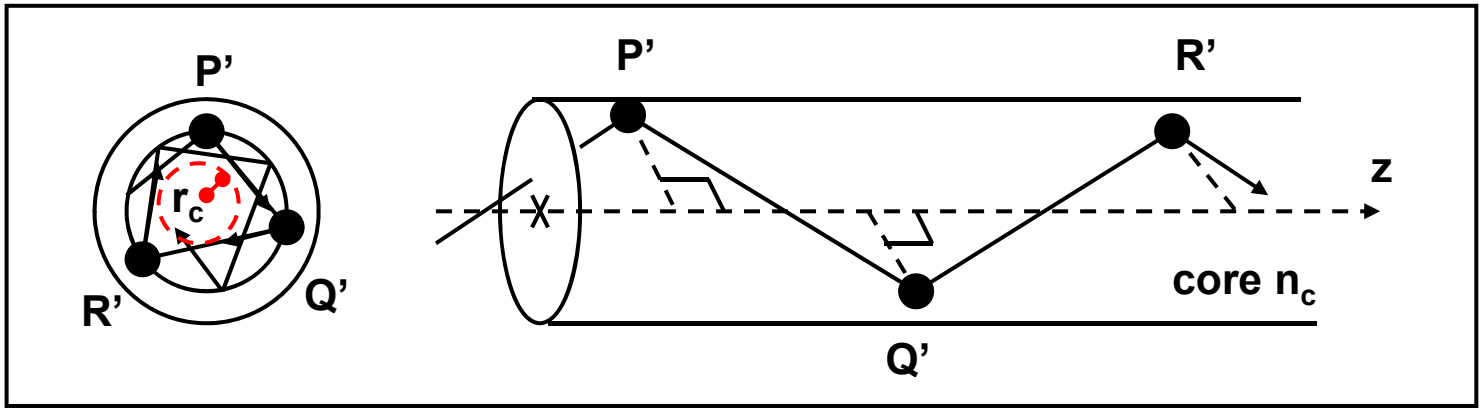

Due to such trajectory, an another angle is judicious ➔ θ_φ (that represents the oblique characteristic of such family-rays)

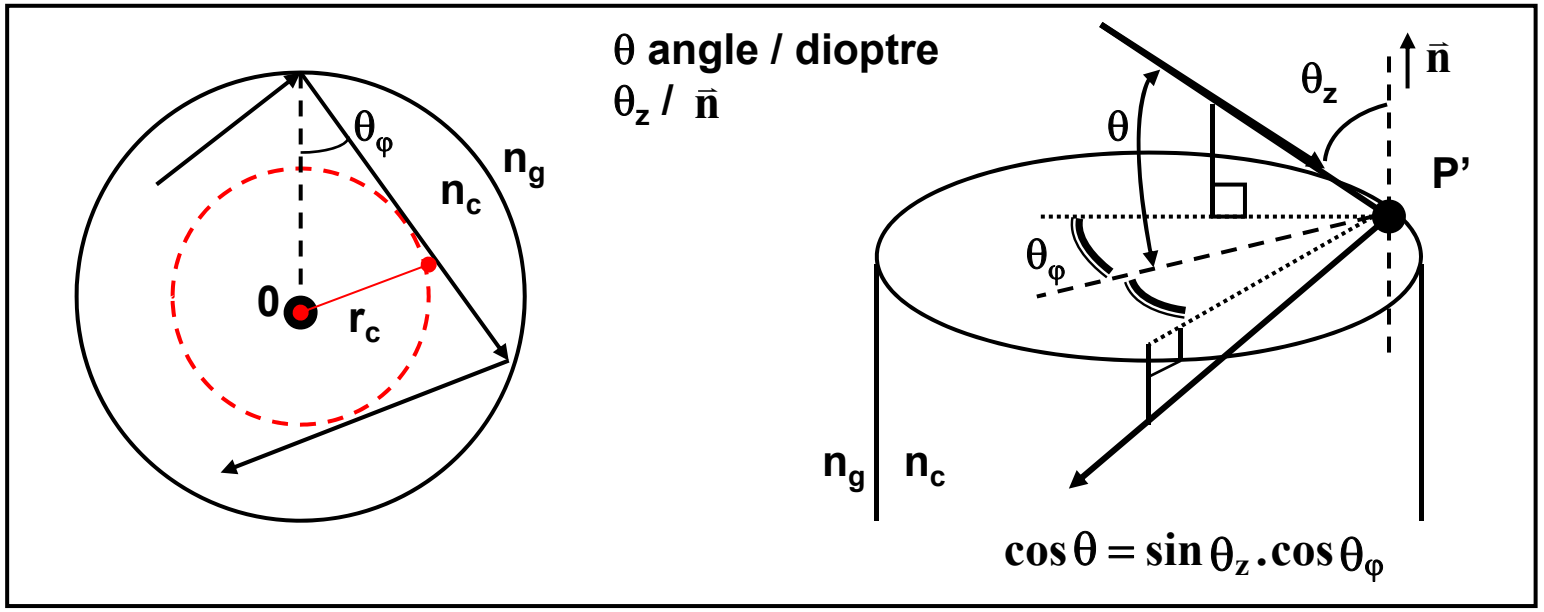

TIR conditions or guiding conditions : $\theta > \theta_c = \arcsin(n_g/n_c)$ + an another one : $\boxed{0 < \theta_z < \theta_{zc}}$

According to the previous diagram considered with θ into the fiber, if $\theta<\theta_c$ refracted rays exist as a new family modes. In conclusion, into such step-fiber structure :

- **Guided rays $0<\theta_z<\theta_{zc}$**
- **Refracted rays $0<\theta<\theta_c$**
- **Leaky rays $\theta_{zc} <\theta_z<(\pi/2)$ and $\theta_c<\theta <(\pi/2)$**

(sometimes, leaky rays designs the both last conditions)

[II-73]

- **Electromagnetic nature of such oblique rays (EH-, HE-, LP- modes):**

Such rays present a *z*-component or longitudinal (E or H) due to the oblique characteristic ➔ EH or HE optical modes (as an example $E_z<H_z$ is called EH modes). It can be noted that such EH-HE modes become LP-optical modes in weakly guiding conditions (lower $\Delta n_{(core/cladding)}$, and weak θ_z). LP-modes are defined by a quasi- linear polarization (see last slide).

- **The number of modes into a step-index fiber is defined by :**

$$\boxed{N \approx \frac{1}{2}V^2 = \frac{2\pi^2 a^2}{\lambda_0^2}\left(n_c^2 - n_g^2\right) \text{ with } V \text{ normalized frequency}}$$

[II-74]

- **Optical intensities of six LP-modes : LP_{01}, LP_{11}, LP_{21}, LP_{02}, LP_{31}, and LP_{12}**

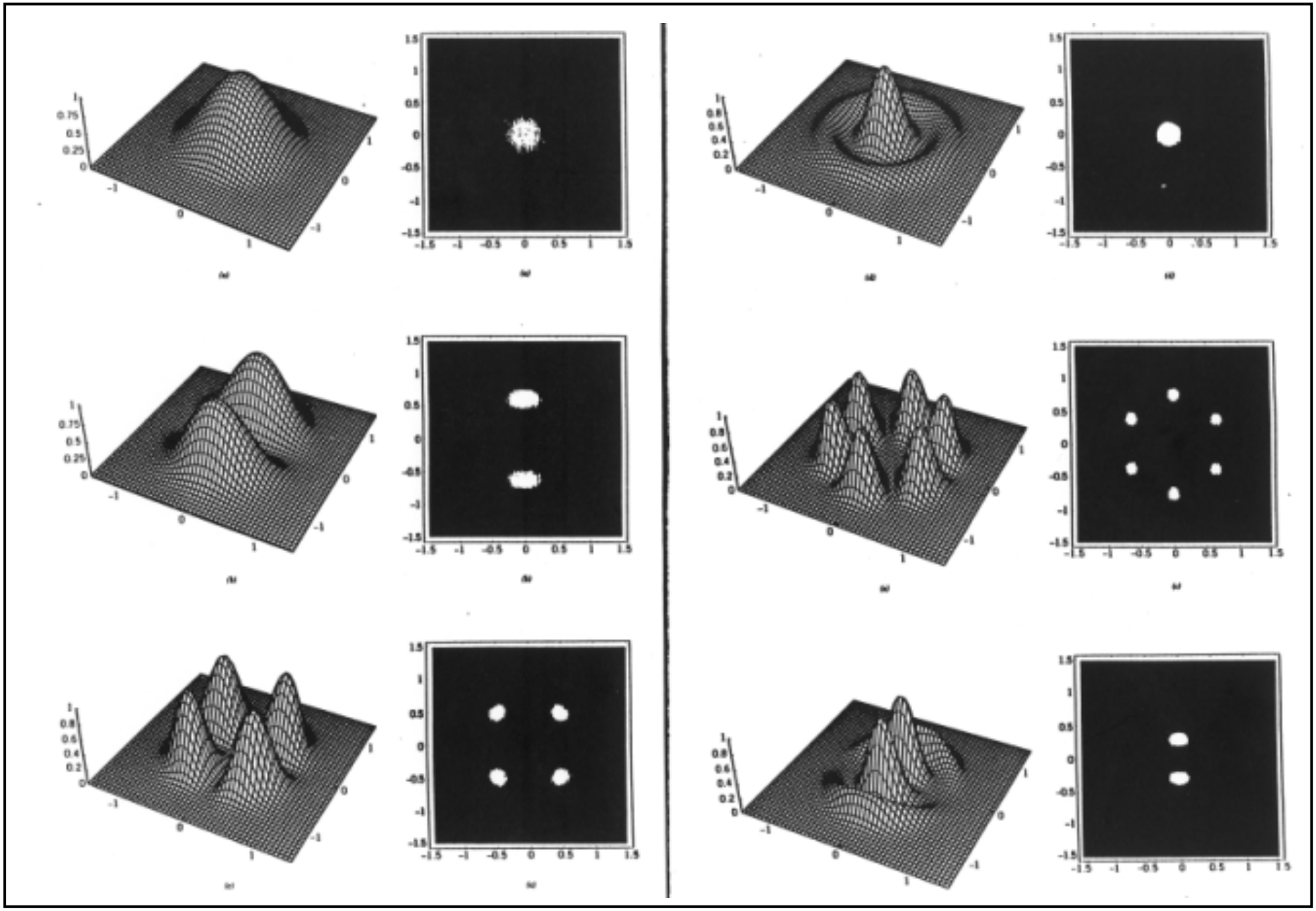

▪ II.6.3 Electromagnetic approach, quantification of the optical modes

▪ Introduction, expressions and relations between the transverses and longitudinales components fields

By considering the propagation stem from the z-axis $\Rightarrow e^{j(\omega t-\beta z)}$ on a cylindrical symmetry and coordinates, we can bring out from Maxwell equations [II.7] and highlight the expressions of E_r H_r and E_φ H_φ function of E_z and H_z.

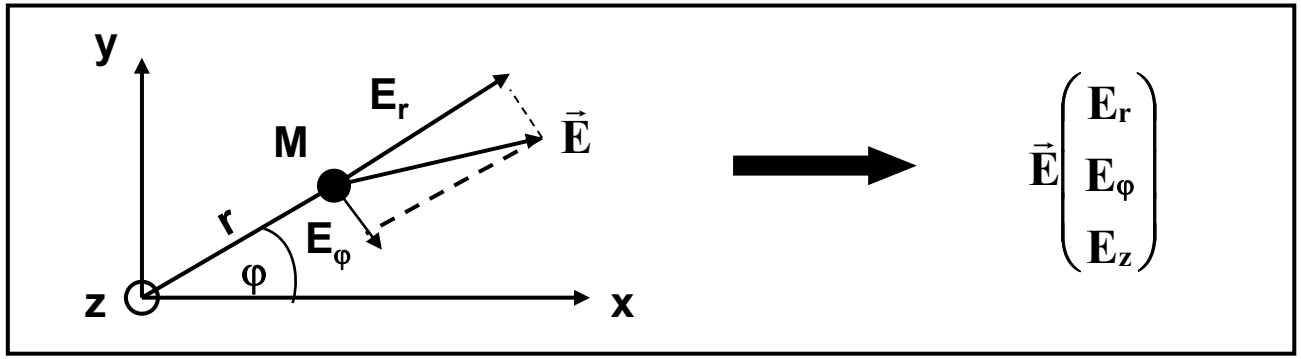

$$\begin{cases} E_r = \dfrac{-j}{\chi_i^2}\left[\beta\dfrac{\partial E_z}{\partial r} + \dfrac{\omega\mu_0}{r}\dfrac{\partial H_z}{\partial\varphi}\right] \\ E_\varphi = \dfrac{j}{\chi_i^2}\left[-\dfrac{\beta}{r}\dfrac{\partial E_z}{\partial\varphi} + \omega\mu_0\dfrac{\partial H_z}{\partial r}\right] \\ H_r = \dfrac{-j}{\chi_i^2}\left[\beta\dfrac{\partial H_z}{\partial r} - \dfrac{\omega\varepsilon_i}{r}\dfrac{\partial E_z}{\partial\varphi}\right] \\ H_\varphi = \dfrac{-j}{\chi_i^2}\left[\dfrac{\beta}{r}\dfrac{\partial H_z}{\partial\varphi} - \omega\varepsilon_i\dfrac{\partial E_z}{\partial r}\right] \end{cases} \quad \text{with } \chi_i^2 = \omega^2\varepsilon_i\mu_0 - \beta^2 = k_0^2 n_i^2(r) - \beta^2 \quad (i \equiv c \text{ et } g) \qquad \text{[II-75]}$$

- **Resolution of the propagation equation, expressions of the optical modes and eigenvalues equation**

- **We search the global field solution by a separated variable method on cylindrical coordinates :**

$$\boxed{\psi_t = \psi_1(r)\psi_2(\varphi)e^{j(\omega t-\beta z)}}$$

[II-76]

$$\boxed{\frac{\partial^2\psi_t}{\partial r^2}+\frac{1}{r}\frac{\partial\psi_t}{\partial r}+\frac{1}{r^2}\frac{\partial^2\psi_t}{\partial\varphi^2}+\frac{\partial^2\psi_t}{\partial z^2}+k_0^2n_i^2(r)\psi_t=0}$$

$$\longrightarrow \quad \frac{\psi_1''(r)}{\psi_1(r)}+\frac{1}{r}\frac{\psi_1'(r)}{\psi_1(r)}+\frac{1}{r^2}\frac{\psi_2''(\varphi)}{\psi_2(\varphi)}+\chi_i^2=0 \quad \text{with} \quad \chi_i^2=\left(k_0^2n_i^2(r)-\beta^2\right)$$

$$\longrightarrow \quad \boxed{\frac{r^2}{\psi_1(r)}\left[\psi_1''(r)+\frac{1}{r}\psi_1'(r)\right]+\chi_i^2r^2=-\frac{\psi_2''(\varphi)}{\psi_2(\varphi)}}$$

[II-77]

Resolution assumes that each member are equal to a constant, for example ν^2 for the second member.

Physical sense mod [2π] = cylindrical symmetry / φ

$$\boxed{\begin{array}{c}\psi_2(\varphi)=C\,e^{j\nu\varphi}\\ \text{with } \nu \text{ integer} = \text{'azimutal' number of the mode and } C \text{ cste}\end{array}}$$

[II-78]

[II-77 & 78] $\longrightarrow$

$$\boxed{\frac{d^2\psi_1(r)}{dr^2}+\frac{1}{r}\frac{d\psi_1(r)}{dr}+\left[\chi_i^2-\frac{\nu^2}{r^2}\right]\psi_1(r)=0}$$ [II-79]

$\downarrow$ into each area

$$\begin{cases}\dfrac{d^2\psi_1(r)}{dr^2}+\dfrac{1}{r}\dfrac{d\psi_1(r)}{dr}+\left[\chi_c^2-\dfrac{\nu^2}{r^2}\right]\psi_1(r)=0 & r<a \ \text{(core)}\\[2ex] \dfrac{d^2\psi_1(r)}{dr^2}+\dfrac{1}{r}\dfrac{d\psi_1(r)}{dr}-\left[\chi_g^2+\dfrac{\nu^2}{r^2}\right]\psi_1(r)=0 & r\geq a \ \text{(cladding)}\end{cases}$$ [II-80]

$$\text{with}\quad \chi_c^2=\left(k_0^2n_c^2(r)-\beta^2\right)>0$$
$$\text{and}\quad \chi_g^2=\left(\beta^2-k_0^2n_g^2(r)\right)>0$$

$\downarrow$ Bessel family functions

[II-81]

$$\Psi_1(r)=a_\nu J_\nu\left(u\frac{r}{a}\right)=a_\nu J_\nu(\chi_c r)\quad \text{with}\quad u=a\sqrt{k_0^2n_c^2-\beta^2}$$

Core r<a
1st kind ν order Bessel

$$\Psi_1(r)=a'_\nu K_\nu\left(v\frac{r}{a}\right)=a'_\nu K_\nu(\chi_g r)\quad \text{with}\quad v=a\sqrt{\beta^2-k_0^2n_g^2}$$

Cladding r>a
1st kind ν order Mac Donald

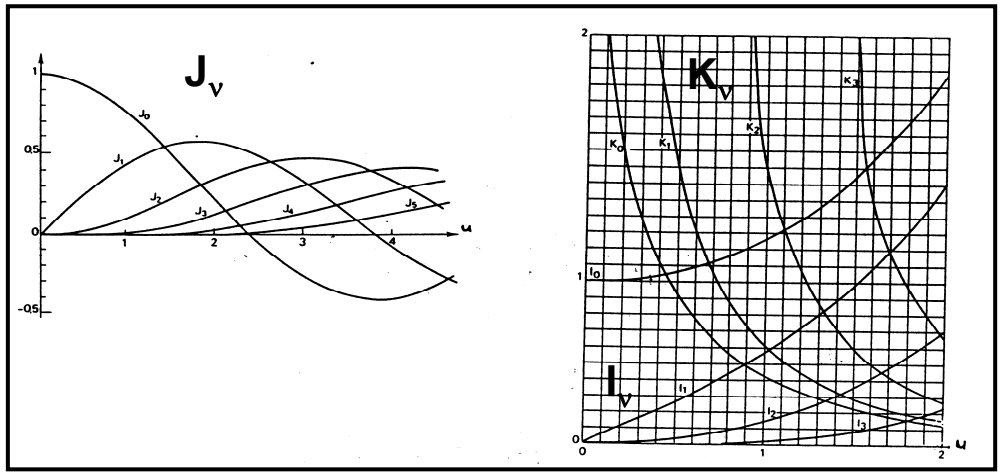

[II-82]

$$\chi_c^2+\chi_g^2=\left(n_c^2-n_g^2\right)k_0^2=(NA)^2k_0^2$$

According to [II.76] , ψ_t we obtain :

[II-83]

$$r \le a \text{ (core area)} \quad \begin{cases} E_z = a_\nu J_\nu\left(\frac{u}{a}r\right)e^{j\nu\varphi}e^{j(\omega t-\beta z)} \\ H_z = b_\nu J_\nu\left(\frac{u}{a}r\right)e^{j\nu\varphi}e^{j(\omega t-\beta z)} \end{cases}$$

$$r \ge a \text{ (cladding area)} \quad \begin{cases} E_z = a'_\nu K_\nu\left(\frac{v}{a}r\right)e^{j\nu\varphi}e^{j(\omega t-\beta z)} \\ H_z = b'_\nu K_\nu\left(\frac{v}{a}r\right)e^{j\nu\varphi}e^{j(\omega t-\beta z)} \end{cases}$$

[II.83 & 75]

[II.84]

$r \le a$ (core):

$$\begin{cases} E_r = -j\frac{a^2}{u^2}\left[\beta\frac{u}{a}a_\nu J'_\nu\left(\frac{u}{a}r\right)\cos(\nu\varphi) - \frac{\omega\mu_0}{r}b_\nu J_\nu\left(\frac{u}{a}r\right)\nu\sin(\nu\varphi)\right]e^{j(\omega t-\beta z)} \\ E_\varphi = -j\frac{a^2}{u^2}\left[-\frac{\beta}{r}a_\nu J_\nu\left(\frac{u}{a}r\right)\nu\sin(\nu\varphi) - \omega\mu_0\frac{u}{a}b_\nu J'_\nu\left(\frac{u}{a}r\right)\cos(\nu\varphi)\right]e^{j(\omega t-\beta z)} \\ H_r = -j\frac{a^2}{u^2}\left[\beta\frac{u}{a}b_\nu J_\nu\left(\frac{u}{a}r\right)\cos(\nu\varphi) + \frac{\omega\varepsilon_c}{r}a_\nu J_\nu\left(\frac{u}{a}r\right)\nu\sin(\nu\varphi)\right]e^{j(\omega t-\beta z)} \\ H_\varphi = -j\frac{a^2}{u^2}\left[-\frac{\beta}{r}a_\nu J_\nu\left(\frac{u}{a}r\right)\nu\sin(\nu\varphi) - \omega\varepsilon_c\frac{u}{a}a_\nu J'_\nu\left(\frac{u}{a}r\right)\cos(\nu\varphi)\right]e^{j(\omega t-\beta z)} \end{cases}$$

$r \ge a$ (cladding):

$$\begin{cases} E_r = -j\frac{a^2}{v^2}\left[-\beta\frac{v}{a}a'_\nu K'_\nu\left(\frac{v}{a}r\right)\cos(\nu\varphi) + \frac{\omega\mu_0}{r}b'_\nu K_\nu\left(\frac{v}{a}r\right)\nu\sin(\nu\varphi)\right]e^{j(\omega t-\beta z)} \\ E_\varphi = -j\frac{a^2}{v^2}\left[\frac{\beta}{r}a'_\nu K_\nu\left(\frac{v}{a}r\right)\nu\sin(\nu\varphi) + \omega\mu_0\frac{v}{a}b'_\nu K'_\nu\left(\frac{v}{a}r\right)\cos(\nu\varphi)\right]e^{j(\omega t-\beta z)} \\ H_r = -j\frac{a^2}{v^2}\left[-\beta\frac{v}{a}b'_\nu K'_\nu\left(\frac{v}{a}r\right)\cos(\nu\varphi) + \frac{\omega\varepsilon_g}{r}\frac{v}{a}a'_\nu K'_\nu\left(\frac{v}{a}r\right)\cos(\nu\varphi)\right]e^{j(\omega t-\beta z)} \\ H_\varphi = -j\frac{a^2}{v^2}\left[\frac{\beta}{r}b'_\nu K_\nu\left(\frac{v}{a}r\right)\nu\sin(\nu\varphi) - \omega\varepsilon_g\frac{v}{a}a'_\nu K'_\nu\left(\frac{v}{a}r\right)\cos(\nu\varphi)\right]e^{j(\omega t-\beta z)} \end{cases}$$

▪ Determination of the eigenvalues equation

By using the continuities of the tangential components (that is E_z, H_z, E_φ and H_φ) at r=a, and the weakly guiding conditions ($\Delta n \ll n_c$) we can shape the quantification of such optical modes.

[II.85]

$$\frac{J'_\nu(u)}{u\,J_\nu(u)} + \frac{K'_\nu(v)}{v\,K_\nu(v)} = \pm\nu\left(\frac{1}{u^2} + \frac{1}{v^2}\right)$$

$$\longrightarrow \quad \boxed{\frac{J_{\nu\pm1}(u)}{u\,J_\nu(u)} \pm \frac{K_{\nu\pm1}(v)}{v\,K_\nu(v)} = 0} \qquad \boxed{u^2 + v^2 = V^2 = a^2 k_0^2 \left(n_c^2 - n_g^2\right)} \qquad [II.86]$$

with, (+) ➔ $EH_{\nu\mu}$ modes and (-) ➔ $HE_{\nu\mu}$ modes

BESSEL and MAC DONALD functions

Definition: $J_\nu(u) = \frac{1}{\pi}\int_0^\pi \cos\left[u\sin(\alpha) - \nu\alpha\right] d\alpha$ (pour ν integer)

Properties:

$J_{\nu-1}(u) = J'_\nu(u) + \frac{\nu}{u} J_\nu(u)$	$K_{\nu-1}(u) = -K'_\nu(u) - \frac{\nu}{u} K_\nu(u)$
$J_{\nu+1}(u) = -J'_\nu(u) + \frac{\nu}{u} J_\nu(u)$	$K_{\nu+1}(u) = -K'_\nu(u) + \frac{\nu}{u} K_\nu(u)$
$J_{-\nu}(u) = (-1)^\nu J_\nu(u)$	$K_{-\nu}(u) = -K_\nu(u)$
$J_{\nu-1}(u) + J_{\nu+1}(u) = 2\frac{\nu}{u} J_\nu(u)$	$K_{\nu-1}(u) + K_{\nu+1}(u) = -2\,K'_\nu(u)$
$J_{\nu-1}(u) - J_{\nu+1}(u) = 2\,J'_\nu(u)$	$K_{\nu-1}(u) - K_{\nu+1}(u) = -2\frac{\nu}{u} K_\nu(u)$
$J_1(u) = -J'_0(u)$ $J_{-1}(u) = J'_0(u)$	DL at 0 of K function : $K_0(v) \approx -\mathrm{Log}(v);\ K_1(v) \approx \frac{1}{v};\ K_2(v) \approx \frac{2}{v^2};$ $K_\nu(v) \approx \frac{2^{\nu-1}}{v^\nu}(\nu-1)!;$

In [II.86], for a *V* fixed value (determinated by the opto-geometric parameters of the fiber waveguide), the *u* and *v* values will stem from the intersections of curves [II.86] with such circle V^2. This leads to μ-solutions for each ν fixed value. The, effective propagation constants could be assess from these results. The optical modes can be stand for by injecting the *u*- and *v*-roots into [II.84].

[ν=0 represent the TE and TM modes and $\nu \geq 1$ the HE and EH optical modes]

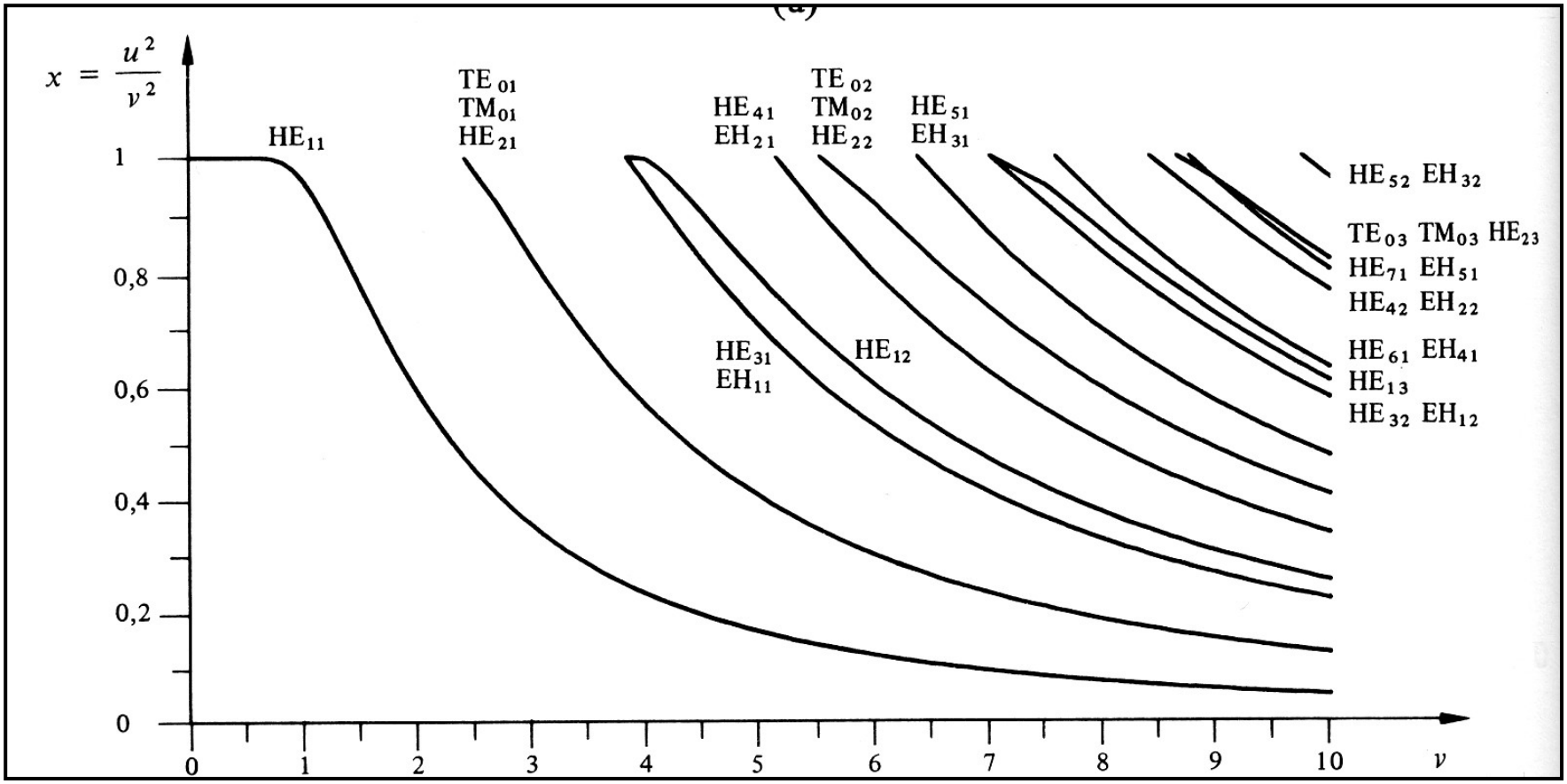

▪ II.7 : Coupled mode theory representation, notions of super-modes

▪ Coupled mode equations and resolution

This formalism that described the coupling between two optical modes is important, and has to be resolved in many cases of optical components and systems : couplers, routers, polarization converters, accordable filters (by electro- or acousto-optic), parametric conversion (non-linear optics), and so on.

By considering such a coupled waveguides structure defined with two n_1 and n_2 guides 'buried' into a n_s-substrate, each index profile can be resumed as :

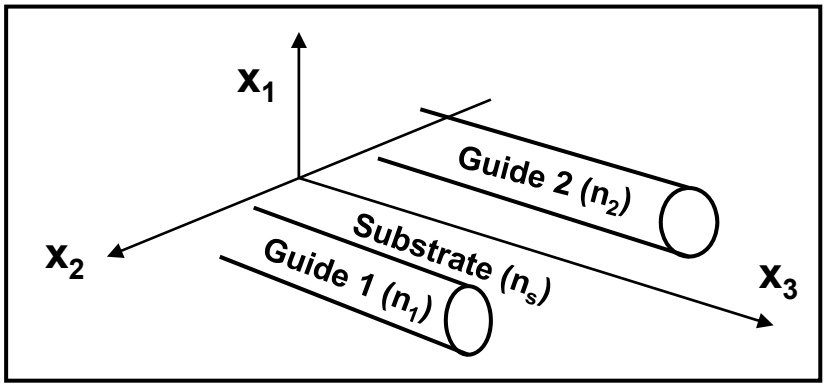

$$\boxed{n_i(x_1,x_2) = n_s\left[1+\Delta_i(x_1,x_2)\right]}$$

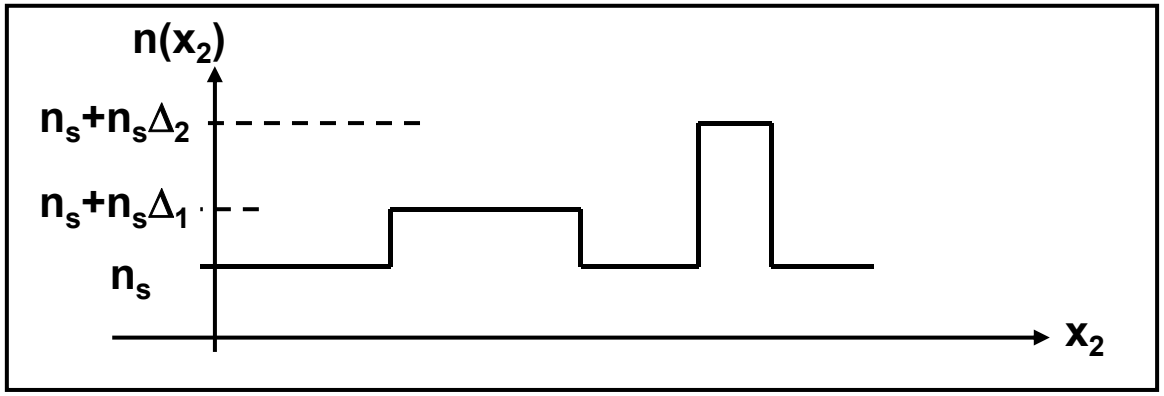

with, weakly guiding conditions Δ_i<<1 : $n_i^2(x_1,x_2) \approx n_s^2\left[1+2\Delta_i(x_1,x_2)\right]$

Global index profile $\longrightarrow$ $\boxed{n_i^2(x_1,x_2) \approx n_s^2\left[1+2\Delta_1(x_1,x_2)+2\Delta_2(x_1,x_2)\right]}$ **[II.87]**

Considering two optical modes (unperturbed) with effective propagation constants $\beta_i=(2\pi/\lambda_0).n_{i\text{-eff}}$, solutions of the propagation equation into proper guides :

$$\boxed{\begin{cases} E_1^o(x_1,x_2,x_3,t) = E_1^o(x_1,x_2)\exp j[\omega t - \beta_1 x_3] \\ E_2^o(x_1,x_2,x_3,t) = E_2^o(x_1,x_2)\exp j[\omega t - \beta_2 x_3] \end{cases}} \quad \text{[II.88]} \qquad \boxed{\nabla^2 E_i^o + k_0^2 n_s^2 (1 + 2\Delta_i(x_1,x_2)) E_i^o = 0}$$

$$\downarrow \nabla_t^2 + \frac{\partial^2}{\partial x_3^2} = \nabla^2$$

For i=1 and 2

$$\boxed{\nabla_t^2 E_i^o(x_1,x_2) - \left[\beta_i^2 - k_0^2 n_s^2 (1 + 2\Delta_i(x_1,x_2))\right] E_i^o(x_1,x_2)\exp j[\omega t - \beta_i x_3] = 0} \quad \text{[II.89]}$$

Another approach is to consider the field as a total optical mode ψ which is solution of an equation of propagation into the global index structures [II.87] :

$$\boxed{\nabla^2 \psi + k_0^2 n_s^2 (1 + 2\Delta_1(x_1,x_2) + 2\Delta_2(x_1,x_2))\psi = 0}$$

$$\boxed{\psi = \sum_{i=1}^{2} A_i(x_3) E_i^0(x_1,x_2,x_3,t) = \sum_{i=1}^{2} A_i(x_3) E_i^o(x_1,x_2)\exp j[\omega t - \beta_i x_3]} \quad \text{[II.90]}$$

***A_i* are not constants in [II.90], because E^o_i are not defined as the eigenvectors of the global index structures [II.87] and ψ could not be developed as an linear combination of E^o_i (that is with A_i constants).**

The idea is to project the total (perturbed) mode ψ on the vectors basis E^o_i that is the proper eigenvectors (unperturbed) of each single guide.

[II.90] →

$$\sum_{i=1}^{2}\left\{\nabla_t^2 . - \left[\beta_i^2 - k_0^2 n_s^2 (1+2\Delta_i)\right]\right\} E_i^o(x_1,x_2)\exp[-j\beta_i x_3] . A_i(x_3)$$

=0 (see [II.89])

$$+ 2k_0^2 n_s^2 \left[\Delta_2 A_1(x_3) E_1^o(x_1,x_2)\exp[-j\beta_1 x_3] + \Delta_1 A_2(x_3) E_2^o(x_1,x_2)\exp[-j\beta_2 x_3]\right]$$

$$-2j\sum_{i=1}^{2}\left\{\beta_i \frac{d A_i(x_3)}{d x_3} E_i^o(x_1,x_2)\exp[-j\beta_i x_3]\right\} + \sum_{i=1}^{2}\left\{\frac{d^2 A_i(x_3)}{d x_3^2} E_i^o(x_1,x_2)\exp[-j\beta_i x_3]\right\} = 0$$

[II.91]

SVE approximation (Slow Varying Envelop)

$$\left|\frac{d^2 A_i(x_3)}{d x_3^2}\right| << \left|\beta_i \frac{d\ A_i(x_3)}{d x_3}\right|$$

$\times E_1^{o*}$ and $\iint ... d x_1 d x_2$

$$k_0^2 n_s^2 \left[A_1(x_3) \iint_S \Delta_2(x_1,x_2) \left|E_1^0(x_1,x_2)\right|^2 dx_1 dx_2 + A_2(x_3) e^{j(\beta_1-\beta_2)x_3} \iint_S \Delta_1(x_1,x_2) E_2^0(x_1,x_2) E_1^{0*}(x_1,x_2) dx_1 dx_2 \right]$$

0

$$-j\left[\beta_1 \frac{d A_1(x_3)}{d x_3} \iint_S \left|E_1^0(x_1,x_2)\right|^2 dx_1 dx_2 + \beta_2 \frac{d A_2(x_3)}{d x_3} e^{j(\beta_1-\beta_2)x_3} \iint_S E_2^0(x_1,x_2) E_1^{0*}(x_1,x_2) dx_1 dx_2\right] = 0$$

0

[II.92]

By estimating each overlap integral, considering the domain of such functions (Δ_i and E^O_i), we obtain the differential equation that manages the amplitude modes evolution E^O_1 along x_3-axis propagation (κ_{12} is the coupling factor).

$$\frac{d\,A_1(x_3)}{d\,x_3} = -j\kappa_{12} A_2(x_3) e^{-j(\Delta\beta)x_3} \quad \text{with} \quad \Delta\beta = \beta_2 - \beta_1$$

with

$$\kappa_{12} = \frac{k_0^2 n_s^2}{\beta_1} \frac{\iint_S E_2^0(x_1,x_2)\Delta_1(x_1,x_2)E_1^{0*}(x_1,x_2)dx_1dx_2}{\iint_S \left|E_1^0(x_1,x_2)\right|^2 dx_1dx_2}$$

[II.93]

Perturbation method analogy

$$\frac{\langle E_1^o|\Delta_1|E_2^o\rangle}{\langle E_1^o|E_1^o\rangle}$$

Conversely,

$$\frac{d\,A_2(x_3)}{d\,x_3} = -j\kappa_{21} A_1(x_3) e^{j(\Delta\beta)x_3}$$

[II.94]

In conclusion, system [II.93 &94] resumes the energy coupling evolution between two waveguide or into previous defined super-structure [II.87]

- **Note :** In various case, Δ_i is the global perturbation that perturb the optical field propagation. Here, this is an another index profile of a neighboring waveguide, but it can be an electric field, an acoustic wave, an another optical field, ('notion of quasi phase matching' $\Delta\beta=\beta_2-\beta_1-2\pi/\Lambda$)...

▪ **Resolution of such system [II.93 & 94] can be obtain by considering for example ($\kappa_{12}=\kappa_{21}=\kappa$) plus the energy conservation along x_3-axis**

$$\frac{d}{dx_3}\left(\left|A_1(x_3)\right|^2+\left|A_2(x_3)\right|^2\right)=0$$

with initials conditions $A_1(x_3=0)$ fixed and $A_2(x_3=0)=0$.

$$\begin{cases} A_1(x_3)=e^{-j\left(\frac{\Delta\beta}{2}\right)x_3}\left[\cos(bx_3)+j\frac{\Delta\beta}{2b}\sin(bx_3)\right]A_1(0) \\ A_2(x_3)=e^{j\left(\frac{\Delta\beta}{2}\right)x_3}\left[j\frac{\kappa}{b}\sin(bx_3)\right]A_1(0) \end{cases} \quad \text{with, } b=\sqrt{|\kappa|^2+\left(\frac{\Delta\beta}{2}\right)^2},\ \Delta\beta=\beta_2-\beta_1 \qquad \text{[II.95]}$$

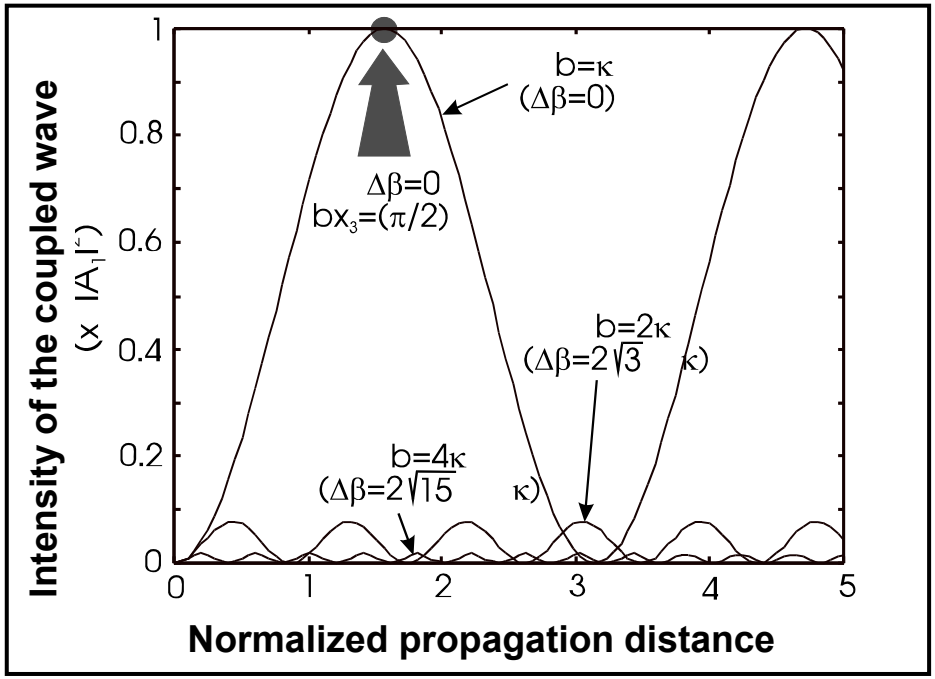

Efficient coupling strongly decrease when difference between propagation constants increase ($\Delta\beta \neq 0$, that is no judicious phase matching!)

Efficiency :

$$\eta=\left|\frac{A_2(x_3)}{A_1(0)}\right|^2=\frac{|\kappa|^2}{b^2}\sin^2[b\,x_3] \qquad \text{[II.96]}$$

▪ Approach by super-modes ψ, effective propagation constants and amplitude of optical super-modes

Ψ can be considered as the eigenvector of the global structure defined previously in [II.87]:

$$\boxed{\psi_{e,o} = \psi(x_1, x_2)\, e^{j(\omega t - \beta_{e,o} x_3)}} \quad \text{[II.97]}$$

Such expression is equal to [II.90] ; by differencing (two time /x_3) such expressions, using [II.93 & 94], we obtain :

$$\boxed{\begin{aligned} & E_1^o(x_1, x_2)\left[j A_1 (\beta_{e,o} - \beta_1) + \kappa A_2 e^{j\Delta\beta\, x_3}\right] \\ & + E_2^o(x_1, x_2)\left[j A_2 (\beta_{e,o} - \beta_2) + \kappa A_1 e^{-j\Delta\beta\, x_3}\right] = 0 \end{aligned}} \quad \text{[II.98]}$$

System det. must vanish

[II.98]

$$\boxed{\begin{aligned} & \beta_{e,o} = \frac{\beta_1 + \beta_2}{2} \pm b \quad \text{with} \quad b = \sqrt{\kappa^2 + \left(\frac{\Delta\beta}{2}\right)^2} \\ & \left[\frac{A_2}{A_1}\right]_{e,o} = e^{-j\Delta\beta x_3}\left[j\frac{\Delta\beta}{2\kappa} \mp \sqrt{1 - \left(\frac{\Delta\beta}{2\kappa}\right)^2}\right] \end{aligned}}$$

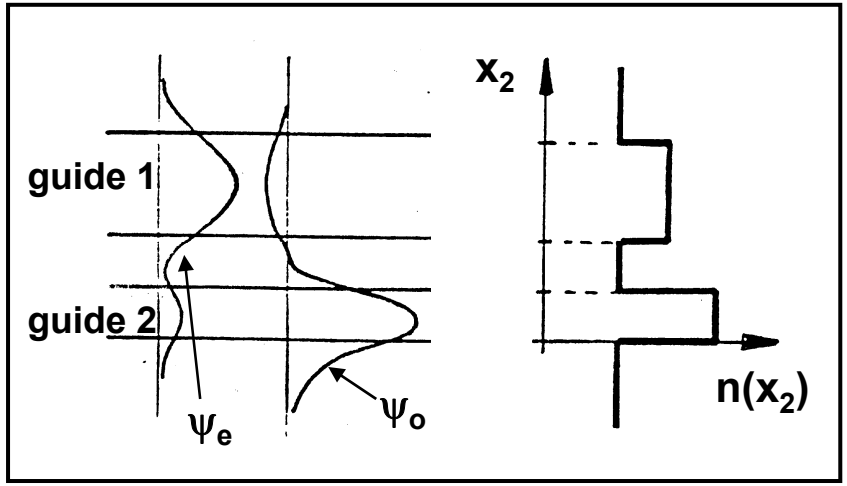

Les solitons

Ces ondes ne subissent ni dispersion ni affaiblissement et conservent presque indéfiniment leur forme et leur amplitude. Une nouvelle approche permet de considérer les solitons comme des particules élémentaires de grande masse.

par Claudio Rebbi

Depuis la formulation de la mécanique quantique entre 1920 et 1930, les théories physiques associent étroitement ondes et particules. On a découvert ces dernières années une autre relation entre ondes et corpuscules, et son origine est assez surprenante : elle découle de l'étude de certaines équations qui ne font pas partie de la mécanique quantique mais qui apparaissent en physique classique. Les solutions de ces équations correspondent à des ondes qui, contrairement aux autres ondes, ne s'étalent pas et ne subissent aucune dispersion; au contraire, leur forme et leur amplitude se conservent indéfiniment. On peut considérer que ces ondes représentent une concentration d'énergie, à tout instant confinée dans une région bien définie de l'espace. Quand l'onde se déplace, elle ne dissipe pas son énergie en s'étalant; de plus, lorsque deux ondes de ce type entrent en collision, elles conservent leurs caractéristiques propres : chacune repart sans que la collision l'ait modifiée. Lorsqu'une onde rencontre une « anti-onde », elles peuvent s'annihiler. Un tel comportement, s'il est inhabituel en physique ondulatoire, est en revanche bien connu dans d'autres domaines : le physicien désigne par particule tout objet qui possède ces propriétés.

Depuis longtemps les spécialistes de l'hydrodynamique savent qu'il existe des ondes qui se propagent sans dispersion; on les appelle « ondes solitaires » ou solitons. Ce qu'on vient de découvrir récemment, c'est que certaines équations proposées pour décrire des particules élémentaires ont aussi des solutions qui représentent des ondes sans dissipation.

On a également baptisé ces objets « solitons »; nous allons décrire ici une seule sorte de solitons, ceux pour lesquels l'impossibilité de s'étaler provient d'une contrainte topologique. Ils ne peuvent se désintégrer par étalement pour la même raison qu'on ne peut défaire un nœud fait sur une corde infinie sans couper cette corde.

Pour l'instant, les solitons de la physique des particules élémentaires ne sont que des créations de l'esprit et il se pourrait qu'ils n'existent pas dans la nature. En revanche, si parmi les équations qui décrivent les particules élémentaires, certaines admettent comme solution des solitons, alors les solitons doivent exister dans la nature; ces particules sont très lourdes, peut-être des milliers de fois plus lourdes que le proton. Une particule soliton peut avoir aussi des propriétés très spéciales; ainsi, selon une théorie proposée récemment, chaque soliton doit être porteur d'un monopole magnétique : soit un pôle Nord soit un pôle Sud isolé. Il faut avouer qu'en dépit de nombreuses tentatives, nul n'a encore observé de tels monopoles.

Même si de tels monopoles n'existent pas, les solitons peuvent quand même s'intégrer à la physique des particules élémentaires comme des objets qui sont confinés non seulement dans une région déterminée de l'espace, mais aussi dans un intervalle de temps. De tels solitons s'appellent des « instantons ». Un instanton n'est pas une particule mais plutôt une transition entre deux états d'un système; l'instanton serait lié au phénomène appelé effet tunnel. Les instantons se sont déjà révélés utiles : on a invoqué des transitions provoquées par des instantons pour expliquer une distribution des masses des particules qui, pendant longtemps, était restée une énigme pour les théoriciens.

Pour comprendre le caractère remarquable d'une onde qui ne s'étale pas au cours du temps, il suffit de considérer une onde dissipative ordinaire, par exemple celle qui prend naissance lorsqu'on jette un caillou dans un bassin rempli d'eau calme. Une telle onde de forme annulaire se déplace à la surface de l'eau, l'anneau grandissant au cours du temps. On constate que l'amplitude de l'onde décroît au fur et à mesure que l'onde s'éloigne du point de chute du caillou, pour finalement disparaître complètement. Ceci n'est dû qu'à la conservation de l'énergie. Le rayon du front d'onde croissant, l'amplitude de l'onde varie de façon inversement proportionnelle au rayon, même en l'absence de toute viscosité. La viscosité du milieu (qui traduit le frottement) est souvent un facteur autre de cette décroissance. Toutefois, dans certains milieux, des ondes planes (comme par exemple les ondes se propageant dans un canal à parois planes) se propagent « sans frottement » mais sont tout de même atténuées : même si on remplit le canal d'un liquide dépourvu de viscosité, les ondes finiront par disparaître. La raison est la suivante : une onde résulte de la superposition de composantes ondulatoires à des longueurs d'onde différentes. Les ondes correspondant à ces longueurs d'onde distinctes se propagent à des vitesses différentes, répartissant ainsi l'énergie de l'onde sur une grande surface. Lorsqu'on observe l'onde en coupe, on remarque qu'elle s'étend de plus en plus et que son amplitude devient par conséquent de plus en plus faible. Si elle peut aller jusqu'à l'infini, elle se disperse sur une surface infinie et donc disparaît.

On ne peut pas dire que les solitons sont à proprement parler insensibles à la dispersion; en fait, cette dispersion est exactement compensée par un autre phénomène. Cette compensation n'est possible que pour une certaine classe d'ondes, à savoir celles dont l'équation de mouvement est « non linéaire ». La propagation d'une telle onde dépend non seulement de la forme de la perturbation mais encore de son amplitude.

(en 1834)

C'est John Scott Russel, un ingénieur du génie maritime, qui a décrit pour la première fois un soliton il y a près de 150 ans. Il relata son observation à l'Association britannique pour l'avancement des sciences : « J'observais le mouvement d'un bateau qui était tiré rapidement le long d'un canal étroit par deux chevaux, quand soudain le bateau s'arrêta; il n'en fut pas de même pour la masse d'eau qu'il avait mise en mouvement : elle s'accumula autour de la proue du bateau dans un bouillonnement violent puis soudainement s'en sépara pour progresser vers l'avant à grande vitesse, telle une grande bosse solitaire, aux contours doux et bien définis, qui continua sa course le long du canal, apparemment sans changer de forme ni diminuer de vitesse. Je la suivis à cheval et la dépassai alors qu'elle roulait encore à la vitesse de huit à neuf miles à l'heure, préservant sa forme

"Great Solitary Wave"

.../...

.../...

...nale de 30 pieds de long et d'un pied ...emi de hauteur. La hauteur diminua ...eu à peu et après une poursuite de ...un à deux miles je la perdis dans les méandres du canal. »

D'après John Scott Russel, la stabilité de l'onde résultait des propriétés intrinsèques du mouvement de l'onde et non des circonstances de son apparition; ce point de vue ne fut pas tout de suite accepté. Ce ne fut qu'en 1895 que D. Korteweg et Hendrik de Vries donnèrent une solution analytique complète d'une équation non linéaire de l'hydrodynamique et montrèrent qu'il pouvait exister des ondes localisées non dissipatives. Depuis cette date, on a observé le phénomène soliton dans divers domaines de la physique et des mathématiques appliquées.

Fiber nonlinearity and solitons

The fiber is nonlinear, that is, its index can be written as

$$\boxed{n = n_0 + n_2 I,} \qquad (1)$$

where I is the intensity in W/cm^2 and $n_2 = 3.2 \times 10^{-16}$ cm^2/W for quartz glass. When effects of the nonlinearity are included, pulse propagation in the fiber is governed by the nonlinear Schrödinger equation:

$$\boxed{i\frac{\partial u}{\partial \xi} = \frac{1}{2}\frac{\partial^2 u}{\partial s^2} + |u|^2 u - i\Gamma u,} \qquad (2)$$

(NLSE)

(ξ = direction de propagation)

where all quantities are in dimensionless form. In particular, u is the pulse envelope function, ξ is z measured in units of $2z_0/\pi$ (see Eq. 4), s is time as perceived by an observer moving with the pulse, measured in units related to the pulse width, and Γ corresponds to α_{eff} times z_0/π. In Eq. 2, the first term on the right describes the effects of dispersion, while the second is derived from the index nonlinearity.

For a fiber with negligible gain or loss ($\Gamma \equiv 0$), the soliton is the special solution

$$\boxed{u(\xi, s) = \mathrm{sech}(s)e^{i\xi/2}} \qquad (3)$$

Solution de (2)

a pulse of constant amplitude, shape, and width.

→ effet Kerr optique (électro-optique, indice = Φ (Intensité))

⇒ l'indice optique de certains milieux varie linéairement avec l'intensité. ⇒ On parle de milieu "Autofocalisant" ≡

ex : CS_2 (liquide)

} ds cas 1D, ∃ solution analytique. (Zakharov et Shabat Sov. phys. JETP 1972)

⇒ Les profils de phase et en amplitude reste invariants !

⇒ profil spatial, ou profil temporel.

⇒ Compétition diffraction et focalisation (effet Kerr)

$P < P_c$ $\qquad$ $(P > P_c)$

∃ notion de puissance critique (P_c) (basculement selon le "mode" de propagation) limite entre les 2 comportements.

APPLICATIONS PHOTONIQUE INTÉGRÉE
Guides Auto-Induits

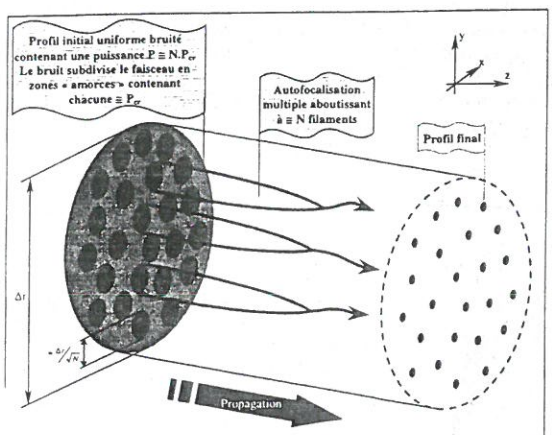

Autofocalisation multiple aboutissant à la dislocation du faisceau.

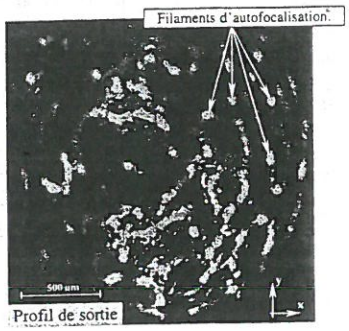

Dislocation. Profil d'un faisceau gaussien monomode après 2 cm de propagation dans une cuve de bisulfure de carbone. La puissance transportée est largement supérieure à la puissance critique ($P_{cr} \equiv 3.4$ kW). L'effet de dislocation se traduit par un profil aléatoire composé de points d'autofocalisation et un speckle en champ lointain.

Chapter III). Microphotonic components

- **III.1 : Principles and perturbation of the optical wave, example of the coherence (de)-modulation technique**

- **III.1.1 Global principles for optical telecommunications and sensors applications**

- **From passives structures waveguides, many components are developed on various substrates for Micro-Optical-Electronic and Mechanical Systems (MOEMS) devoted to optical telecommunications or sensors and measurements applications. Such actives components have many functionalities for the optical signal treatment. Each component is based on various devices that imply modulation or modification of physical attributes (or characteristic) of the optical wave :**

  - the amplitude (or intensity)
  - the phase
  - the frequency
  - the polarization
  - the direction of propagation
  - the temporal coherence (to be developed)

- **Artificial perturbations of the materials, physical effects**

Functions realized by the active components are based on the crystallographic symmetry of the material [32 classes + tensor physical effects, permittivity and susceptibility (non linear), electrooptic (Pockels), elastooptic, rigidity, and so on]

➔ Propagation equation into anisotropic and perturbed material

$$\nabla^2 E_i^o - \mu_0 \varepsilon_0 \varepsilon_{ij} \left(\frac{\partial^2}{\partial t^2} E_i^o \right) = \mu_0 \left(\frac{\partial^2}{\partial t^2} \Delta P_i^{total} \right) \qquad (i, j = 1 \text{ to } 3)$$ [III-1]

with, ε_0 vacuum permittivity, ε_{ij} relative permittivity tensor, E^o_i components of the optical mode, and $\Delta P_i^{total} = \Delta P_i^L + \Delta P_i^{NL}$ components of the variation of total polarization (linear and non-linear parts)

$$\Delta P_i^{NL} = \varepsilon 0 \left[\chi_{ijk}^{<2>} E_j^o E_k^o + \chi_{ijkl}^{<3>} E_j^o E_k^o E_l^o + \ldots \right]$$

$$\Delta P_i^L = -\varepsilon_0 \varepsilon_{ij} \left[p_{jkmn} S_{mn} + r_{jkm} E_m^e \right] \varepsilon_{kd} E_d^o$$ [III-2]

[III-3]

Perturbation of the optical wave by electro- and elasto-optic effects

$$\Delta B_{jk} = p_{jkld} S_{ld} + r_{jkl} E_l^e \quad (j, k, l, d = 1 \text{ to } 3)$$

- Variation of impermeability tensor B_{jk}, defined as the inverse of tensor permittivity $(\varepsilon_{ij}).(B_{jk}) = \delta_{ik}$ with $\Delta \varepsilon_{il} = -\varepsilon_{ij} \Delta B_{jk} \varepsilon_{kl}$.

-Deformation of the indices ellipsoïd, rotation of the neutral lines of the material, …

- Application of an electric field E^e_m along particular directions *l* via the electrooptic tensors terms r_{ijk}.

- Application of a strain $S_{ld} = \frac{1}{2}\left(\frac{\partial u_l}{\partial x_d} + \frac{\partial u_d}{\partial x_l} \right)$ via the elastooptic tensors terms p_{ijkl} (x_i axis= crystallographic reference). Use of transducers (or electrodes) to generate acoustic waves (surface or volume, u_i displacements) by piezoelectric effect $S_{ld} = e_{uld} E^e_u$.

▪ Potential of the telecom components (➔ a perturbed mode will present a new eigenvalue n_{eff} or β)

- Coupling between many physical fields or modes (see formalism developed in chapter II): optical fields in parametric conversion, non-linear optics, optical fields and electric fields (for opto-hyper-frequency components using electrooptic effect), optical fields and acoustic waves (for acousto-optic components), and so on.
- Modulations (amplitude or intensity, phase, frequency, and temporal coherence of the optical guided wave), modulators, filters components, Wavelength Division Multiplexing components for DWDM, PHASAR, and so on.
- Control of the state of polarization (integrated polarizers, polarization converters, tunable filters, WDM, amplifiers…)
- Control of the direction of propagation β (Y-, X- junctions, couplers, routers, splitters and networks)

▪ III.1.2 An example of modulation technique: the temporal coherence modulation *[the other modulations (intensity, phase, …) are considered as known]*

▪ III.1.2.1 Global notions

- Optical coherence is relative to the capacity of a wave to obtain interference phenomena. Optical source = emission and superposition of uncertain and successive set of waves totally decorrelated between them (that is a train can create interferences just with itself).

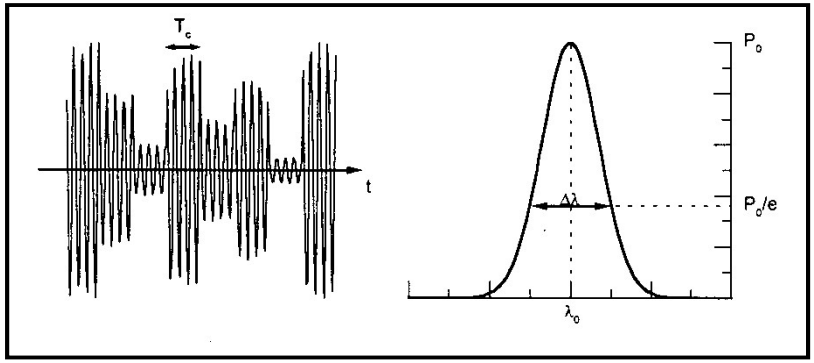

T_c= time during phase and amplitude are constants.

$$L_c = c\,T_c = \frac{c}{\Delta\nu} = \frac{\lambda_0^2}{\Delta\lambda} \quad \text{[III-4]}$$

Source	Wavelength	Spectral width	Coherence length
White light	0.6µm	400 nm	≈ 1µm
Superluminescence diode	1.3µm	40 nm	≈ 40µm
Monochromatic Laser	1.06µm	0.01 nm	≈ 10cm

- Two-waves interferometer, spectral transfer function P(σ) :

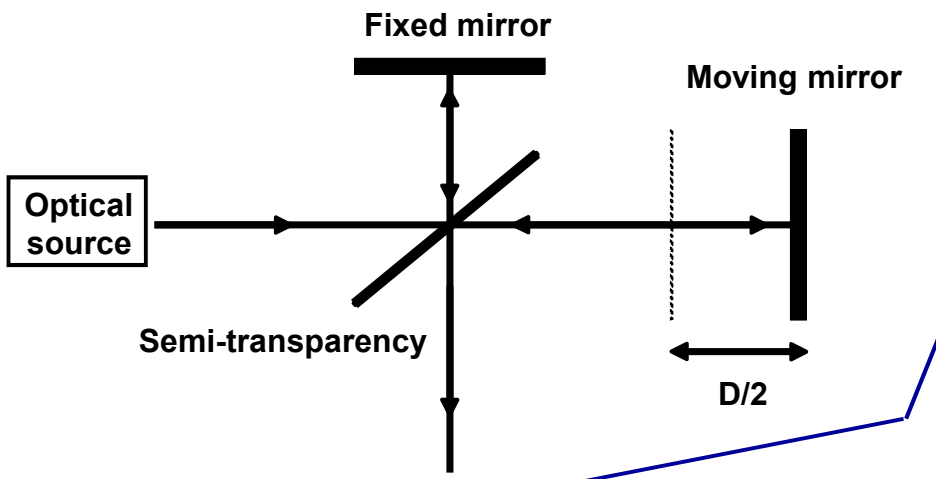

P(σ) represents the spectral power density of the emitter, with $\sigma=1/\lambda$ wave number.

$$P^m(\sigma)=\frac{P(\sigma)}{2}\left[1+\cos(2\pi\sigma D)\right]$$ [III-5] → Modulated transfer function (contrast =1) of such interferometer

▪ **III.1.2.2 Coherence modulation/demodulation**

• **Coherence modulation : by considering a normalized Gaussian spectral distribution concerning the emitter,**

$$P(\sigma) = \frac{2P_0}{\Delta\sigma\sqrt{\pi}} \exp\left(\frac{-4(\sigma-\sigma_0)^2}{\Delta\sigma^2}\right) \quad \text{with } \Delta\sigma = \frac{\Delta\lambda}{\lambda_0^2} = \frac{1}{L_c} \qquad \text{[III-6]}$$

calculus of the modulated intensity at the exit of modulators can be expressed by the integration on all the spectral components:

[III-5 & 6] ⟶

$$I^m(\sigma) = \frac{P_0}{2}\left[1 + \exp\left(-\frac{\pi^2}{4}\frac{D^2}{L_c^2}\right)\cos(2\pi\sigma_0 D)\right] \quad \text{with } D = D_0 + D_v(t) \qquad \text{[III-7]}$$

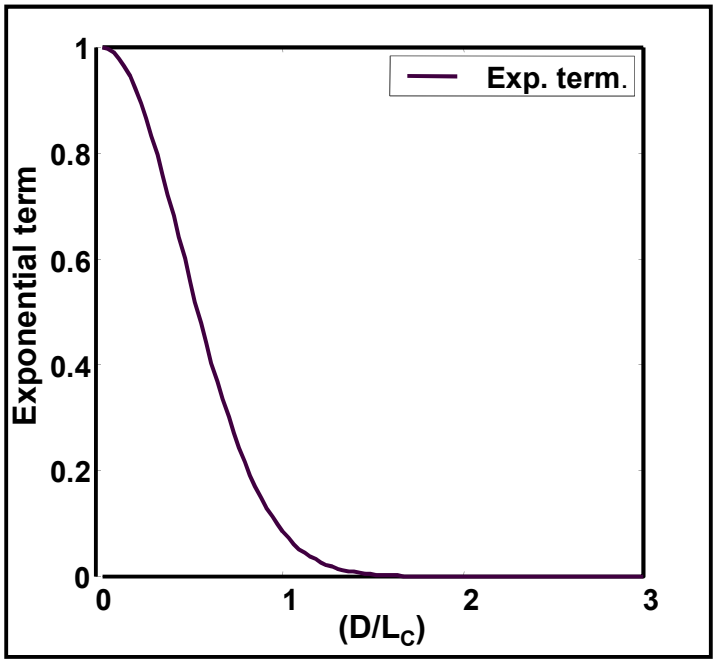

Evolution of the exp. Term function of (D/L_C). Such a term can be neglected when $D \gg L_C$:

$$I^m(D \gg L_c) = \frac{P_0}{2} \qquad \text{[III-8]}$$

The information (crypts on the delay between the set or train of waves) is not accessible at the exit of modulator (that introduces a delay $D \gg L_C$) by a photodiode; indeed, this one just can detect a continuous intensity and no modulation according to [III.8].

Such a coherence modulator component can be defined by a integrated imbalanced Mach-Zehnder (MZ) interferometer constituted by Y-junctions two S-bend arms waveguides; D_0 is a high static delay and $D_v(t)$ is the modulated delay (for example from an electrooptic or acoustooptic *v* signal for telecommunication applications, or modulate delay created by various physico-chemical detections concerning sensors applications.

• Coherence demodulation : such demodulation (that allows to obtain the previous modulated information) is accessible by an another interferometer that presents a D_0 static delay. Then, at the exit of this one, spectral density power can be expressed as :

[III-5] [III-6]

$$\boxed{P^d(\sigma) = \frac{P^m(\sigma)}{2}\left[1+\cos(2\pi\sigma D_0)\right] = \frac{P(\sigma)}{4}\left[1+\cos(2\pi\sigma D)\right]\left[1+\cos(2\pi\sigma D_0)\right]} \quad \text{[III-9]}$$

The intensity is deduced by integration on all the spectral components with conditions D, D_0, $D+D_0 >> L_C$:

1

$$\boxed{I^d(\sigma) = \frac{P_0}{4}\left[1+\frac{1}{2}\exp\left(-\frac{\pi^2}{4}\frac{D_v(t)^2}{L_c^2}\right)\cos(2\pi\sigma_0 D_v(t))\right]}$$

$$\boxed{I^d(D_v(t) << L_c) = \frac{P_0}{4}\left[1+\frac{1}{2}\cos\left(\frac{2\pi}{\lambda_0}D_v(t)\right)\right]} \quad \text{[III-10]}$$

The $D_v(t)$ is now directly accessible by a classical photodiode.

• **Principles and physical interpretation of the coherence (de)-modulation :**
[as an example, modulated delay $D_v(t)$=perturbation P(t) measuring in sensors applications]

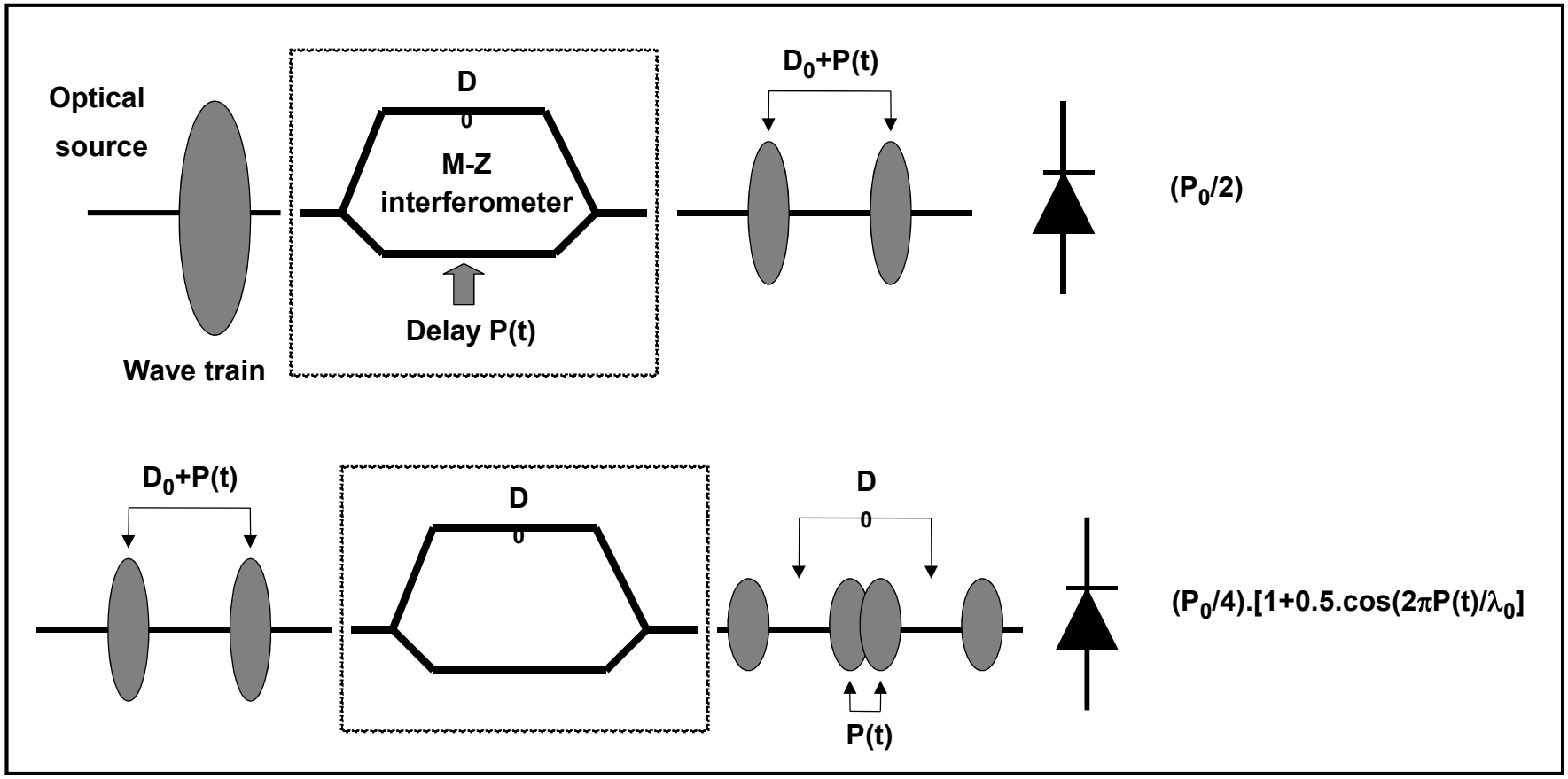

• **Notes : Such principle can be used on parallels and series architectures local networks for multiplexing applications (static delays D_0, D_1, D_2, … D_N). Dispersion on propagation limits this technique. Moreover, such coherence modulation can be developed into only one rib waveguide (and not a MZ structure) that presents a birefringence between the two polarizations (in this case, TE and TM polarizations don't see the same delay); For example, by an electrooptic effect, a proper electrode can only created a variable delay $D_v(T)$ (or P(t)) relative to one polarization (multiplexing on the polarization is then possible)…**

- **Example : a tri-axis Si accelerometer**

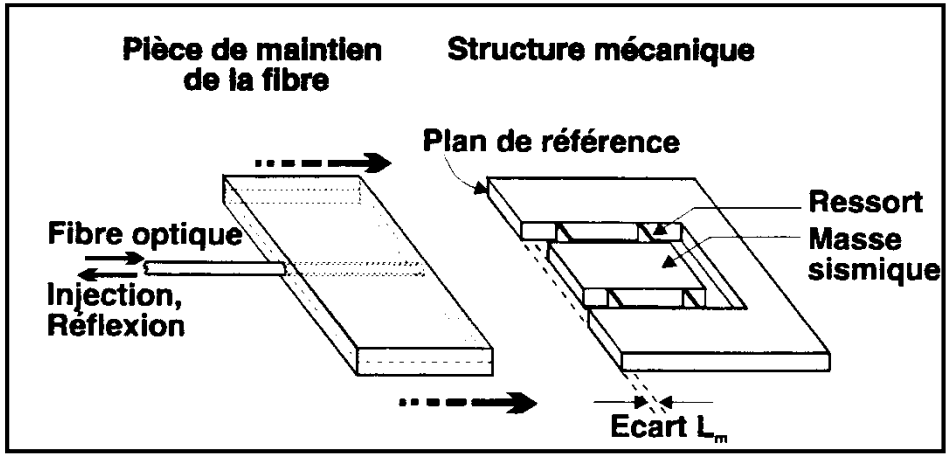

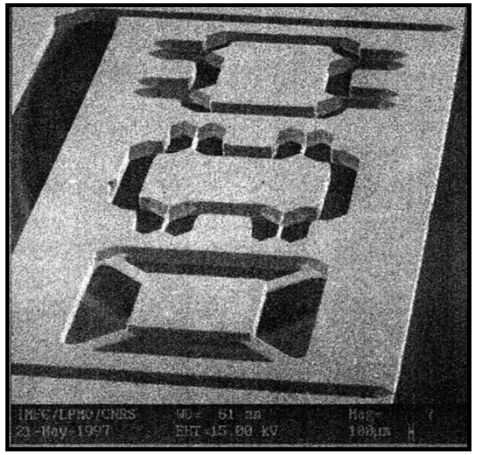

- **lectures and studies of both references :**

JOURNAL OF LIGHTWAVE TECHNOLOGY, VOL. 17, NO. 1, JANUARY 1999 10

A GaAlAs-GaAs Integrated Coherence Modulator

Sabry Khalfallah, *Associate Member, IEEE,* Pascal Dubreuil, Laurent Escotte, René Legros, Chantal Fontaine, Antonio Muñoz-Yagüe, Bruno Beche, and Henri Porte

Abstract—This paper presents a novel integrated III–V semiconductor waveguide modulator specially designed to generate optical delays of several hundred micrometers. This is achieved by simultaneous propagation of transverse electric (TE) and transverse magnetic (TM) lowest order modes in an original layered waveguide exhibiting a group birefringence greater than 0.02 at 1.3 μm. The device has 40% contrast, a switching voltage of 7 V with a 10-mm long electrode and is suitable for transmission and multiplexing of signals by coherence modulation of light in an optical fiber network powered by a short coherence source such as a superluminescent diode.

Index Terms—Birefringence, coherence modulation, electrooptic modulation, III–V compound semiconductors, multiplexing, optical delay, optical waveguide, superluminescent diodes.

15 August 1999

ELSEVIER

Optics Communications 167 (1999) 67–76

OPTICS COMMUNICATIONS

www.elsevier.com/locate/optcom

Highly unbalanced GaAlAs–GaAs integrated Mach–Zehnder interferometer for coherence modulation at 1.3 μm

Sabry Khalfallah [a,*,1], Pascal Dubreuil [a], Rene Legros [a], Chantal Fontaine [a], Antonio Munoz-Yagüe [a], Bruno Beche [b], Henri Porte [b], Rafal Warno [c], Miroslaw Karpierz [c]

[a] *Laboratoire d'Analyse et d'Architecture des Systemes du CNRS, 7, avenue du Colonel Roche, 31077 Toulouse Cedex, France*
[b] *Laboratoire d'Optique P.M.Duffieux, URA CNRS 214, UFR Sciences et Techniques Universite de Franche-Comte, 25030 Besançon Cedex, France*
[c] *Warsaw University of Technology, Pl. Politechniki 1, 00-661 Warsaw, Poland*

Received 15 April 1999; accepted 26 May 1999

Abstract

A novel integrated III–V semiconductor waveguide modulator specially designed to generate an optical delay of 100 μm is presented. This is achieved by simultaneous propagation of the TE fundamental mode in both of the arms of a highly unbalanced Mach–Zehnder interferometer with a 29 μm length difference between both arms. In order to minimize the losses in this complex curved structure, trenches were etched on the outsides of curved sections. The modulator has a contrast of 34%, a switching voltage of 6 V with a 10 mm long electrode and is suitable for the transmission and multiplexing of signals by coherence modulation of light in an optical fiber network powered by a short coherence source, such as a 1.3 μm superluminescent diode. © 1999 Published by Elsevier Science B.V. All rights reserved.

PACS: 42.79.Sz; 42.87.Bg; 42.82.Et; 85.60.Bt
Keywords: Coherence modulation; Electro-optic modulation; III–V compound semiconductors; Multiplexing; Mach–Zehnder interferometer; Optical delay; Optical waveguide; Superluminescent diodes

▪ III.2 : Microphotonic components

▪ III.2.1 Integrated optics in telecommunications applications : some examples

▪ **Y-junction element : symmetric 50 / 50 (or asymmetric (100-x) / x)**

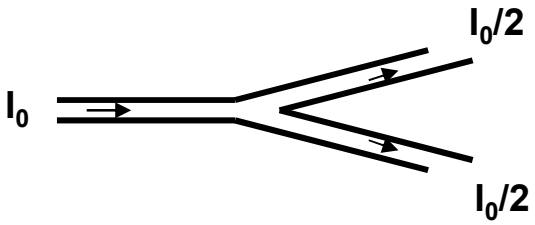

Such a role is to separate the optical beam. It can be noted that X-junctions are used too.

▪ **Fabry-Perot, Mach-Zehnder, and Michelson interferometers integrated versions**

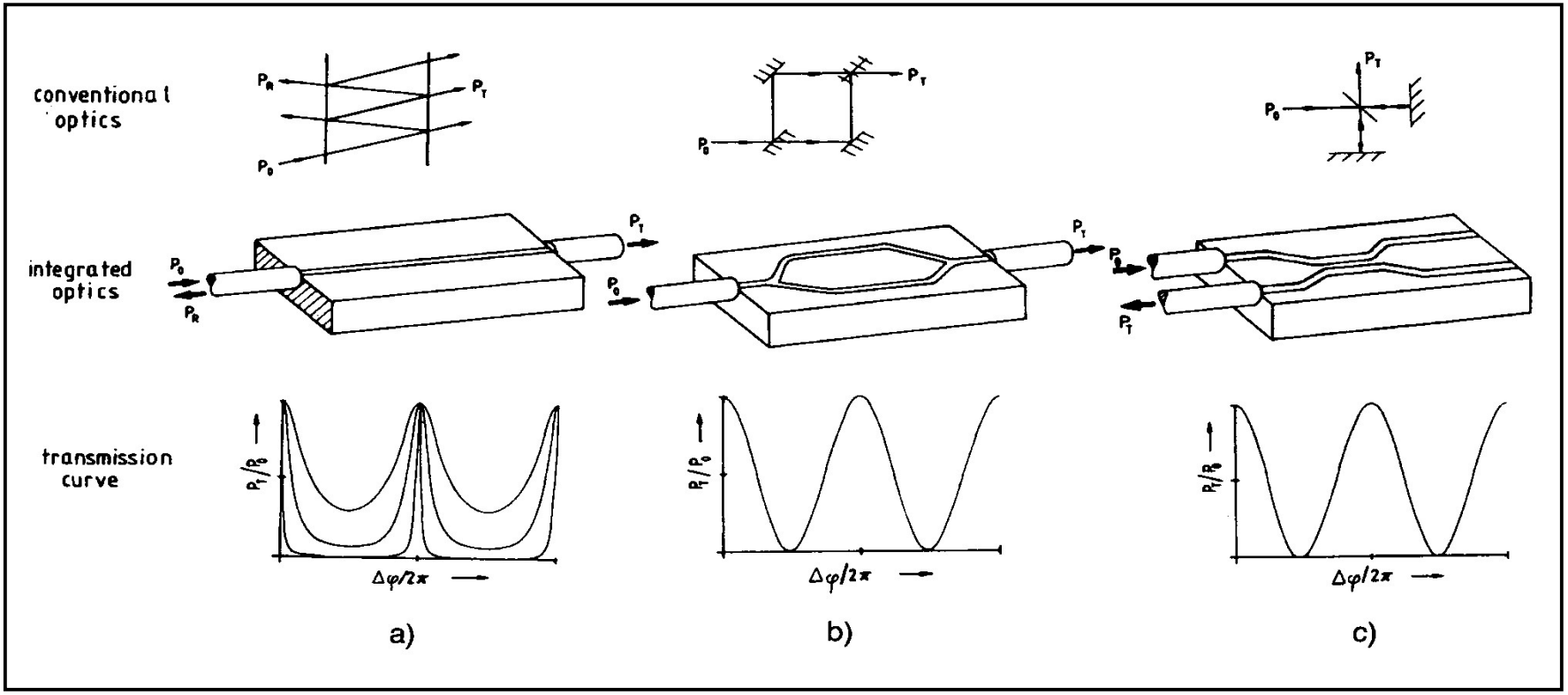

▪ Schematic diagram components in telecommunications applications ($LiNbO_3$ case)

Example 1 : a polarizer ➔ metal layer is deposited on the top of the waveguide (TM polarization is totally suppressed).

Note or example 2 of an another polarizer : by using the exchange-proton technique on $LiNbO_3$, n_e increases and such corresponding polarization is guided and n_O decreases and the other polarization can became a radiation field respectively).

Example 3 : a phase modulator ➔ an electrode changes the effective propagation constant β and print the information (modulation) on the physical attribute 'phase'.

Example 4 : a intensity MZ modulator (symmetric) ➔ the wave is splited at the Y-junction. On one of the arm waveguide, an electrode change the effective index of the 'perturbed' optical mode (➔ delay, see phase modulation at this level). Then, the two waves is recombined by an another Y-juntion and create interferences or intensity modulation that can be detected on a photodiode.

Note or example 5 : An un-balanced MZ structure will operate in coherence modulation schema.

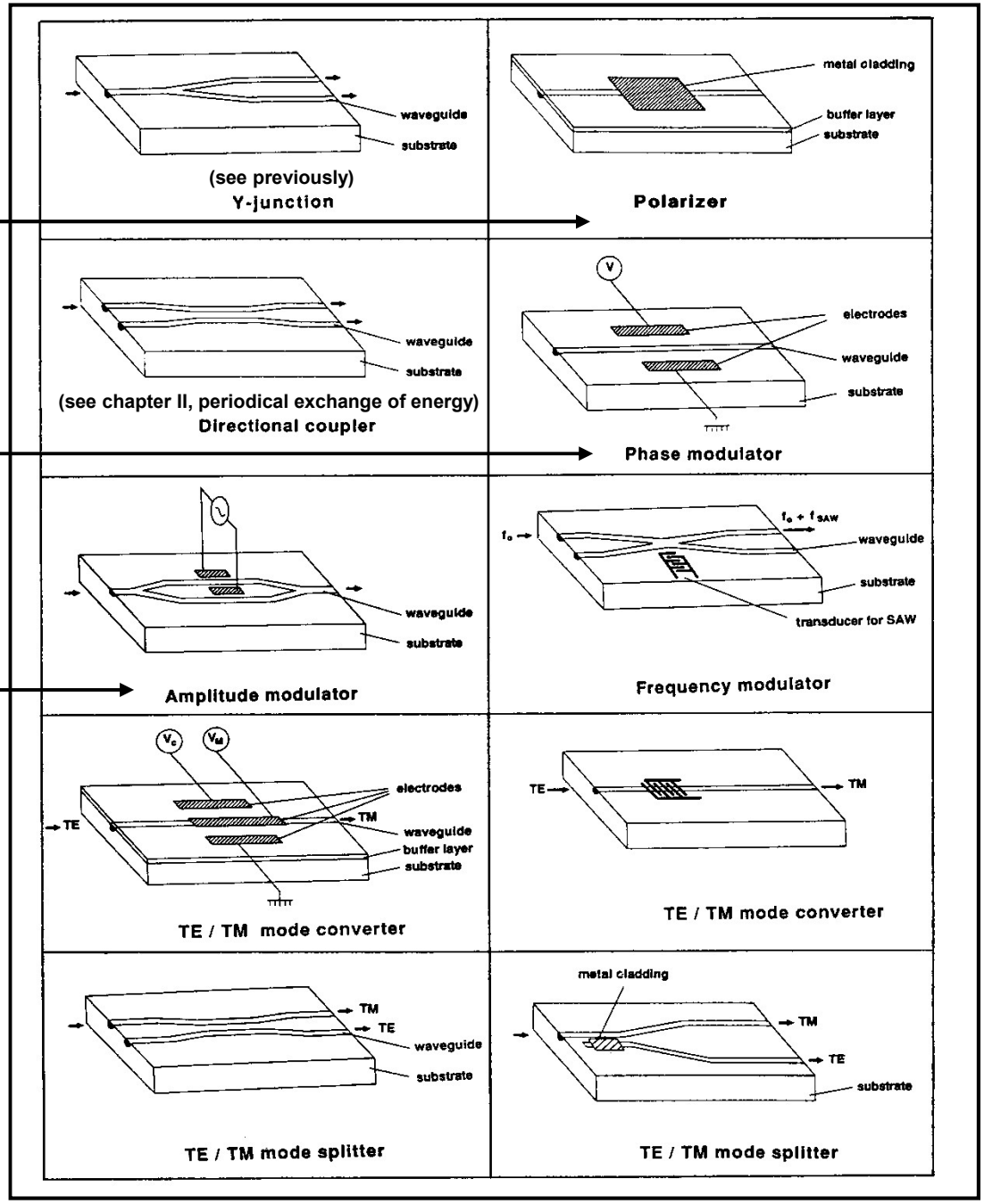

Example 6 : a polarization converter operate with three planar electrodes. A electric field is applied horizontally and allow the energy transfer (coupling process) from a polarization to the another in the same waveguide. A second electrode creates a vertically electric field that optimizes the phase matching condition $\Delta\beta=\beta_{TE}-\beta_{TM}$ (see chapter II) and allow to obtain a 100% efficiency in polarization conversion.

Example 7 : a polarization converter and a tunable filter (WDM applications) ➔ TE-TM conversion can be obtain by inter- or digital electrodes of Λ-periodicity by using the integrated version of the Sölc bulk filters (based on electrooptic effect). In such a case, the quasi-phase matching condition defined infra is obtain by the effective-geometric wave vector $2\pi/\Lambda$. Acoustooptic effect can be used, Λ_a will represent the real wavelength of acoustic wave. The tunable filter function is obtain by changing one of the $\beta_{(TE\ orTM)}$ attribute in the quasi-phase-matching condition [III.11] for example by an another planar electrode (electrooptic) or a shift of acoustic frequency ν_a on the digital transducers (acoustooptic effect).

Quasi-Phase Matching (QPM) condition

$$\beta_{TE}(\lambda_0)-\beta_{TM}(\lambda_0)=\frac{2\pi}{\Lambda}\equiv K \quad \text{or} \quad \beta_{TE}(\lambda_0)-\beta_{TM}(\lambda_0)=\frac{2\pi}{\Lambda_a}=\frac{2\pi\nu_a}{v_a} \qquad \text{[III-11]}$$

Tunable functions

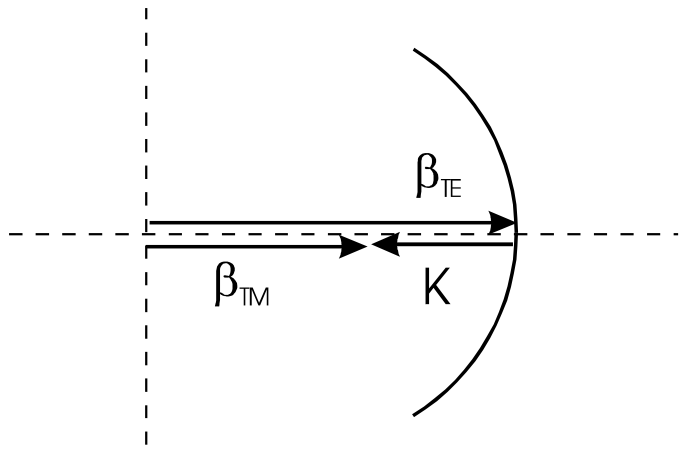

- **lectures and studies of the references :**

820 IEEE JOURNAL OF QUANTUM ELECTRONICS, VOL. 35, NO. 5, MAY 1999

A Tunable Filter with Collinear Acoustooptical TE–TM Mode Conversion in a GaAs–AlAs Multiquantum-Well Waveguide

Bruno Beche, Henri Porte, Jean-Pierre Goedgebuer, and Chantal Fontaine

Abstract—**We investigate theoretically an acoustooptic tunable filter (AOTF) based on TE–TM mode conversion by collinear acoustooptic interaction, using the high form birefringence that occurs in a GaAs–AlAs multiquantum-well (MQW) rib waveguide. Mode conversion is achieved using a transverse piezoelectric surface acoustic wave. We propose to use a piezoelectric layer (ZnO or AlN) of 6-mm symmetry, which can be deposited by plasma-enhanced chemical vapor deposition. The *c* axis is then parallel to the plane of the layer. Under this condition, a transverse piezoelectric surface acoustic wave excited by inderdigital electrodes can propagate within the GaAs–AlAs MQW optical waveguide. TE–TM conversion is then possible with a relatively low acoustic frequency (some tens of megahertz), yielding a high diffraction efficiency and a figure of merit 14 times higher than that of conventional $LiNbO_3$ filters based on AOTF's.**

Index Terms—**Acoustooptics, multilayers, tunable filters.**

15 November 2000

ELSEVIER

Optics Communications 185 (2000) 325–329

OPTICS COMMUNICATIONS

www.elsevier.com/locate/optcom

A tunable filter with electrooptical TE–TM mode conversion in a GaAs/AlAs multiquantum-well waveguide

B. Bêche [a,*], E. Gaviot [a], N. Grossard [b], H. Porte [b]

[a] *ENSIM – Micro_Cap_Ouest, Laboratoire d'Acoustique de l'Université du Maine, LAUM – UMR CNRS 6613, 72000 Le Mans, France*
[b] *Laboratoire d'Optique P.M. Duffieux UMR CNRS 6603, Université de Franche Comté, 25000 Besançon, France*

Received 27 July 2000; accepted 19 September 2000

Abstract

In this paper, the theoretical study of a new electrooptic tunable filter based on TE–TM mode conversion, and the high form birefringence that occurs in a GaAs/AlAs multiquantum-well waveguide is presented. Then TE–TM conversion can be achieved with a relatively low voltage (30 V). Such a filter shows off a tuning rate voltage ranging around 7 V/channel, and as regards selectivity a 1.3 nm filter bandwidth can be obtained. © 2000 Elsevier Science B.V. All rights reserved.

Keywords: Electrooptic effect; Multilayers; Integrated optics; Tunable filters

830 IEEE PHOTONICS TECHNOLOGY LETTERS, VOL. 13, NO. 8, AUGUST 2001

AlGaAs–GaAs Polarization Converter with Electrooptic Phase Mismatch Control

Nicolas Grossard, Henri Porte, Jean-Pierre Vilcot, Bruno Bèche, and Jean-Pierre Goedgebuer

Abstract—**In this letter, we designed and fabricated an electrooptic transverse magnetic-transverse electric mode converter with phase mismatch control integrated in AlGaAs GaAs. The electrode scheme, which is reported for the first time in such a device, insures a high polarization conversion efficiency with low-driving voltages.**

Index Terms—**Electroooptic modulators, integrated optics, modal birefringence, polarization, semiconductor waveguides.**

Example 8 : PHASAR for WDM applications ➔ principle developed in course

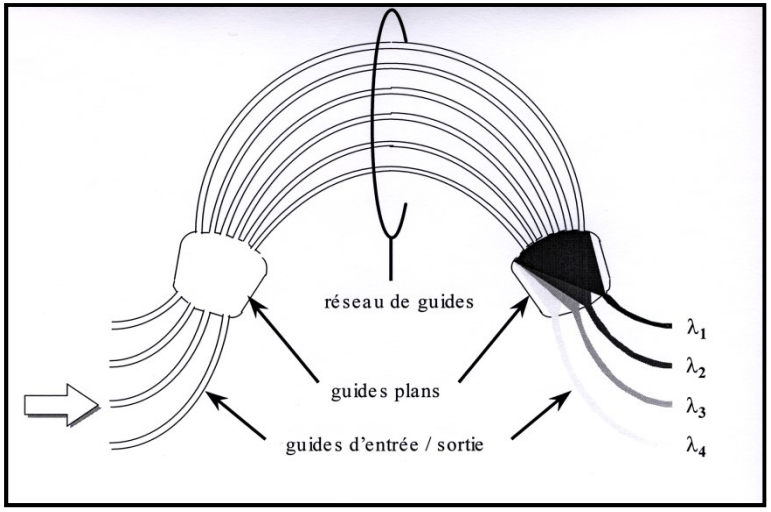

Symmetric components composed of two-star-couplers (n × m) waveguides, two free-propagation areas, and a tunable array of waveguides.

As an example : wavelength de-multiplexing applications

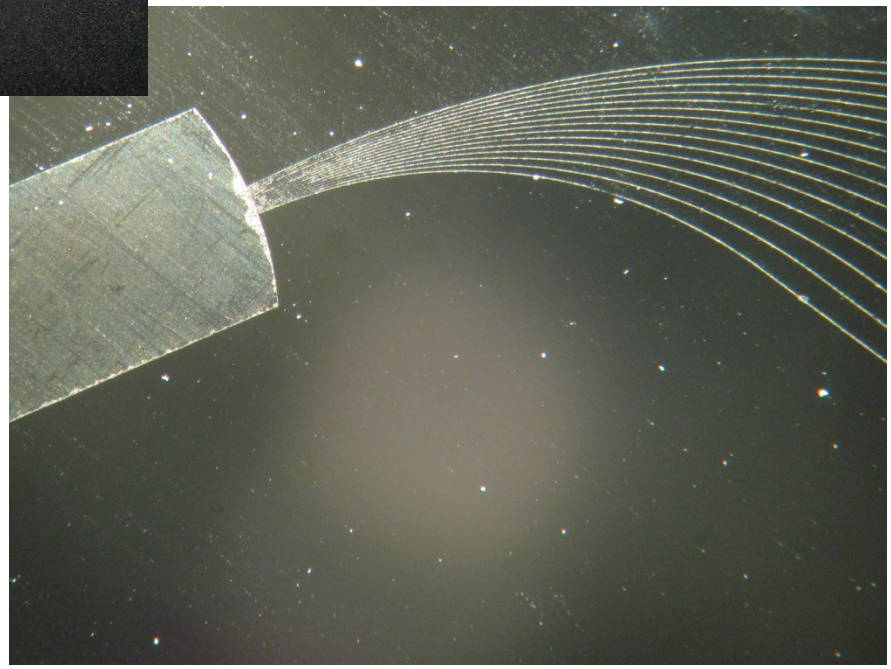

▪ III.2.2 Integrated optics in measurements and sensors applications : some examples

▪ **Introduction : the principles (detection and architecture) are equivalent to the telecom applications but the idea is to use the optical wave as a probe for the measurement or detection of an information conversely to a print of information for transmissions and telecommunications. The physical or chemical attributes to measure are various, gas detections, liquid, chemical- or bio- species (DNA), biomedical detection, gage pressure measurements, acceleration, humidity, magnetic field (using magneto-optic effect), thermal flux, and so on…**

▪ **Gas sensors**

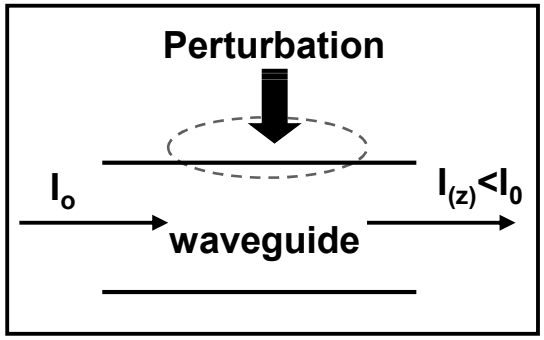

Principle : evanescent wave = probe for the detection applications ➔ radiation field / $I_{(z)}<I_0$.

- Example with a reference arm in order to compare the intensity (H_2 detection ➔ 20 ppm) :

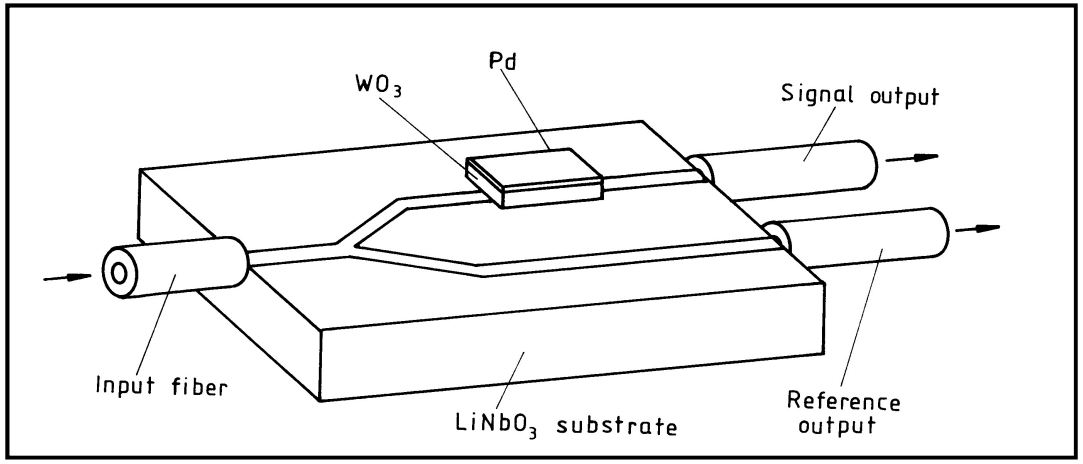

- Examples of NH_3 detection by a polaronic effect or resonance on a polymeric conductor

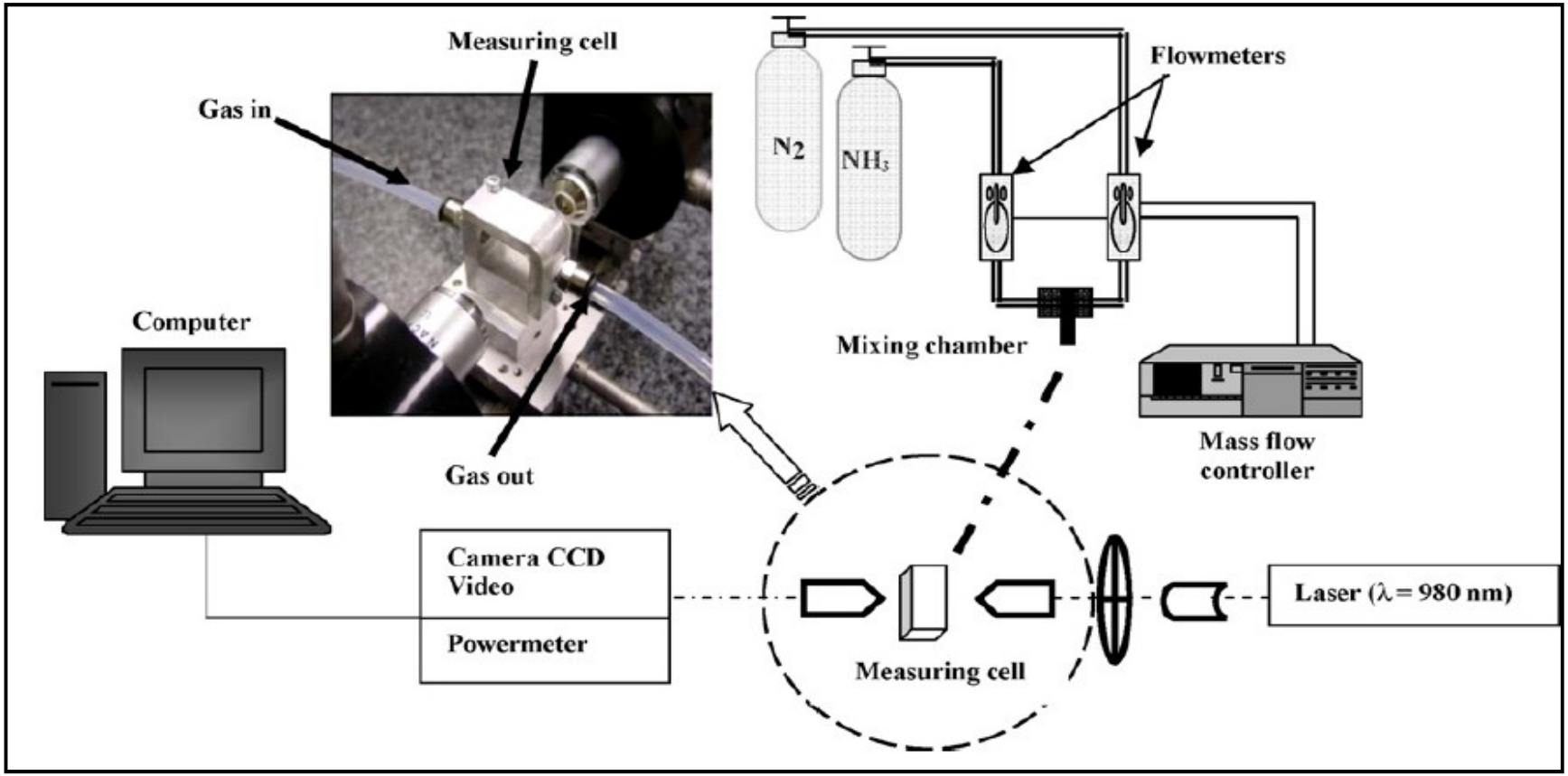

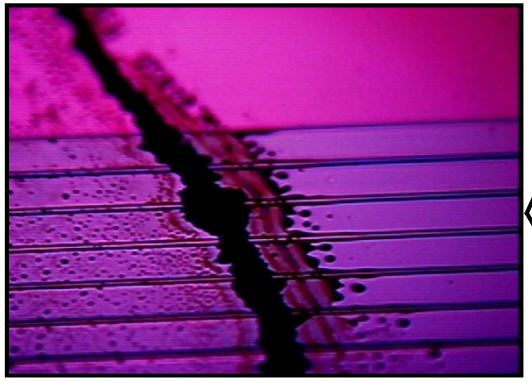

SU8 core /PMMA upper cladding-I /PANI upper cladding-II

[Various families]

SU8 core /composite upper cladding [PMMA/PANI]

- Kinetic measurements of the (de)-absorption of the NH_3 gas

$$T_{opt} \propto \Psi(t,C) \equiv \frac{N(t)}{N^*} = A\left[1 - e^{-(t/t_A)}\right]$$

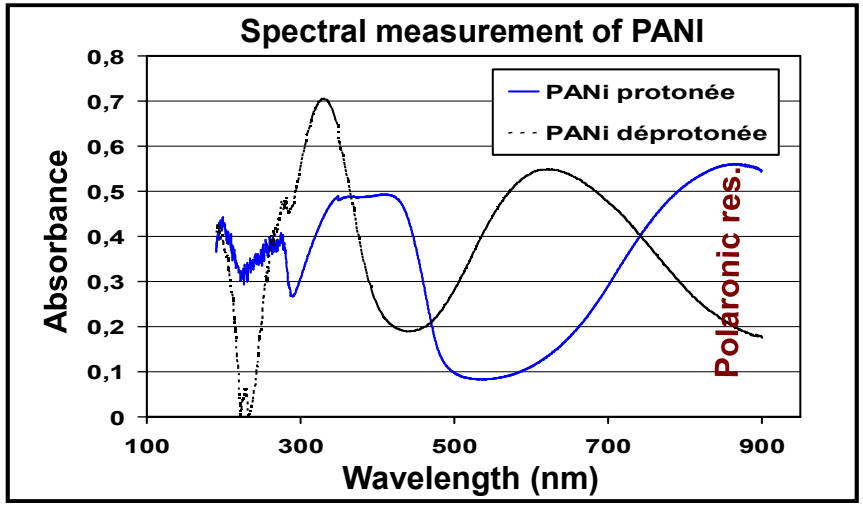

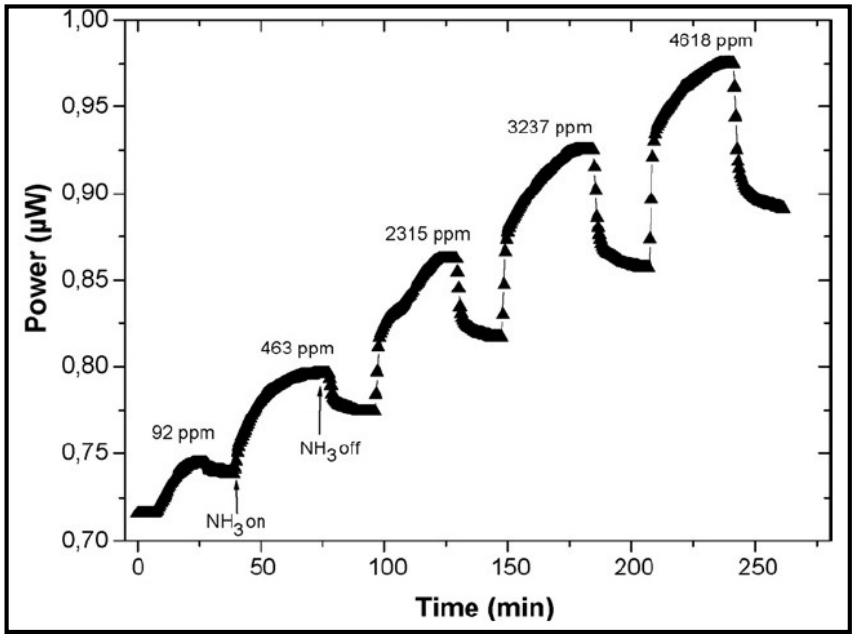

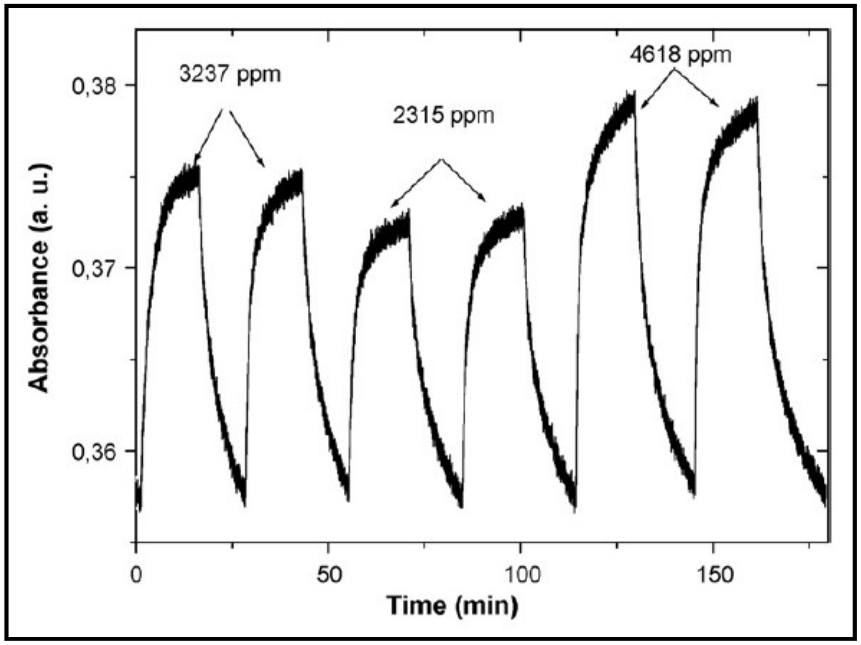

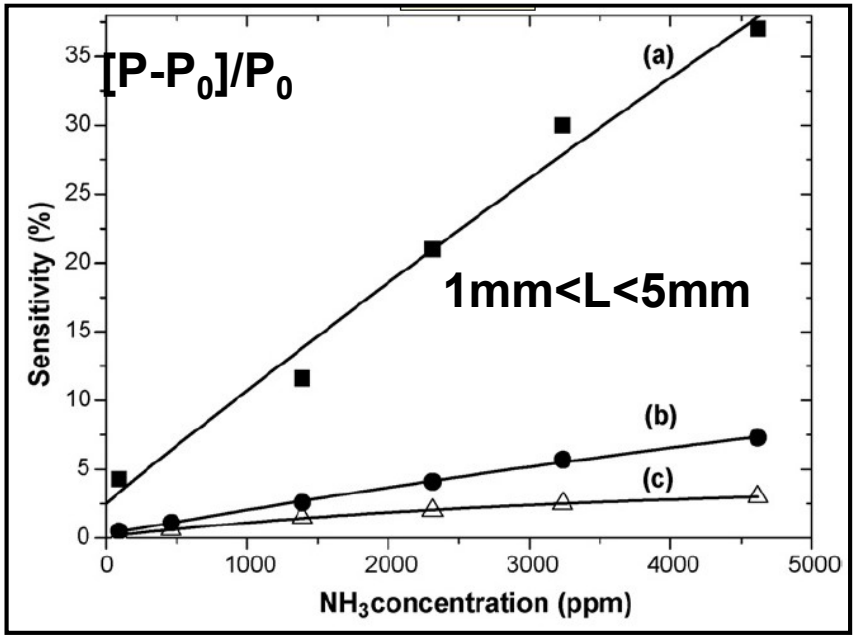

- **lectures and studies of the references :**

Talanta 76 (2008) 314–319

Contents lists available at ScienceDirect

Talanta

journal homepage: www.elsevier.com/locate/talanta

A new evanescent wave ammonia sensor based on polyaniline composite

A. Airoudj[a,b], D. Debarnot[a,*], B. Bêche[c], F. Poncin-Epaillard[a]

[a] Laboratoire Polymères, Colloïdes, Interfaces, UMR 6120, Université du Maine, Avenue Olivier Messiaen, 72085 Le Mans, France
[b] Laboratoire d'Acoustique de l'Université du Maine, UMR-CNRS 6613, Avenue Olivier Messiaen, 72085 Le Mans, France
[c] Laboratoire PALMS-GMCM, UMR-CNRS 6627-6626, Institut de Physique de Rennes, 35042 Rennes, France

ARTICLE INFO

Article history:
Received 18 December 2007
Received in revised form 19 February 2008
Accepted 26 February 2008
Available online 18 March 2008

Keywords:
Ammonia detection
Polymer sensitive layer
Planar waveguide sensor
Light power variations

ABSTRACT

A single-mode TE_0–TM_0 optical planar waveguide ammonia sensor based on polyaniline/polymethyl methacrylate (PANI/PMMA) composite is designed and developed. The sensing properties of the photonic sensor to ammonia at room temperature are studied. A significant change is observed in the guided light output power of the sensor after it is exposed to ammonia gas. The metrological parameters (sensitivity, response time and recovery time) of the sensor are strongly influenced by the interaction length (length of sensing region). Compared with the conventional optical ammonia sensor based on absorption spectroscopy, the integrated optical sensor is more sensitive to ammonia.

© 2008 Elsevier B.V. All rights reserved.

ANALYTICA CHIMICA ACTA 626 (2008) 44–52

available at www.sciencedirect.com

ScienceDirect

journal homepage: www.elsevier.com/locate/aca

New sensitive layer based on pulsed plasma-polymerized aniline for integrated optical ammonia sensor

A. Airoudj[a,b], D. Debarnot[a,*], B. Bêche[c], F. Poncin-Epaillard[a]

[a] Laboratoire Polymères, Colloïdes, Interfaces, UMR 6120, Université du Maine, Avenue Olivier Messiaen, 72085 Le Mans, France
[b] Laboratoire d'Acoustique de l'Université du Maine, UMR 6613, Avenue Olivier Messiaen, 72085 Le Mans, France
[c] Institut de Physique de Rennes, Université de Rennes I, IPR UMR CNRS 6251, 35042 Rennes, France

ARTICLE INFO

Article history:
Received 12 March 2008
Received in revised form
21 July 2008
Accepted 22 July 2008
Published on line 6 August 2008

Keywords:
Polyaniline
Plasma polymerization
Planar waveguide
Integrated optical sensor
Ammonia sensor

ABSTRACT

A new integrated optical sensor based on plasma-polyaniline sensitive layer for ammonia detection is designed and developed. The sensor is based on polyaniline elaborated by the plasma technique (Plasma Enhanced Chemical Vapor Deposition, PECVD) and deposited on a small section of a single-mode planar SU-8 waveguide. The sensing properties of the integrated optical sensor to ammonia at room temperature are presented. A significant change in the guided light output power of the sensor is observed after exposition to ammonia gas. This new ammonia sensor exhibits fast response and recovery times, good reversibility and repeatability. The metrological parameters (sensitivity, response time and recovery time) of the sensor are strongly influenced by the interaction length (length of sensing region), the type of dopant and the light polarization. The sensor has a logarithmic linear optical response within the ammonia concentration range between 92 and 4618 ppm.

© 2008 Elsevier B.V. All rights reserved.

Optics Communications 282 (2009) 3839–3845

Contents lists available at ScienceDirect

Optics Communications

journal homepage: www.elsevier.com/locate/optcom

Integrated SU-8 photonic gas sensors based on PANI polymer devices: Comparison between metrological parameters

A. Airoudj [a,b,*], B. Bêche [c], D. Debarnot [a], E. Gaviot [b], F. Poncin-Epaillard [a]

[a] Laboratoire Polymères, Colloïdes, Interfaces, UMR–CNRS 6120, Université du Maine, Avenue Olivier Messiaen, 72085 Le Mans, France
[b] Laboratoire d'Acoustique de l'Université du Maine, UMR–CNRS 6613, Avenue Olivier Messiaen, 72085 Le Mans, France
[c] Institut de Physique de Rennes, IPR UMR–CNRS 6251, Université de Rennes, 35042 Rennes, France

ARTICLE INFO

Article history:
Received 24 March 2009
Received in revised form 15 June 2009
Accepted 16 June 2009

Keywords:
Integrated photonics
Sensor components
Polyaniline
SU-8 polymer
Ammonia detection

ABSTRACT

In this work, we have designed and developed three families of integrated photonic sensors for ammonia detection. These photonic sensors are integrated onto single-mode TE_0–TM_0 SU-8 polymer planar waveguides and based on a polyaniline (PANI) sensitive polymer material. The first family relies on the deposit of a PANI–polymethyl methacrylate (PMMA) composite sensitive layer on a given SU-8 waveguide. The second family relies on a PMMA passive layer deposited on the SU-8 waveguide before applying the PANI sensitive layer on the PMMA passive layer. The third family takes advantage of a PANI layer deposited by plasma technique directly onto the SU-8 waveguide. The working principle of such sensors is based on the optical intensity modulation induced within the single-mode waveguide owing to the interaction between the evanescent field and the sensitive layer. The sensing proprieties of these integrated photonic sensors to ammonia gas at room temperature were characterized and the comparison between these different families of photonic sensors is presented. Experimental results show that the sensor based on new plasma–PANI as sensitive layer has the better metrological parameters.

© 2009 Elsevier B.V. All rights reserved.

▪ **Liquid and bio- species detection by a coupling between the grating and the waveguide (coupling between the optical field on the third direction with the guided modes)**

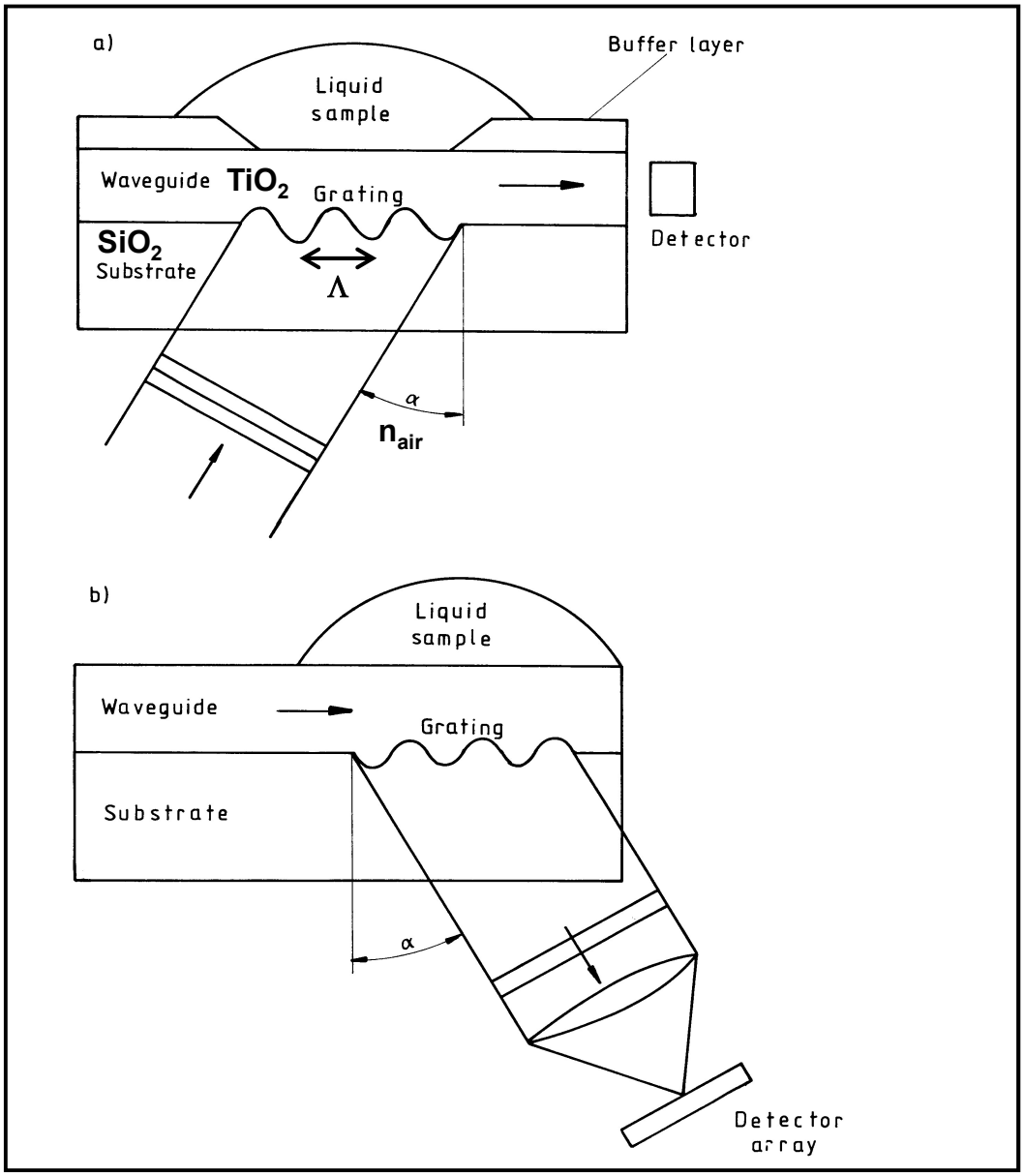

[III-12]

$$n_{eff\,(mode\,guidé)} = n_{air} \sin\alpha + m\frac{\lambda_0}{\Lambda}$$

with, m integer and diffraction order, Λ periodicity of the grating.

For the detection, variation on the n_{eff} value implies various α-angles [III-12] that can be detected by a array of photodiodes

Note : This schematic detection can be used for the measurement of index change of liquid ($\Delta n=10^{-6}$)

- **Pressure measurements and sensors based on MZ structures**

TE_{00} (λ_0=980 nm)

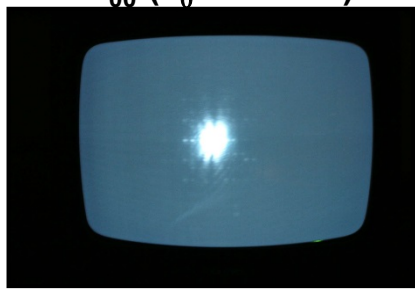

Upper view

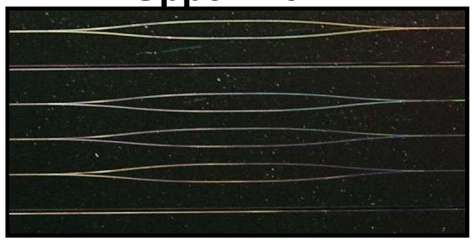

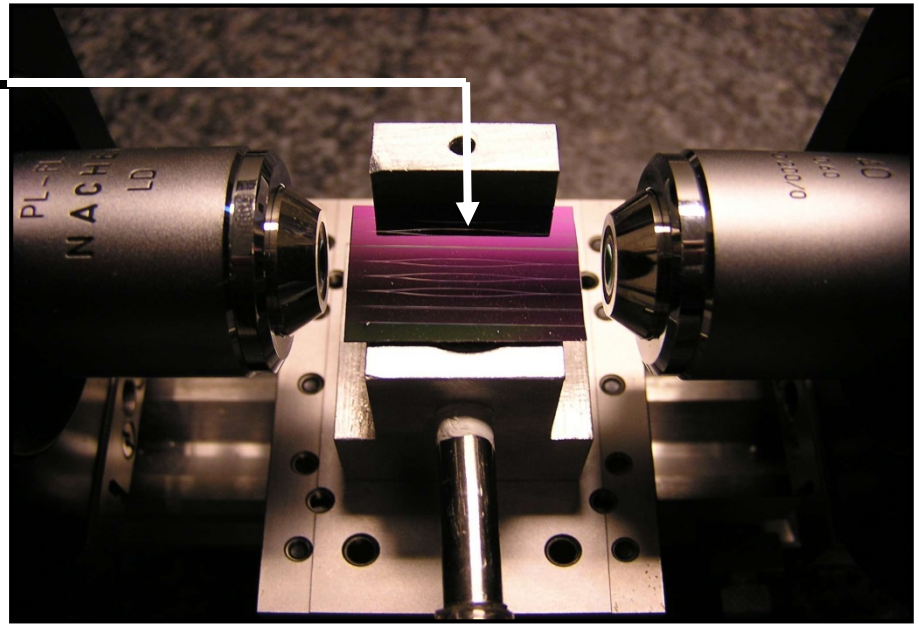

Propagation single-mode TE_{00}/TM_{00}
High optical confinement

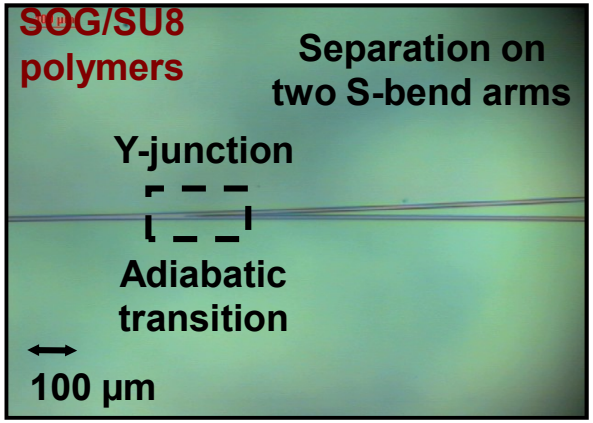

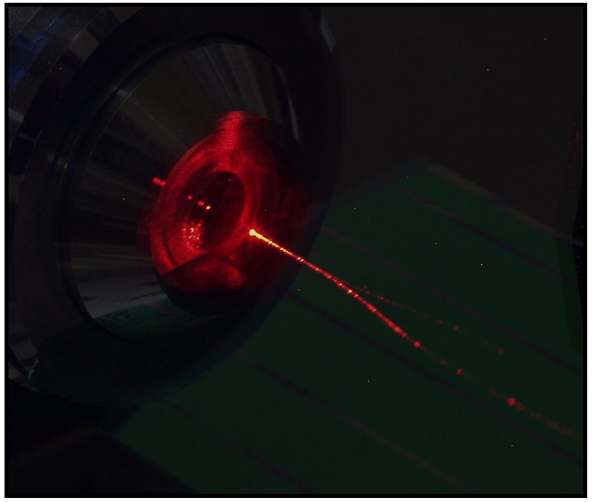

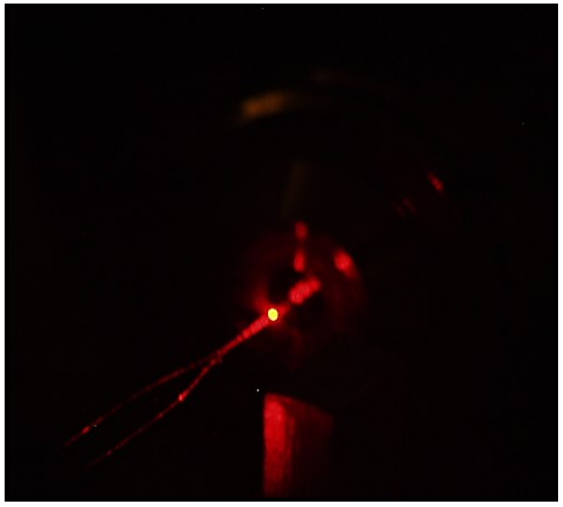

[III-13]

$$\nabla^4 u(x_2, x_3, t) = \frac{P}{D} \qquad D = \frac{e^3 E}{12(1-\nu^2)} \longrightarrow P = \frac{E}{1-\nu}\frac{e^3 h_0}{a^4}\left(\frac{1}{12\alpha(1+\nu)} + C\frac{h_0^2}{e^2}\right)$$

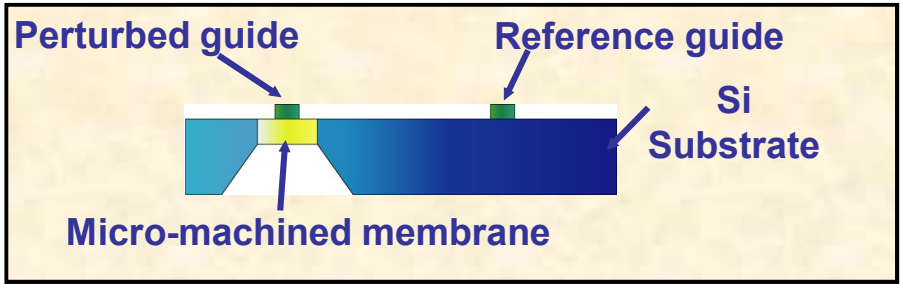

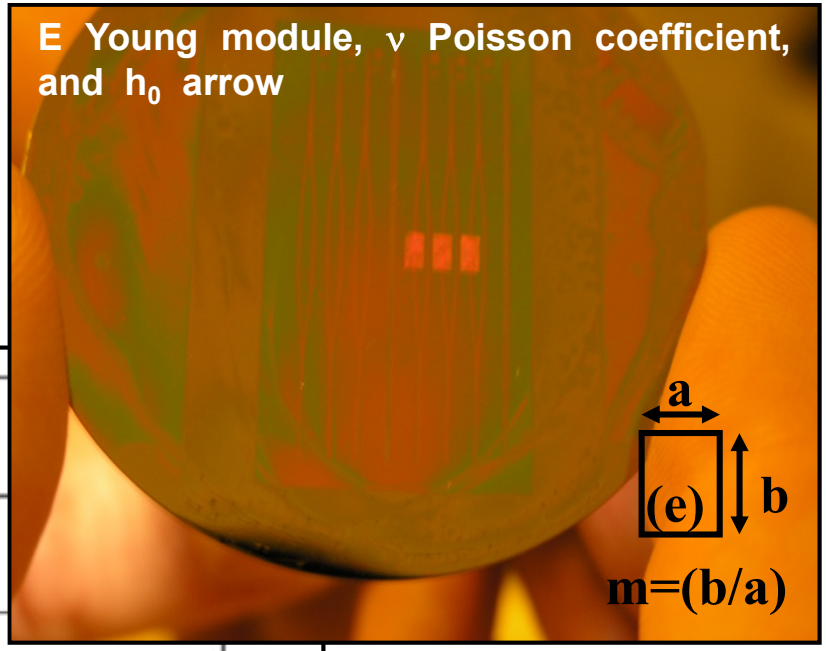

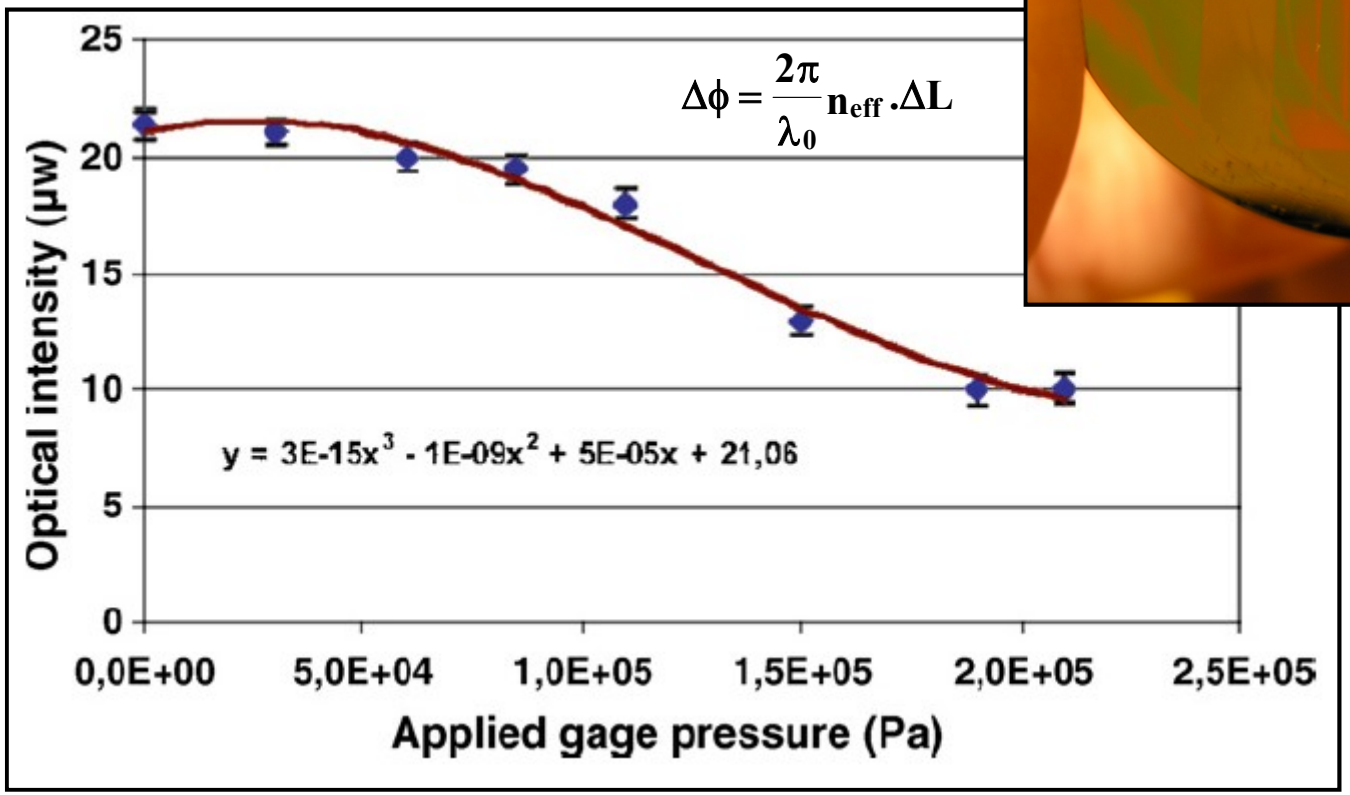

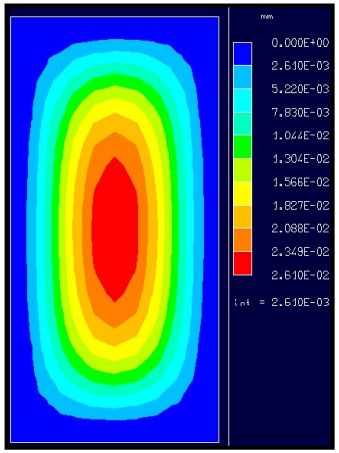

- **lectures and studies of the references :**

IEEE SENSORS JOURNAL, VOL. 6, NO. 3, JUNE 2006

Single-Mode Rib Optical Waveguides on SOG/SU-8 Polymer and Integrated Mach–Zehnder for Designing Thermal Sensors

N. Pelletier, B. Bêche, E. Gaviot, L. Camberlein, N. Grossard, F. Polet, and J. Zyss

Abstract—This paper presents a successful design, realization, and characterization of single-mode rib optical waveguides on SOG/SU-8 polymers in order to highlight a new approach to designing heat sensors. The basic principle of this new thermal-sensing method relies on the differential thermal behavior regarding both acting arms of a micro Mach–Zehnder Interferometer (MZI). First, two families of single-mode straight rib waveguides composed of SOG/SU-8 polymers are analyzed. Hence, optical losses for TE_{00} and TM_{00} optical modes for structures on $Si/SiO_2/SU-8$ have been estimated respectively as $1{,}36 \pm 0{,}02$ and $2{,}01 \pm 0{,}02$ dB $\cdot$ cm^{-1}, while the second one composed of $Si/SiO_2/SOG/SU-8$ presented losses of $2{,}33 \pm 0{,}02$ and $2{,}95 \pm 0{,}02$ dB $\cdot$ cm^{-1}. Then, owing to modeling results, an experimental sensor is realized as an integrated device made up of SU-8 polymer mounted on a standard silicon wafer. When subjected to a radiant source, as a laser light (980 nm) is injected across the cleaved input face of the MZI, the significant change of output signal allows us to consider a new approach to measuring radiant heat flow rate. Experimental results are given regarding the obtained phase shift against the subjected thermal power. According to the modeling results, one can expect new highly sensitive devices to be developed in the next coming years, with advantageous prospective industrial applications.

Index Terms—Heat flow rate sensor, integrated optics, Mach–Zehnder interferometer (MZI), optical losses measurement, optical rib waveguides, polymer, spin-on-glass (SOG), SU-8.

Available online at www.sciencedirect.com
ScienceDirect
Sensors and Actuators A 135 (2007) 179–184
SENSORS AND ACTUATORS A PHYSICAL
www.elsevier.com/locate/sna

SU-8 waveguiding interferometric micro-sensor for gage pressure measurement

N. Pelletier[a,*], B. Bêche[b], N. Tahani[a], J. Zyss[c], L. Camberlein[a], E. Gaviot[a]

[a] *Laboratoire d'Acoustique de l'Université du Maine, Micro_Cap_Ouest, LAUM UMR CNRS 6613, 72085 Le Mans, France*
[b] *Institut de Physique, Université de Rennes1, GMCM-PALMS UMR CNRS 6626-6627, 35042 Rennes, France*
[c] *Laboratoire de Photonique Quantique et Moléculaire, LPQM UMR CNRS 8537, ENS-Cachan, 94235 Cachan, France*

Received 2 February 2006; received in revised form 14 June 2006; accepted 5 July 2006
Available online 5 September 2006

Abstract

The authors present a successful modeling, realization and characterization of a new micro-sensor based on a convenient optical principle, namely an integrated Mach–Zehnder interferometer (MZI). This MZI device is designed with a view to measuring pressure disturbances due to optical path variations. Such a system is arranged in order to work in intensity modulation scheme. Moreover, the MZI is made up of straight and bent rib optical waveguides composed of SU-8 polymer. The mainstay of the device is based on differential measurements performed by a sensing arm arranged with a micromachined membrane and actuated by a given pressure disturbance, while the second arm of the interferometer is considered as a reference one. The main parameters of each element are given by way of two modeling approaches: an optical modeling with a semi-vectorial finite difference method together with a conformal transformation, and a mechanical modeling with a finite-element method associated to the mechanical theory of membranes. So, as the pressure to be measured is applied upon the diaphragm, an optical path variation of the acting arm is induced. After the combination of both signals, the variation at the output of the system is measured. A prototype is characterized by way of a micro-optical injection bench specifically designed to allow an efficient end-fire coupling into the waveguides.
© 2006 Elsevier B.V. All rights reserved.

Keywords: Microtechnologies; Integrated optics; SU-8 polymer; Optical sensor; Mach–Zehnder interferometer; Micromachined membrane; Gage pressure sensor

▪ III.2.3 Integrated optics with micro-resonators (2D, 2.5D and 3D), whispering gallery modes

▪ **Micro-resonators** = seductive objects to control the electromagnetic fields, meaning localization or strong confinement into a restricted V space-volume allowing a quantification on optical modes (called whispering gallery modes'), and increase of their life time τ into such cavities

➔ Merit factor of an optical mode : $$F = \frac{(\tau / V)}{(T / \lambda^3)} \propto \text{Purcell factor}$$ [III-14]

▪ Theoretical aspects in QED (discrete modes coupling electromagnetic modes and atomic) ➔ Rabi oscillation and intricated states ; Application aspects on physical cavities and Laser (spontaneous recombination / stimulate), in optical telecommunications ((de)-multiplexing in wavelength or filters), in sensors (optical probe strongly localized and interactive➔ measurements with shift of the resonance), and so on..

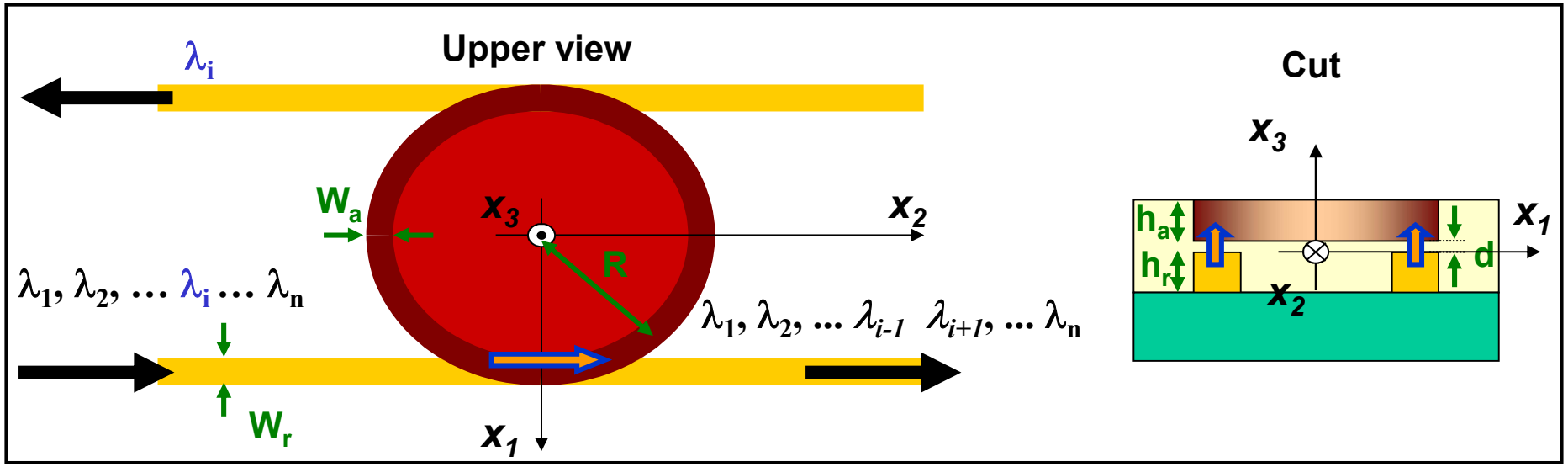

- Notion of evanescent wave (probe) and optical tunnel effect: $e^{(-x/d)}$

$$d < \left(\frac{\lambda}{2\pi}\right)\left(n_{eff}^2 - n_{gaine}^2\right)^{-1/2}$$ [III-15]

$(d \approx [10 - 150]\text{nm for optical } \lambda_0) \longrightarrow$ e-beam technology for 2D

[III-16]

- Principle : spectral resonance: $$FSR = \frac{\lambda_0^2}{2\pi R n_{eff,gpe}}, \quad \delta\lambda = \frac{\lambda_0^2}{2\pi^2 R n_{eff,\varphi}}\left(\frac{1}{|\tau|}e^{\alpha\pi R} - |\tau| e^{-\alpha\pi R}\right)$$

▪ Conceptions on polymers 2.5D micro-structures (ring, disk) by Ar and O_2 plasma treatments:

➔ Surface energy modification and measurements ($J.m^{-2}$) : $[\gamma = (\partial G/\partial S)_{T,p,n}]$

Dispersive contribution $\gamma^{d-(LW)}$ (forces London Van der Waals)

No-dispersive contribution (or polar) γ^{nd} (Keesom interactions, Debye forces, H-atoms attraction / H_2O, Acido-Basic interactions] $\gamma^{AB} = 2.\left[\gamma^+\gamma^-\right]^{1/2}$

$\gamma^{T-(totale)} \equiv \sum \text{contributions}$

2d Newton law or PFD ($F=\gamma L$)

➔ Young equation at the three interfaces

$$\gamma_S = \gamma_{SL} + \gamma_L \cos(\theta)$$ [III-17]

mesureaments

Van Oss Model (or Acido-Basic)

$$\gamma_{SL} = \gamma_S + \gamma_L - 2\left[\left(\gamma_L^{d-(LW)}\gamma_S^{d-(LW)}\right)^{1/2} + \left(\gamma_L^{nd(+)}\gamma_S^{nd(-)}\right)^{1/2} + \left(\gamma_S^{nd(+)}\gamma_L^{nd(-)}\right)^{1/2}\right]$$

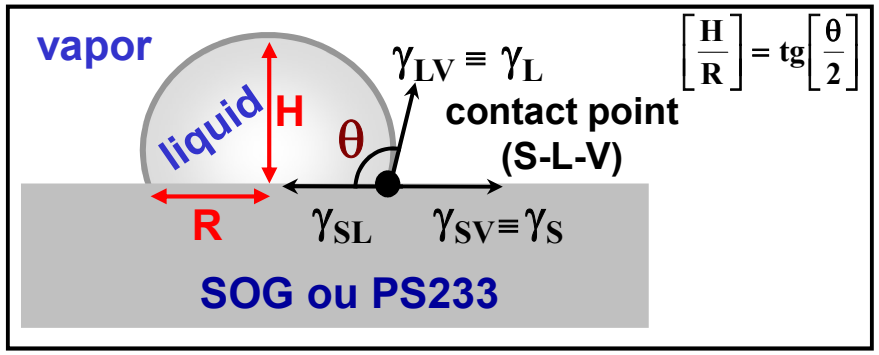

Reference liquid	$\gamma^{T-(total)}$	$\gamma^{d-(LW)}$	$\gamma^{nd(+)}$	$\gamma^{nd(-)}$
Water	72.8	21.8	25.5	25.5
Glycerol	63.3	34.0	3.92	57.4
Diiodomethane	50.8	50.8	0.0	0.0

(Unity : $mJ.m^{-2}$)

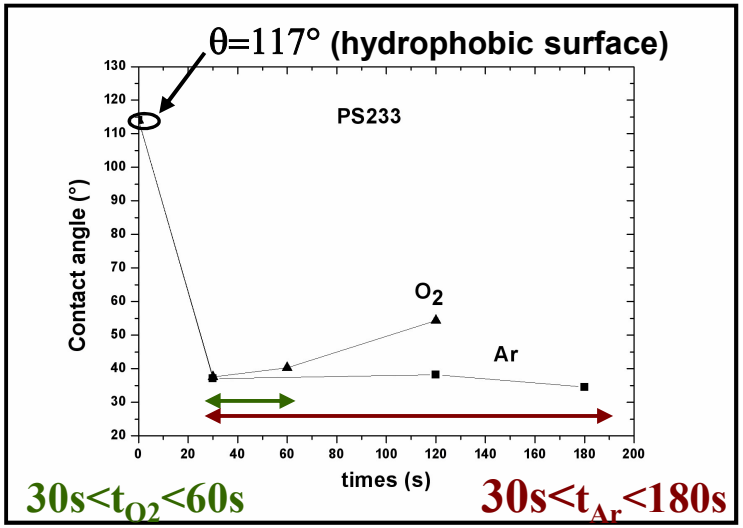

[θ_{water}]

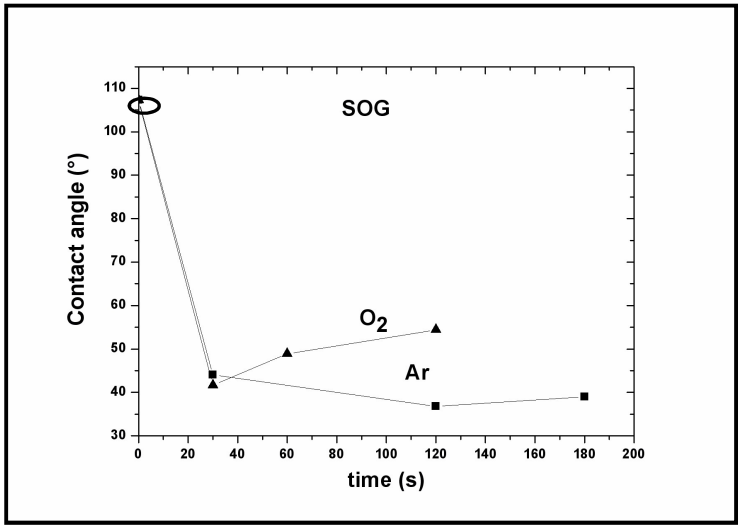

[γ_S/O_2]

maximum

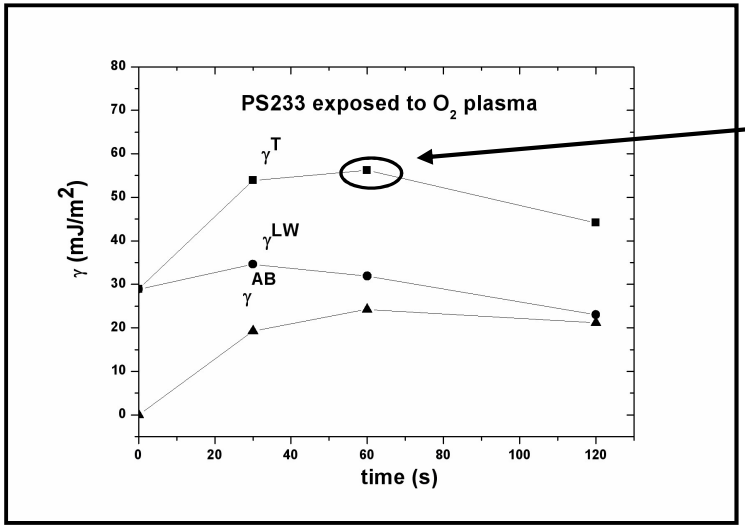

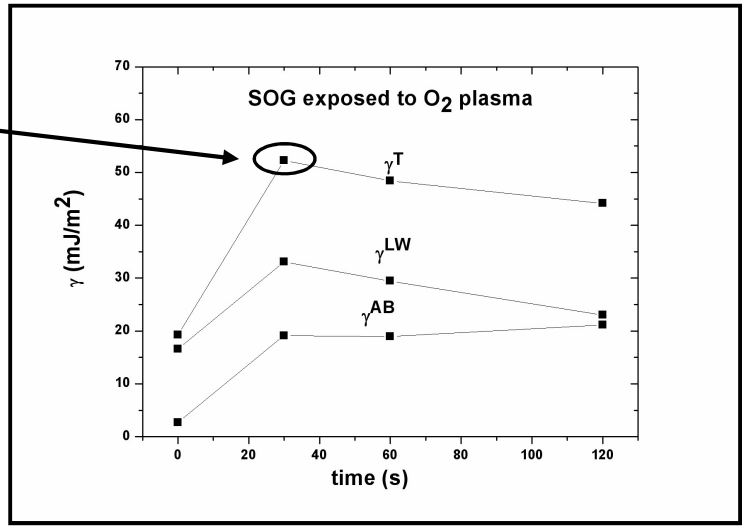

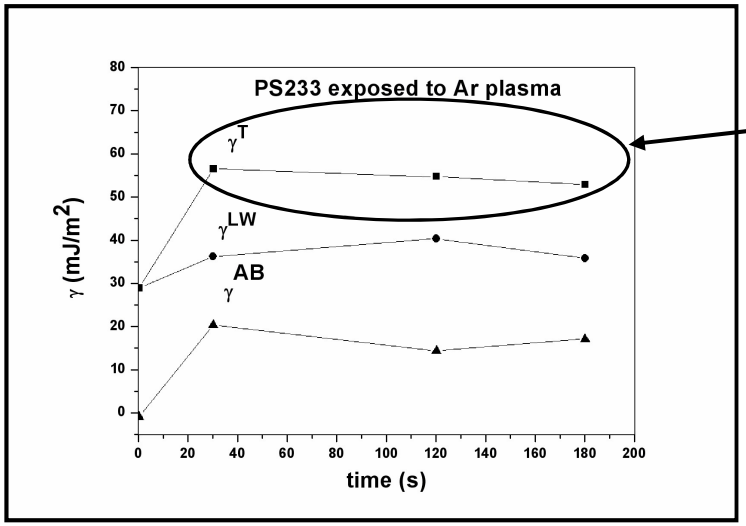

[γ_S/Ar]

plate

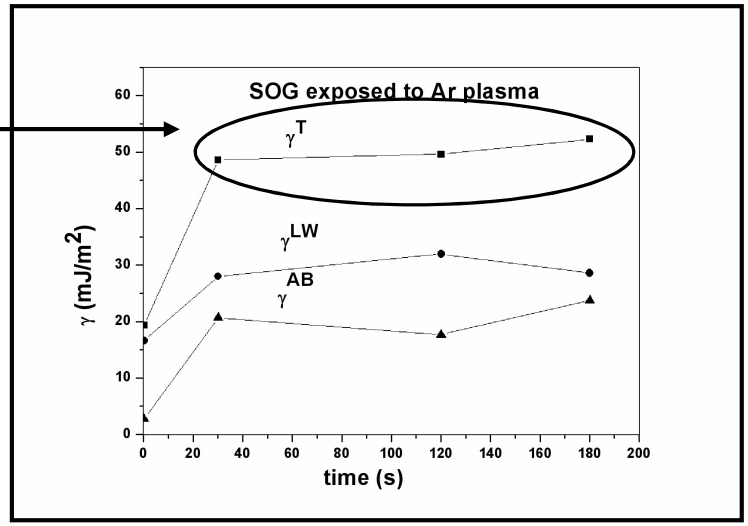

The determination of the set of γ_S materials allow to define the adhesion work at the interface guide (SU8 core) and cladding (nano-gap) PS233 or SOG

$$W_{S1/S2} = 2\left[\left(\gamma_{S1}^{d-(LW)}\gamma_{S2}^{d-(LW)}\right)^{1/2} + \left(\gamma_{S2}^{nd(+)}\gamma_{S1}^{nd(-)}\right)^{1/2} + \left(\gamma_{S1}^{nd(+)}\gamma_{S2}^{nd(-)}\right)^{1/2}\right] \quad \text{[III-18]}$$

with, SU8 : $\gamma^{d-(LW)}$=48.5 mJ/m², $\gamma^{nd-(+)}$=0 mJ/m², $\gamma^{nd-(-)}$=6.9 mJ/m²

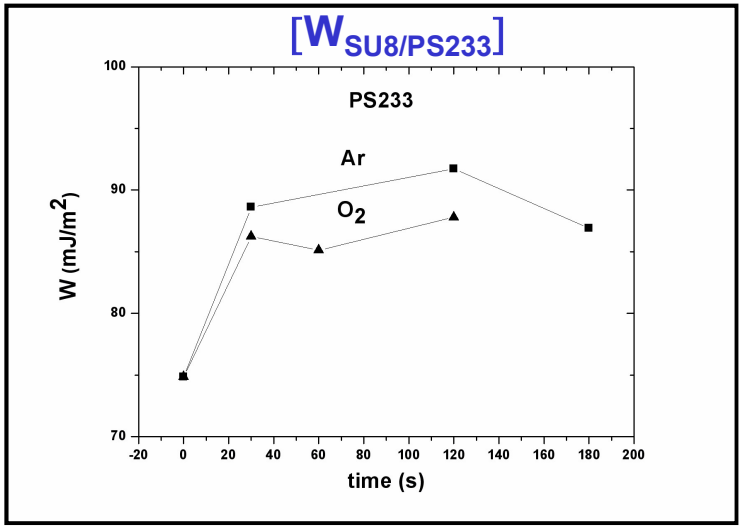

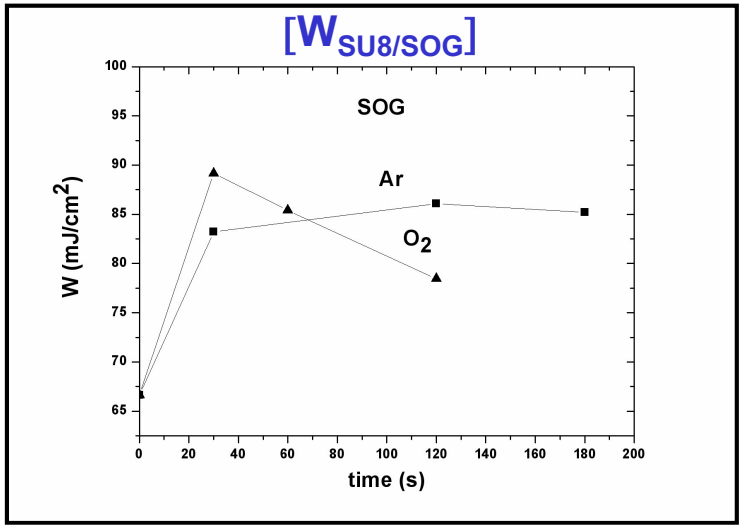

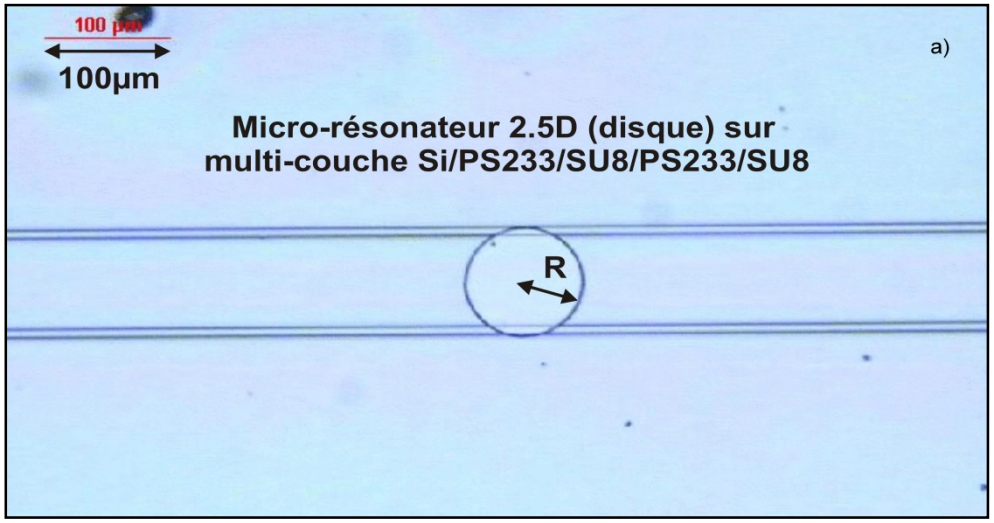

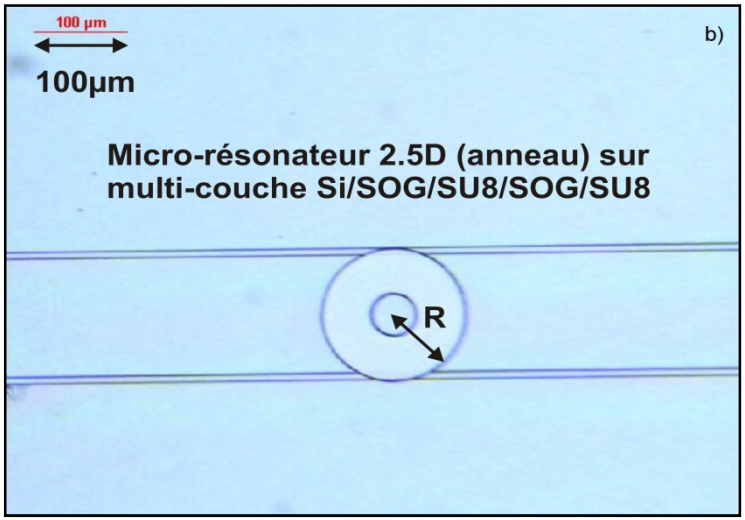

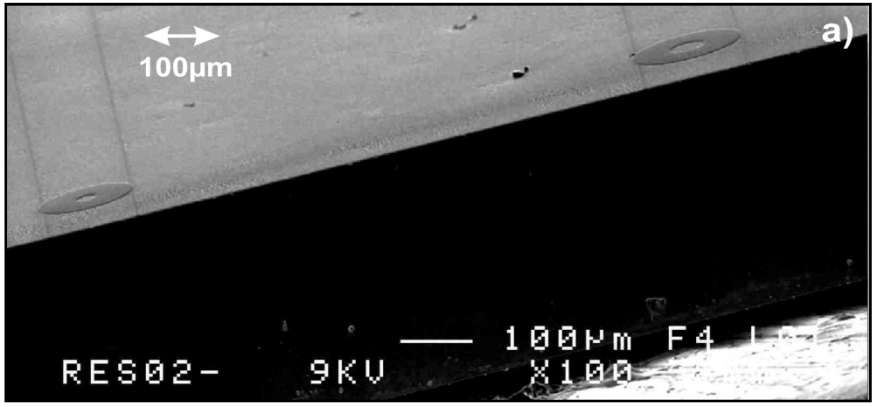

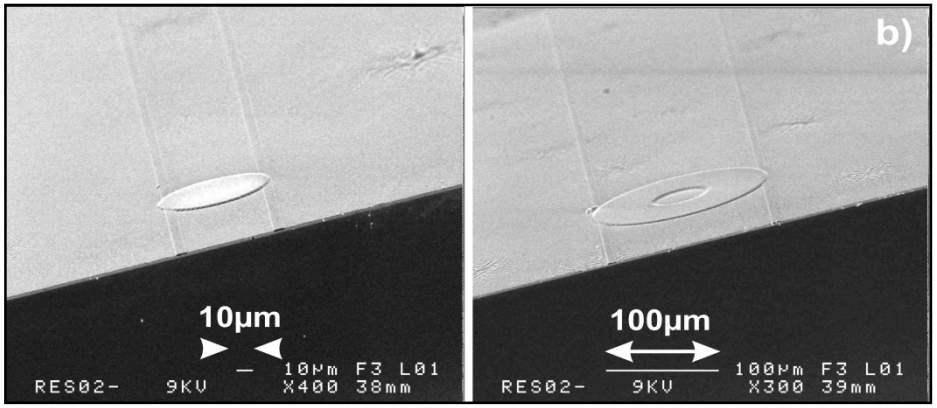

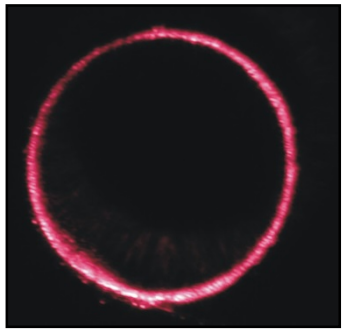

TE_{00} whispering gallery modes into a disk (λ_0=670 nm)

- **lecture and study of the reference :**

Available online at www.sciencedirect.com

ScienceDirect

Thin Solid Films 516 (2008) 8668–8674

thin solid films

www.elsevier.com/locate/tsf

Spin coating and plasma process for 2.5D integrated photonics on multilayer polymers

A. Zebda [a], L. Camberlein [b], B. Bêche [a,*], E. Gaviot [b], E. Bêche [c], D. Duval [a], J. Zyss [d], G. Jézéquel [a], F. Solal [a], C. Godet [a]

[a] *Institut de Physique de Rennes, IPR UMR CNRS 6251, Université de Rennes I, 35042 Rennes, France*
[b] *Laboratoire d'Acoustique de l'Université du Maine, Micro_Cap_Ouest, LAUM-UMR CNRS 6613, 72000 Le Mans, France*
[c] *PROMES UPR CNRS 8521 — Odeillo 66125 Font-Romeu, France*
[d] *IFR d'Alembert, Laboratoire de Photonique Quantique et Moléculaire, ENS Cachan, LPQM-UMR CNRS 8537, 94235 Cachan, France*

Received 22 October 2007; received in revised form 6 March 2008; accepted 18 April 2008
Available online 1 May 2008

Abstract

Polymer spin coating, surface plasma treatment and selective UV-lithography processes have been developed to realize 2.5D photonic micro-resonators, made of disk- or ring-shaped upper rib waveguides, using common polymers such as SU8 (biphenol A ether glycidyl), PS233 (polymeric silane) and SOG (siloxane Spin on Glass). Both oxygen and argon plasma treatments, applied to PS233 and SOG before spin-coating the SU8, improve substantially the grip of multilayer devices (SU8 / PS233 or SU8 / SOG). Surface energy components derived from contact angle measurements have been used to optimize the processing conditions. In such integrated photonic devices, the both single-electromagnetic-modes called transverse electric (TE_{00}) and transverse magnetic (TM_{00}) have been excited in a SU8 micro-disk, with a single mode propagation strongly localized near the edge of the disk (i.e. the so called whispering gallery modes).
© 2008 Elsevier B.V. All rights reserved.

PACS: 42.70Jk; 42.82-m; 78.66Qn; 42.82-Gw
Keywords: Polymers; SU8; PS233; SOG; Integrated photonics; Waveguides; 2.5D micro-optical resonators; Energy surface measurements; Whispering gallery modes

- III.2.3.1 Glass 3D-MR on organic chip – resonant coupling : add-drop filter in glass/SU8 with DPPC biomolecular lipid gap (Langmiur-Blodgett film)

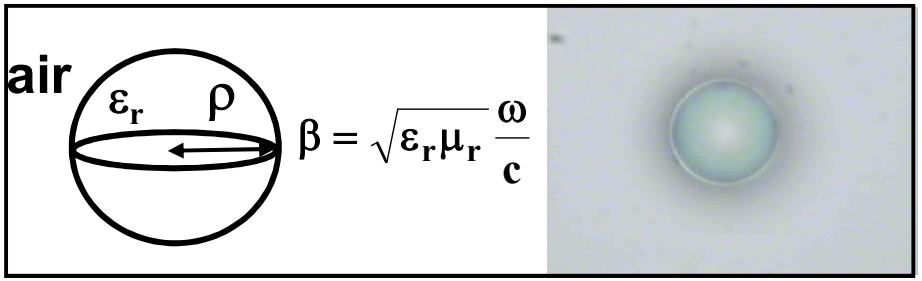

$$\frac{J_{n-1/2}(\beta\rho)}{J_{n+1/2}(\beta\rho)} = \frac{H^{(2)}_{n-1/2}\left(\frac{\beta\rho}{\sqrt{\varepsilon_r}}\right)}{\sqrt{\varepsilon_r}\,H^{(2)}_{n+1/2}\left(\frac{\beta\rho}{\sqrt{\varepsilon_r}}\right)}$$

(TE & TM)*nmr*

Eigenvalues Eqs.

$$\frac{J_{n-1/2}(\beta\rho)}{J_{n+1/2}(\beta\rho)} - \frac{n}{\beta\rho} = \frac{\sqrt{\varepsilon_r}\,H^{(2)}_{n-1/2}\left(\frac{\beta\rho}{\sqrt{\varepsilon_r}}\right)}{H^{(2)}_{n+1/2}\left(\frac{\beta\rho}{\sqrt{\varepsilon_r}}\right)} - \frac{n\varepsilon_r}{\beta\rho}$$

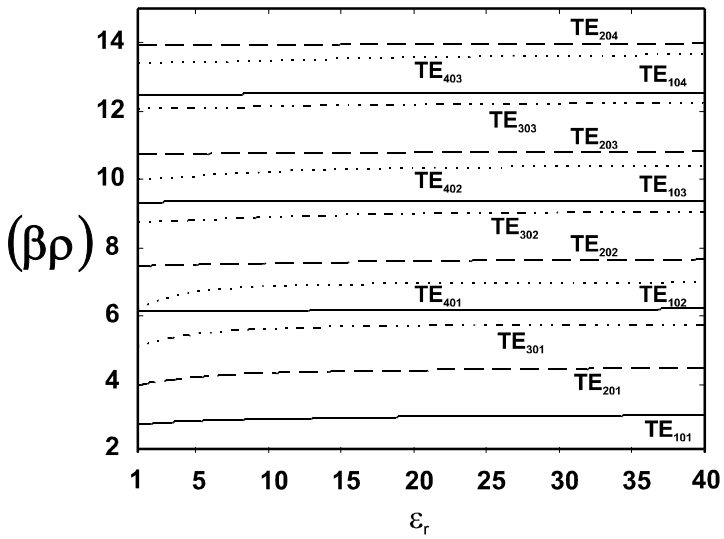

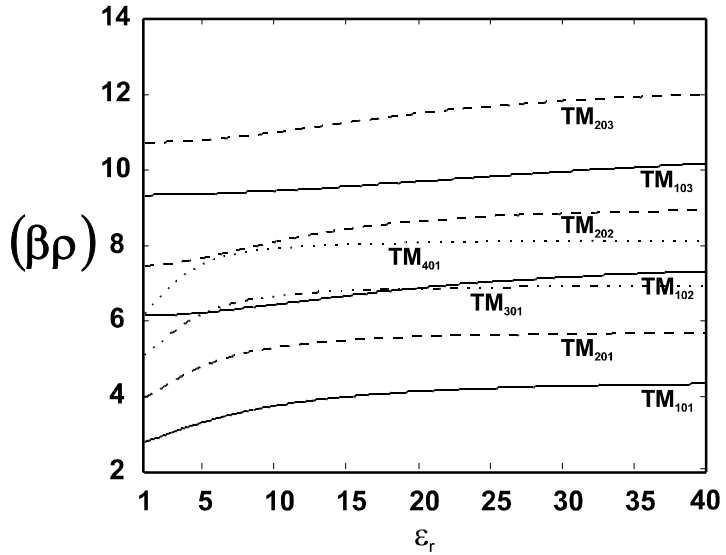

Eigenvectors = modes $\equiv f_1(\rho).f_2(\theta).f_3(\phi)$

$$\rho^2\frac{d^2f_1}{d\rho^2}+2\rho\frac{df_1}{d\rho}+(\beta^2\rho^2-p^2)f_1=0$$

$$\frac{1}{\sin\theta}\frac{d}{d\theta}\left(\sin\theta\frac{df_2}{d\theta}\right)+\left(p^2-\frac{q^2}{\sin^2\theta}\right)f_2=0$$

$$\frac{d^2f_3}{d\phi^2}+q^2f_3=0$$

$$E_\rho=0$$

$$E_\theta=-j\frac{\beta.m}{\rho\sin\theta}\sqrt{\frac{\mu_r}{\varepsilon_r}}\sqrt{\beta\rho}.J_{n+1/2}(\beta\rho)P_n^m(\cos\theta)\Big|_{-\sin(m\phi)}^{\cos(m\phi)}e^{j\omega t}$$

$$E_\phi=j\frac{\beta}{\rho}\sqrt{\frac{\mu_r}{\varepsilon_r}}\sqrt{\beta\rho}.J_{n+1/2}(\beta\rho)\frac{dP_n^m(\cos\theta)}{d\theta}\Big|_{\cos(m\phi)}^{\sin(m\phi)}e^{j\omega t}$$

$$H_\rho=\frac{n(n+1)}{\rho^2}\sqrt{\beta\rho}.J_{n+1/2}(\beta\rho)P_n^m(\cos\theta)\Big|_{\cos(m\phi)}^{\sin(m\phi)}e^{j\omega t}$$

$$H_\theta=\frac{1}{\rho}\frac{d[\sqrt{\beta\rho}.J_{n+1/2}(\beta\rho)]}{d\rho}\frac{dP_n^m(\cos\theta)}{d\theta}\Big|_{\cos(m\phi)}^{\sin(m\phi)}e^{j\omega t}$$

$$H_\phi=\frac{m}{\rho\sin\theta}\frac{d[\sqrt{\beta\rho}.J_{n+1/2}(\beta\rho)]}{d\rho}P_n^m(\cos\theta)\Big|_{-\sin(m\phi)}^{\cos(m\phi)}e^{j\omega t}$$

$$\|\vec{E}\|=\sqrt{E_\rho^2+E_\theta^2+E_\phi^2}$$

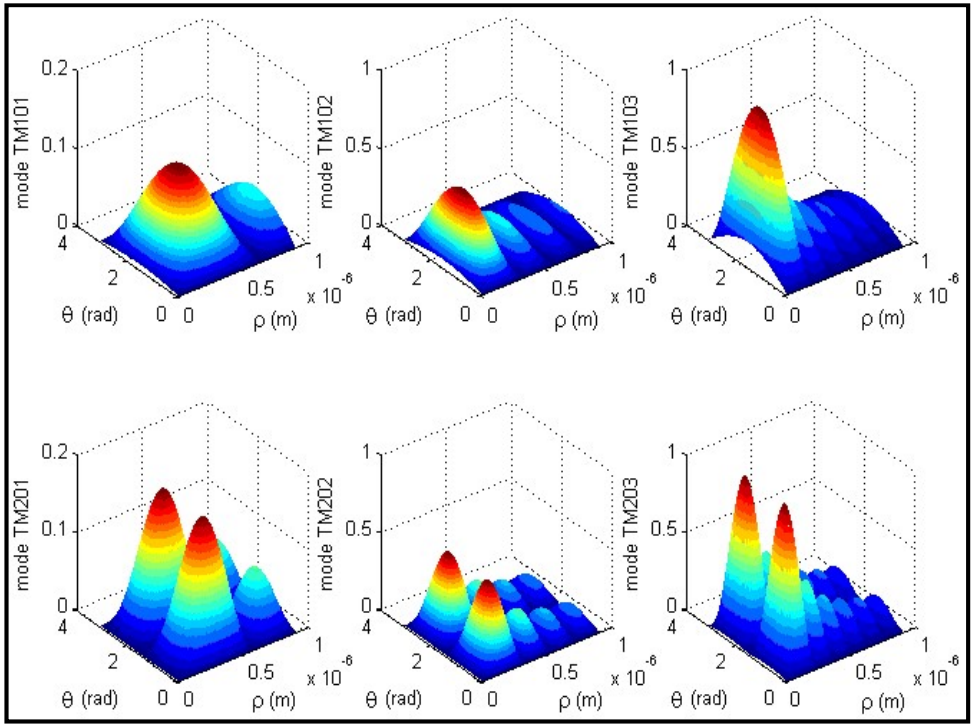

- Realisation of the lipid biomolecular film (DPPC)

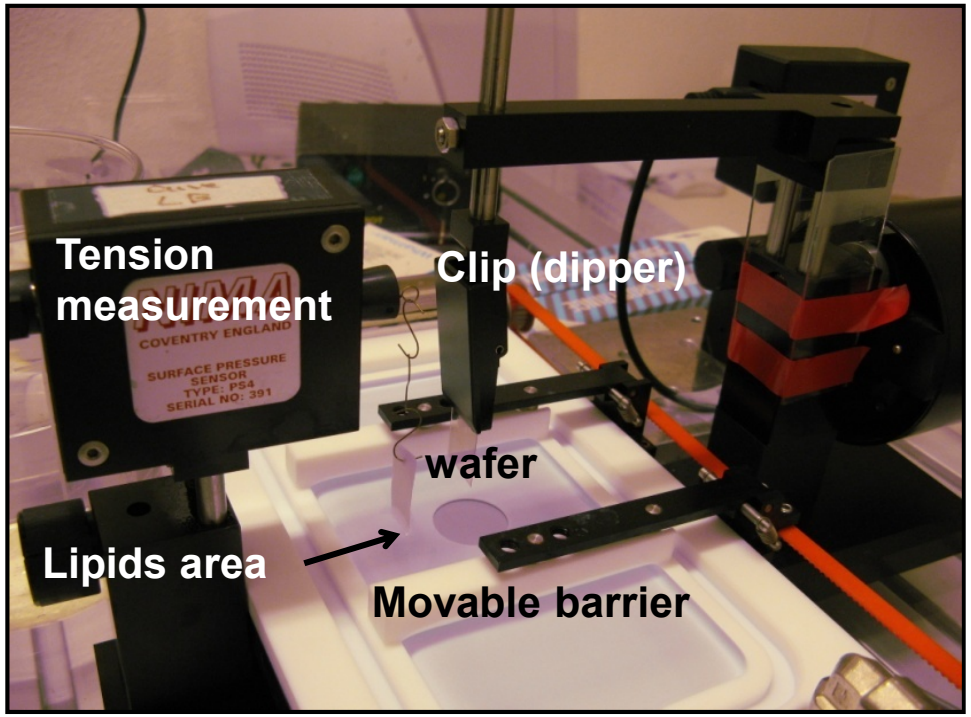

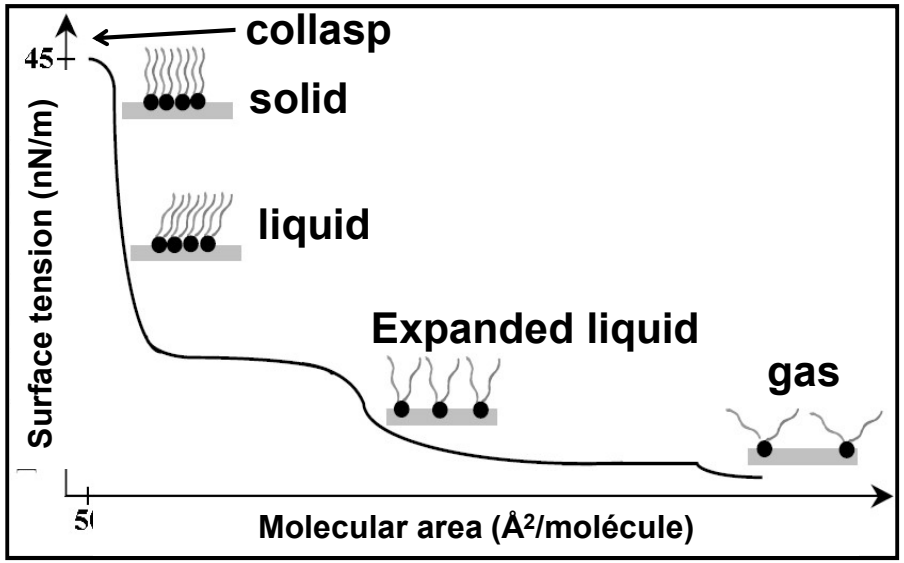

(surface tension) at interface : 35 mN/m

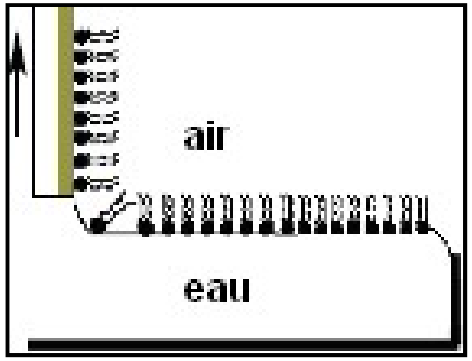

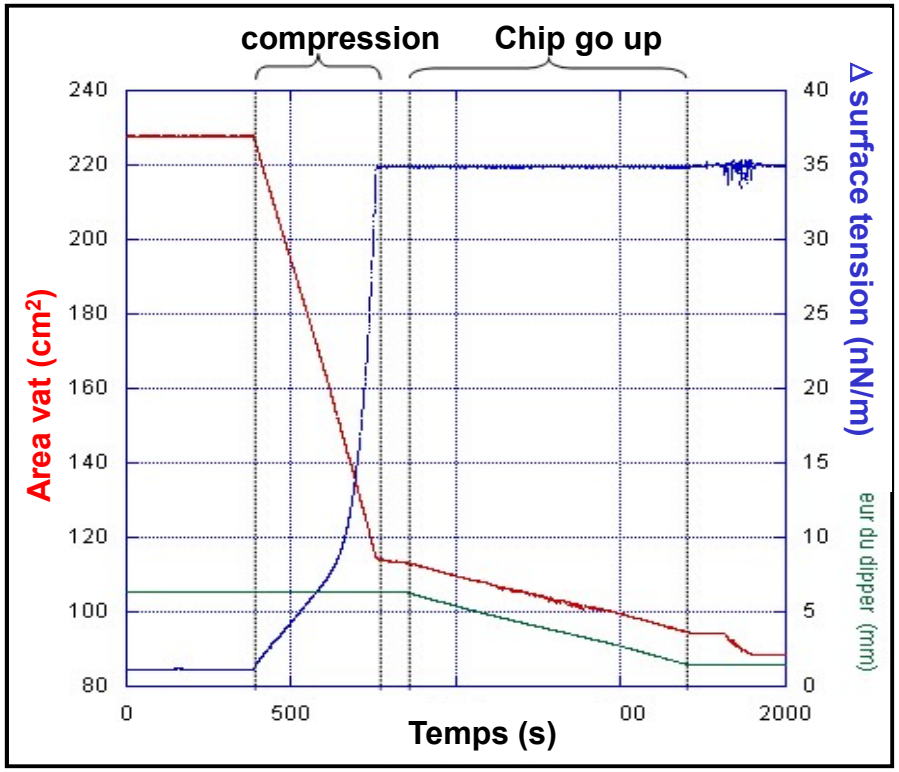

▪ Conception of polymers/glass 3D micro-structures resonators (sphere) :

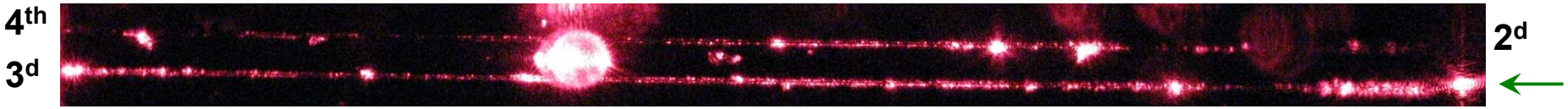

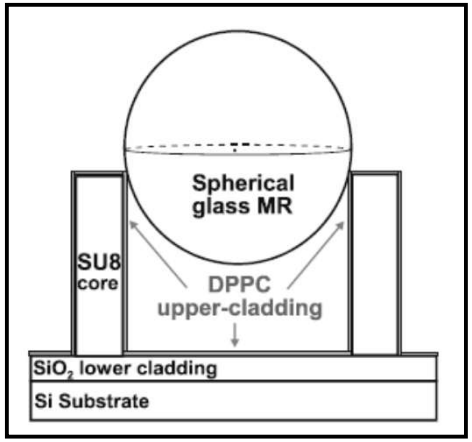

Excitation of whispering gallery modes and coupling to waveguides

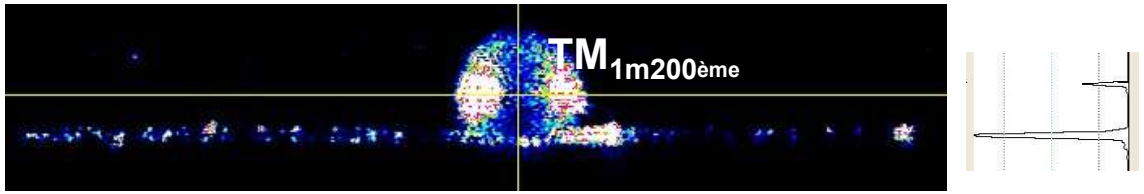

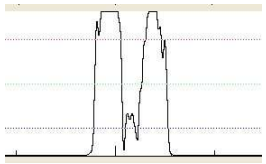

Upper detection (4-ports)

Port-exits 3 and 4

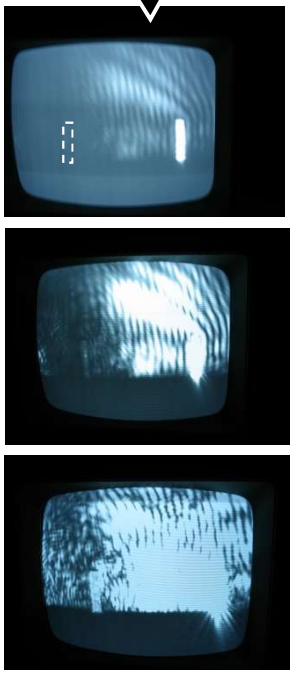

➔ cas TE

$$\left(i^{\text{ème}}\ \text{port} / j^{\text{ème}}\ \text{port}\right)_{i \neq j} \rightarrow \text{cste}\ \forall\, I_{\text{laser}}$$

$$\left(2^{\text{éme}}\text{port} / 1^{\text{er}}\ \text{port}\right) \approx 1.5$$

$$\left(3^{\text{ème}}\ \text{port} / 4^{\text{ème}}\ \text{port}\right) \approx 1.97$$

Spectral resonances

$Q \approx 10^5$

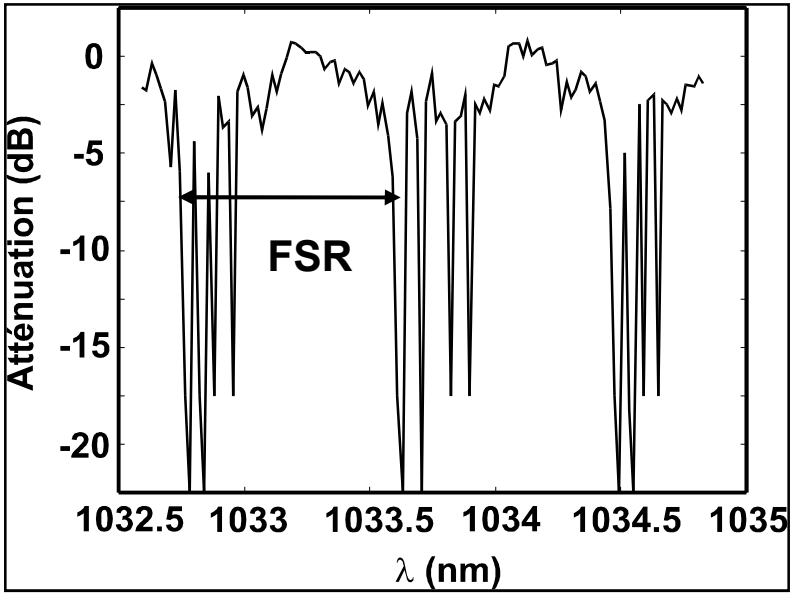

FSR=$\Delta\lambda$=0.97 nm (**FSR/λ_0=T/t_{1t}**)

$$R \approx \left(\lambda_0^2 / 2\pi n_{eff}.\Delta\lambda\right) \approx 105\mu m \text{(radius)}$$

$$t_{tt} = \left(\lambda_0^2 / c.\Delta\lambda\right) \approx 3.7 ps$$

Fineness $\Delta\lambda/\delta\lambda$ reaching 37

Quality factor Q=$\lambda_0/\delta\lambda$ > 4.10^4

Modal photonic life time τ=Q/ω_0=21.9 ps (6 rounds)

- **lecture and study of the reference :**

Optics Communications 283 (2010) 164–168

Contents lists available at ScienceDirect

Optics Communications

journal homepage: www.elsevier.com/locate/optcom

Resonant coupling into hybrid 3D micro-resonator devices on organic/biomolecular film/glass photonic structures

Bruno Bêche [a,*], Arnaud Potel [a], Jérémy Barbe [a], Véronique Vié [a], Joseph Zyss [b], Christian Godet [a], Nolwenn Huby [a], David Pluchon [a], Etienne Gaviot [c]

[a] Institut de Physique de Rennes, IPR UMR CNRS 6251, Université de Rennes 1, 35042 Rennes, France
[b] IFR d'Alembert, Laboratoire de Photonique Quantique et Moléculaire, ENS Cachan, LPQM-UMR CNRS 8537, 94235 Cachan, France
[c] Laboratoire d'Acoustique de l'Université du Maine, Micro_Cap_Ouest, LAUM-UMR CNRS 6613, 72000 Le Mans, France

ARTICLE INFO

Article history:
Received 9 July 2009
Received in revised form 31 August 2009
Accepted 21 September 2009

PACS:
42.82.−m
42.82.Et
42.82.Gw
42.70.Jk

Keywords:
Integrated photonics
3D micro-resonators
Add-drop filters
Whispering gallery-modes
SU-8 polymer
Biomolecular lipid films

ABSTRACT

We have designed and realized an integrated photonic family of micro-resonators (MR) on multilayer SU8/lipidic film/glass materials. Such a family involves hybrid 3D-MR structures composed of spherical glass–MR arranged upon organic pair-SU8-waveguides, an efficient coupling being ensured with a Langmuir–Blodgett Dipalmitoylphosphatidylcholine (DPPC-lipid from Avanti Polar®) film whose thickness is ranging from 12 to 48 nm. We have characterized such add/drop filters, respectively, in intensity and spectral measurements, and experimentally achieved an evanescent resonant–photonic-coupling between the 3D-MR and the 4-ports structure through the DPPC-gap. Spectral resonances have been measured for 4-whispering gallery-modes (WGM) into such 3D-structures, respectively, characterized with a 0.97 nm free spectral range (FSR) and a high quality Q-factor up to 4.10^4.

Crown Copyright © 2009 Published by Elsevier B.V. All rights reserved.

- III.2.3.2 Design of organic 3D microresonators with microfluidics coupled to thin-film processes for photonic applications

▪ Micro-fluidic technology and organic 3D MR conception

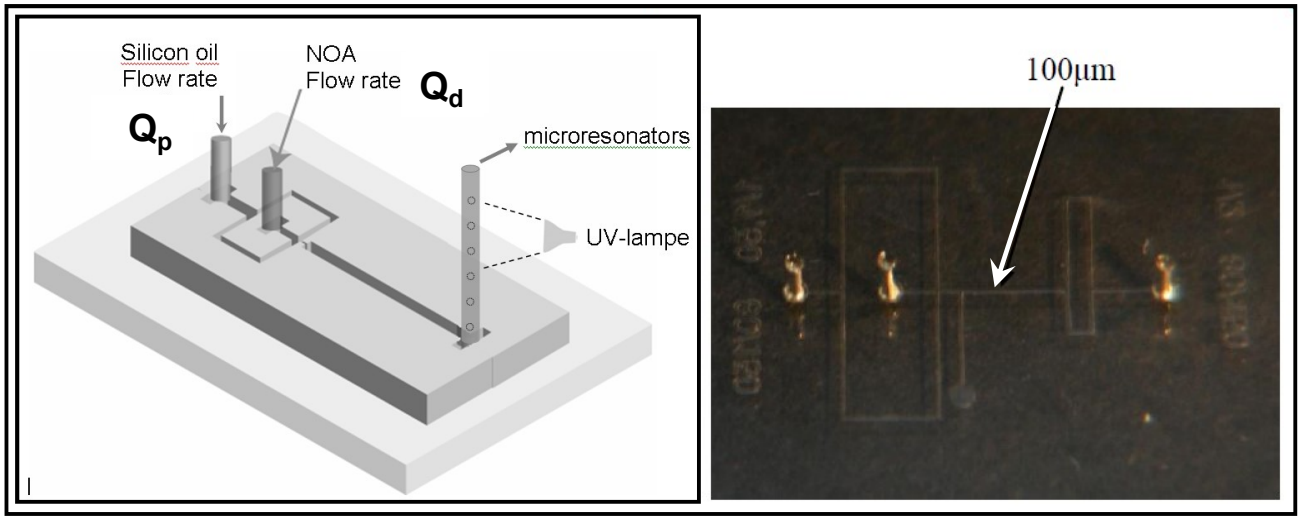

▪ Micro-channels realisation by thin layer processes (clean room) (SU8, PDMS, plasma cleaner…).

▪ Generation of monodisperses droplets train ('T'-junctions flow focusing)

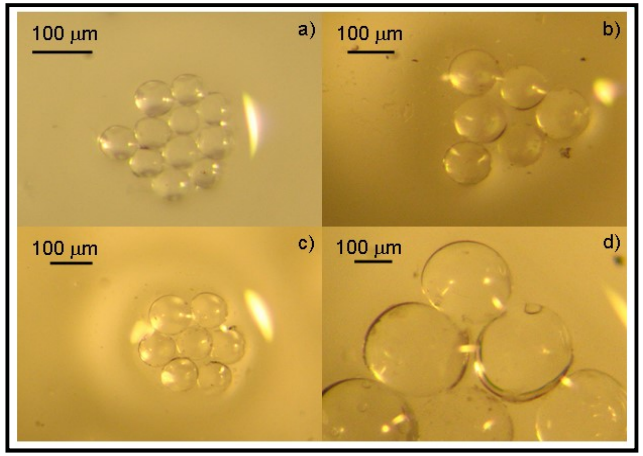

- 'T'- Structure +restriction area : NOA pinching.
- NOA = dispersed phase (Q_d, µL/h) and silicon oil = continuous phase (Q_p, 100-300 µL/h) ➔ 30µm<$R_{spheres}$<200µm.
- Model in two steps τ, flow-rates $Q_{p,d}$ fixe sizes of droplets : $\tau_{drop\text{-}formation} = \tau_{block}+\tau_{pinch}$, V=Q.τ, Q=v.S **Flow-rate**

∃ another parameters γ_{phases}, µ

μ_{NOA}=200mPa.s, γ_{NOA}=4.3mN/m

geometrie

$$V_{droplet} = V_{block} + V_{pinch}\frac{Q_d}{Q_p}$$

▪ Two dynamical flow regimes into the T-flow-focusing

- Jetting regime $t_{jet\text{-}formation} < \tau_{pinch}$, Rayleigh-Plateau instability ➔ minimization of energy lead to formation of droplet-geometry.

- Dripping regime $\tau_{pinch} < t_{jet\text{-}formation}$ (fast-pinch).

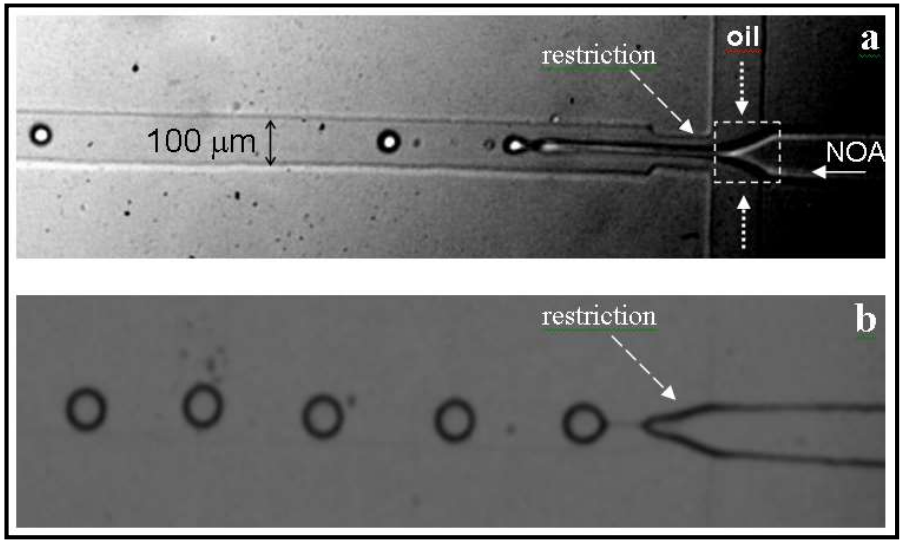

▪ Microphotonic and organic 3D spherical resonances

- Raman excitation set-up (λ=785nm) for isolated 3D MR resonances (Stokes-line, 830 nm)

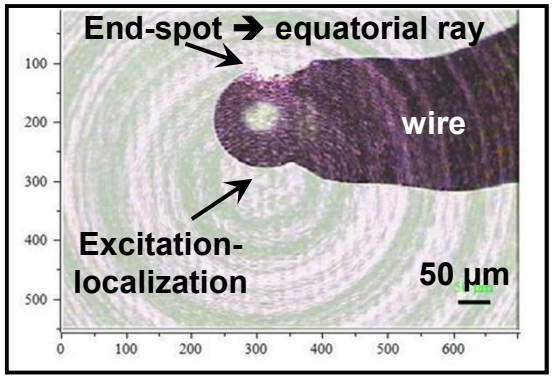

➔FSR (Δλ)= 0.86 nm & 0.88 nm ($D_{sphère}$= 150 µm).

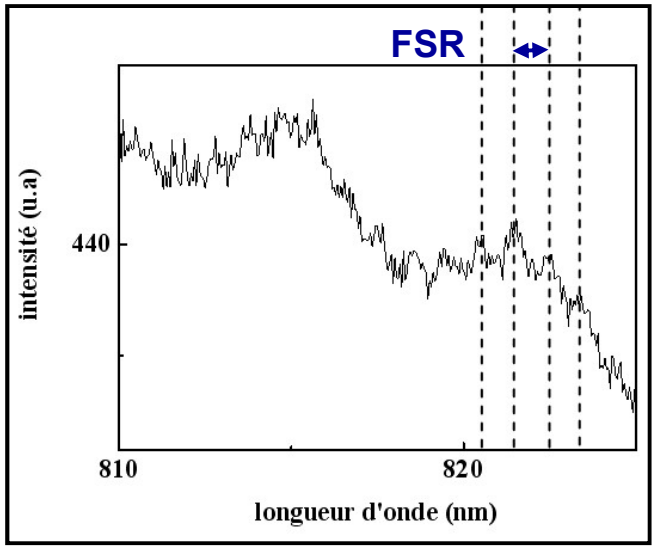

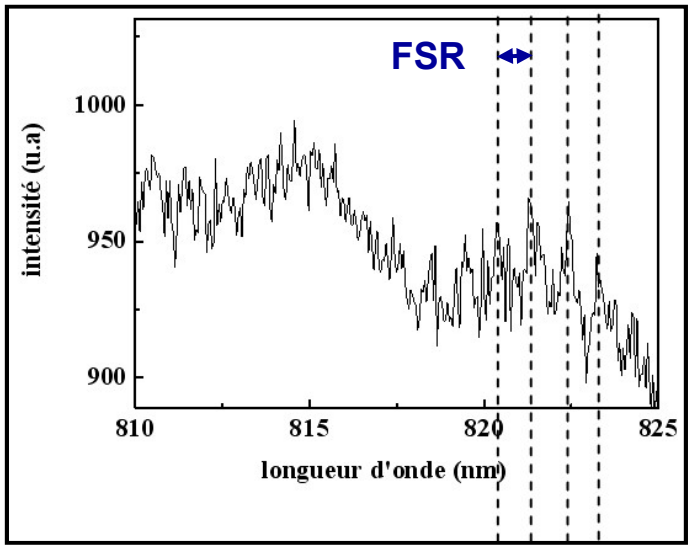

- **Whole organic MR/waveguides, coupling and excitation of Whispering Gallery Modes**
- Clean room processus, SU8 waveguides, SiO_2 gap, and integration of NOA MRs on the chip, MR excitation

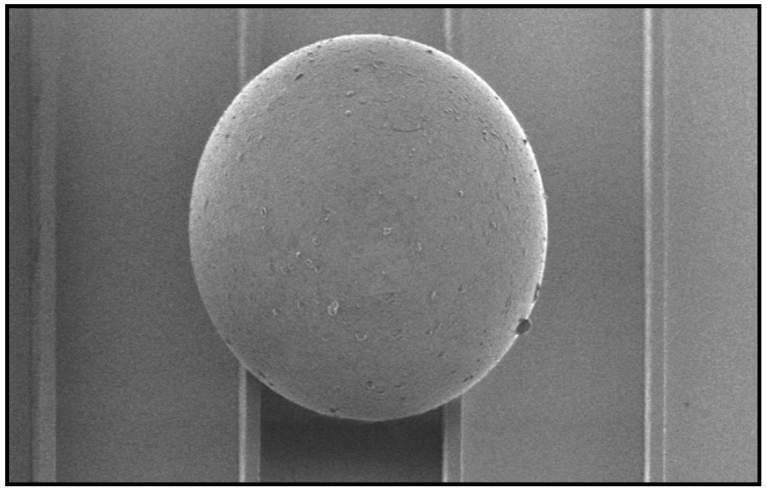

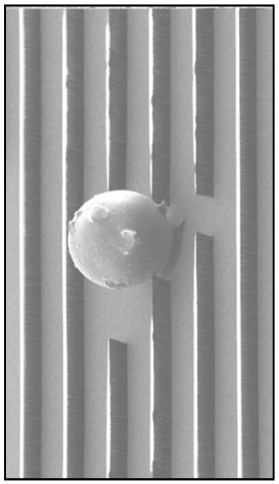

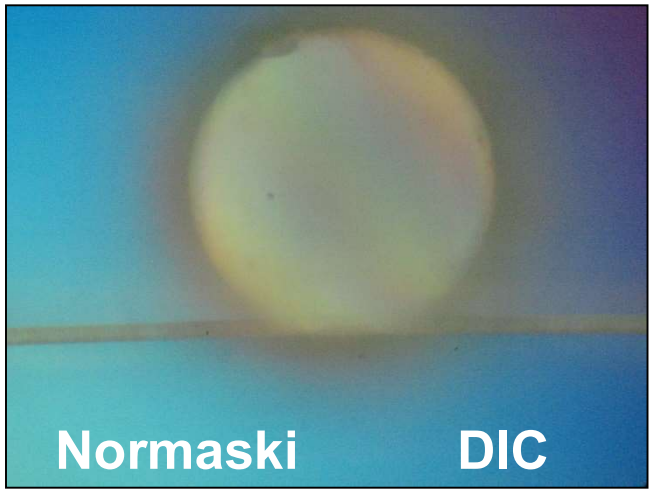

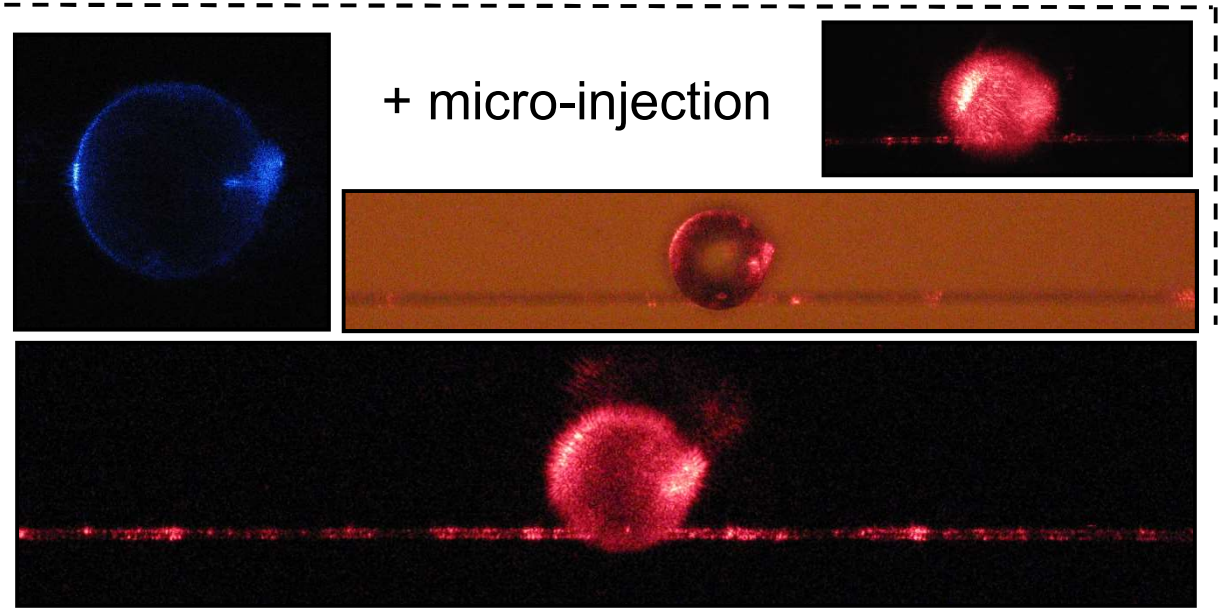

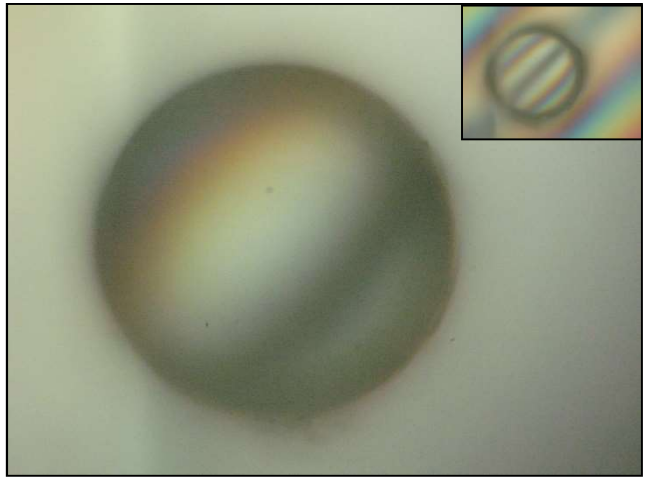

- Spectral characterization in integrated configuration

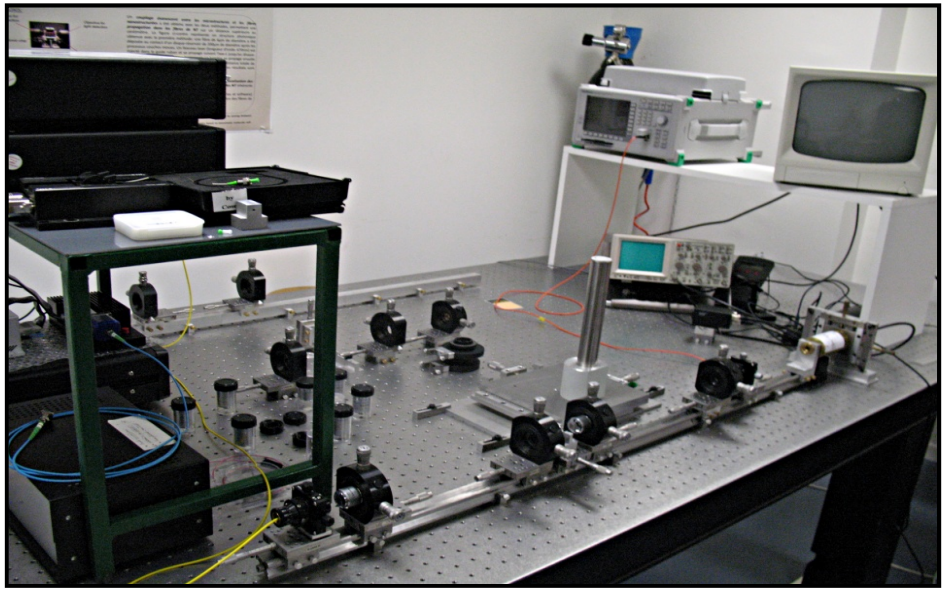

➔FSR ($\Delta\lambda$)= 1.5 nm, total agreements with diametres ($D_{sphère}$=155 µm).

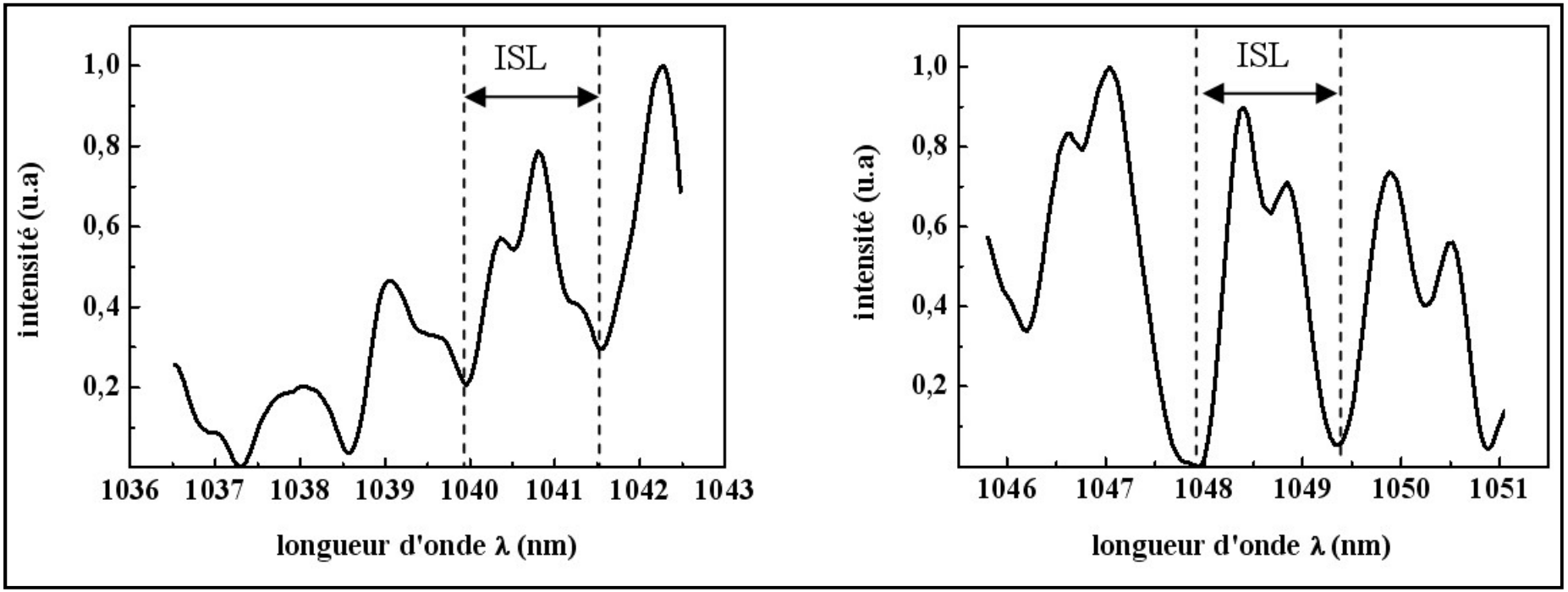

+ Read the distributed documents on fiber-sensors and applications…

- **lecture and study of the reference :**

Optics Communications 283 (2010) 2451–2456

Contents lists available at ScienceDirect

Optics Communications

journal homepage: www.elsevier.com/locate/optcom

Design of organic 3D microresonators with microfluidics coupled to thin-film processes for photonic applications

N. Huby [a], D. Pluchon [a], N. Coulon [b], M. Belloul [a], A. Moreac [a], E. Gaviot [c], P. Panizza [a], B. Bêche [a,d,*]

[a] IPR UMR CNRS 6251, Université de Rennes 1, bât. 11B, 263 avenue Général Leclerc, 35042 Rennes, France
[b] IETR UMR CNRS 6164, Université de Rennes 1, bât. 11B, 263 avenue Général Leclerc CS 74205, 35042 Rennes Cedex, France
[c] LAUM UMR CNRS 6613, Université du Maine, avenue O. Messiaen, 72085 Le Mans Cedex, France
[d] IUF, Institut Universitaire de France, 103 bd Saint-Michel, 75005 Paris, France

ARTICLE INFO

Article history:
Received 19 November 2009
Received in revised form 7 December 2009
Accepted 27 January 2010

Keywords:
Integrated optics
3D organic microresonators
Whispering Gallery Modes
Organic compounds
Applied complex fluid mechanism

ABSTRACT

We report on the design and realization of photonic integrated devices based on 3D organic microresonators (MR) shaped by an applied fluid mechanism technique. Such an interdisciplinary approach has been judiciously achieved by combining microfluidics techniques and thin-film processes, respectively, for the realizations of microfluidic and optical chips. The microfluidic framework with flow rates control allows the fabrication of microresonators with diameters ranging from 30 to 160 μm. The resonance of an isolated sphere in air has been demonstrated by way of a modified Raman spectroscopy devoted to the excitation of Whispering Gallery Modes (WGM). Then the 3D-MR have been integrated onto an organic chip and positioned either close to the extremity of a taper or alongside a rib waveguide. Both devices have proved efficient evanescent coupling mechanisms leading to the excitation of the WGM confined at the surface of the organic 3D-MR. Finally, a band-stop filter has been used to detect the resonance spectra of organic resonators once being integrated. Such spectral resonances have been observed with an integrated configuration and characterized with a $\Delta\lambda = 1.4$ nm free spectral range (FSR), appearing as stemming from a 78 μm-radius MR structure.

© 2010 Elsevier B.V. All rights reserved.

▪ Integrated chip 2D or 2.5D approach

➔ **Process of micro-nanotechnologies**

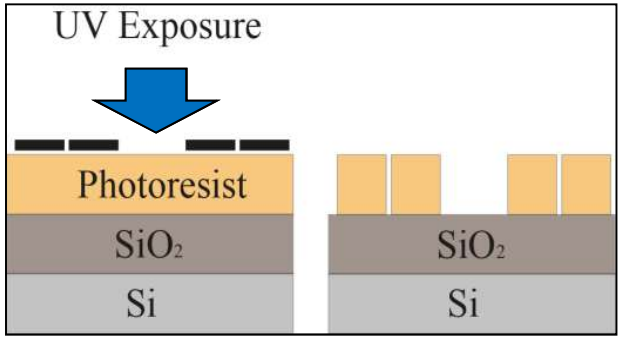

MRs à ➔ 2D (sub-λ gap)

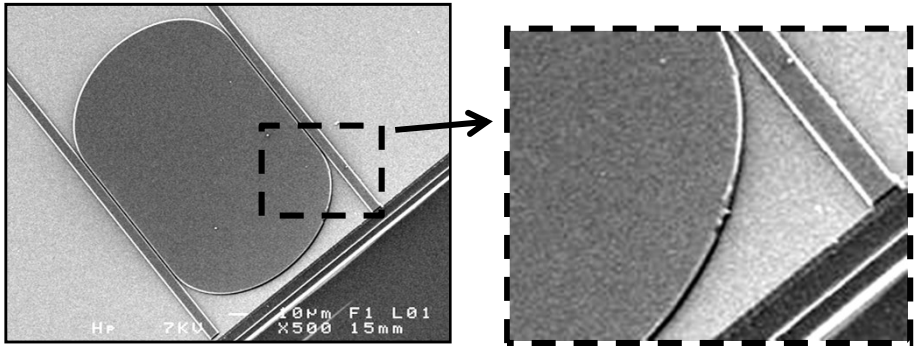

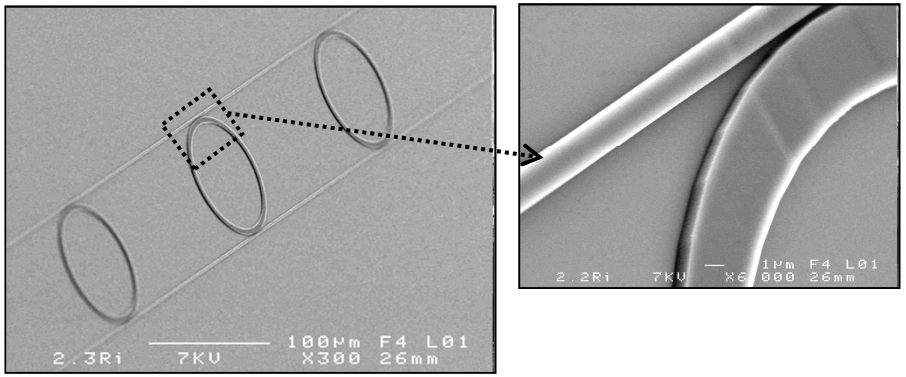

MRs upper view➔ 2.5D

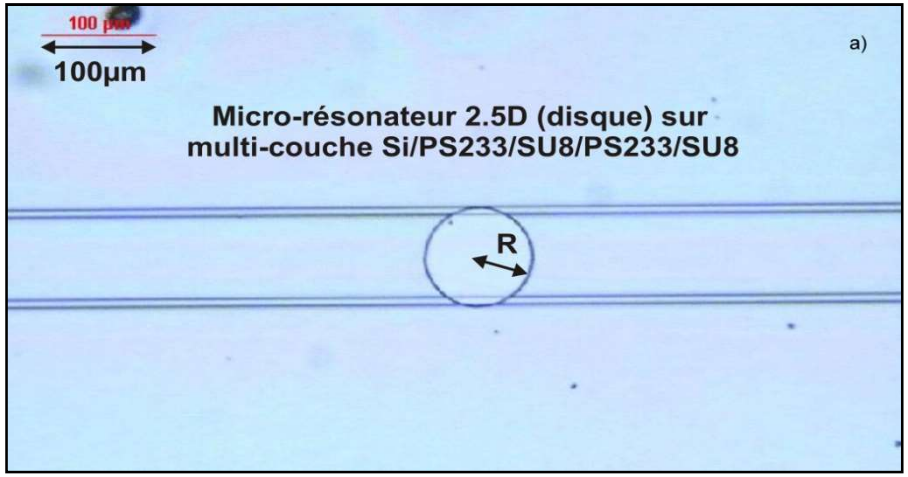

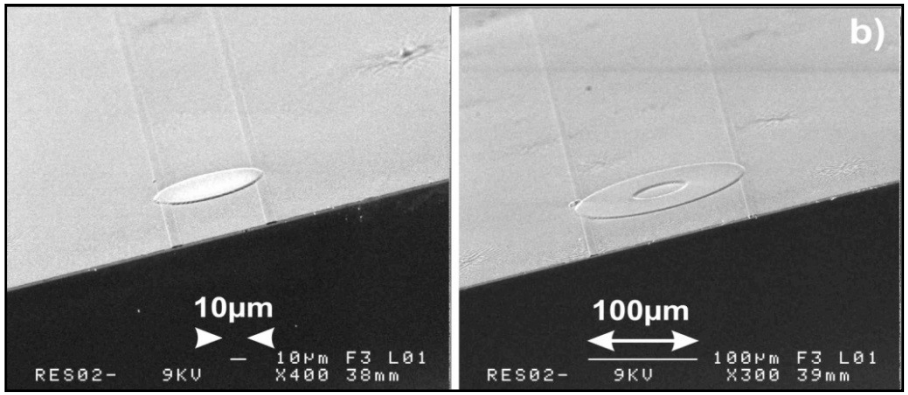

▪ Optical Characterizations of MRs

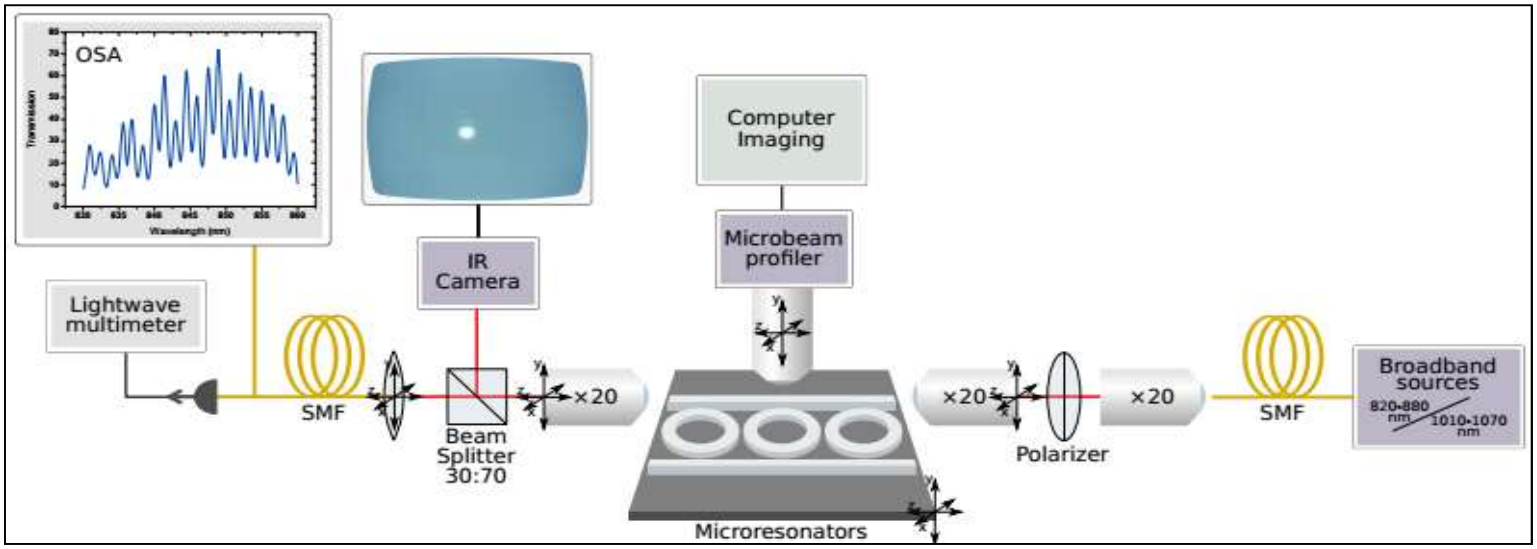

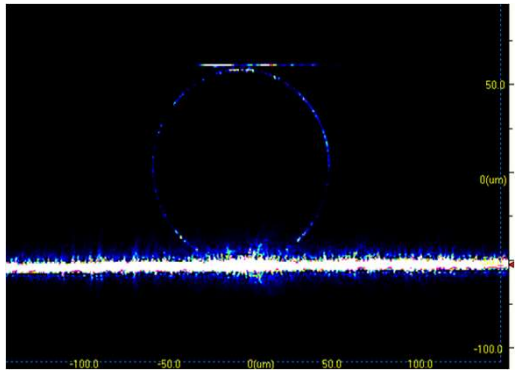

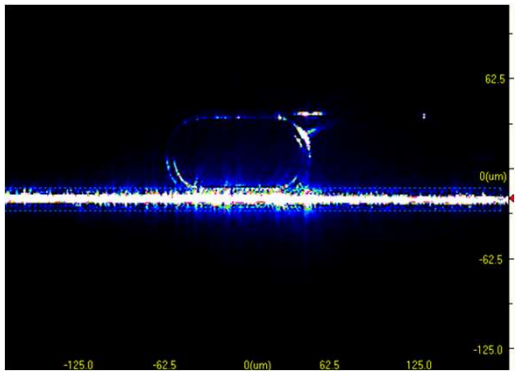

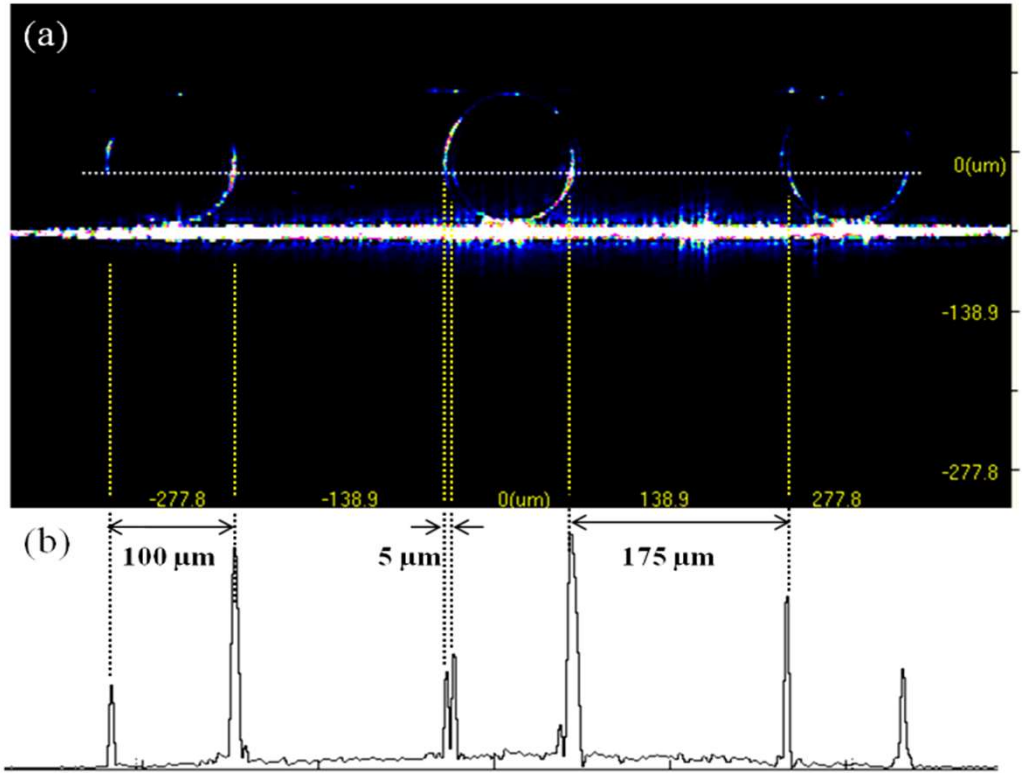

- Réponses spectrales et ISL ($\Delta\lambda$)

Cavité disque: R = 25 µm

Cavité s

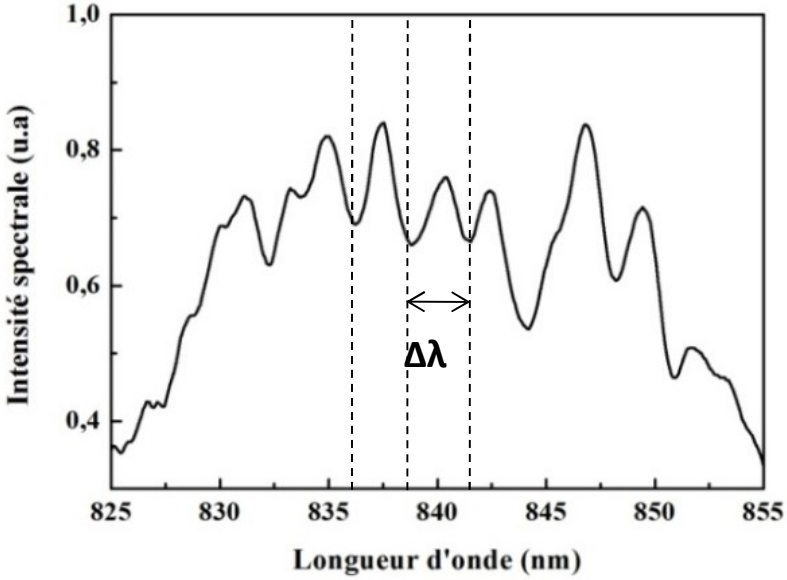

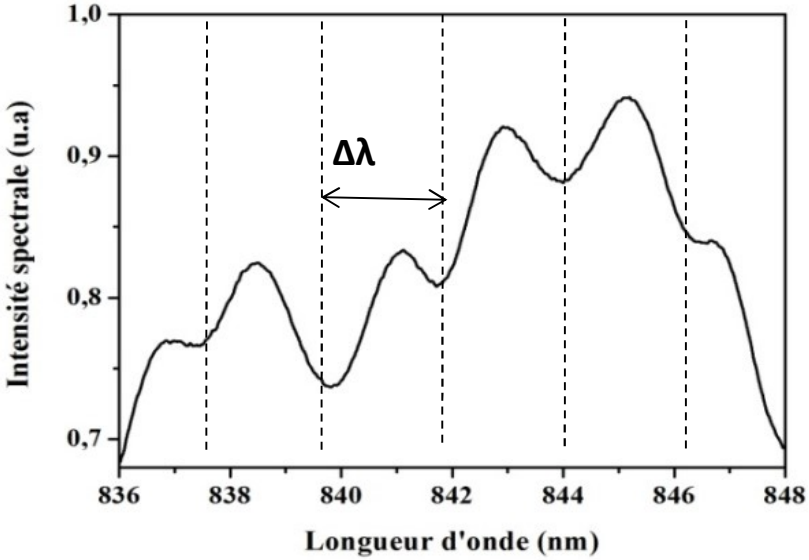

→ Mise en évidence de modes de galerie résonants 'WGM'

Structures / Paramètre R	Disques		Stades	
	25µm	50µm	25µm	50µm
ISL théoriques (nm)	2.92	1.46	1.78	0.89
ISL expérimentaux (nm)	2.70	1.45	1.95	/
Facteurs de qualité Q	700	950	700	

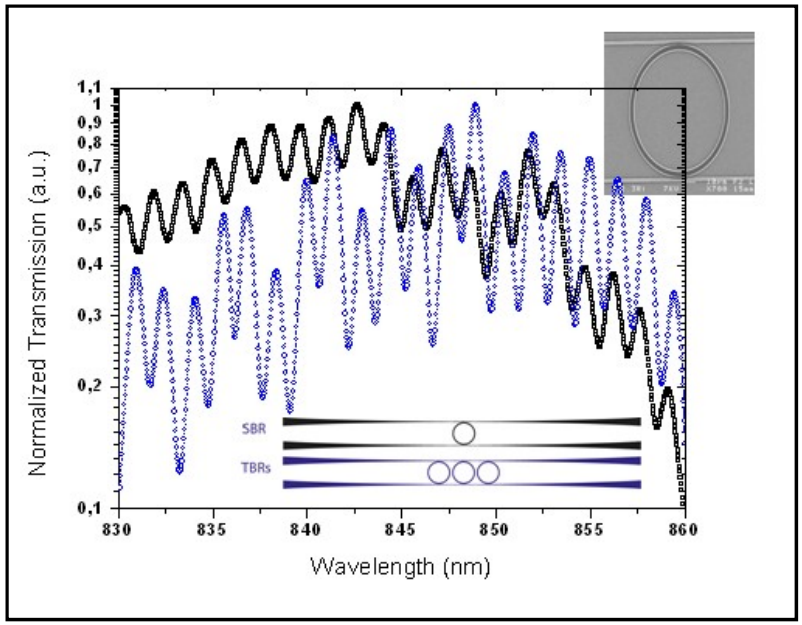

Fourier

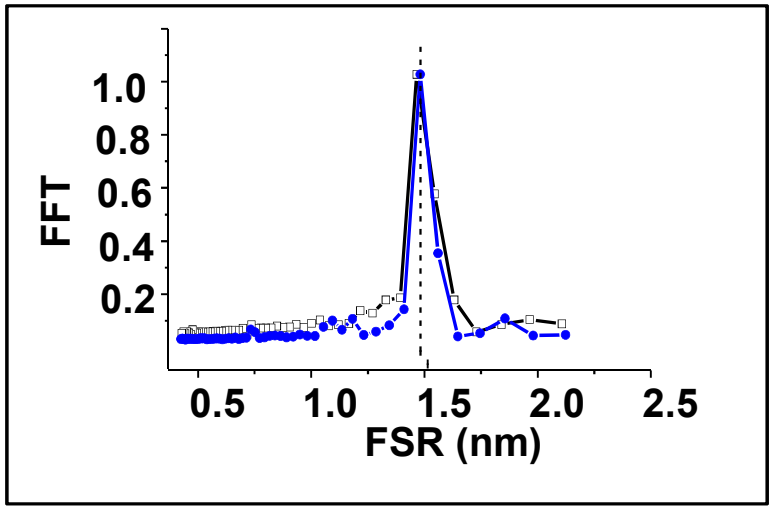

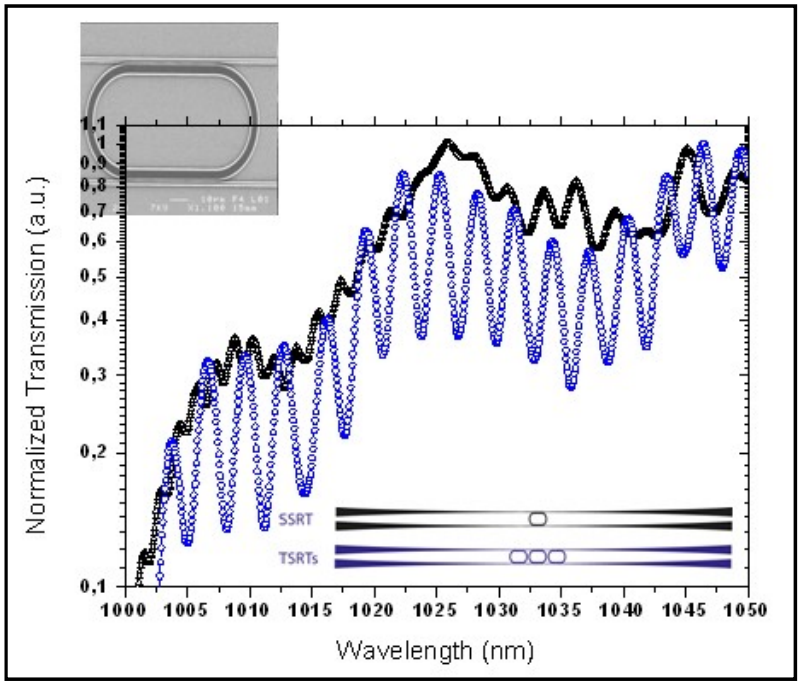

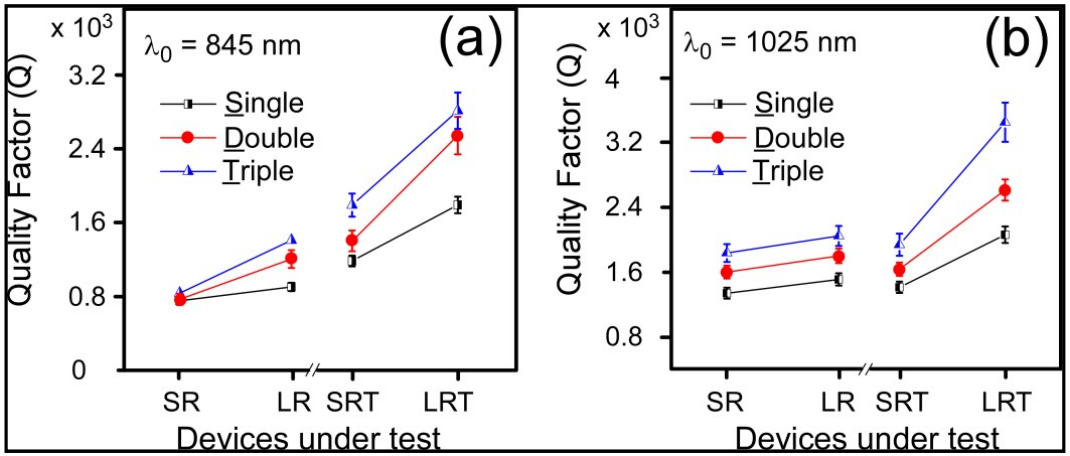

Quality factor Q >3000 at λ_{IR}

- **lecture and study of the reference :**

IOP Publishing Journal of Micromechanics and Microengineering
J. Micromech. Microeng. **24** (2014) 125006 (7pp) doi:10.1088/0960-1317/24/12/125006

Improvement of efficient coupling and optical resonances by using taper-waveguides coupled to cascade of UV210 polymer micro-resonators

R Castro-Beltran[1], N Huby[1], G Loas[1], H Lhermite[2], D Pluchon[1] and B Bêche[1,3]

[1] IPR UMR CNRS 6251, Université de Rennes 1, bât. 11B, 263 avenue Général Leclerc, 35042 Rennes, France
[2] IETR UMR CNRS 6164, Université de Rennes 1, bât. 11B, 263 avenue Général Leclerc CS 74205, 35042 Rennes Cedex, France
[3] IUF, Institut Universitaire de France, 103 bd St Michel, 75005 Paris, France

E-mail: bruno.beche@univ-rennes1.fr and nolwenn.huby@univ-rennes1.fr

Received 25 June 2014, revised 11 September 2014
Accepted for publication 12 September 2014
Published 12 November 2014

Abstract
In this paper, we report the overall design, fabrication and optical characterization of single and multiple resonant micro-structures patterned on UV210 polymer and shaped by using deep-UV lithography procedures. Various families of ring and racetrack forms are investigated with different geometrical dimensions linked to the micro-resonators and the specific taper-waveguides and gaps allowing the optimized coupling. Well defined photonic structures families in the sub-micrometer range obtained by this deep UV-light process are clearly confirmed through scanning electron microscopy. In order to evaluate and quantify the efficiency of the sub-micrometer coupling, the recirculation of the light and the quality of the optical resonance aspects, a global study including top view intensity imaging, spectral measurements and fast Fourier transform analysis is performed for all these devices based on single and multiple family resonators. The experimental TE-mode resonance transmissions reveal a complete agreement with the period of the theoretically expected resonances.
A maximum value of the quality factor $Q = 3.5 \times 10^3$ at 1035 nm with a 3.2 times higher resonance contrast is assessed for cascade of triple micro-resonators with respect to photonic devices based on only one micro-resonator. In addition, UV210 circuits made of specific tapers coupling to cascade loops act directly on the improvement of the evanescent coupling and resonances in terms of quality factor and extinction rate by selecting the optical mode resonance successively and more precisely. All these designs have low cost technological reproducible steps, and the devices and protocol measurements are markedly suitable for mass fabrication and metrology applications.

- **Plateform :**

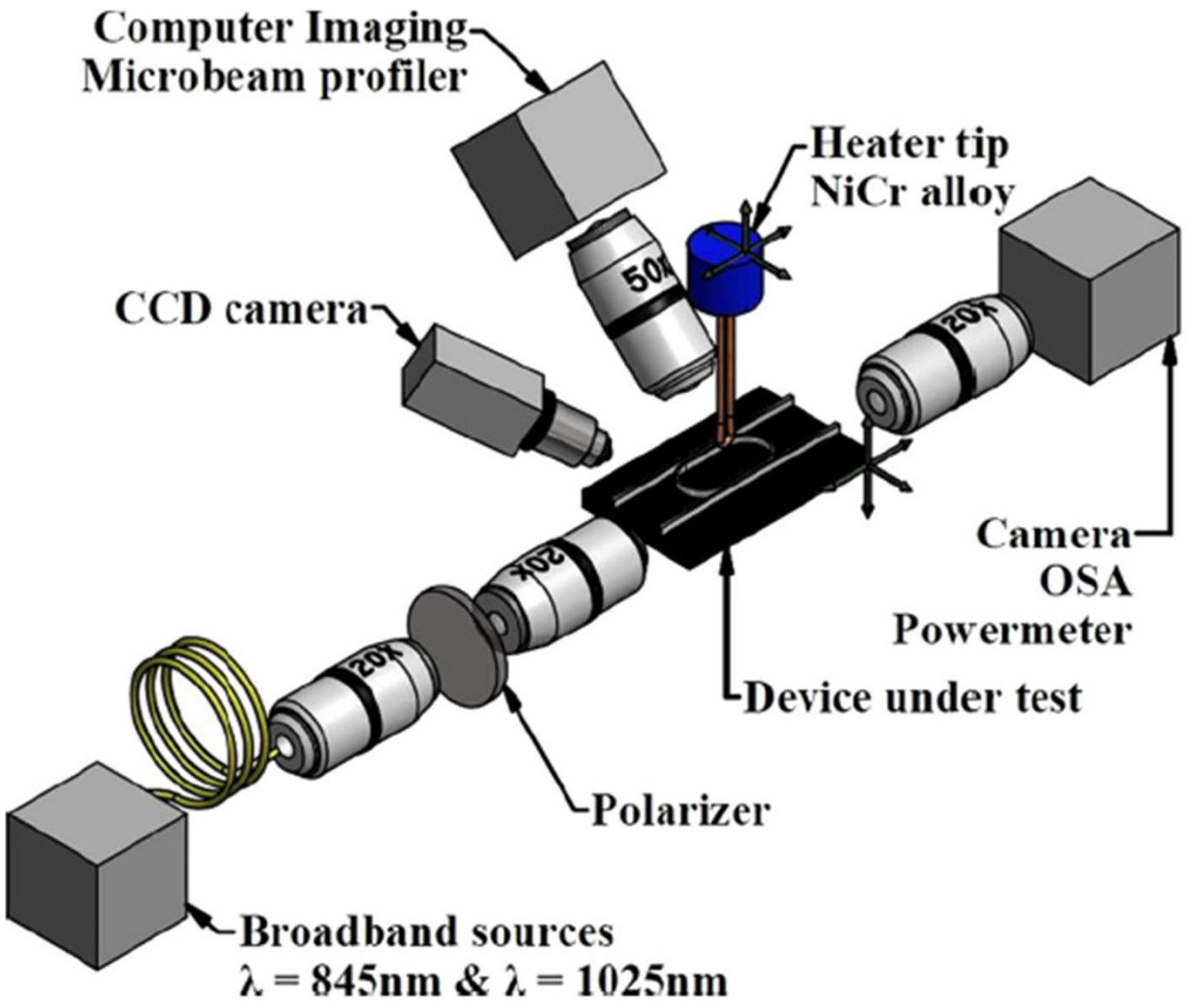
Computer Imaging
Microbeam profiler
Heater tip
NiCr alloy
CCD camera
50x
20x
20x
20x
Camera
OSA
Powermeter
Device under test
Polarizer
Broadband sources
λ = 845nm & λ = 1025nm

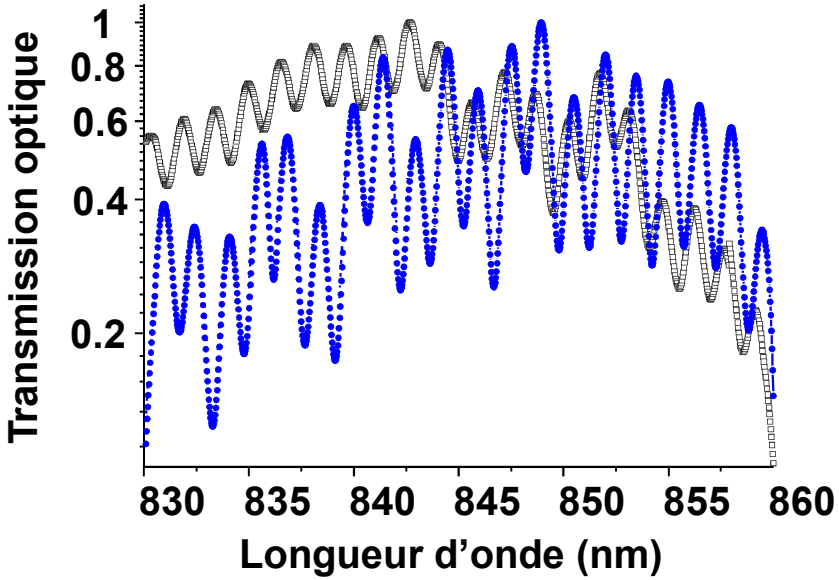

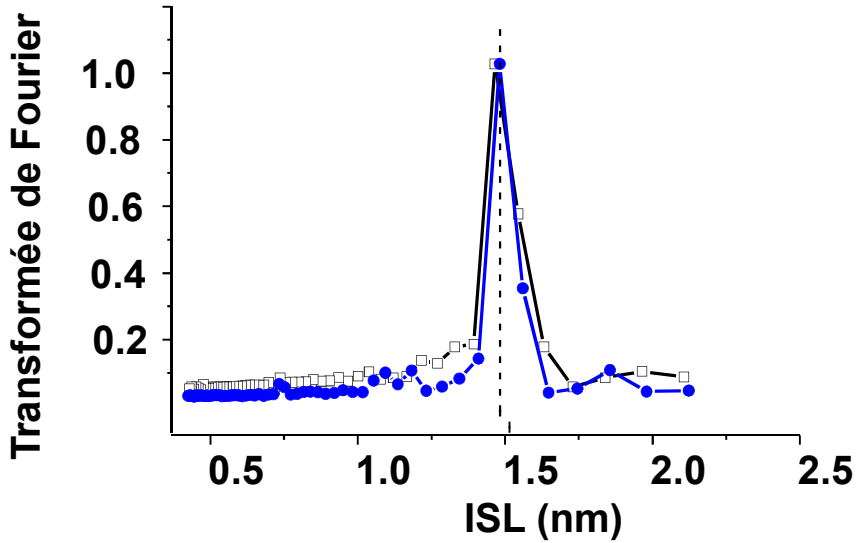

- Vers les applications senseurs ($\Delta n \rightarrow$ décalage $\Delta\lambda$ en longueur d'onde)

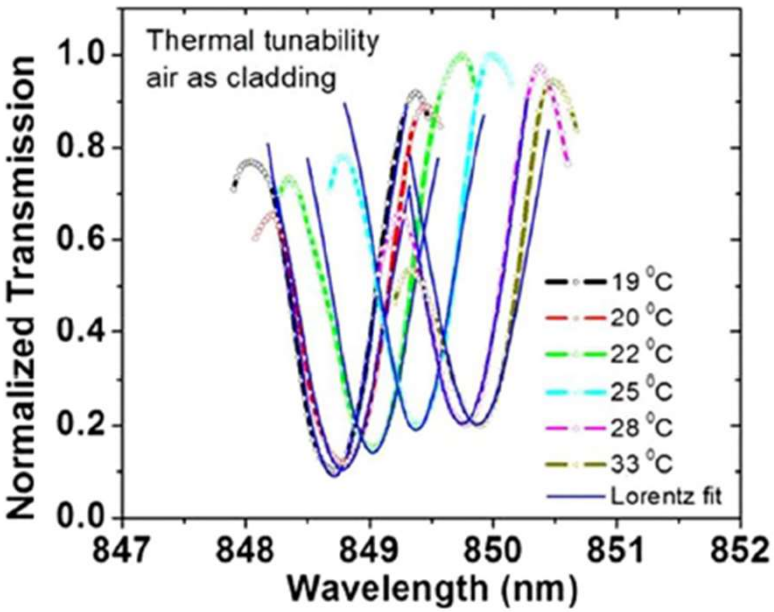

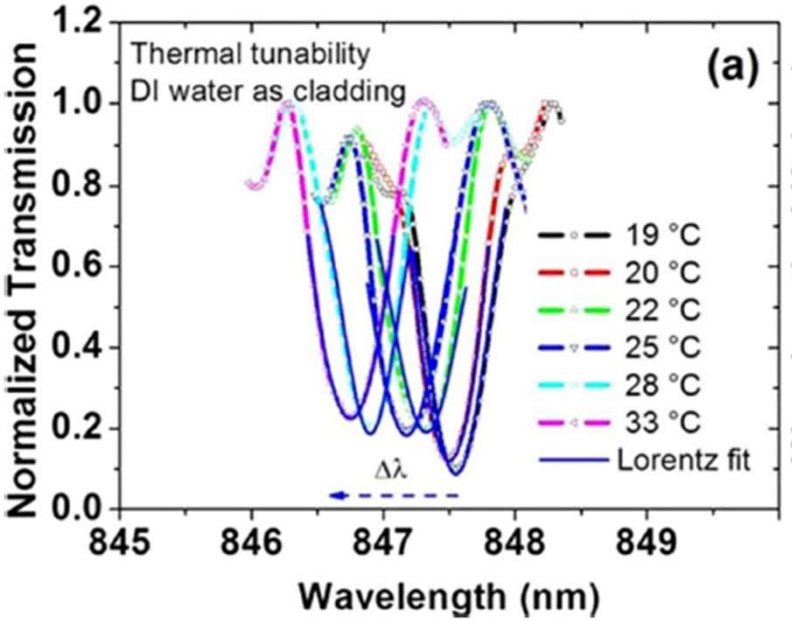

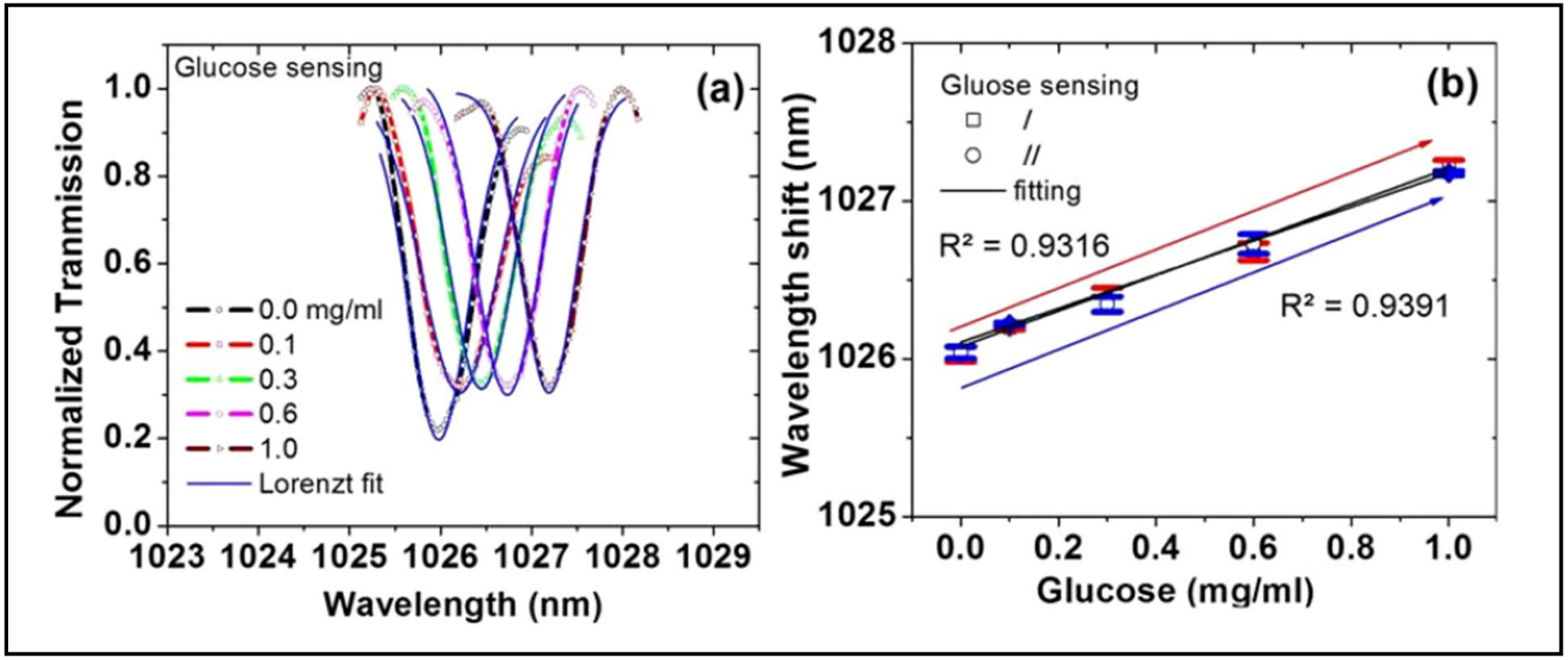

S 280 pm/(mg/ml)
Limit 0,04 mg/ml
$\Delta C \rightarrow \Delta n = 10^{-5}$

- **lecture and study of the reference :**

Advanced Device Materials *Original Research Paper*

A laterally coupled UV210 polymer racetrack micro-resonator for thermal tunability and glucose sensing capability

R. Castro-Beltrán*[1], N. Huby[1], V. Vié[1], H. Lhermite[2], L. Camberlein[3], E. Gaviot[3] and B. Bêche*[1]

[1]Institut de Physique de Rennes, IPR UMR CNRS 6251, Université de Rennes 1, bât. 11E Nanosciences, 263 Avenue Général Leclerc, 35042 Rennes, France
[2]Institut d'Electronique et de Télécommunications de Rennes, IETR UMR CNRS 6164, Université de Rennes 1, bât. 11B, 263 avenue Général Leclerc CS 74205, 35042 Rennes Cedex, France
[3]Laboratoire d'Acoustique de l'Université du Maine, LAUM UMR CNRS 6613, Université du Maine, Avenue Olivier Messiaen, 72085 Le Mans Cedex 9, France

Abstract Authors report and demonstrate the feasibility of a laterally coupled racetrack microresonator based on UV210 photoresist to act as a thermal and glucose sensor. The large thermo-optic coefficient and the detection principle based on the interaction of the evanescent field with different glucose concentrations demonstrate that this sensor displays high sensitivity on detection properties. Deep-UV lithography procedures allow us to develop a laterally coupled microresonator with submicrometer patterns. The thermo-optic response of the racetrack microresonator is interrogated by using a NiCr alloy tip positioned on the top of the device. Temperatures ranging between 19 and 33°C yield a red shift of the resonant wavelength with a linear sensitivity of 220 pm °C^{-1}. Additionally, the thermal tunability is successively demonstrated by covering the resonator with DI water. A blue shift of the resonant wavelength is obtained with a linear sensitivity of 200 pm °C^{-1}. The resonance optical properties under this top cladding conditions lead a Q-factor of 4000 with a finesse of 5.7. Glucose homogeneous sensing capability is also experimentally demonstrated. Different concentrations of glucose solutions result in a red shift of the resonant wavelengths with a linear sensitivity of 280 pm mg^{-1} ml^{-1}. Finally, these results validate the laterally coupled racetrack microresonator as an operative photonic component for integrated optical devices such as optical filters applied on telecommunication, or transducer components devoted to assess biochemical interactions.

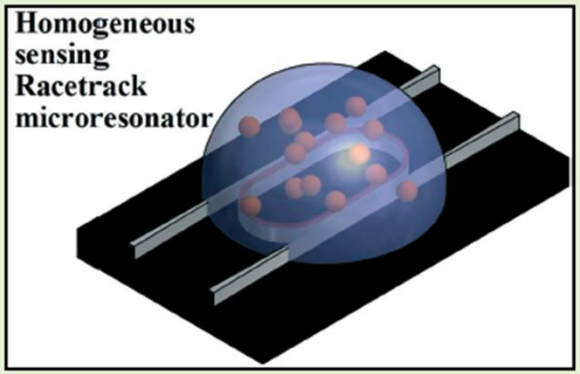

▪ Resonant probes of light to detect and follow the phase-transition in temperature : biology application, lipids (MSM)

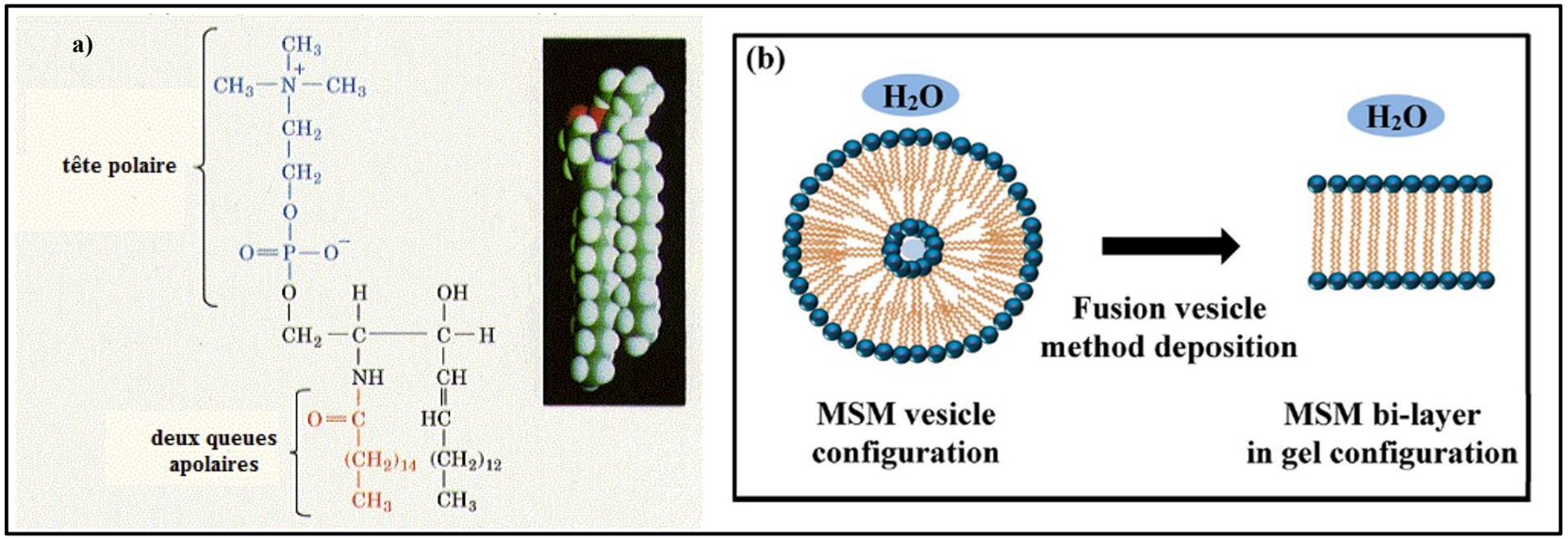

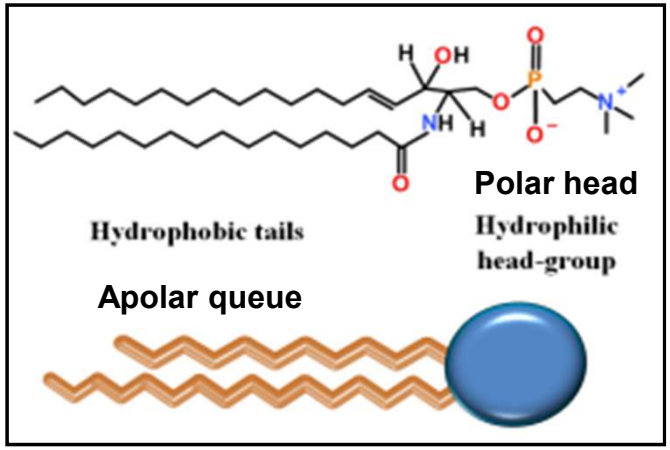

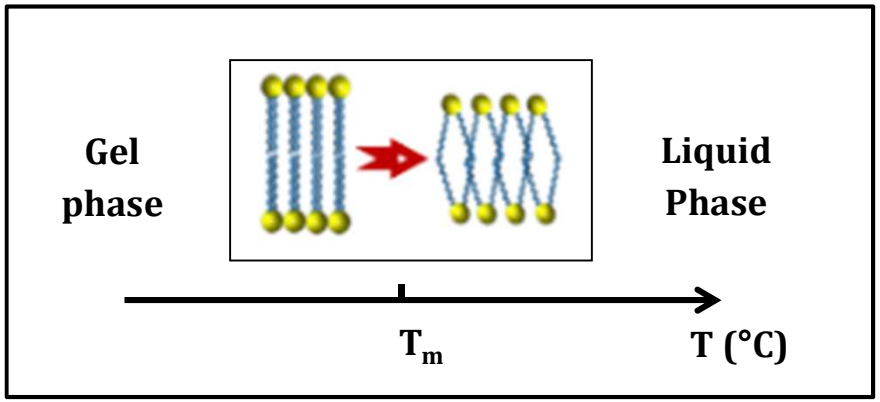

Sensors Actuators : physical A, 2017, 263, 707-717

Photonics injection
Spectral quantification

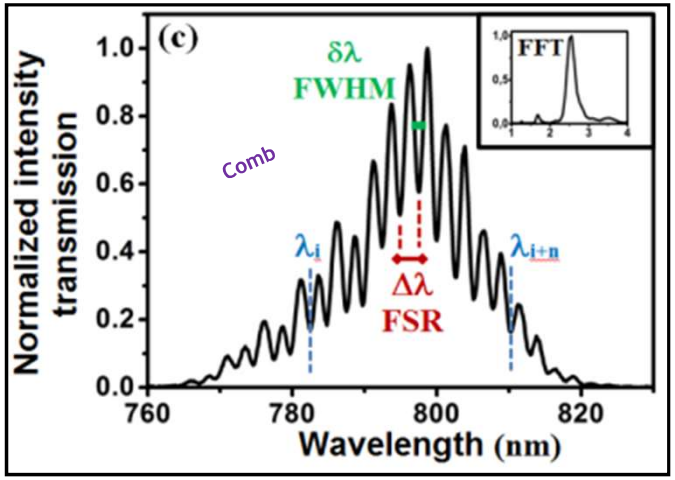

Serial spectral & statistic

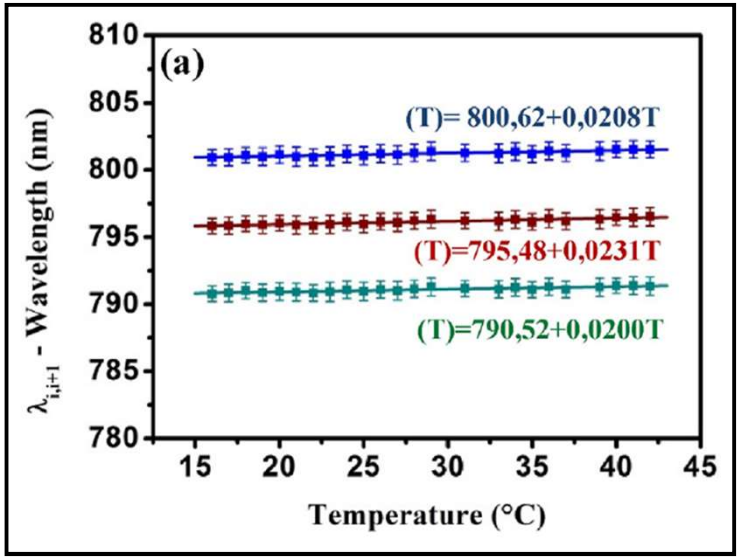

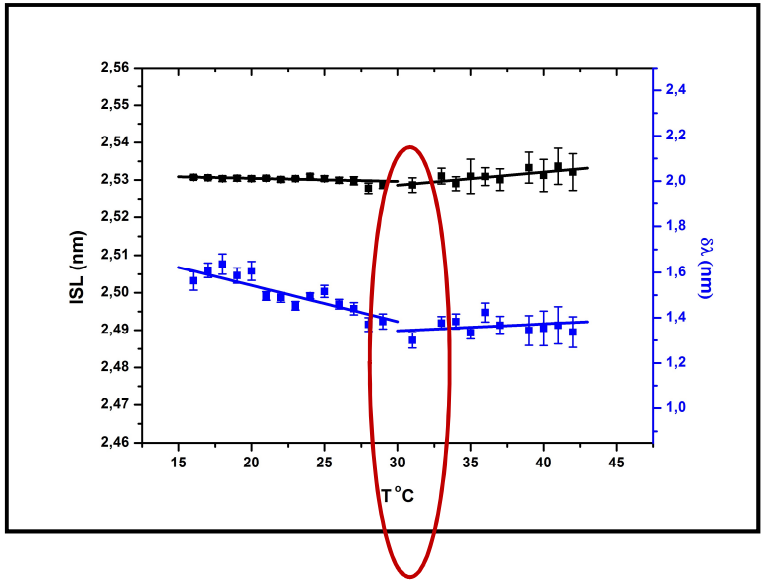

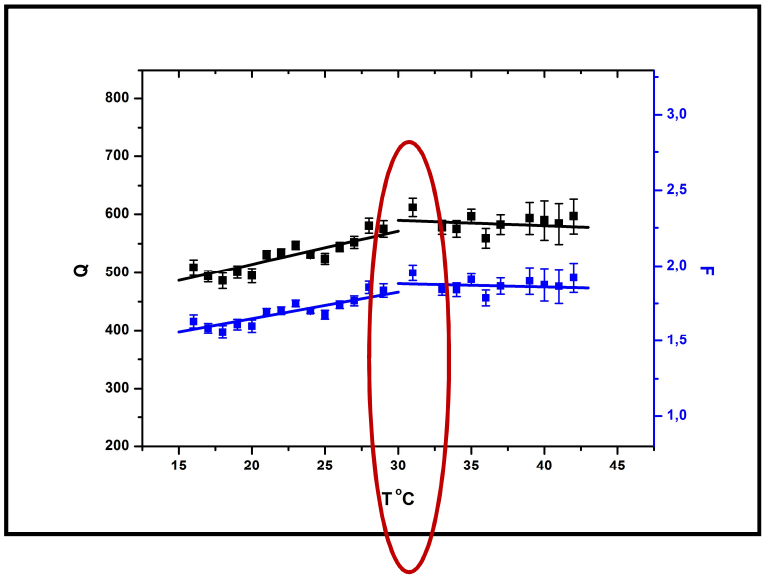

➔ **Phase-transition (gel=>liquid) of MSM-lipids at T_m [31-32]°C**

➔ DSC experiments on milk sphingomyelin

Thermogram (endothermic heat flow up) and determination of the T_m

T_m extracted from the thermograms recorded at different scanning rate

Sensors Actuators : physical A, 2017, 263, 707-717

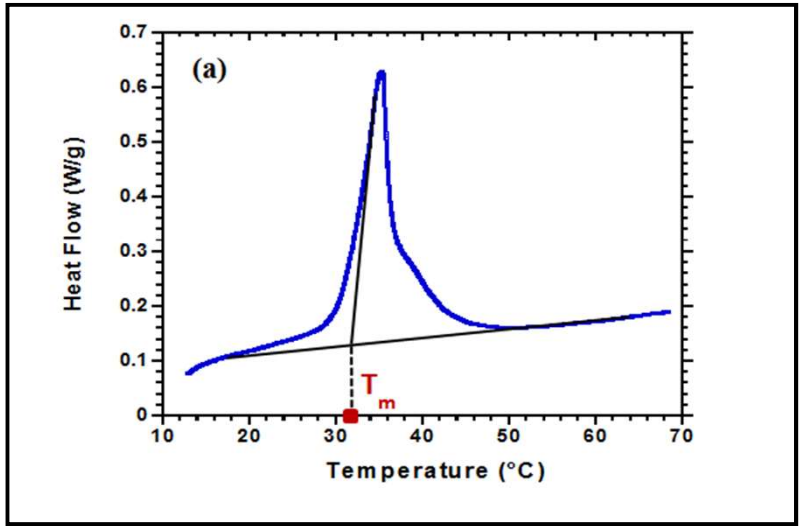

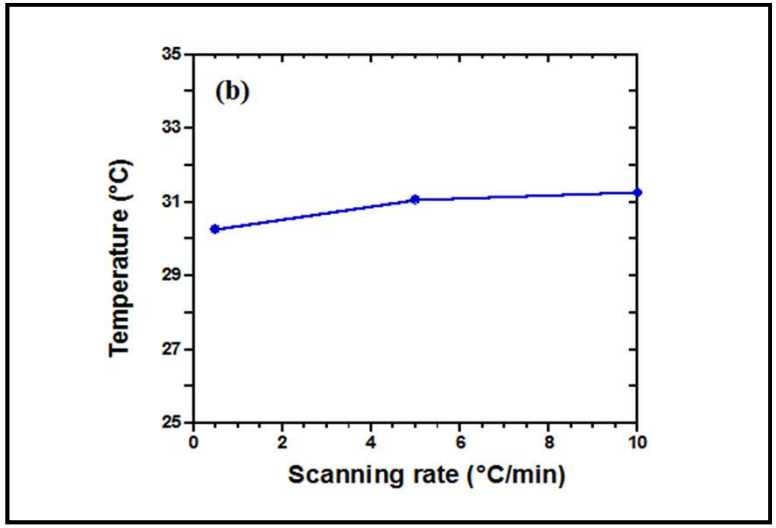

➔ Future : Towards control and measurements at distance and embedded computer systems …

▪ **lecture and study of the reference :**

Sensors and Actuators A 263 (2017) 707–717

Contents lists available at ScienceDirect

Sensors and Actuators A: Physical

journal homepage: www.elsevier.com/locate/sna

Polymer resonators sensors for detection of sphingolipid gel/fluid phase transition and melting temperature measurement

Qingyue Li[a], Véronique Vié[a], Hervé Lhermite[b], Etienne Gaviot[c], Claire Bourlieu[d], Alain Moréac[a], Denis Morineau[a], Didier Dupont[e], Sylvie Beaufils[a], Bruno Bêche[a,*]

[a] Institut de Physique de Rennes, IPR CNRS 6251, Université de Rennes 1, 35042 Rennes, France
[b] Institut d'Electronique et de Télécommunications de Rennes, IETR CNRS 6164, Université de Rennes 1, 35042 Rennes, France
[c] Laboratoire d'Acoustique de l'Université du Maine, LAUM CNRS 6613, Université du Maine, 72000 Le Mans, France
[d] Ingénierie des Agro-polymères et Technologies Émergentes, IATE UMR, CIRAD - Université Montpellier II, 34060 Montpellier, France
[e] Science et Technologie du Lait et de l'Oeuf, STLO INRA 1253, Agrocampus Ouest, 35042 Rennes, France

ARTICLE INFO

Article history:
Received 29 March 2017
Received in revised form 15 June 2017
Accepted 18 July 2017
Available online 22 July 2017

Keywords:
Integrated sensors
Photonics
Resonators
Deep UV polymer
Gel/fluid phase transition
Sphingomyelin lipids

ABSTRACT

This work describes a low-cost biophotonic sensor shaped by way of cheap processes as hybrid silicon/silica/polymer resonators able to detect biological molecule gel/fluid phase transition as lipids at very low concentration (sphingomyelin). The photonic structure is composed of specific amplified deep UV photoresist-polymer waveguides coupled by a sub-wavelength gap with racetrack microresonators allowing a low temperature-dependent operation ranging from 16 to 42 °C. The temperature dependent wavelength shift and the thermo-optic coefficient characterizing the quantified resonances and opto-geometric properties of the device have been evaluated, highlighting an enough low thermal features of the whole system for such application. With an appropriate vesicle lipid deposition process specific in biology associated to an apt experimental bio-thermo-photonic protocol (made of serial optical resonance spectra acquisitions with statistical treatments), the dynamic evolution of the sphingomyelin lipid phase transition was assessed: then, the ability to detect their own gel/fluid transition phase and melting temperature has been demonstrated with a mass product factor 10^7 lower than that of more conventional methods The equilibrium of the regime of the resonators was highlighted as being broken by the dynamic of the sphingomyelin and its own phase transition prior relevant detection.

© 2017 Elsevier B.V. All rights reserved.

▪ **Resonant probes of light to detect and follow the phase-transition in temperature in cosmetic, food… : fatty acid**

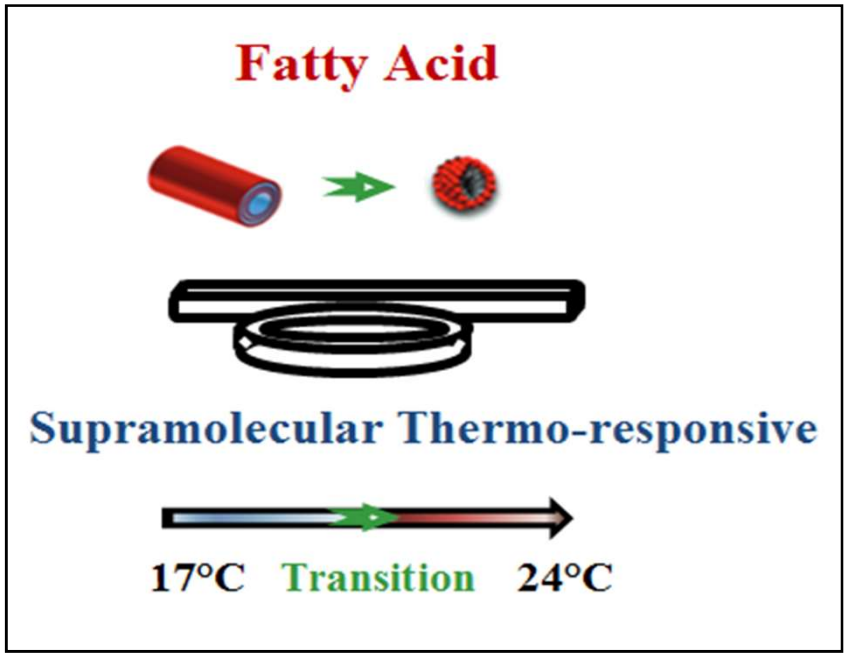

Phase transition : fatty acid 12-hydroxystearic acid (12-HAS)

(associated with alkanolamine counterions,

selection of the 5-amino-1-pentanol (C5) in the alkanolamine group)

Morphologica
l transition !

µm ⇔ nm

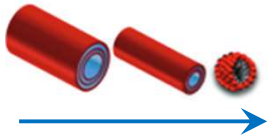

T(°C)

C5 /12-HSA compound shows a large supramolecular polymorphism

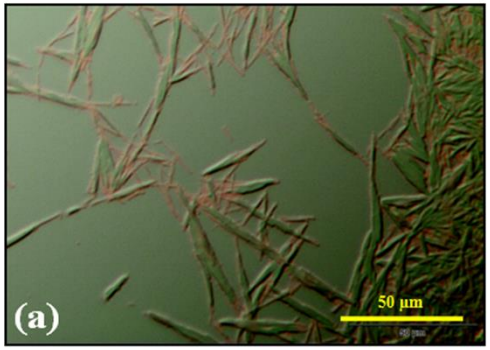

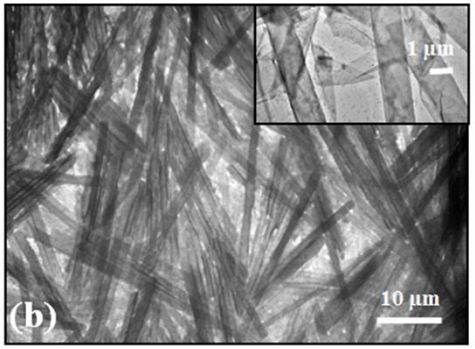

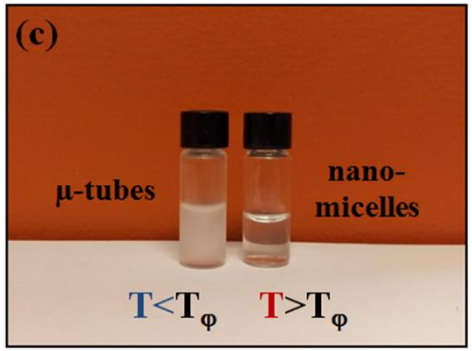

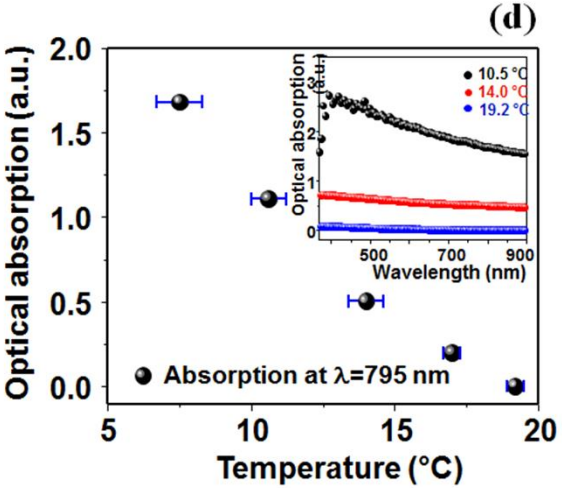

Experimental setup for the full optical characterization of the microcavities

the complete fatty acid phase-transition monitoring protocol

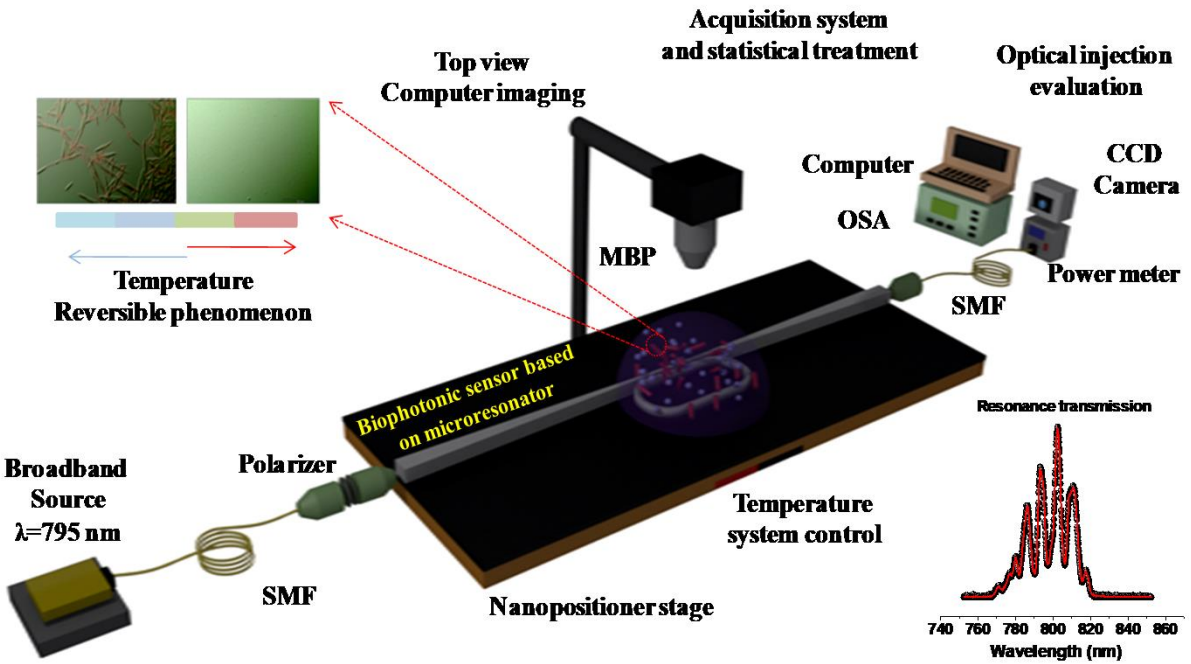

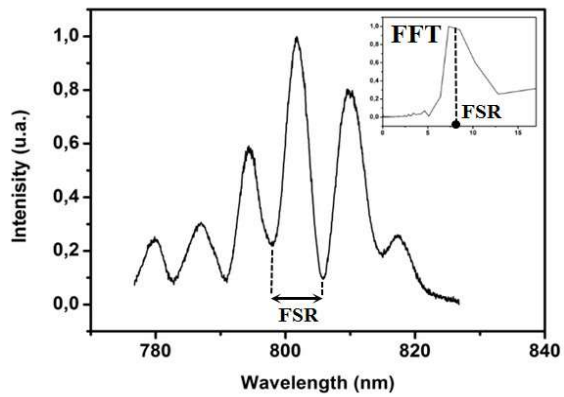

Phase transition : fatty acid (12-HAS)

Integrated Photonics

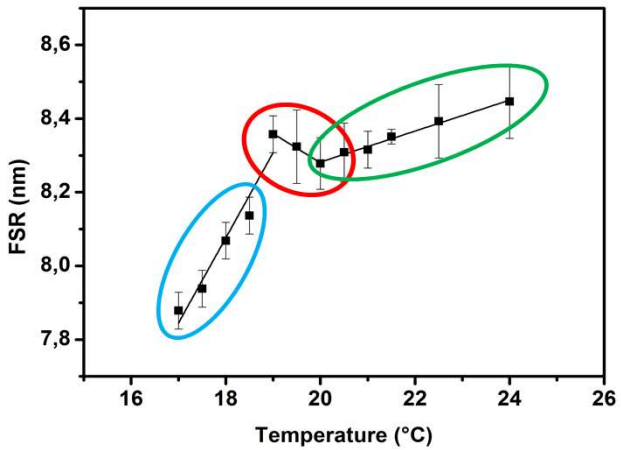

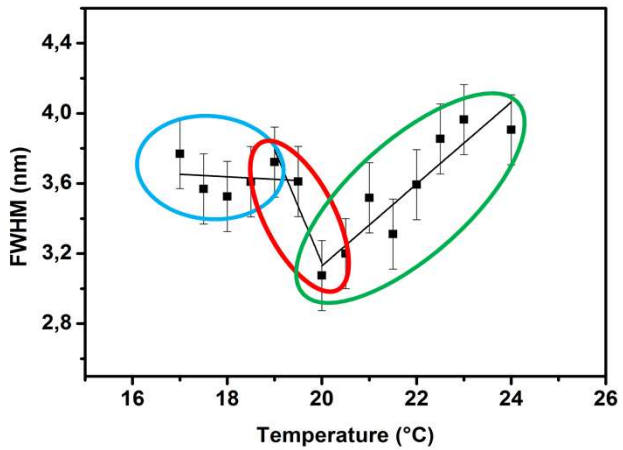

Rheology

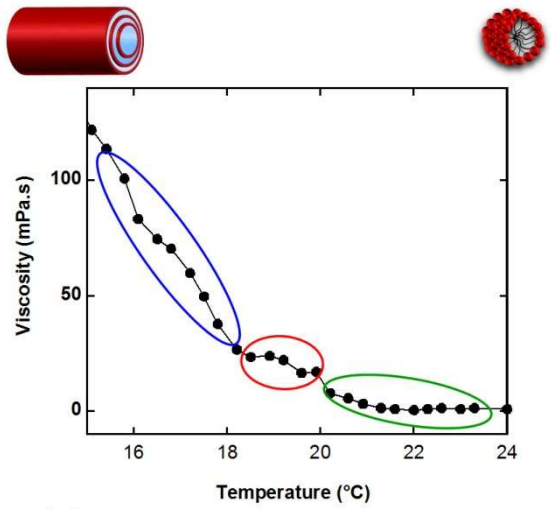

Behavior changes are much sharper in terms of optical properties !

Small volume of analysis

▪ **lecture and study of the reference :**

Optics Communications 468 (2020) 125773

Contents lists available at ScienceDirect

Optics Communications

journal homepage: www.elsevier.com/locate/optcom

Microphotonics for monitoring the supramolecular thermoresponsive behavior of fatty acid surfactant solutions

R. Castro-Beltrán [a], L. Garnier [b], A. Saint-Jalmes [b], H. Lhermite [c], H. Cormerais [c,d], A.-L. Fameau [e], E. Gicquel [b], B. Bêche [b,c,*]

[a] Universidad de Guanajuato, Departamento de Ingeniería Física, División de Ciencias e Ingenierías-León, Guanajuato, Mexico
[b] Univ Rennes, CNRS, IPR (Institut de Physique de Rennes) - UMR 6251, F-35000 Rennes, France
[c] Univ Rennes, CNRS, IETR (Institut d'Electronique et de Télécommunicationde Rennes) - UMR 6164, F-35000 Rennes, France
[d] Centrale/Supelec, Campus de Rennes, 35510, Cesson-Sévigné, France
[e] INRA-BIA, Biopolymères Interactions Assemblages, 44316 Nantes, France

ARTICLE INFO

Keywords:
Micro-technologies
Polymers
Photonics
Fatty acid
Thermos-responsive surfactant system

ABSTRACT

The development and the ability of an optical integrated polymeric resonator, acting as a surface light probe, for monitoring temperature-induced supramolecular phase transitions is presented in this work. The homogeneous detection of the transitions between different self-assembled structures in an aqueous solution of fatty acids (12-hydroxystearic acid, in association with amino-pentanol) was studied by investigating the coupling between the solution and the integrated photonic micro-cavity. Tuning the self-organized assemblies of surfactant is very attractive for many applications, such as cosmetic products, food, drug delivery and medical, and the development of alternative tools – especially those requiring minute amount of solution – to monitor their structural changes are essential. These original studies at temperatures ranging from 17 to 24 °C, based on a statistical treatment of optical resonance spectra, have evidenced the thermoresponsive nature of the optical features, and that different regimes occur with temperature. The optical results were corroborated with the measurement of the solution viscosity as a function of temperature, confirming that we can ascribe the optically-detected regimes to a surfactant assembly shifting reversibly from a tubular shape to a micellar one. The comparison between the optical and the rheological responses showed different accuracies: while the viscosity data exhibited a rather smooth and monotonous transition, the behavior changes were sharper and non-monotonous in terms of optical properties, allowing us to unambiguously identify in intermediate regime between 18.5 and 20 °C. These morphological transition experiments represent a unique opportunity to extend the numbers of available techniques studying these systems through integrated optical techniques with potential opportunities of real time detection and working on low sampling volume.

▪ Resonant probes of light to detect and follow the loss/lack of mass

Towards the notion of resonant photonic microbalance?

Following the mechanism of drying : **single water droplet – *air/water interface effect***

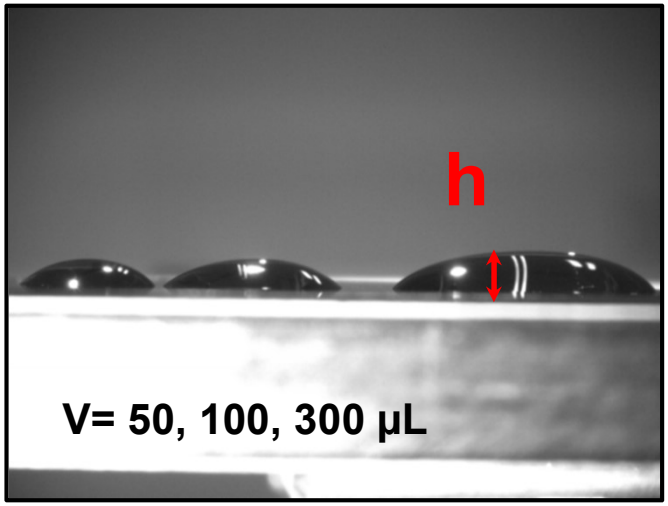

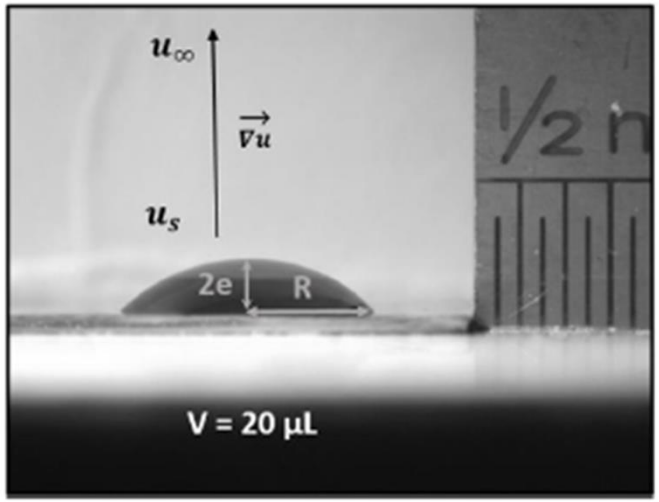

Figure 4. Side view photography of a water sessile droplet. The air is saturated with water in the close surrounding of the droplet (u_s) and drier far from this droplet (u_∞): then, a diffusion process drives the evaporation dynamics.

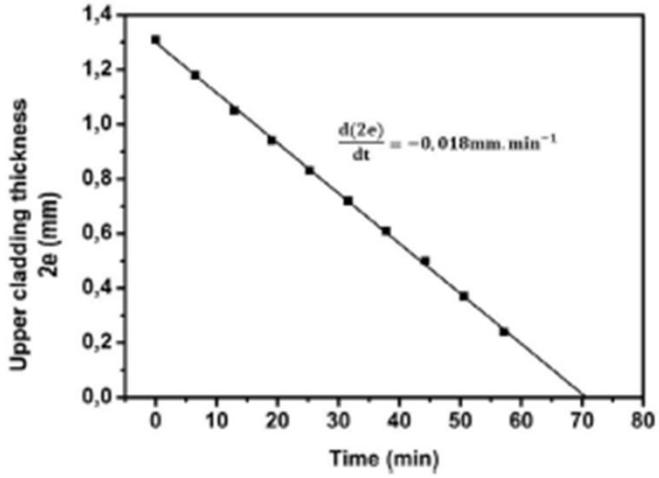

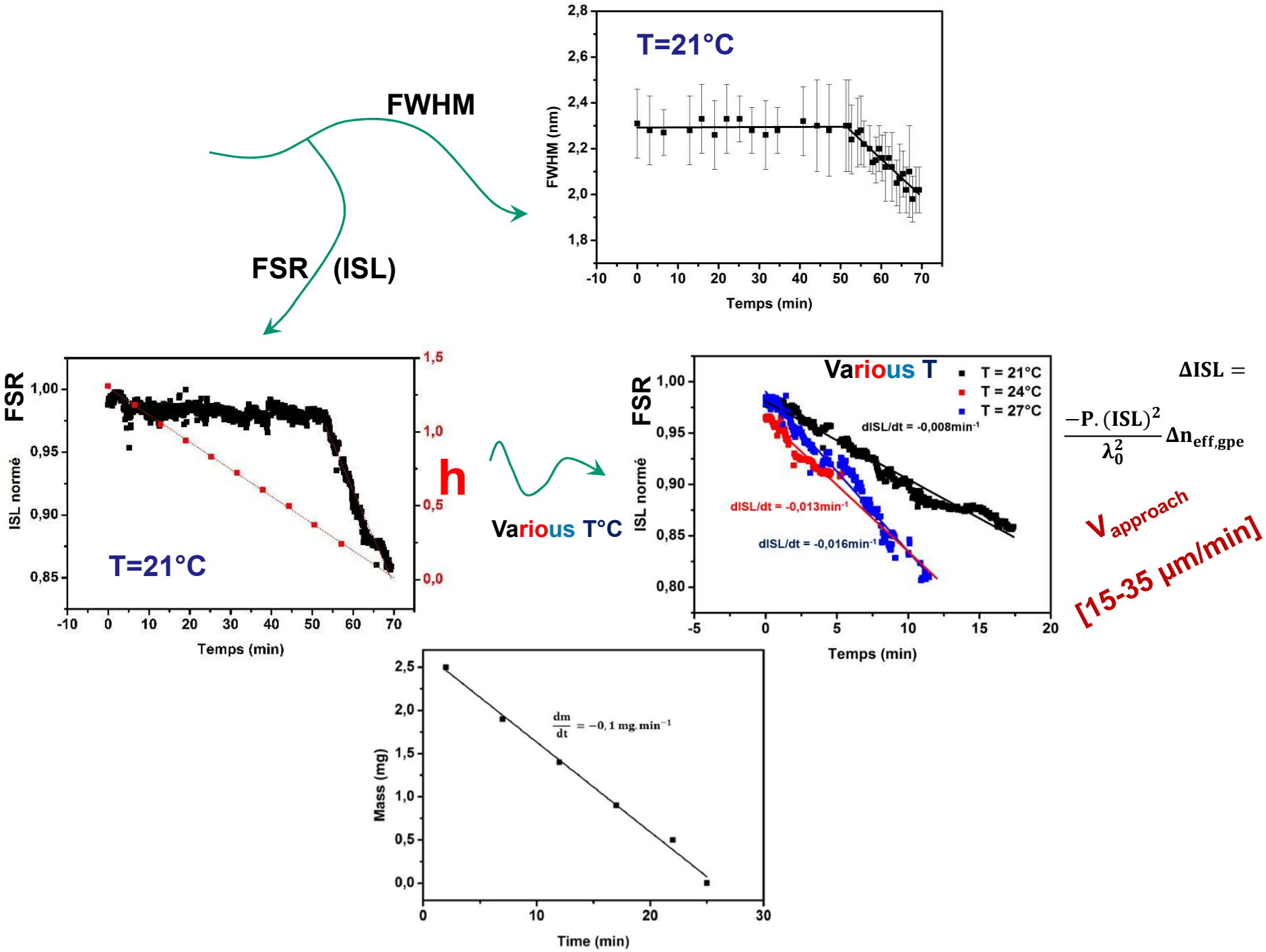
FWHM
FSR (ISL)
T=21°C
FWHM (nm)
Temps (min)
FSR
ISL normé
T=21°C
h
Various T°C
Various T
T = 21°C
T = 24°C
T = 27°C
dISL/dt = -0,008min-1
dISL/dt = -0,013min-1
dISL/dt = -0,016min-1
Temps (min)
$\Delta ISL = \frac{-P.(ISL)^2}{\lambda_0^2}\Delta n_{eff,gpe}$
$V_{approach}$
[15-35 µm/min]
$\frac{dm}{dt} = -0,1\ mg.min^{-1}$
Mass (mg)
Time (min)

IOP Publishing
Journal of Physics D: Applied Physics
J. Phys. D: Appl. Phys. 53 (2020) 125107 (10pp)
https://doi.org/10.1088/1361-6463/ab651d

Monitoring the evaporation of a sessile water droplet by means of integrated photonic resonator

Lucas Garnier[1], Hervé Lhermite[2], Véronique Vié[1], Octave Pin[3], Quentin Liddell[3], Hervé Cormerais[2,3], Etienne Gaviot[4] and Bruno Bêche[1,2]

[1] Université de Rennes 1, CNRS (Institut de Physique de Rennes)—UMR 6251, F-35000 Rennes, France
[2] Université de Rennes 1, CNRS (Institut d'Electronique et de Télécommunications de Rennes)—UMR 6164, F-35000 Rennes, France
[3] Centrale/Supelec, Campus de Rennes, F-35510 Cesson-Sévigné, France
[4] Université du Maine, CNRS (Laboratoire d'Acoustique de l'Université du Maine—UMR 6613, F-72000 Le Mans, France

E-mail: lucas.garnier@univ-rennes1.fr and bruno.beche@univ-rennes1.fr

Received 7 October 2019, revised 11 December 2019
Accepted for publication 23 December 2019
Published 13 January 2020

Abstract

We have investigated the behavior of the optical transduced signal of a photonic integrated polymer micro resonator as an evaporating water droplet is positioned upon it. The photonic chip is fabricated by means of deep-UV photolithography, and the circuits are made of polymer UV210. The device is then arranged in an optical bench so as to perform relevant measurements thanks to a broadband laser for the excitation of the resonators and an optical spectrum analyzer remotely controlled by a Matlab software for the acquisition and treatment of data. By dynamically tracking the free spectral range (FSR) of the optical mode, we come up with a signature of the thermodynamic evaporation process. In order to correlate this signature to the evaporation speed of the water droplet, a lateral camera is disposed to measure the evolution of the geometrical characteristics of the droplet, while weight measurements are performed thanks to a precision balance. These measurements provide a numerical link between the temporal variation of the FSR and the variation of the distance between the apex of the droplet and the substrate, correlating clearly the variation of the FSR with the mass change of the droplet. The measurements have been performed with 20 μl droplets for three different substrate temperatures: 21 °C, 24 °C and 27 °C. Then, theoretical investigations have been also performed in order to interpret the dynamics of the FSR in terms of guiding theory.

Chapter IV). Nanophotonic and nano-components

- **IV.1 : Electron-photon analogies, development of the basics on photonic crystals (PC); wave equation and eigenvalues; one-dimensional model (PC-1D or Bragg mirror); Bloch's theorem and Fourier expansion of dielectric functions; plane waves method decomposition; spatial periodicities and photonics band gap; two- and three-dimensional crystals cases (PC-2D and -3D); bands engineering and control of the photonic dispersion curves; localized defect modes**

IV.1.1 Electron-photon analogies, curtain call and quantum mechanical considerations

- **Wave notion and wavelength associated to such quantum particle : photon**

[IV-1]

Particle ← → wavelength

Particle world
Spot of light : photon
(m=0)

Wave world
(and quantum → h)

$$E = h\nu = hc/\lambda = \hbar\omega$$

$$\vec{p} = (m.\vec{c}) = \hbar\vec{k} \Rightarrow \|\vec{p}\| = h/\lambda$$

(kinetic quantity, pressure radiation → Crookes experience)

$$(E = c^2.m)$$

$$\|\vec{m}_t\|(\equiv S) = \pm\hbar$$

(Kinetic moment, angular = circular polarization → torsion experience)

▪ Complex wavelength function associated to photon = photonic mode

$$\boxed{\begin{array}{l} \mathrm{Op.}\left[\vec{X}\right] = \nabla^2 \vec{X} - \mu_0 \varepsilon_0 \varepsilon_{ij} \dfrac{\partial^2 \vec{X}}{\partial t^2} = \text{propagation into the space-time} \\ \vec{X} \equiv \vec{E} \text{ or } \vec{H} \end{array}} \quad \text{[IV-2]}$$

$$\vec{E}(\vec{r},t) = A(\vec{r}).\exp j\left[\omega t - \vec{k}.\vec{r} + \varphi_0\right].\vec{e}_{polar}$$ + Maxwell eq. (fields and causes)

▪ The quantum (photon) propagates along the $\vec{k}$-direction (propagation constant or wavelength vector), with kinetic quantity $\vec{p}$, and E -energy. Such a particle possess an intrinsic angular moment $\vec{m}_t$ quantified on two values (S –spin) that are link up to the polarization ; its mass is considering as null.

▪ The quantum-probability to observe a photon in an area at a t -time (during Δt) is proportional to the intensity of the optical (or photonic) -mode (associated to such space-time area :

$$\boxed{\mathrm{proba.dV.dt} \propto \mathrm{Intensity}\left(= \left\|\vec{E}(\bar{r},t)\right\|\right).\mathrm{dV.dt}} \quad \text{[IV-3]}$$

▪ Energy-time relation (Heisenberg) : $\boxed{\Delta E.\Delta t \geq \hbar/2}$ [IV-4]

✎ Quantum mechanics restrict the possibility of different dynamics variables existence into the same Δt measurements :

$$\boxed{\Delta p.\Delta t \approx \hbar/c} \longrightarrow \boxed{\text{position } \Delta x \approx \lambda} \quad \text{[IV-5]}$$

Relativistic quantum expression of a limit : the notion of ray or trajectory or 'classical coordinates' have no sense at sub-λ-dimensions (nano-photonics) !

Optik 127 (2016) 3643–3645

Contents lists available at ScienceDirect

Optik

journal homepage: www.elsevier.de/ijleo

Short note

About the Heisenberg's uncertainty principle and the determination of effective optical indices in integrated photonics at high sub-wavelength regime

B. Bêche [a,b,*], E. Gaviot [c]

[a] Institut de Physique de Rennes – IPR UMR CNRS 6251, Université de Rennes 1, Rennes 35042, France
[b] Institut Universitaire de France – IUF, Paris 75005, France
[c] Laboratoire d'Acoustique de l'Université du Maine – LAUM UMR CNRS 6613, Université du Maine, Le Mans 72000, France

ARTICLE INFO

Article history:
Received 15 September 2015
Accepted 28 December 2015

Keywords:
Integrated photonics
Heisenberg's principle

ABSTRACT

Within the Heisenberg's uncertainty principle it is explicitly discussed the impact of these inequalities on the theory of integrated photonics at sub-wavelength regime. More especially, the uncertainty of the effective index values in nanophotonics at sub-wavelength regime, which is defined as the eigenvalue of the overall opto-geometric problems in integrated photonics, appears directly stemming from Heisenberg's uncertainty. An apt formula is obtained allowing us to assume that the incertitude and the notion of eigenvalue called effective optical index or propagation constant is inversely proportional to the spatial dimensions of a given nanostructure yielding a transfer of the fuzziness on relevant senses of eigenvalues below a specific limit's volume.

© 2016 Elsevier GmbH. All rights reserved.

▪ **Quantification process of the photon in Quantum Electro Dynamics (QED)**

Total kinetic (or angular) moment can be developed for a non-relativistic particle as :

$$\boxed{\vec{j} = \vec{l} + \vec{s}} \quad \text{[IV-6]}$$

Intrinsic moment (/fixed mark) (photon, s=1) Symmetric even spinor of 2s-rank (that is 2s+1 components)

Orbital kinetic moment = localization aspect : linear combination of spherical wavelength function 'l'-order Y_{lm}

- Note : There is no rest-referential for the photon (because relativistic or *c* -aspect). With [IV.5], the potential-vector $\vec{A}$ for the photon theoretically is not perfectly an amplitude of probability. But, if the same quantification process [IV.6] (than quantum electronics) is applied, we can shape:

$\vec{A}(\vec{k})$ **: Potential vector or 2-rank-spinor ≈ vectorial amplitude function for the photon**

$$\boxed{\begin{array}{l} \Delta\vec{A} - \dfrac{1}{v^2}\dfrac{\partial^2 \vec{A}}{\partial t^2} = \ldots \text{ with } \overrightarrow{\mathrm{rot}\vec{A}} = \vec{\nabla} \wedge \vec{A} = \vec{B} \text{ and } -\vec{A} = \vec{E} + \vec{\nabla}\phi \\ \vec{A} \equiv \vec{A} + \vec{\nabla}(\text{space} - \text{time function}) \quad \text{(invariance of Jauge)} \end{array}} \quad \text{[IV-7]}$$

Such Jauge's invariance is important and valid for many attribute of the 'photon-wave' (for example the state of polarization : $\vec{e}^{(\alpha)} \equiv \vec{e}^{(\alpha)} + [\text{space} - \text{time } \overrightarrow{\text{function}}]$, α=1,2)

- Note : Due to the *c*-relativistic aspect, photon particle presents strong symmetry along its *z*-propagation-axis (helical-aspect) ➔ the projection of the moment takes two values : +/- 1 that corresponding to the two eigenvalues of the spin-projection-operator (+ for the right circular polarization and – for the left circular aspect).

- Note : Another theory based on a 2-rank tensor (or matrix) can represents the mixing state of polarization of the photon particle, called polarization density matrix ρ. Each $\vec{e}$ state of polarization can be decomposed along two basic perpendicular polarizations : $\vec{e}^{(1)}.\vec{e}^{(2)} = 0$

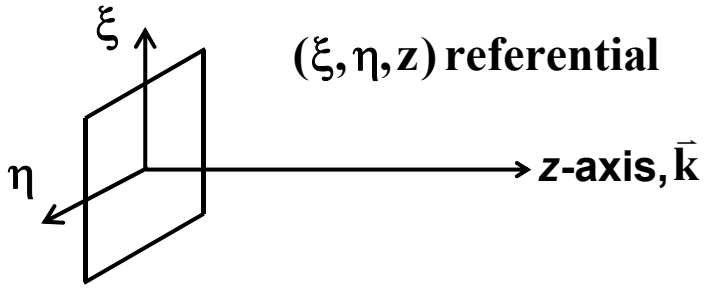

(ξ, η, z) referential

$\forall\ \vec{e} = e_1.\vec{e}^{(1)} + e_2.\vec{e}^{(2)}$

with e_i probability of $\vec{e}^{(i)}$-polarization-state

Probability that the photon presents a $\rho_{ij}\vec{e}^{(1)}.\vec{e}^{*(2)}$ polarization is $\left\langle e^{(1)} \middle| \rho \middle| e^{(2)} \right\rangle$

$$\rho = \frac{1}{2}\begin{pmatrix} 1+S_3 & S_1 - jS_2 \\ S_1 + jS_2 & 1-S_3 \end{pmatrix}$$

with $-1 \le S_i \le 1$ Stockes-parameters; S_1 is the parameter relative to the rectilinear polarization along the (+/-) $\pi/4$ from ξ-axis; S_2 represent the degree of circular polarization; S_3 characterizes the linear polarization along the ξ and η directions.

$\sum_{i=1}^{3} S_i = 1$ characterizes a total polarized state.

$S_{i=1\ \text{to}\ 3} = 0$ characterizes a non-polarized particle state.

▪ **Another electron/photon particles analogies :**

- Diffraction, capacity to interferences phenomena (coherence), physical laws at interfaces (reflection, transmission T and tunnel effect, evanescent penetration)…

[IV-9]

- Tunnel effect -

- Quantum mechanics

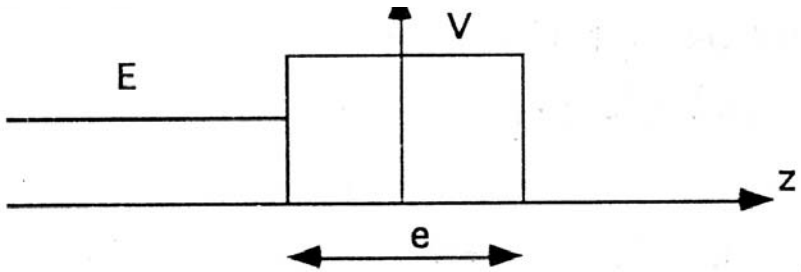

$$T = \frac{1}{\alpha . sh^2(e\,\gamma)+1}$$

$$\alpha = \frac{V^2}{4E(V-E)}$$

$$\gamma = 2\pi\frac{\sqrt{2m(V-E)}}{h}$$

électron

Analogie

- Optical and photonics

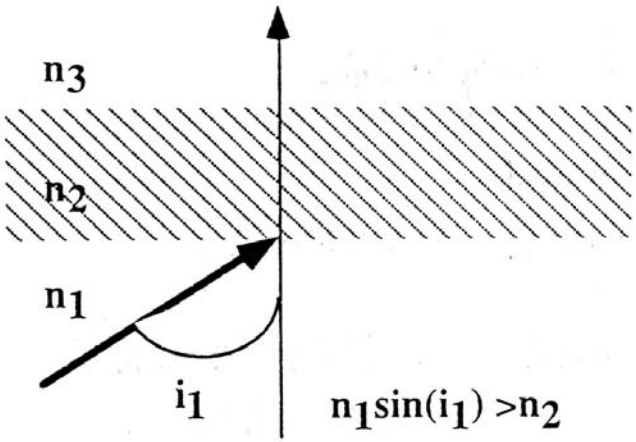

$$T = \frac{1}{\alpha . sh^2(e\,\gamma)+\beta}$$

photon

$$\gamma = \frac{2\pi n_2 e}{\lambda}\sqrt{N^2\sin^2(i_1) - 1}$$

$$n = \frac{n_3}{n_1} \qquad N = \frac{n_1}{n_2}$$

$$\alpha_{TE} = \frac{(N^2 - 1)(n^2N^2 - 1)}{4N^2\cos(i_1)(N^2\sin^2(i_1) - 1)\sqrt{n^2 - \sin^2(i_1)}}$$

$$\alpha_{TM} = \frac{\alpha_{TE}}{n^2}[(N^2 + 1)\sin^2(i_1) - 1)]\,][\,(n^2N^2 + 1)\sin^2(i_1) - n^2)]$$

$$\beta_{TE} = \frac{[\sqrt{n^2 - \sin^2(i_1)} + \cos(i_1)]^2}{4\cos(i_1)\sqrt{n^2 - \sin^2(i_1)}} \qquad \beta_{TM} = \frac{[\sqrt{n^2 - \sin^2(i_1)} + n^2\cos(i_1)]^2}{4n^2\cos(i_1)\sqrt{n^2 - \sin^2(i_1)}}$$

si $n_1 = n_3 = N \quad n_2 = 1$

$$\beta_{TE} = \beta_{TM} = 1 \quad T = \frac{1}{\alpha sh^2(e\gamma) + 1}$$

$$\alpha_{TE} = \frac{(N - 1)^2}{4N^2}\frac{1}{\cos^2(i_1)(N^2\sin^2(i_1) - 1)} \qquad \alpha_{TM} = \alpha_{TE}[(N^2 + 1)\sin^2(i_1) - 1]^2$$

$$\gamma = \frac{2\pi e}{\lambda}\sqrt{N^2\sin^2(i_1) - 1}$$

➔ See Scanning Tunneling (near field) Optical Microscopy (STOM, SNOM, attenuated total reflection method) ; Singe (1928) + Pohl and Betzig (1984).

- Same type of quantification-process, eigen -values and -vectors problem, confinement and energy level, same extrema-integral-formulation on space-time (QED, Feynman)

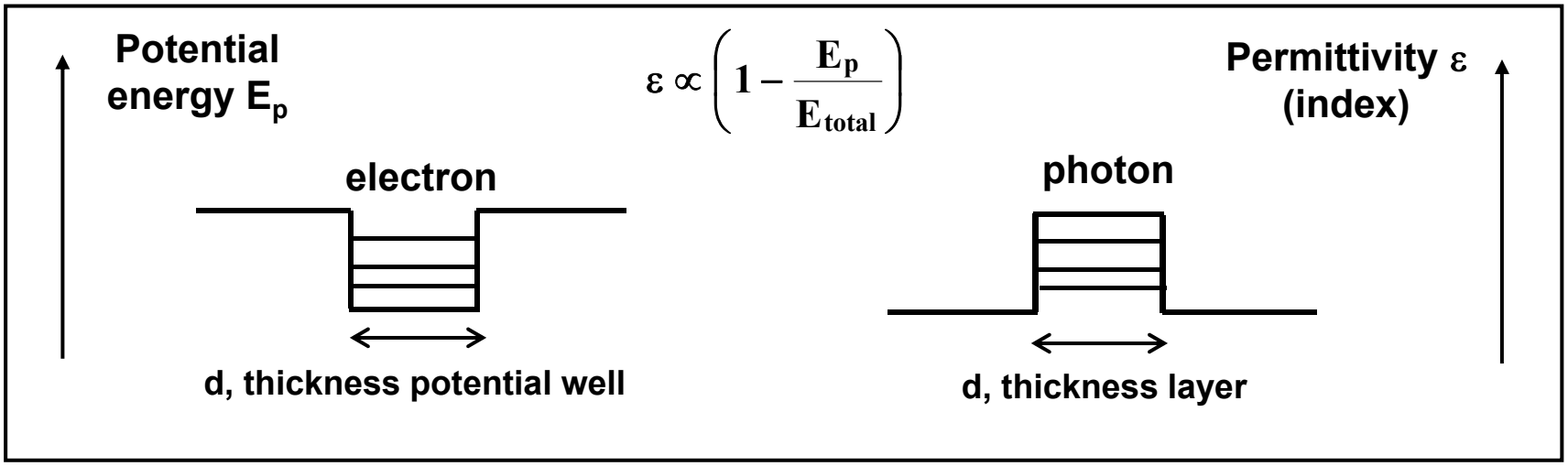

- **Extended comparison between quantum mechanics in a periodic potential and electromagnetism in a periodic dielectric structure (*J.D. Joannopoulos, 'Photonics Crystals : molding the flow of light', Princeton, 1995*)**

	QUANTUM MECHANICS IN A PERIODIC POTENTIAL (CRYSTAL)	ELECTROMAGNETISM IN A PERIODIC DIELECTRIC (PHOTONIC CRYSTAL)
What is the "main function" that contains all of the information?	The scalar wave function $\Psi(\mathbf{r}, t)$.	The magnetic vector field $\mathbf{H}(\mathbf{r}, t)$.
How do we separate out the time dependence of the function (into normal modes)?	$\Psi(\mathbf{r}, t) = \sum_E c_E \Psi_E(\mathbf{r}) e^{iEt/h}$ Expand in a set of energy eigenstates $\Psi_E(\mathbf{r})$	$\mathbf{H}(\mathbf{r}, t) = \sum_\omega c_\omega \mathbf{H}_\omega(\mathbf{r}) e^{i\omega t}$ Expand in a set of harmonic modes $\mathbf{H}_\omega(\mathbf{r})$.
What is the "master equation" that determines the normal modes of the system?	$\left(\frac{p^2}{2m} + V(\mathbf{r})\right)\Psi_E(\mathbf{r}) = E\,\Psi_E(\mathbf{r})$ The Schrödinger equation.	$\boxed{\nabla \times \frac{1}{\varepsilon(\mathbf{r})} \nabla \times \mathbf{H}_\omega(\mathbf{r}) = \frac{\omega^2}{c^2}\mathbf{H}_\omega(\mathbf{r})}$ (par ex. l'éq. de propagation pour $\vec{H}$) The Maxwell equations.
Are there any other conditions on the main function?	Yes, it must be normalizable.	Yes, the field must be both normalizable and transverse: $\nabla \cdot \mathbf{H} = 0$.
Where does the periodicity of the system enter?	The potential: $V(\mathbf{r}) = V(\mathbf{r} + \mathbf{R})$, for all lattice vectors R.	The dielectric: $\boxed{\varepsilon(\mathbf{r}) = \varepsilon(\mathbf{r} + \mathbf{R})}$, for all lattice vectors R. ↳ périodicité de la permittivité
Is there any interaction between normal modes?	Yes, there is an electron-electron repulsive interaction that makes large-scale computation difficult.	In the linear regime, light modes can pass right through one another undisturbed, and can be calculated independently.

(Voir calcul dans cours)
- valeurs propres ω_n
- et vecteurs propres (modes) H_{ω_n}

photocopie de : J. D. Joannopoulos, 'Photonics Crystals', Molding the flow of light, Princeton University Press (1995). [livre tout public] (1ère lecture sur BIP)

What important properties do the normal modes have in common?	Eigenstates with different energies are orthogonal, they have real eigenvalues, and can be found with a variational principle.	Modes with different frequencies are orthogonal, they have real positive eigenvalues, and can be found with a variational principle.
On what fact about the master equation do the important properties rely?	The Hamiltonian H is a linear, Hermitian operator.	The Maxwell operator Θ is a linear, Hermitian operator.
What is the variational theorem we use to determine the normal modes and frequencies?	$E_{var} = \frac{\langle\Psi \mid H \mid \Psi\rangle}{\langle\Psi \mid \Psi\rangle}$ } principe variationnel { E_{var} is minimized when Ψ is an eigenstate of H.	$E_{var} = \frac{(\mathbf{H}, \Theta\mathbf{H})}{(\mathbf{H}, \mathbf{H})}$ E_{var} is minimized when $\mathbf{H}$ is a normal mode of Θ.
What is the heuristic that goes along with the variational theorem?	The wave function concentrates in regions of low potential, while remaining orthogonal to lower states.	The fields concentrate their electrical energy in high-ε regions, while remaining orthogonal to lower modes.
What is the physical *energy of the system?*	The eigenvalue E of the Hamiltonian.	$E = \left(\frac{1}{8\pi}\right)\int d\mathbf{r}\left(\frac{1}{\varepsilon}\lvert\mathbf{D}\rvert^2 + \lvert\mathbf{H}\rvert^2\right)$ The electromagnetic energy.
Is there a natural length scale to the system?	Usually, because constants such as the Bohr radius set the length scale.	No, solutions are scalable to any length scale.
What is the mathematical statement that says: "A is a symmetry of the system"?	A commutes with the Hamiltonian: $[A, H] = 0$.	A commutes with the Maxwell operator: $[A, \Theta] = 0$.

	Quantum Mechanics in a Periodic Potential (Crystal)	Electromagnetism in a Periodic Dielectric (Photonic Crystal)
How do we classify the normal modes using a system's symmetries?	Distinguish them by how they transform under a symmetry operation A.	Distinguish them by how they transform under a symmetry operation A.
What does the discrete translational symmetry of a crystal allow us to do?	$\Psi_{\mathbf{k}}(\mathbf{r}) = u_{\mathbf{k}}(\mathbf{r})e^{i\mathbf{k}\cdot\mathbf{r}}$ Write the wave function in Bloch form.	$\mathbf{H}_{\mathbf{k}}(\mathbf{r}) = \mathbf{u}_{\mathbf{k}}(\mathbf{r})e^{i\mathbf{k}\cdot\mathbf{r}}$ Write the harmonic modes in Bloch form.
What are the allowable values for the wave vvector $\mathbf{k}$?	They lie in the Brillouin zone in reciprocal space.	They lie in the Brillouin zone in reciprocal space.
What do we mean by the term "band structure"?	The functions $E_n(\mathbf{k})$, which tell us the energies of the allowed eigenstates.	The functions $\omega_n(\mathbf{k})$, which tell us the frequencies of the allowed harmonic modes.
What is the physical origin of the band structure?	The electron wave scatters coherently from the different potential regions.	The electromagnetic fields scatter coherently at the interfaces between different dielectric regions.
What happens inside a gap in the band structure?	No propagating electrons in that energy range are allowed to exist, regardless of wave vector.	No extended modes in that frequency range are allowed to exist, regardless of wave vector.
What do we call the bands immediately above and below the gap?	The band above the gap is the *conduction band;* the band below the gap is the *valence band.*	The band above the gap is the *air band;* the band below the gap is the *dielectric band.*
How do we introduce defects into the system?	By adding foreign atoms to the crystal, which breaks the translational symmetry of the atomic potential.	By changing the dielectric constant of certain regions, which breaks the translational symmetry of $\varepsilon(\mathbf{r})$.
What is the result of introducing a defect?	It might create an allowed state in a band gap, thereby permitting a localized electron state around the defect.	It might create an allowed state in a band gap, thereby permitting a localized mode around the defect.
How do we classify different types of defects?	Donor atoms pull states from the conduction band into the gap; acceptor atoms pull states from the valence band into the gap.	Dielectric defects pull states from the air band into the gap; air defects pull states from the dielectric band into the gap.
In short, why is the study of the physics of the system important?	We can tailor the *electronic* properties of materials to our needs.	We can tailor the *optical* properties of materials to our needs.

- **IV.1.2 Development of the basics on photonic crystals (PC); one-dimensional model (Bragg mirror vision and PC-1D); Bloch's theorem and Fourier expansion of dielectric functions; wave equation and eigenvalues; plane waves method decomposition; spatial periodicities and photonics band gap; two- and three-dimensional crystals cases (PC-2D and -3D); bands engineering and control of the photonic dispersion curves, notion of defect and localized modes.**

- **Physical effect of a spatial periodicity, notion of photonic crystals, topologic structures examples**

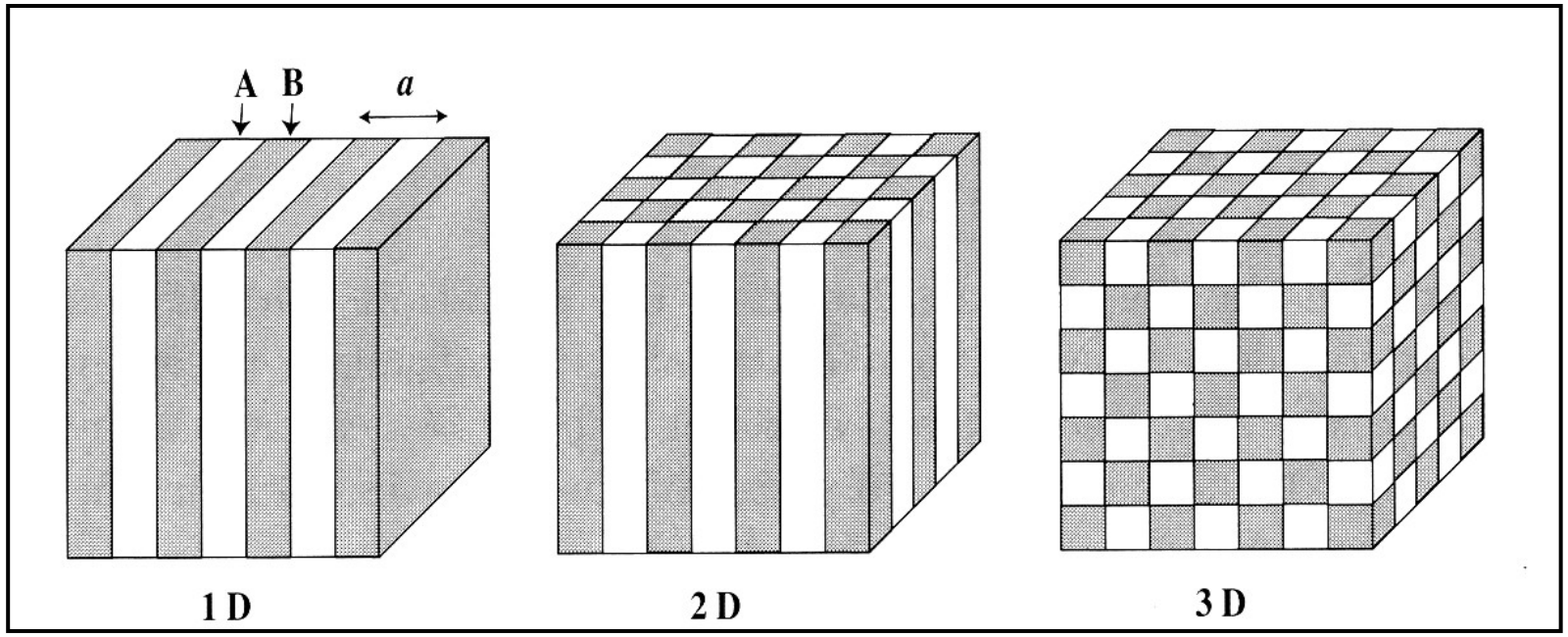

▪ Photonics crystal notion (PC) 1D or Bragg mirror : optical approach

➔ case $n_2 > n_1$

Incident ray (*considered perpendicular to the element surface*)

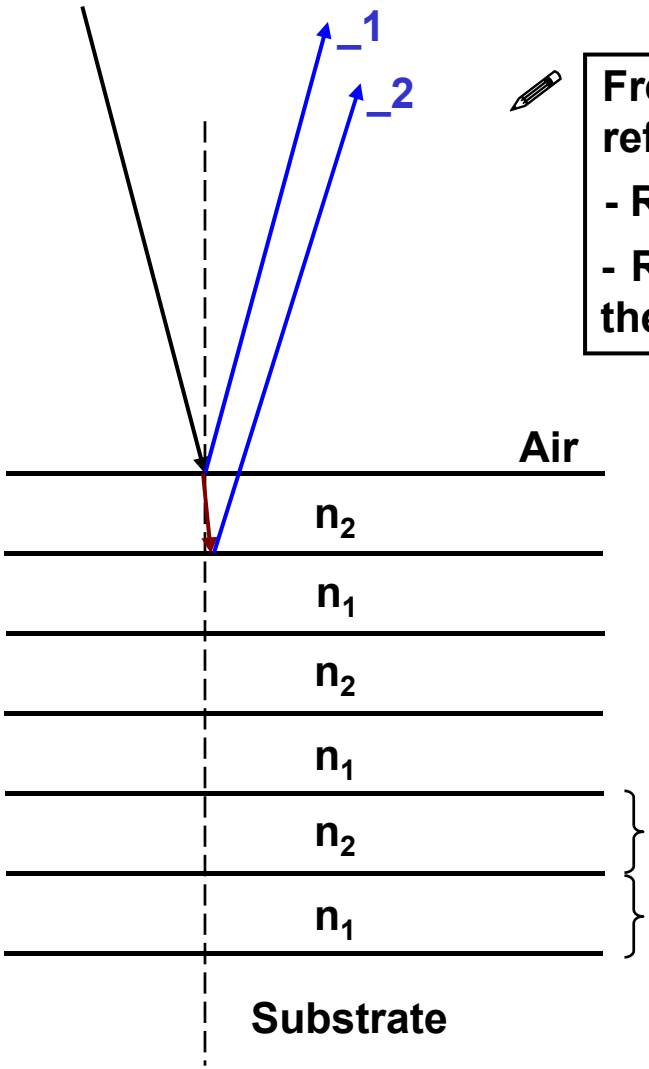

Fresnel's calculus of successive phase at each reflection

- Reflect ray number_1: π-phase at the interface

- Reflect ray number_2: no- reflected phase at the interface

d_2 thickness= $\frac{\lambda}{4n_2}$

d_1 thickness= $\frac{\lambda}{4n_1}$

(called "λ/4-layers")

▪ Main properties of such PC-1D, Photonic Band Gap PBG-1D or Bragg mirror

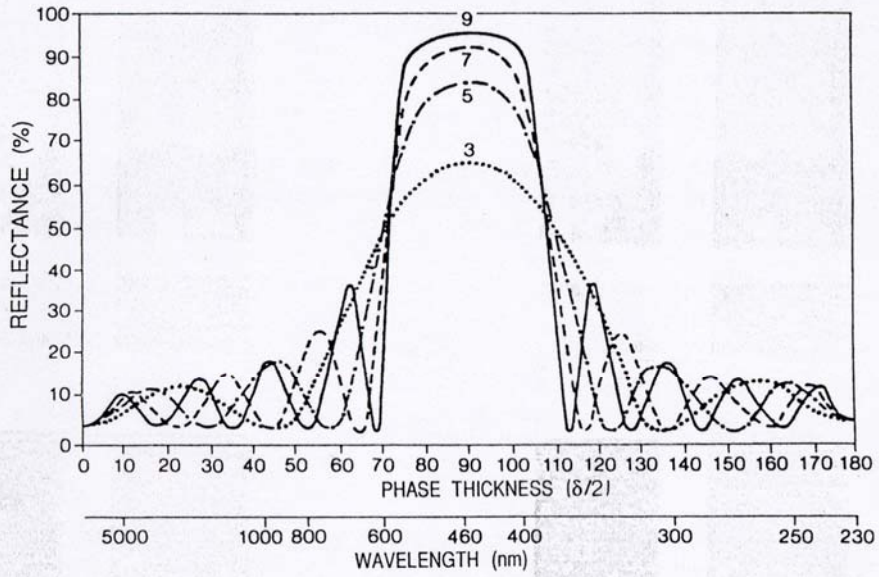

(a)

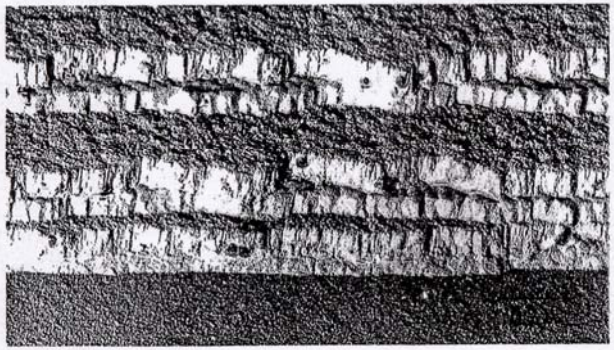

(b)

(a) Spectral characteristics of multilayer stacks formed of alternating $\lambda/4$ layers of ZnS and MgF_2 on glass ($n_2 = 1.52$) as a function of $2\pi nd/\lambda$. Normally incident light with $\lambda = 4600$ Å assumed. Number of layers in each stack is indicated. (From Ref. 18). (b) Transmission electron micrograph of a replica of the ZnS/MgF_2 multilayer cross section. (Courtesy of K. H. Guenther).

- Each successive reflected ray is in phase at the infinite ➔ mirror-object for previous λ (or fixed spectral width) !

- The maximum reflectance R is obtained into such width spectral with high number of 'n_1/n_2 bi-layers' (R>99.5% can be obtained).

- Spectral width characteristic increase with the contrast index or (n_2/n_1) ratio.

- Existence of second order Bragg-peak : $\lambda_p=\lambda_{Bragg}/(2p+1)$

- If the incidence changes, the position of the spectral characteristic is shifts too.

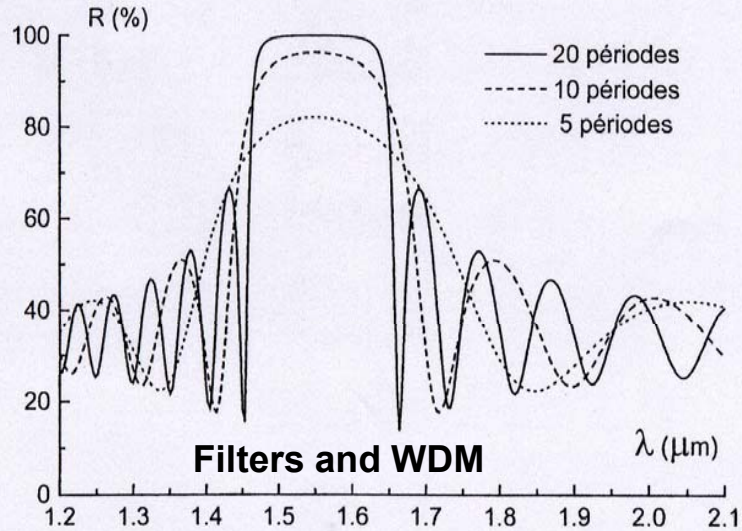

Pouvoir réflecteur d'un miroir de Bragg idéal, centré à λ=1,55 µm, en fonction du nombre de périodes (Malzac J.P. - 1996)

▪ **In conclusion, the photon-particles (into the spectral band gap) are not allow to propagate into such multilayer material or stack (but there is no absorption process, it is forbidden for such photon to exist into such new stack or periodical object) ➔ notion of spectral forbidden band and Photonic Band Gap crystals (PBG crystals).**

▪ **Physical properties and dispersion curves of such PBG crystals :**

- For respectively the bulk materials or the 'classical' integrated optics circuits the dispersion curves or the light cone that limiting the dispersion curves of optical guided modes are linear relations ➔ propagation constant $k=\omega n/c$ or $\omega(k)=ck/n$ (inverse or reciprocal space), with n index of the bulk material or index of the core or cladding layer (see chapter II).
- If a the material is composed by a dielectric multilayer stack (or heterostructure) that present a permittivity-periodicity $\varepsilon(x)=\varepsilon(x+a)$ along the *x*-direction of photon propagation, it can be shown by a Fourier expansion and a band calculation by plane-wave expansion method that the photon dispersion curves (in the inverse space) are fall back.
- Moreover, if the ratio of permittivity $(\varepsilon_2/\varepsilon_1)>2$, then such fall-back dispersion curves can open forbidden areas at the end of first Brillouin zone.

⬇

Such engineering ultimate band control concepts for the photon-particles can be developed for the realization of new devices in nanophotonics and nano-components.

▪ Photonics Band Gap crystals notion (PBG-1D) : physical approach

Calculus of the PBG or forbidden zone for a PC-1D

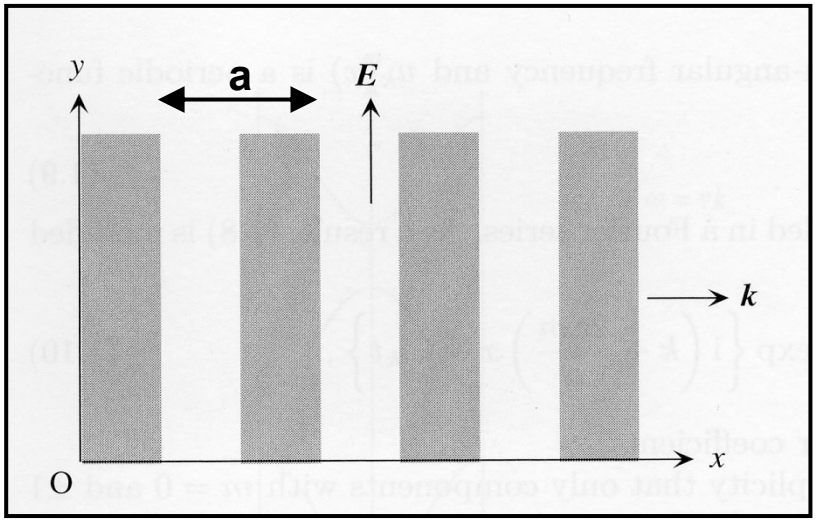

[IV-10]

$$\frac{c^2}{\varepsilon(x)}\frac{\partial^2 E(x,t)}{\partial x^2} = \frac{\partial^2 E(x,t)}{\partial t^2}$$

with periodicity $\varepsilon(x+a) = \varepsilon(x)$

[IV-11]

$$\varepsilon^{-1}(x) = \sum_{m\to-\infty}^{m\to+\infty} \kappa_m . \exp\left[j\frac{2\pi m}{a} x \right]$$

Bloch Floquet theorem

[IV-12]

$$E_k(x,t) = \sum_{m\to-\infty}^{m\to+\infty} E_m . \exp\left[j\left(k + \frac{2\pi m}{a} \right) x - j\omega_k t \right]$$

[IV-10 to 12] + development at +/-1 order (that is m=0 and m=+/-1)

[IV-13]

At the end of 1st Brillouin zone ($k \to \frac{\pi}{a}$)

$$\begin{cases} \left(\omega_k^2 - \kappa_0 c^2 k^2\right) E_0 - \kappa_1 c^2 \left(k - \frac{2\pi}{a}\right)^2 E_{-1} = 0 \\ -\kappa_{-1} c^2 k^2 E_0 + \left[\omega_k^2 - \kappa_0 c^2 \left(k - \frac{2\pi}{a}\right)^2\right] E_{-1} = 0 \end{cases}$$

[IV-14]

$$\omega_\pm \approx \frac{\pi c}{a}\sqrt{\kappa_0 \pm |\kappa_1|} \pm \frac{ac}{\pi |\kappa_1| \sqrt{\kappa_0}}\left(\kappa_0^2 - \frac{|\kappa_1^2|^2}{4}\right)\left(k - \frac{\pi}{a}\right)^2$$

For $k \to \frac{\pi}{a}$

[IV-15]

$$\text{PBG}: \frac{\pi c}{a}\sqrt{\kappa_0 - |\kappa_1|} < \omega < \frac{\pi c}{a}\sqrt{\kappa_0 + |\kappa_1|}$$

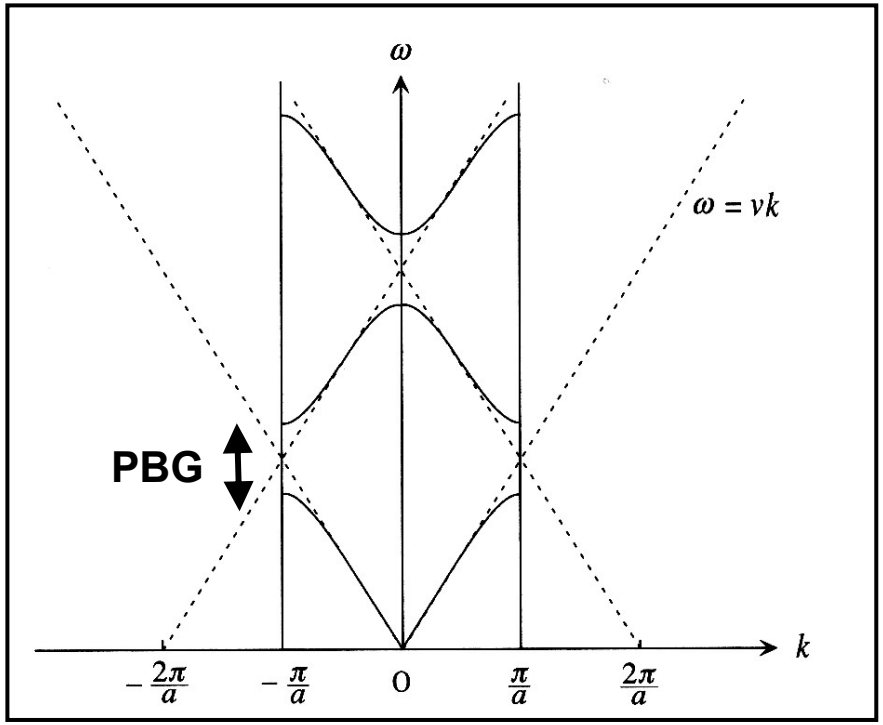

▪ Photonics Band Gap crystals notion (PBG-2D and 3D) : generalization

Periodicity entails $\varepsilon(\vec{r}+\vec{a}_i)=\varepsilon(\vec{r})$ (i=1 à 3) , $\{\vec{a}_i\}$ vectors of the direct space of PC

$\vec{G}=\sum_{i=1}^{3} l_i \vec{b}_i$, vectors of reciprocal space, $\vec{a}_i \cdot \vec{b}_j = 2\pi\,\delta_{ij}$

➔ $\varepsilon^{-1}(\vec{r})=\sum_{\vec{G}} \kappa(\vec{G}).\exp[j\vec{G}.\vec{r}]$ ➔ Optical field : $\vec{E}(\vec{r},t)=\vec{E}(\vec{r}).e^{-j\omega t}$

[IV-16]

$$\frac{1}{\varepsilon(\vec{r})}\nabla\wedge\left(\nabla\wedge\vec{E}(\vec{r},t)\right)=-\frac{1}{c^2}\frac{\partial^2\vec{E}(\vec{r},t)}{\partial t^2} \longrightarrow \frac{1}{\varepsilon(\vec{r})}\nabla\wedge\left(\nabla\wedge\vec{E}(\vec{r})\right)=\frac{\omega^2}{c^2}\vec{E}(\vec{r})$$

[IV-17]

Fourier development of the optical field : $\vec{E}(\vec{r})\equiv\vec{E}_{\vec{k}n}(\vec{r})=\vec{u}_{\vec{k}n}(\vec{r}).e^{j\vec{k}.\vec{r}}$ with

$$\vec{E}_{\vec{k}n}(\vec{r})=\sum_{\vec{G}}\vec{E}_{\vec{k}n}(\vec{G}).\exp\left[j(\vec{k}+\vec{G}).\vec{r}\right]$$

Eigenvalues equation of the dispersion curves:

[IV-18]

[IV-16 & 17] ⟶

$$-\sum_{\vec{G}'}\kappa(\vec{G}-\vec{G}').(\vec{k}+\vec{G}')\wedge\left[(\vec{k}+\vec{G}')\wedge\vec{E}_{\vec{k}n}(\vec{G}')\right]=\frac{\omega_{\vec{k}n}^2}{c^2}\vec{E}_{\vec{k}n}(\vec{G})$$

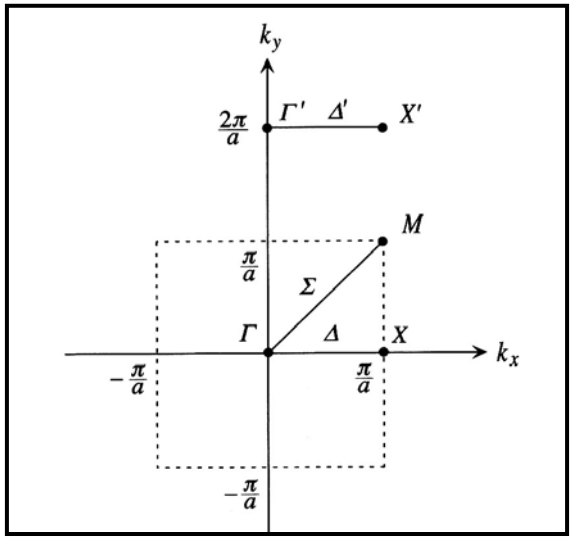

Reciprocal lattice space of the 2D square photonic crystal with the lattice constant *a*.

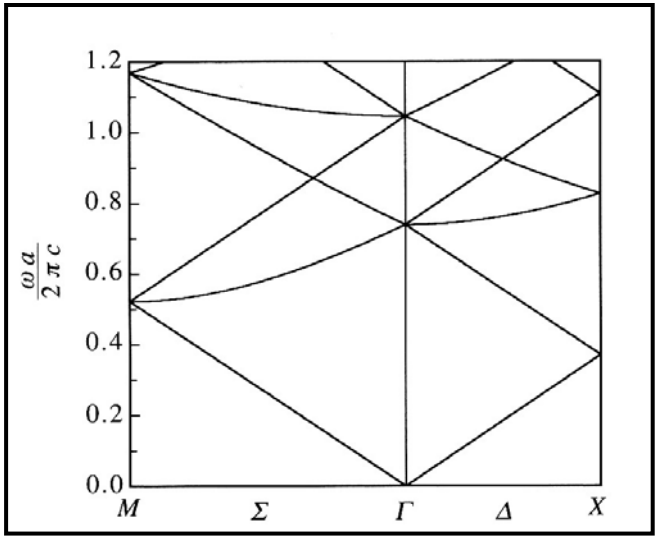

Dispersion relation for a 2D photonic crystal with infinitesimally small spatial variation of the dielectric constant. The abscissa represents the wave vector in the first Brillouin zone. The ordinate is normalized frequency where *a* stands for the lattice constant.

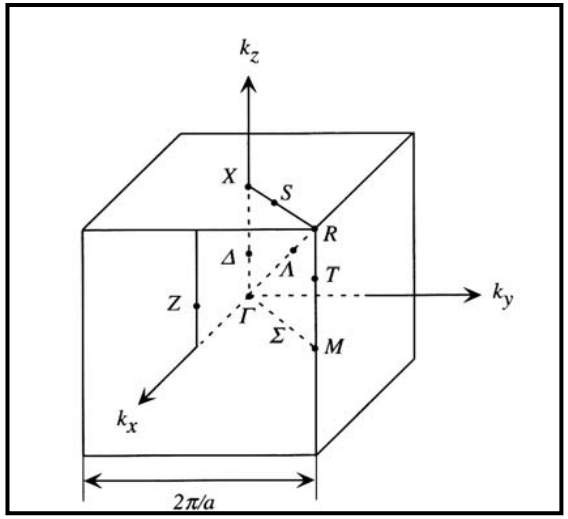

First Brillouin zone of the simple cubic lattice.

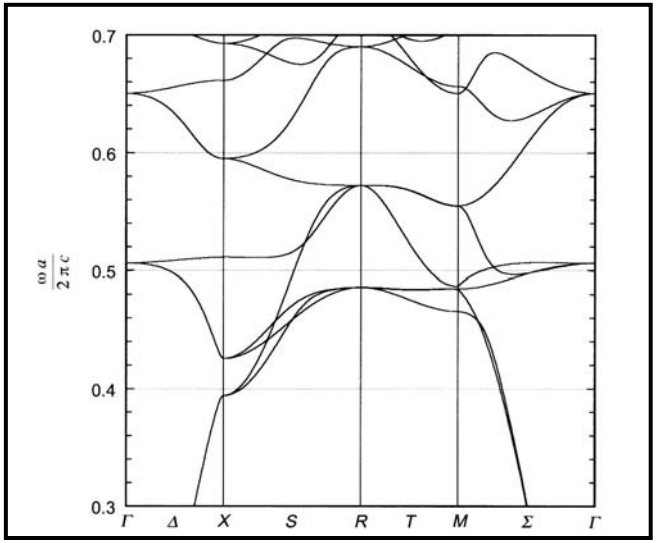

Photonic band structure of a simple cubic lattice (ε=1) with a dielectric sphere at each lattice point (ε=13). The ratio of the lattice constant to the radius of the sphere is (1/0.3).

- **Notion of punctual default or defect (analogy with presence of discrete electronic defect into the forbidden energy gap)**

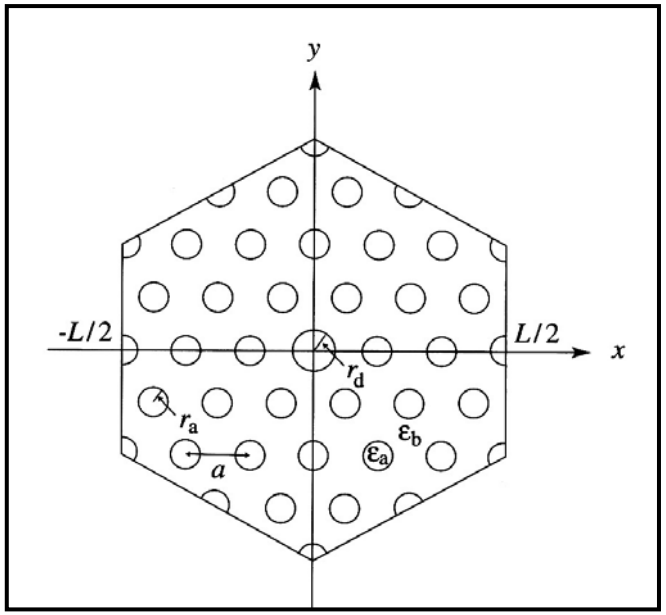

Top view of a super-cell of 2D hexagonal array of circular rods (ε_a and r_a) ; r_d is the radius of a defect rod.

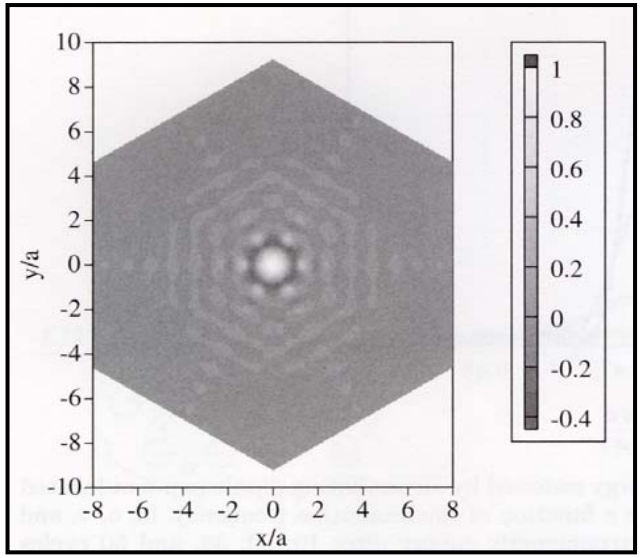

Distribution of the electric field radiated at ($\omega a/2\pi c$)=0.468 or ($\omega/2\pi$)=11GHz. Localized eigenmode, created by such a defect, called A_1-mode (totally symmetric mode that exists at r_d=0).

K. Sakoda, 'Optical properties of photonic crystals', Ed. Springer-Verlag, (2005).

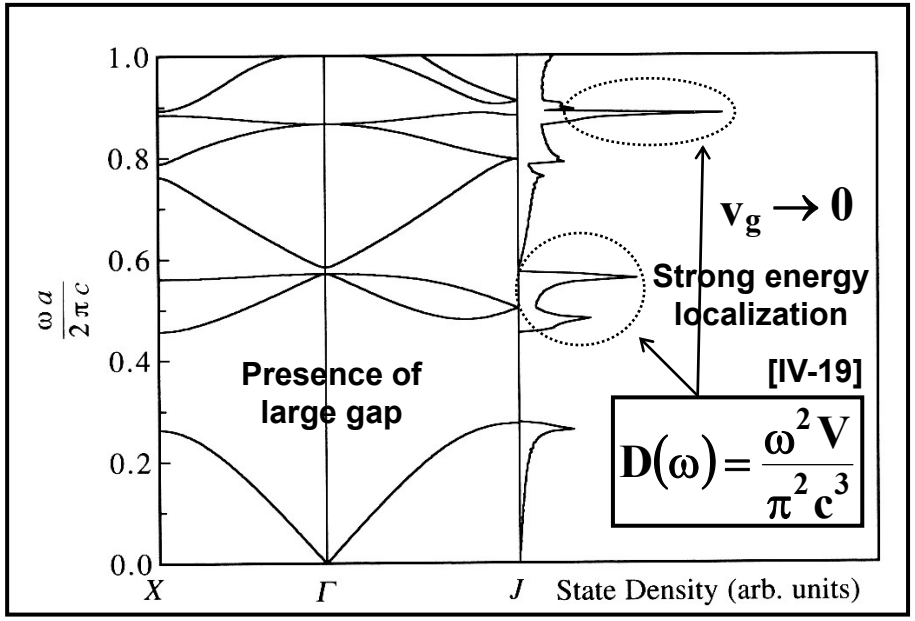

Photonic band structure and state density of the previous hexagonal lattice of circular rods with central r_d defect for TE-polarization (r_a/a=0.2, ε_a=13 and ε_b=1).

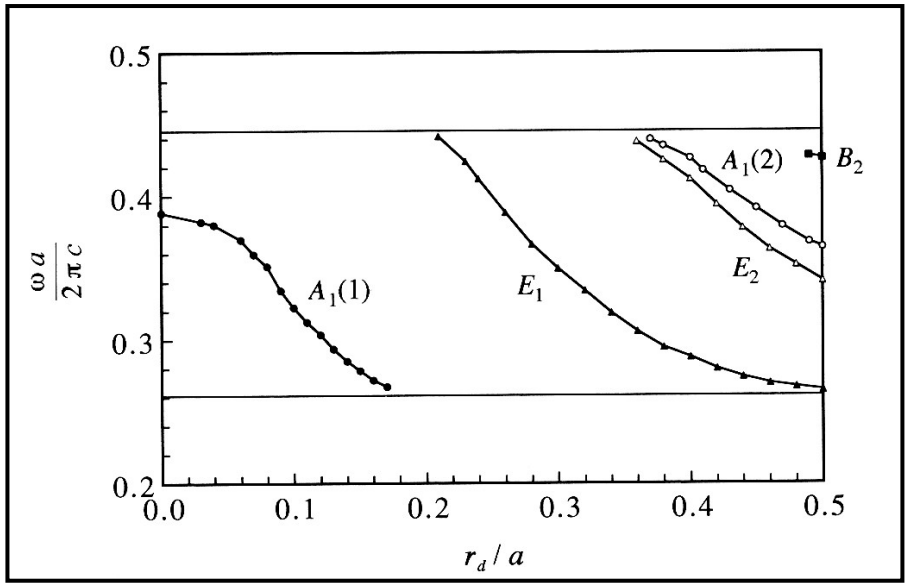

Eigen-frequency of the localized defect modes as function of the defect rod radius r_d.

Distribution of the correspondent electric field of the called A_1, E_1, E_2 and B_2 defect-modes.

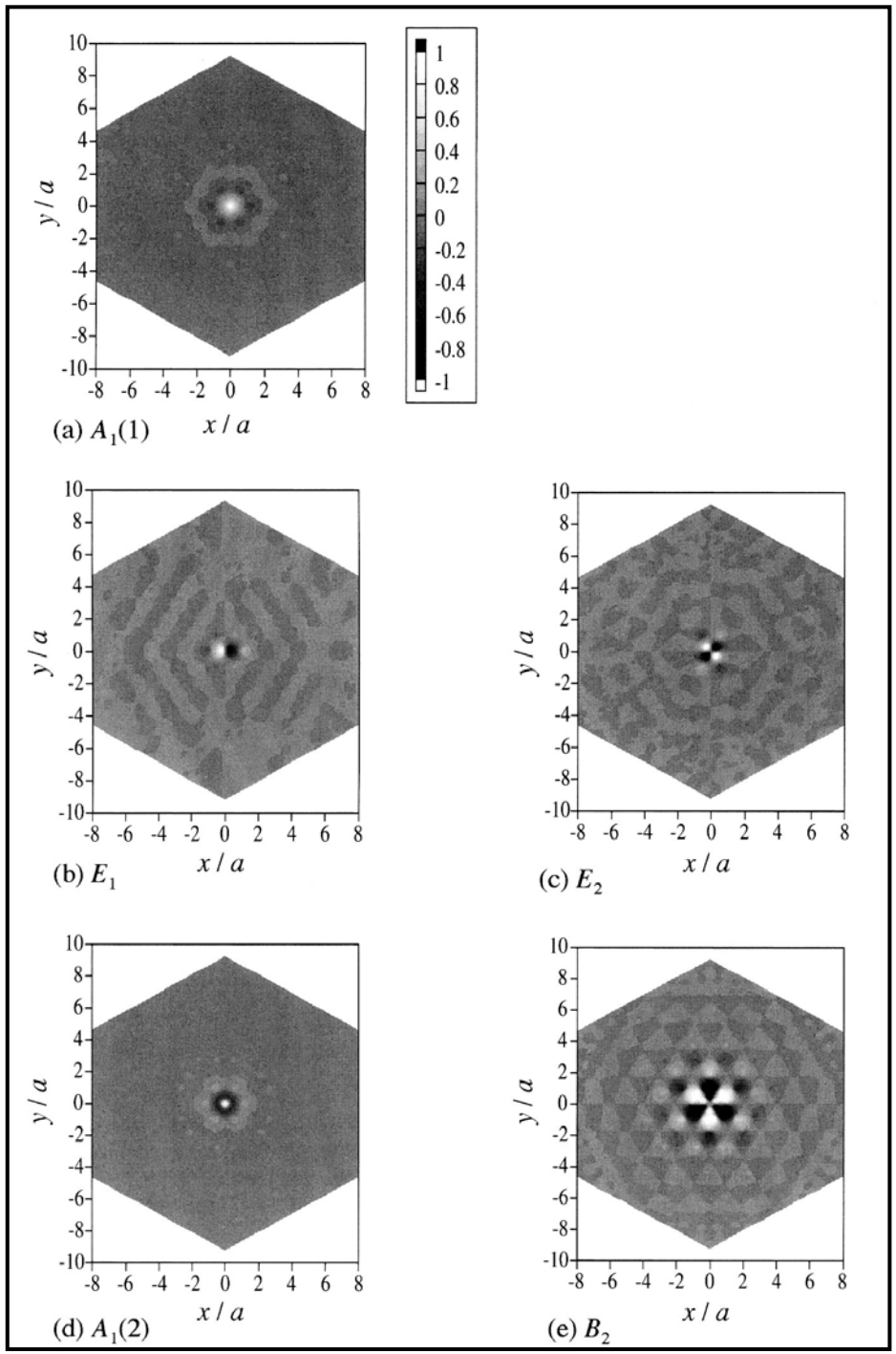

Many defect can be designed such as optical cavities, waveguides-lines, and so on.

PC-waveguides called W1 type A and B, type B_{ratio} can be defined.

- **IV.2 Photonic structures based on photonic crystals (PC-waveguides, resonators, couplers, filters, mirrors, lasers); 2.5D-PC-components examples; technical characterisations of structures; mapping of CP-research in France.**

- **IV.2.1 Periodic optical crystal structures in the nature, historic and first development of such structures at hyper-frequencies, toward the optical wavelength**

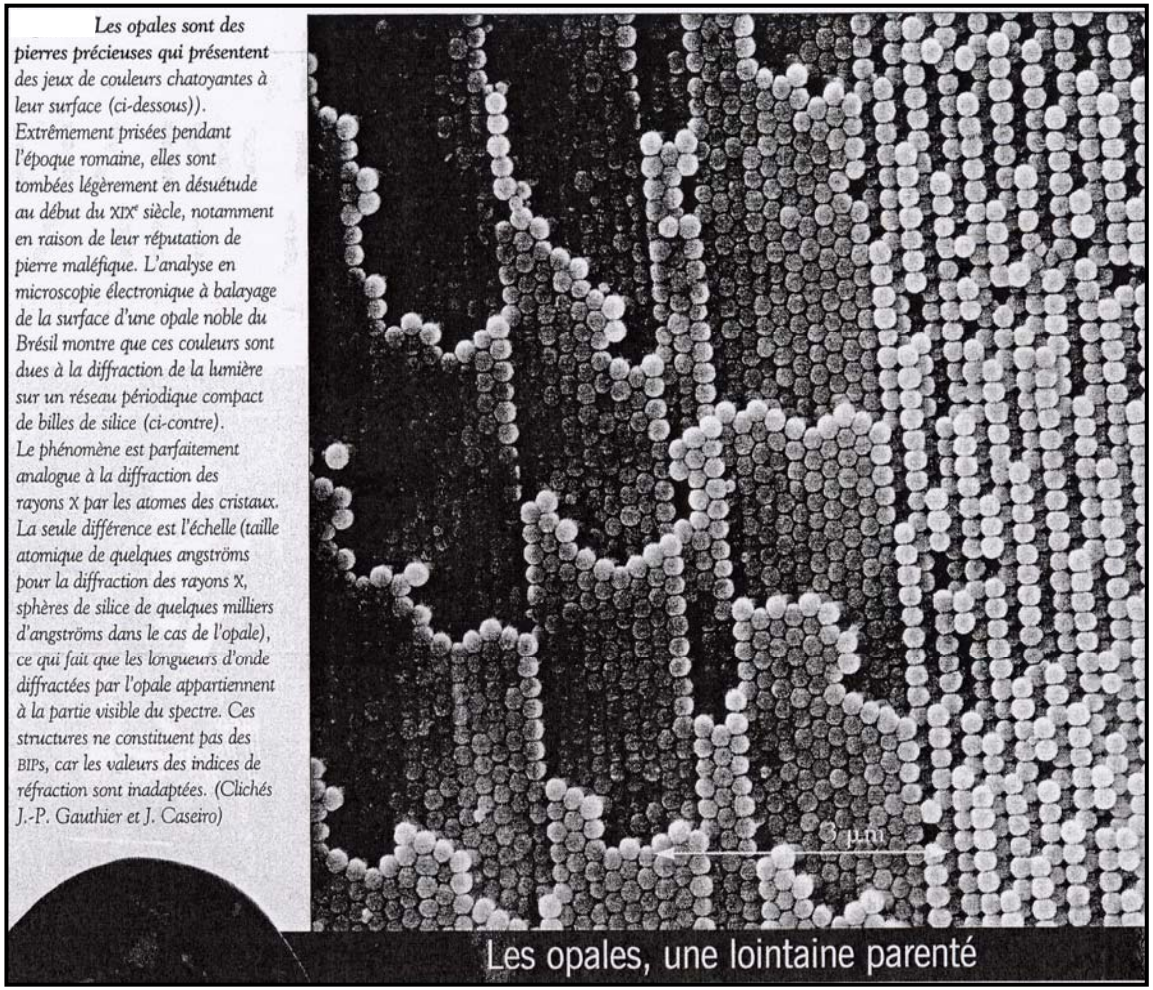

⟵ As an example, opal colors.

Wing's butterfly...

- **Eli Yablonovitch** (1980, first development of 3D-hyperfrequency-electromagnetic structures)

Spectral transmission of the first e.m. structures realized by E. Yablonovitch (hyperfrequency λ=2cm).

$$\nu = \frac{c}{\lambda} = 15\,\mathrm{GHz}$$

La « yablonovite »
est la première structure à bande interdite photonique qui ait été réalisée (cliché A, en vue de dessus). Elle interdit la pénétration de rayonnement électromagnétique pour des longueurs d'onde voisines de 2 cm.
Elle a été fabriquée en perçant dans du Plexiglas trois séries de cylindres parallèles rangés selon un réseau hexagonal, et orientés avec un angle de 35° par rapport à la verticale (B, d'après[4]).
Les trois réseaux se déduisent l'un de l'autre par une rotation de 120° autour de la verticale. La fabrication de cette structure pour des longueurs d'onde centimétriques est simple puisqu'elle requiert l'usage d'une simple perceuse.
Pour les longueurs d'onde de l'infrarouge proche, les échelles recherchées (submicroniques) nécessiteront des techniques très sophistiquées de gravure (par exemple gravure par faisceaux d'ions).
(Cliché A : E. Yablonovitch)

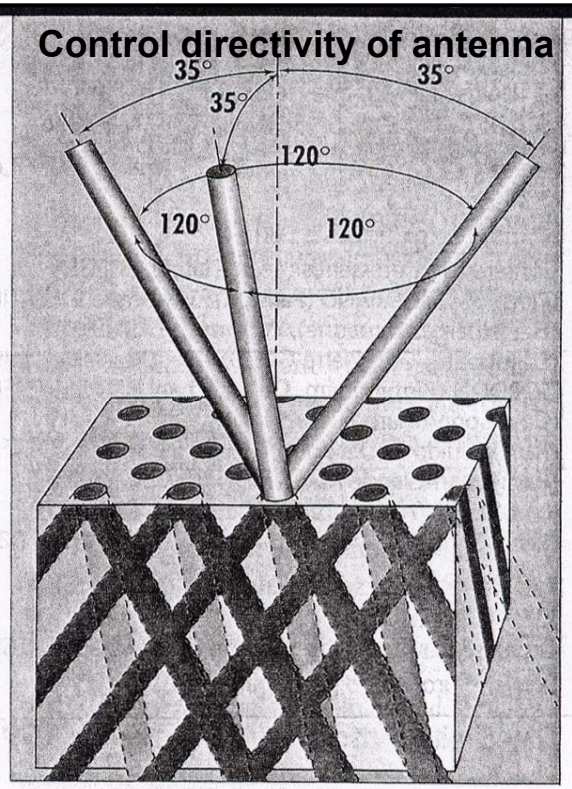

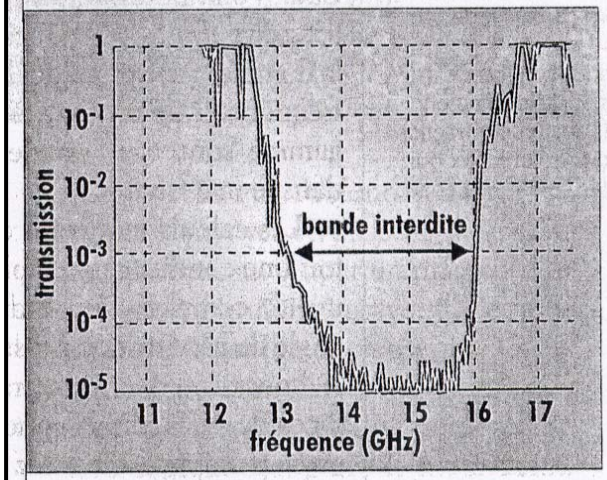

Spectre de transmission
d'un échantillon de la yablonovite (fig. 1). Pour toutes les longueurs d'onde (ou fréquences) situées à l'intérieur de la bande interdite, le BIP réfléchit presque totalement le rayonnement. Pour un matériau contenant seulement 8 périodes (soit une structure d'environ 8 centimètres au total), la part transmise est inférieure à 1 sur 100 000. (D'après[4]).

3D YABLONOVITE in SILICON by FOCUSED ION BEAM ("FIB") ETCHING OF MACROPOROUS SILICON

A FULL 3D PHOTONIC BAND GAP AT ~3µm

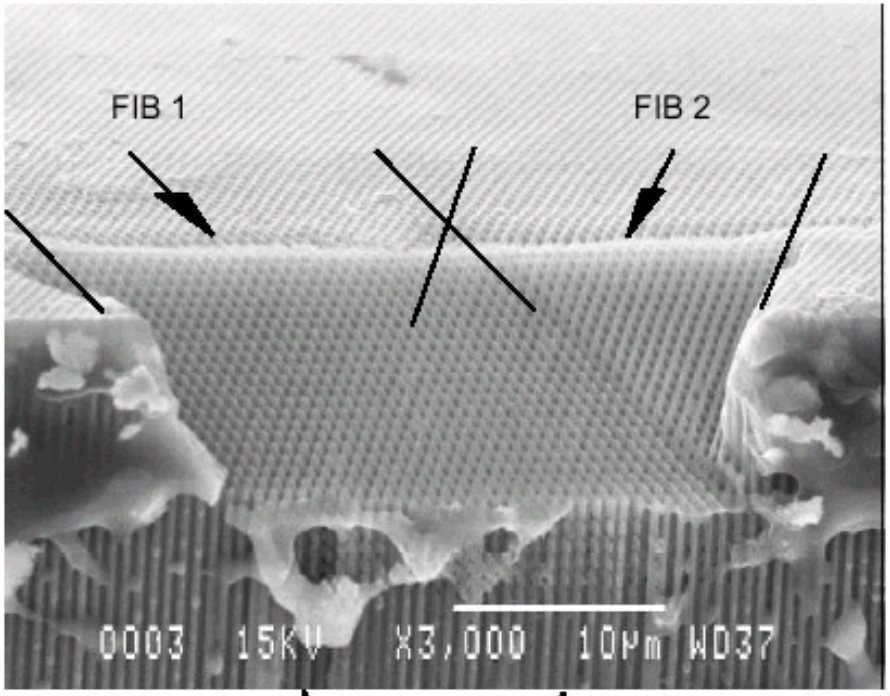

Original macropores obtained by photo-electro-chemical etching

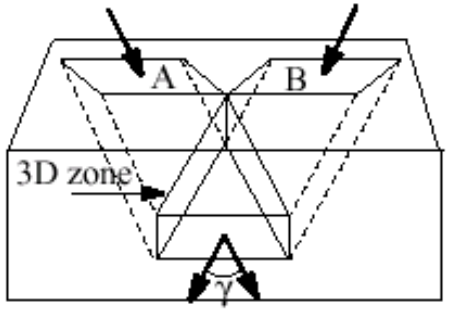

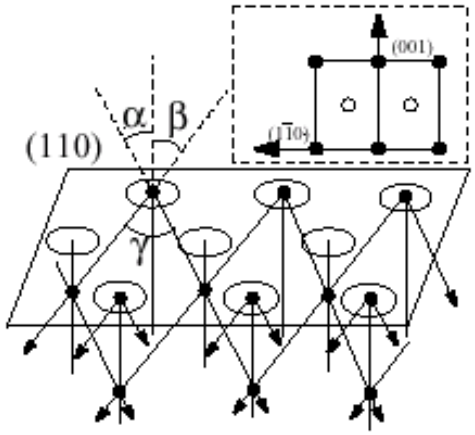

▪ **Nanotechnologies development for optical wavelength devices, toward the PBG-structures**

Development of new technical process for nano-lithographies (e-beam, and so on), proper nano-etching process of nano- or sub-wavelength elements ($\lambda/3$ or $\lambda/4$ dimensions) for the realization of PBG-components.

Hexagonal (or trigonal) 2D PBG-structures on GaAlAs (0.4µm of lattice parameter)

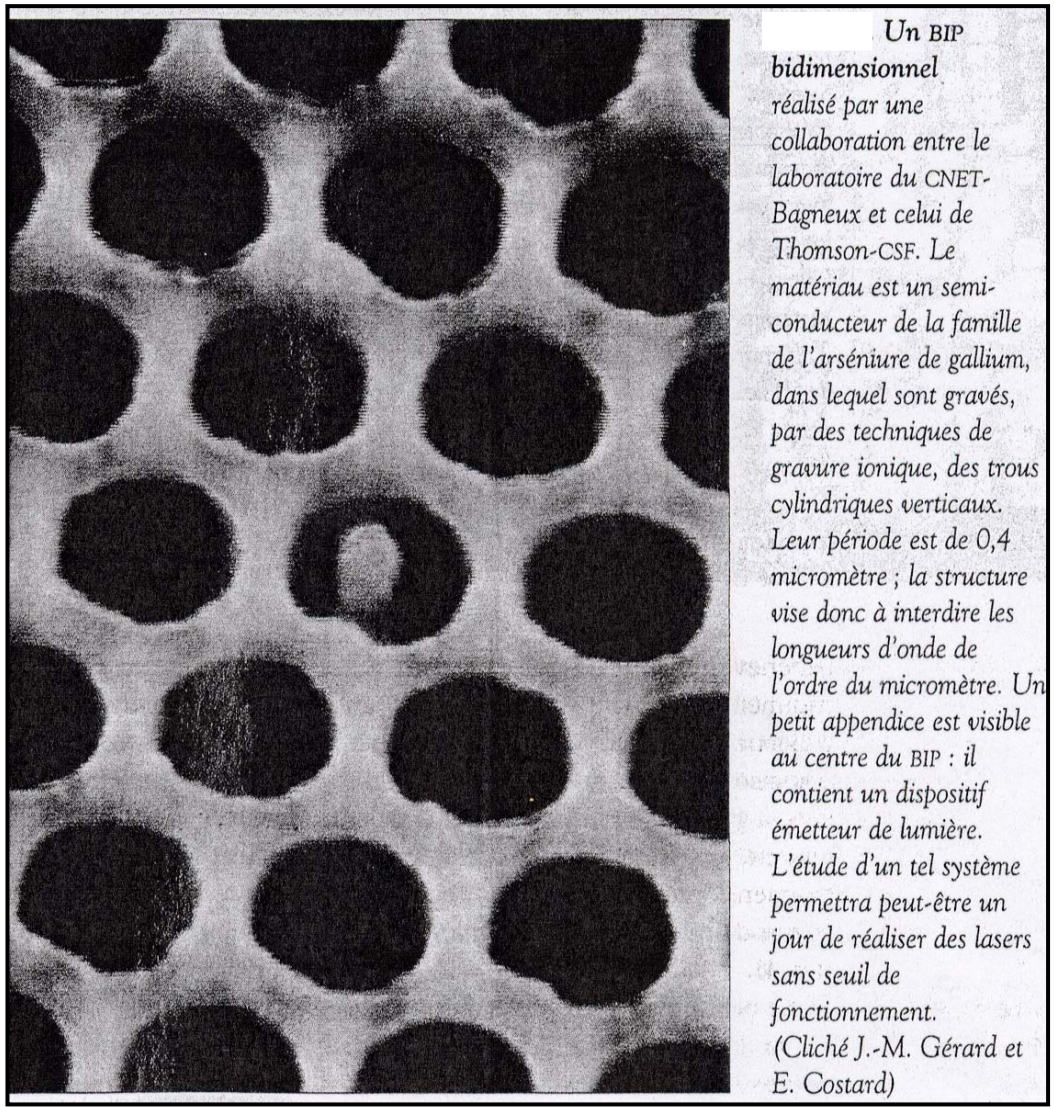

Un BIP bidimensionnel *réalisé par une collaboration entre le laboratoire du CNET-Bagneux et celui de Thomson-CSF. Le matériau est un semi-conducteur de la famille de l'arséniure de gallium, dans lequel sont gravés, par des techniques de gravure ionique, des trous cylindriques verticaux. Leur période est de 0,4 micromètre ; la structure vise donc à interdire les longueurs d'onde de l'ordre du micromètre. Un petit appendice est visible au centre du BIP : il contient un dispositif émetteur de lumière. L'étude d'un tel système permettra peut-être un jour de réaliser des lasers sans seuil de fonctionnement. (Cliché J.-M. Gérard et E. Costard)*

Hexagonal 2D PBG-structures on $Ga_{0.9}Al_{0.1}As/GaAs$

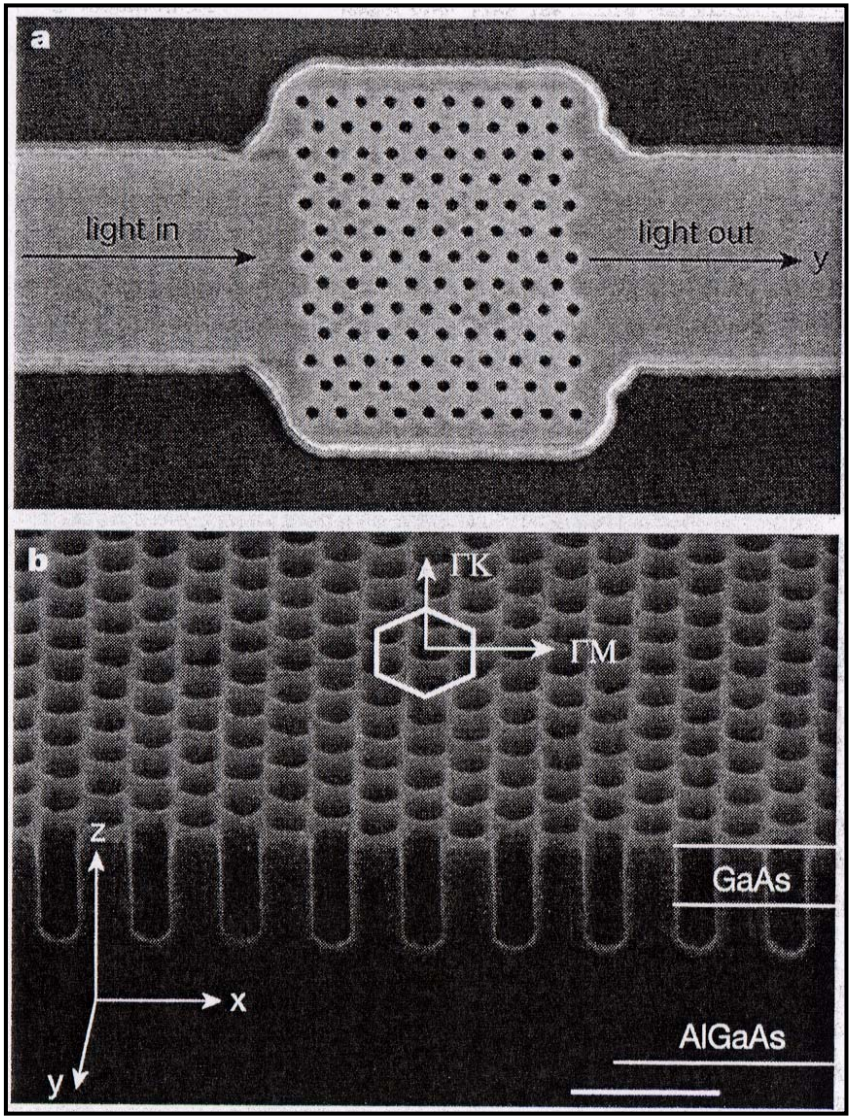

Dispersion relation function to the direction of photonic propagation $\omega=\phi(k)$

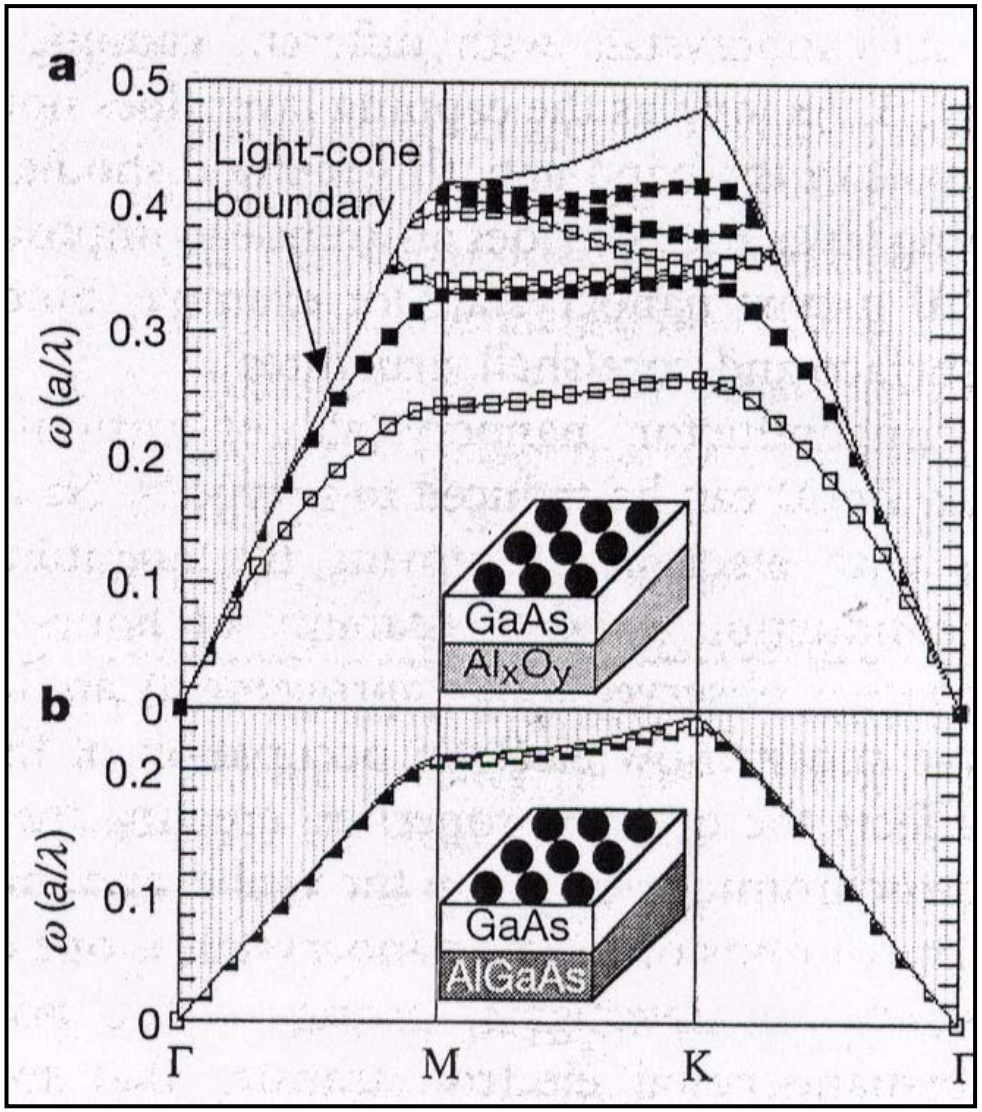

▪ IV.2.2 Photonic structures based on photonic crystals (PC-waveguides, resonators, couplers, filters, mirrors, lasers); 2.5D-PC-components examples; technical characterisations of structures.

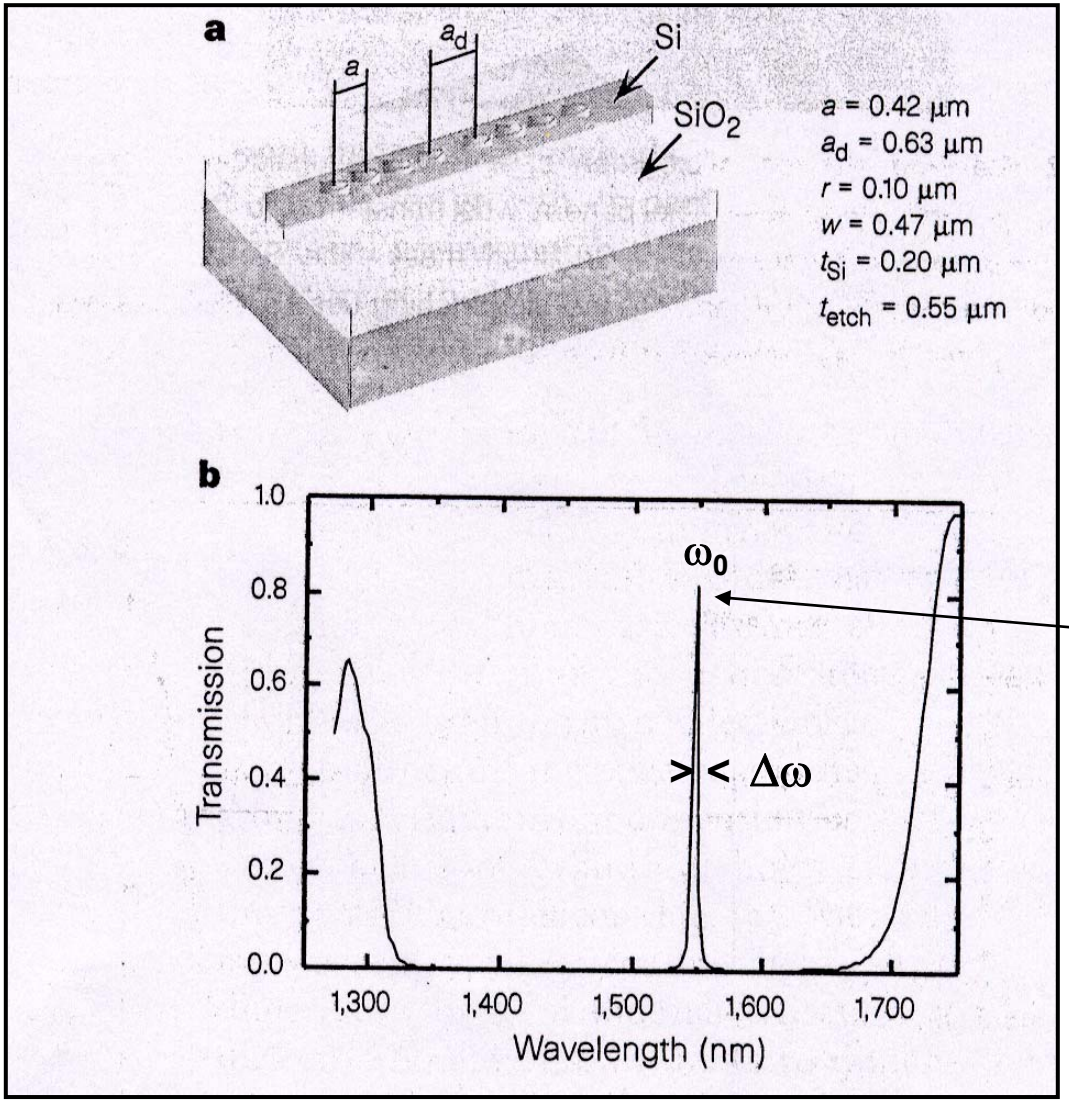

SOI-components **(for example at Institut d'Electronique Fondamental, Paris)**

Micro-cavity with punctual a_d-defect (that allow the existence of light) in a Si/SiO_2 rib waveguide. Permittivity contrast (ratio) ε_{Si}=12.1 and ε_{air}=1 at 1.55µm.

Notion of Q (quality) factor that characterizes the optical resonance of the cavity.

$$Q = \omega_0 \frac{U}{-\frac{dU}{dt}} \quad \text{[IV-20]}$$

✎ **Determination of the evolution equation of the energy U(t) into the cavity and the associated spectral band.**

$$\longrightarrow \boxed{U(t) = U_0 . \exp\left[-\frac{\omega_0}{Q} t\right] \equiv E \ . E^*} \quad \text{[IV-21]} \longrightarrow \boxed{E(t) = E_0 . e^{\left(-\frac{\omega_0}{2Q} t\right)} . e^{-j(\omega_0 + \Delta\omega)t}}$$

$$\downarrow$$

Equation of the spectral resonance peak : $$\boxed{|E(\omega)|^2 = \frac{1}{(\omega - \omega_0 - \Delta\omega)^2 + \left(\frac{\omega}{2Q}\right)^2}} \quad \text{[IV-22]}$$

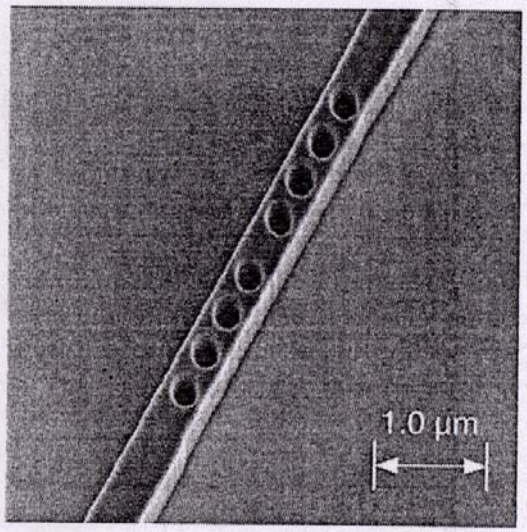

Scanning electron micrograph of a PBG waveguide microcavity fabricated by X-ray lithography. The pattern was transferred to the Unibond silicon-on-insulator substrate with a Cr lift-off mask. The Si etching was performed in a plasma of CF_4 and O_2; the SiO_2 etching used a CHF_3 plasma. After etching, the Cr was removed and the samples were cut and polished for testing.

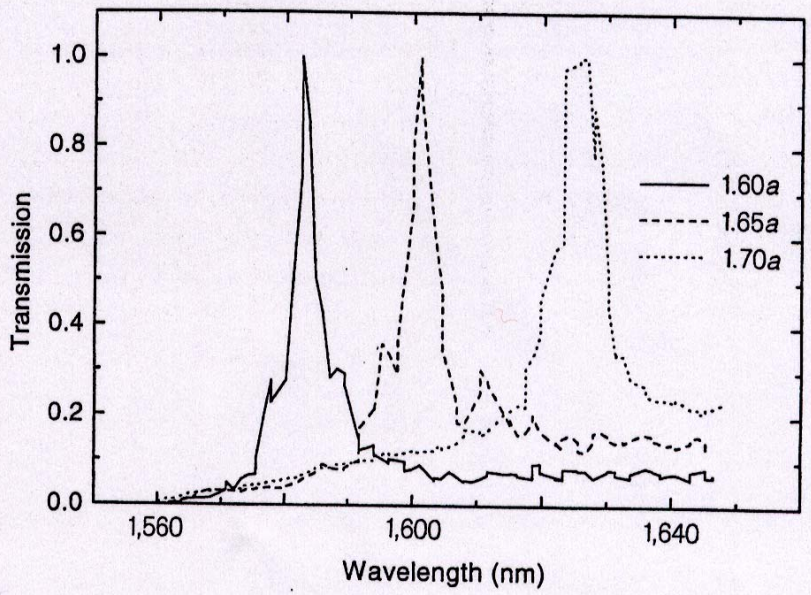

Transmission characteristic of PBG waveguide microcavities for various defect lengths. Three different defect lengths are shown. The resonance peak shifts to longer wavelengths with increasing defect length.

▪ IV.2.3 Mapping of CP-research in France : example of the LEOM INL realizations on nanophotonic at Lyon.

▪ **This part of slides is devoted to the presentation of PBG-devices and realization that have been shaped at LEOM UMR CNRS 5270 / Institut des Nanotechnologies de Lyon (INL) at Ecole Centrale de Lyon (ECL-Ecully).**

➔ Three references of this LEOM team and some actors involved in such photonic crystals activities:

- **P. Viktorovitch, 'Photonics Crystals : from micro-photonics to nano-photonics', Chapters 1st in Nanophotonics, Ed. ISTE, (2006).**
- **P. Viktorovitch, E. Drouard, M. Garrigues, J.L. Leclerq, X. Letartre, P. Rojo-Romeo, C. Seassal, 'Photonic crystals: basic concepts and devices', Special issue 'Recent advances in crystal optics' of the Compte-Rendus de l'Académie des Sciences, vol. 8, p. 253, (2007).**
- **X. Letartre, J. Mouette, C. Seassal, P. Rojo-Romeo, J.L. Leclercq, P. Viktorovitch, 'Switching devices with spatial and spectral resolution combining photonic crystal and MOEMS structures', Journal of Lightwave Technology, vol. 21, p. 1691, (2003).**

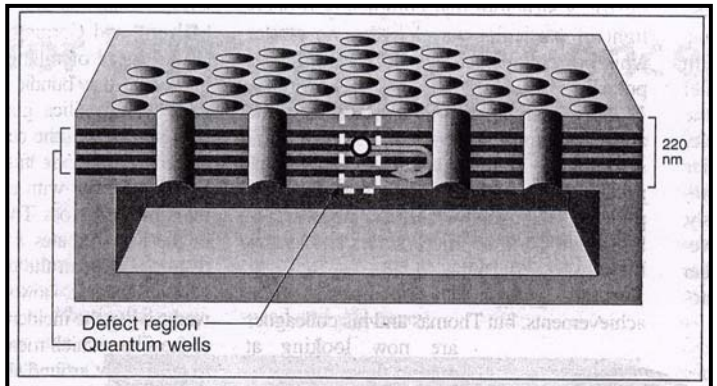

Littlest laser. Light emitted from thin layers called quantum wells cannot propagate through a thicker slab of optical material because it meets a photonic bandgap created by an array of holes. Trapped in a volume of just a fraction of a cubic micrometer, it builds up to laser intensity.

▪ **Micro-cavities / coupling between PBG waveguide and cavities / 2.5D PBG structures devices (Institut des Nanotechnologies de Lyon / INL-LEOM at ECL-Lyon)**

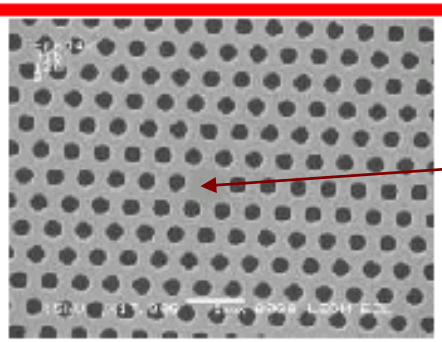

H1

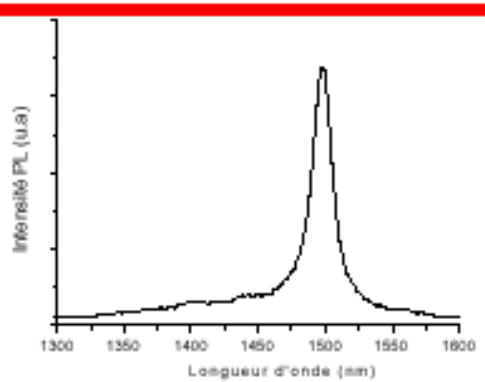

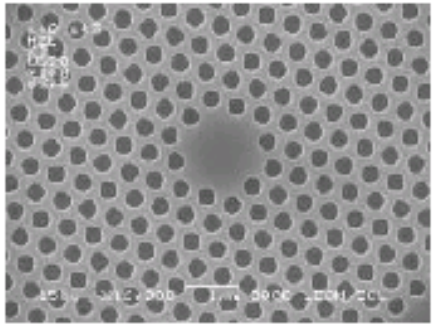

H2

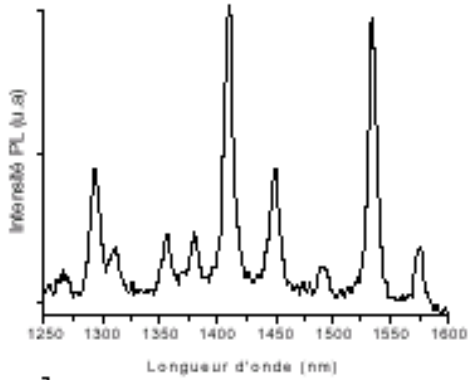

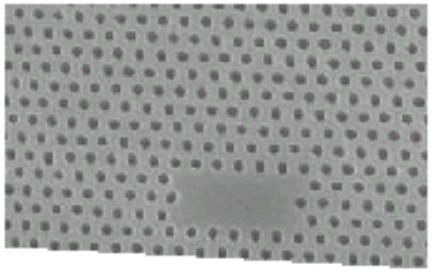

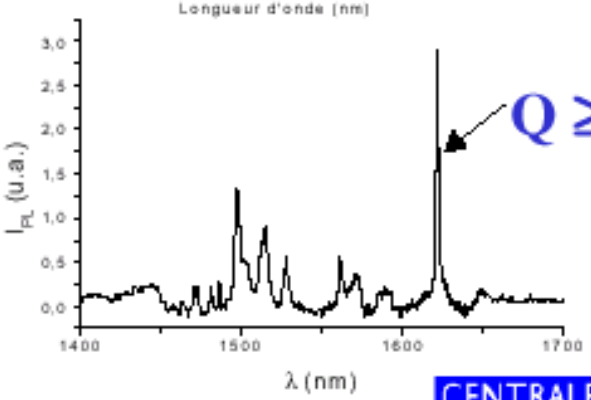

Q ≥ 1300

POSTER JNMO C. MONAT

LEOM

JNMO 2001

CENTRALE LYON

CNRS

▪ **Possibilities of PBG-devices-coupling between waveguides and cavities**

Photonic crystals

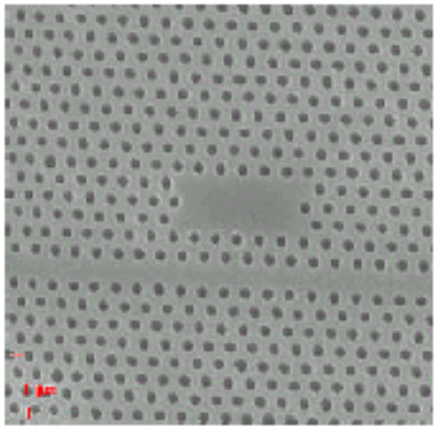

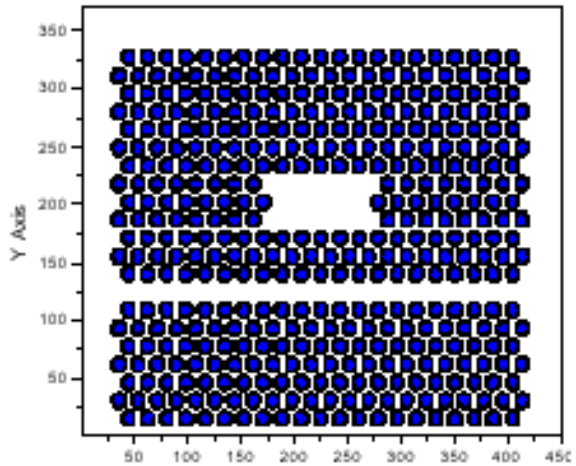

PL spectra (pumping in the cavity)

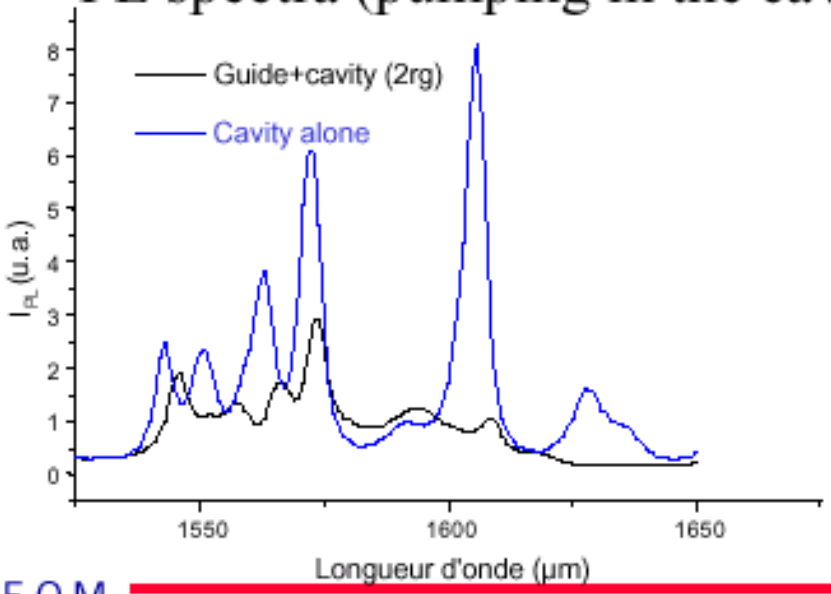

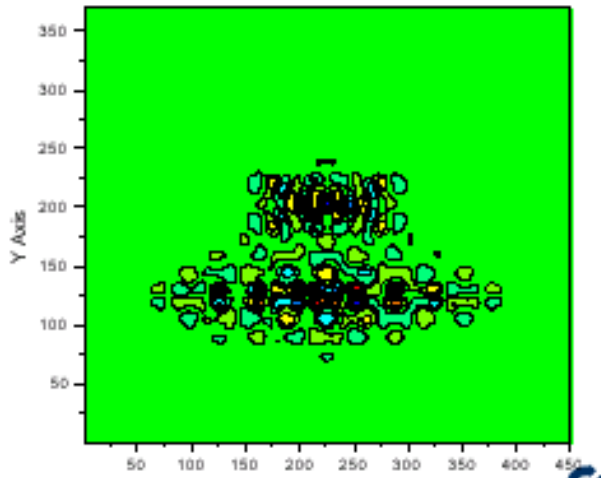

⇨ ***PC waveguide with a single missing row***: single-mode

• losses < 150 dB/cm ➔ 30µm propagation

PHOTOLUMINESCENCE

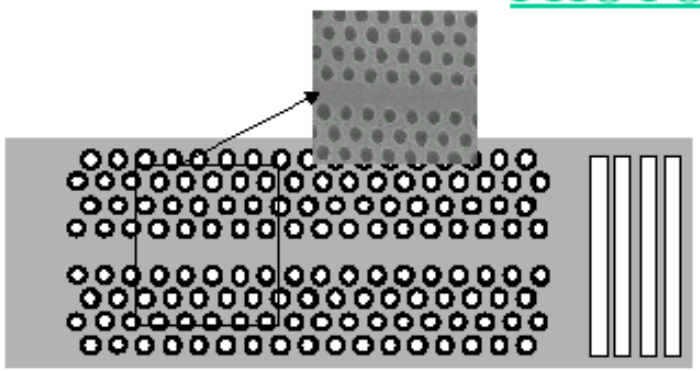

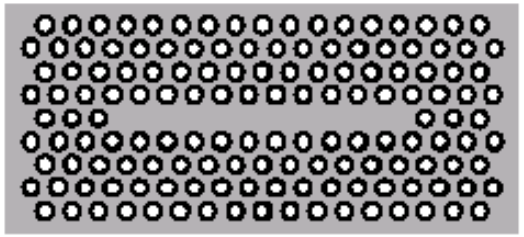

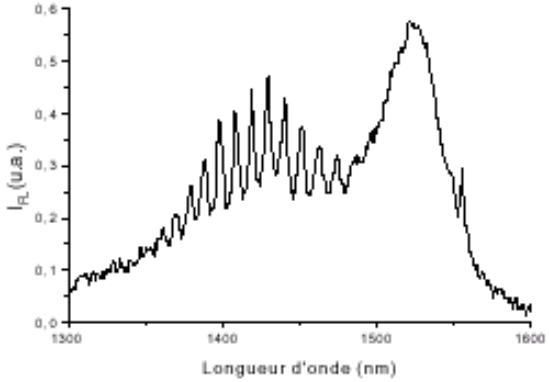

POSTER JNMO Y. DESIERES

POSTER JNMO C. GRILLET

▪ **Coupling the 2.5D and 3D photonic technologies for new PC-devices : tunable laser components and photo-detectors applications**

« OUVRIR LES CRISTAUX PHOTONIQUES SUR LE MONDE EXTERIEUR »

ESPACE LIBRE - MOEMS

OPTIQUE GUIDEE - BIP

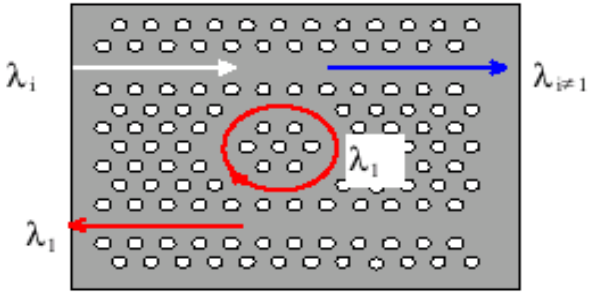

DMOEMS (Diffractive MOEMS)

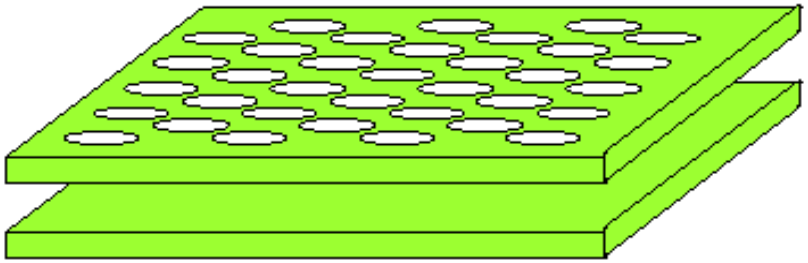

▪ **INL / LEOM realizations : highlight of difficulty process for such 2.5D devices**

Etch selectivity

Structural/etch-stop layer	Sacrificial layer	Etch solution	Selectivity
InP	InGaAs	FeCl3	infinite
InP	InGaAs	HF:H2O2:H2O	infinite
InGaAs	InP	HCl:H2O	infinite
InGaAlAs (Al<0.2)	InAlAs	HCl/H2O	2000

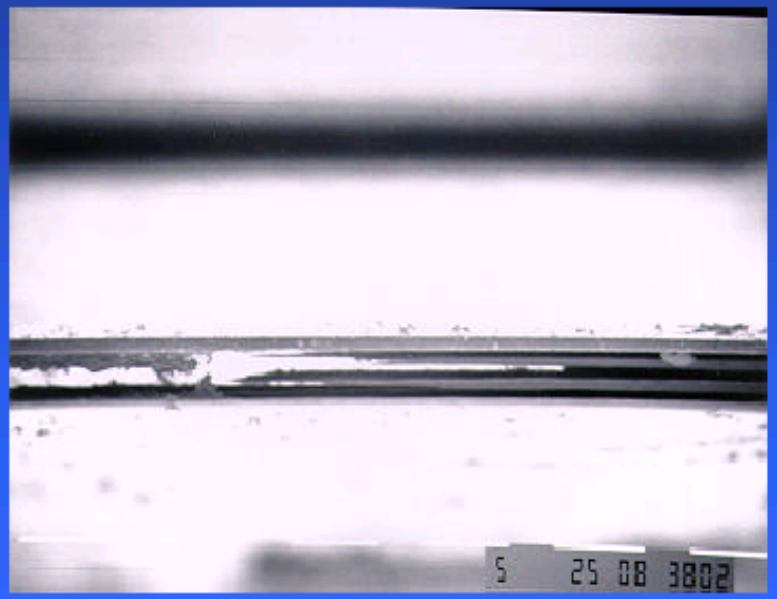

Insufficient selectivity

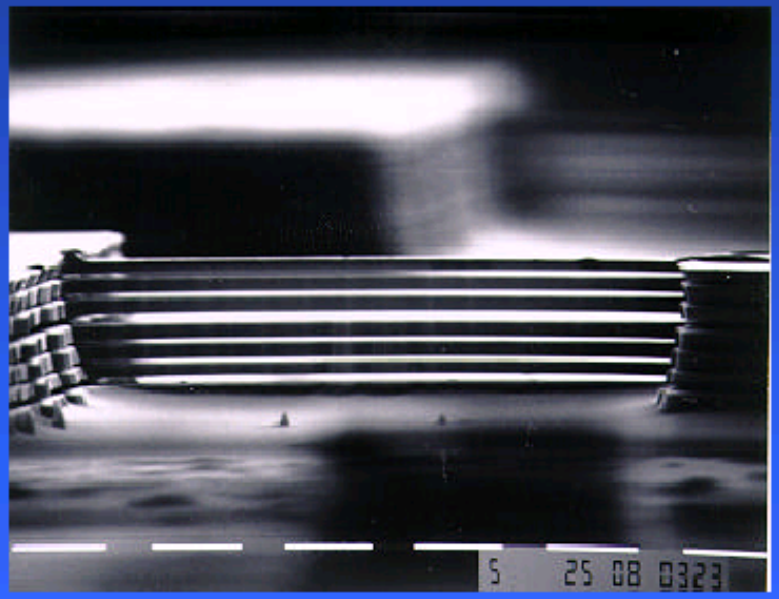

Total selectivity

Sticking phenomena

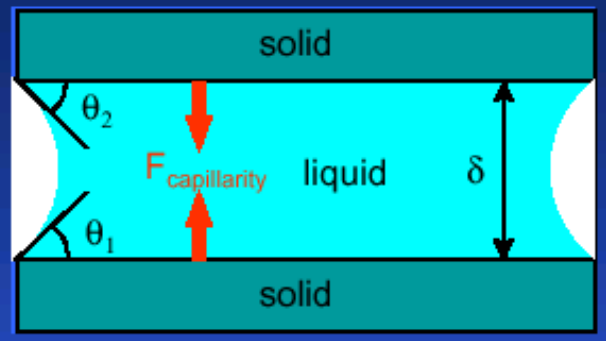

Removal of the rinsing liquid

⇨ **capillary forces**

self attraction between the suspended layers

⇨ **permanent sticking**

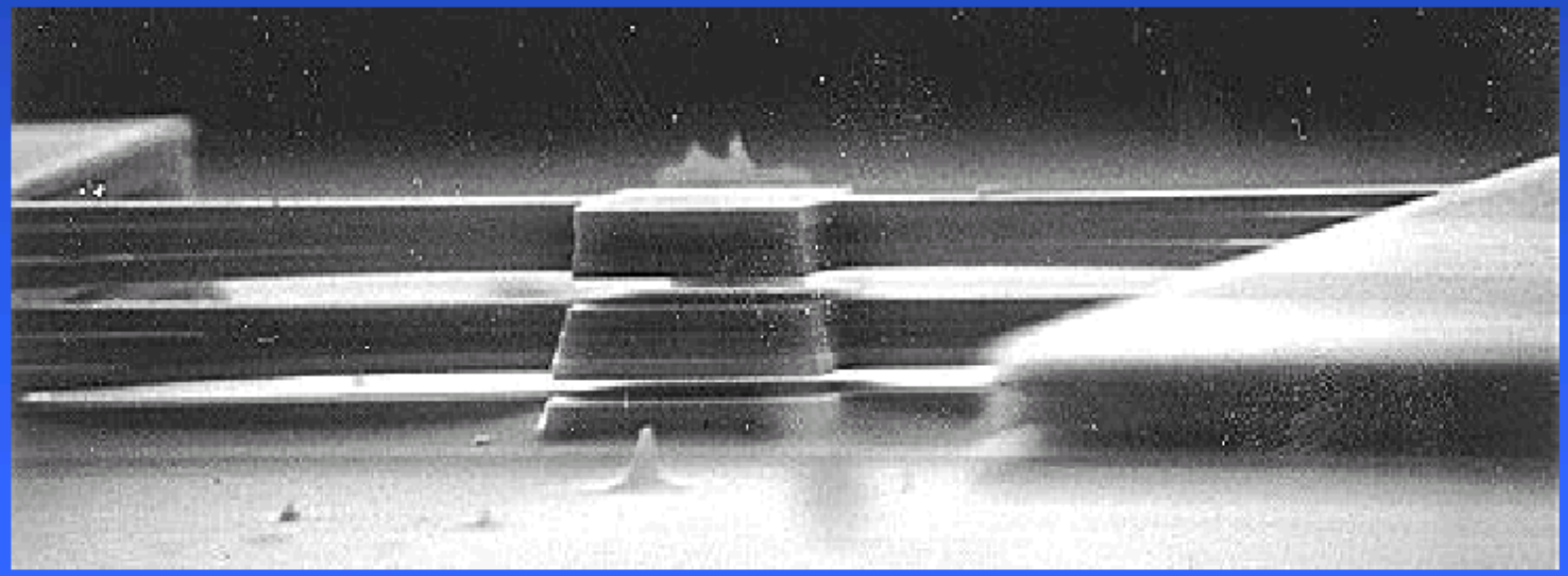

How to control the residual stress ?

❶ "critical" solution : adjustment of the growth conditions

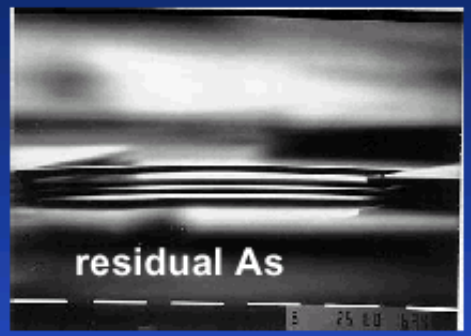

❷ "practical" solution : compensation of As by Ga

micro-mechanical engineering (pre-stressed tensile InGa(As)P layer)

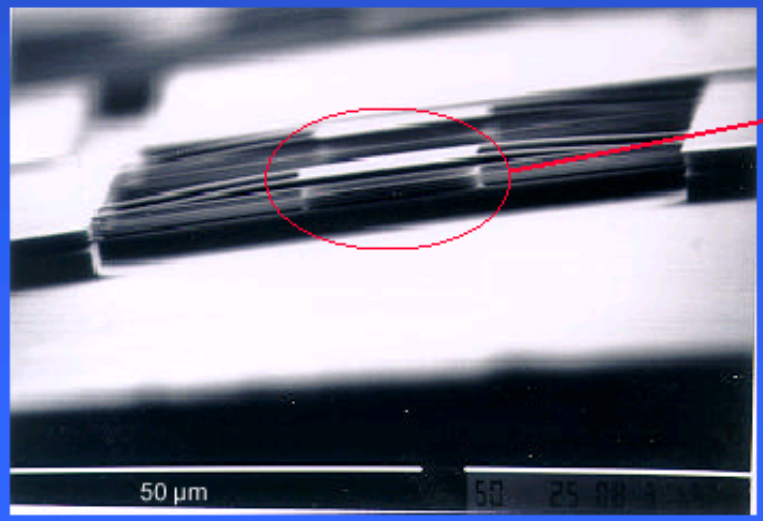

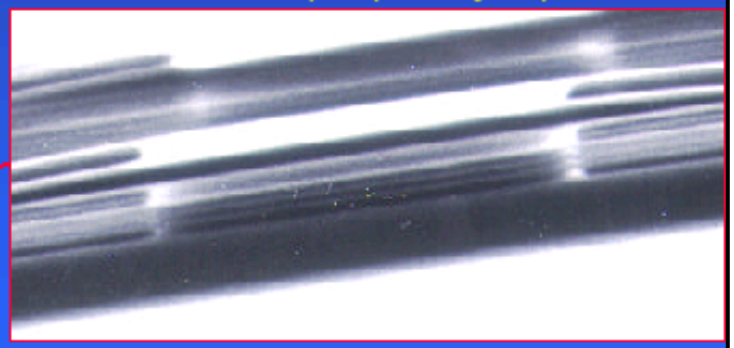

1x { 370 nm In(As)P layer
360 nm air gap

3x { 370 nm $In_{.99}Ga_{.01}(As)P$ layer
360 nm air gap

Drying method

Super-critical CO_2 drying (CPD)

liquid ➡ super-critical fluid ➡ vapor

multi-gaps air / InP suspended layers
with very high aspect ratio

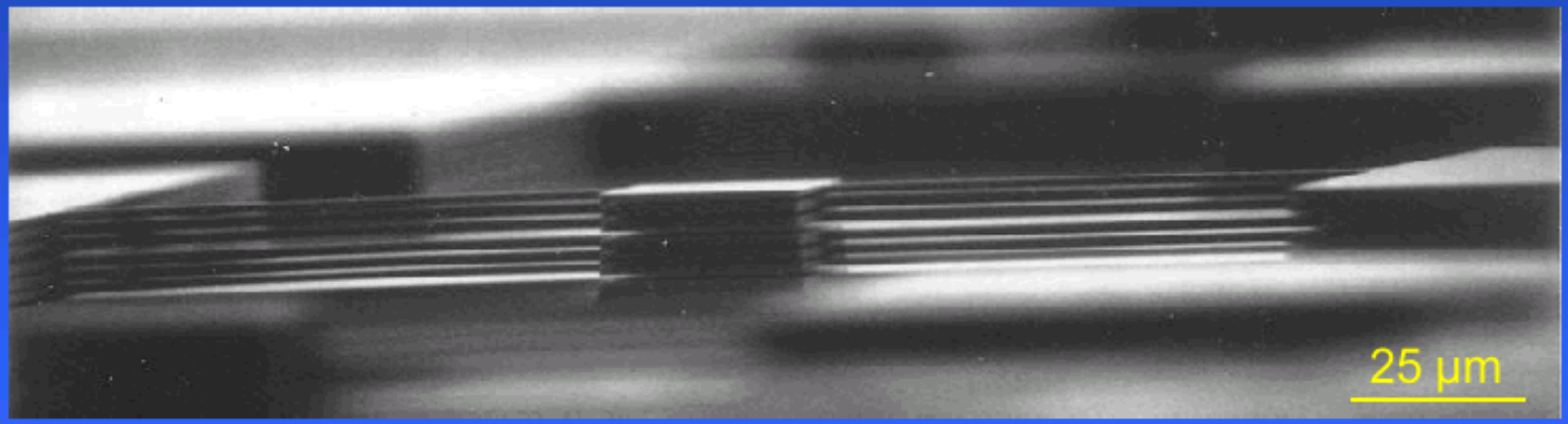

Successful realization (INL-LEOM)

Examples

8 x InP/ Air

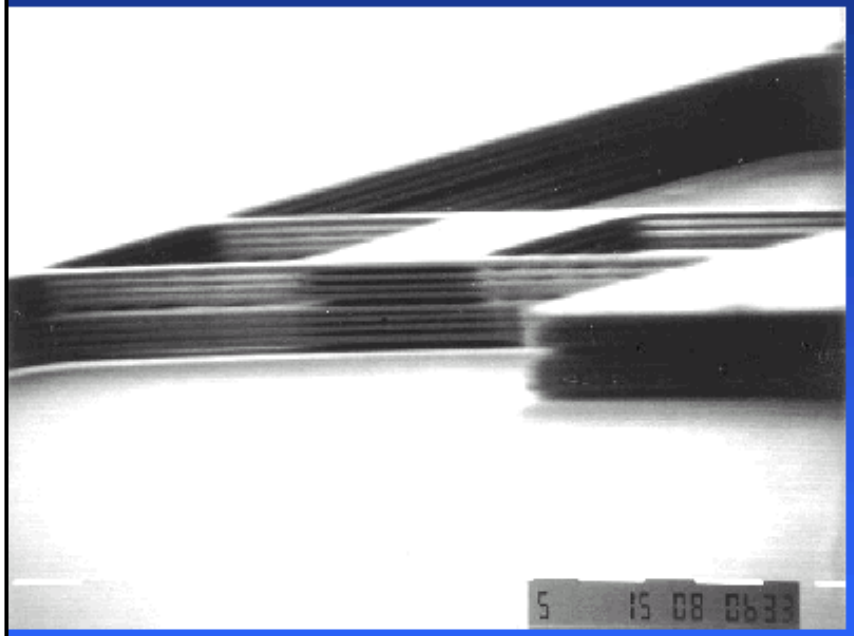

MOCVD - LCR

10 x GaAlAs / Air

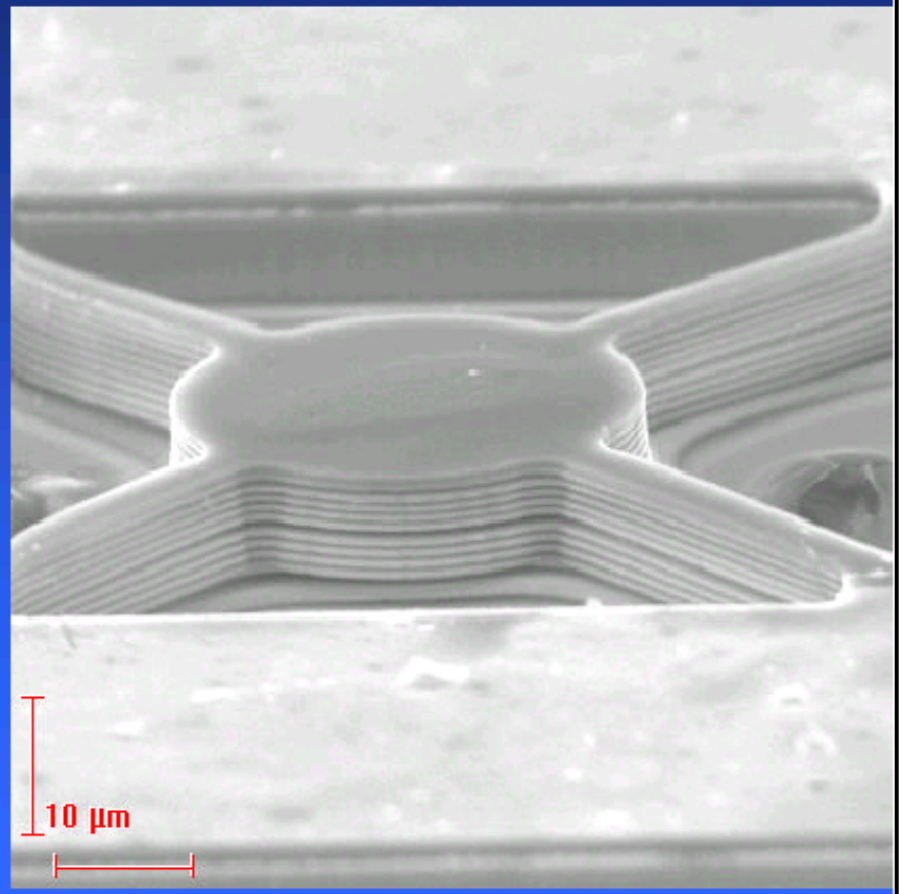

MOCVD - CDP

Tunable photodetectors applications (INL-LEOM)

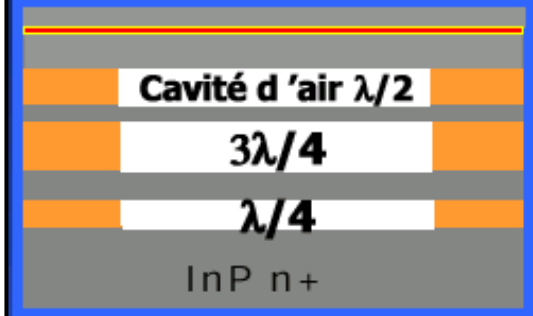

Plans de boîtes quantiques d'InAs

Validation experimentale

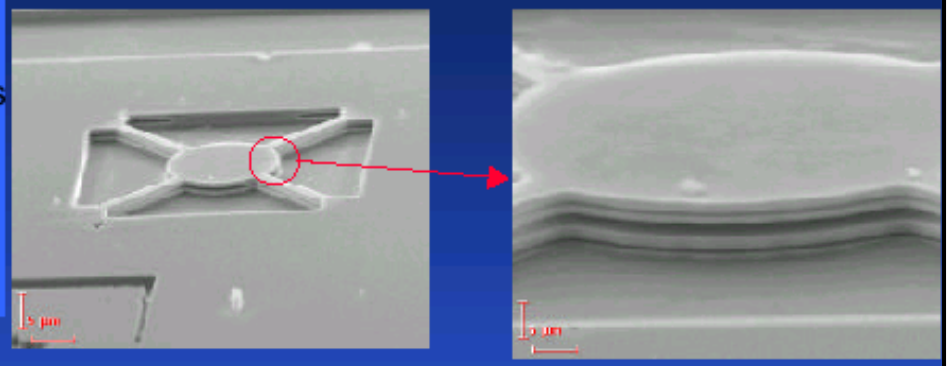

Tuned

Detuned

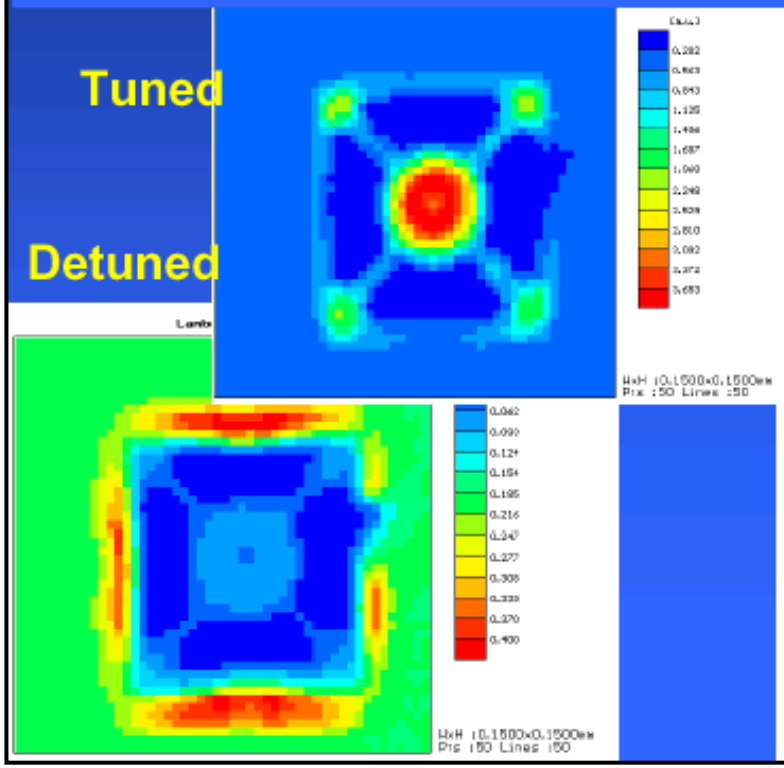

Réponse sous pompage optique en fonction de la tension d'actuation

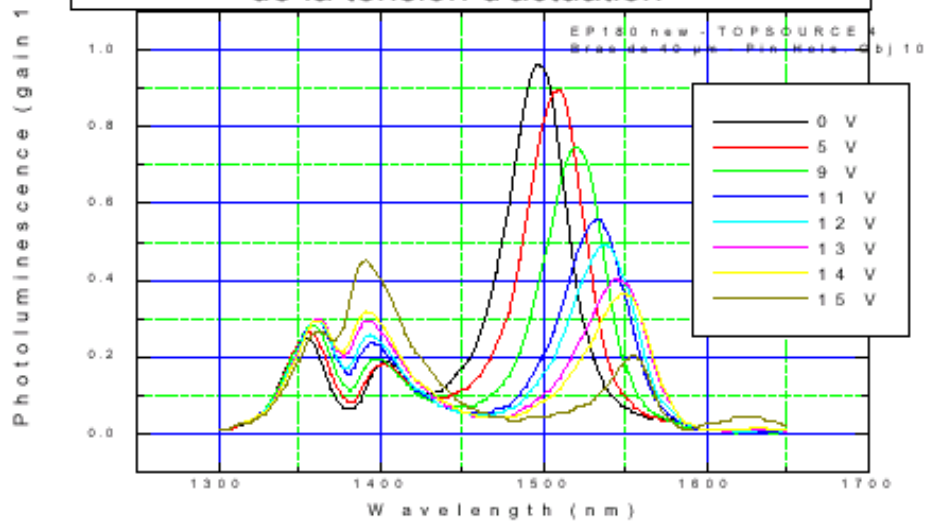

(INL-LEOM)

Photodétecteur accordable

Détecteur en cavité RCEPD

Concepts établis pour l'intégration monolithique

Filtre + Détecteur

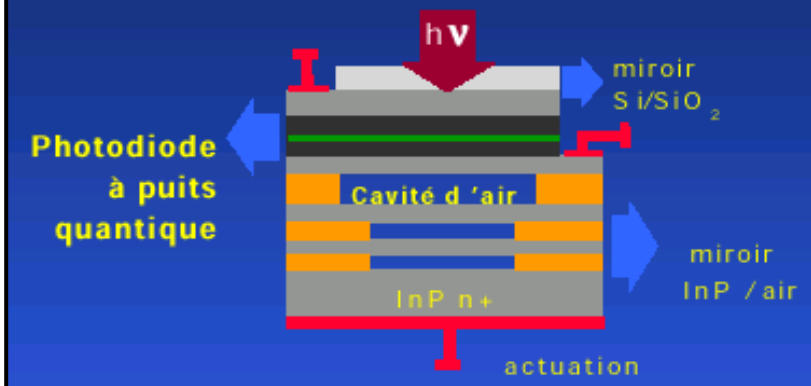

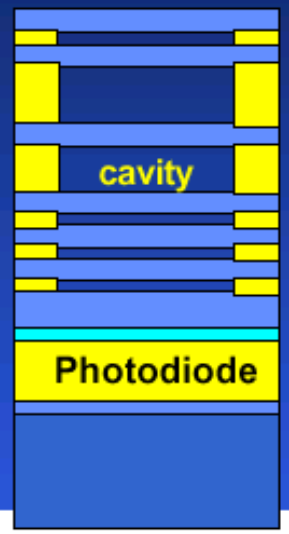

Techno. complexe

fort RC

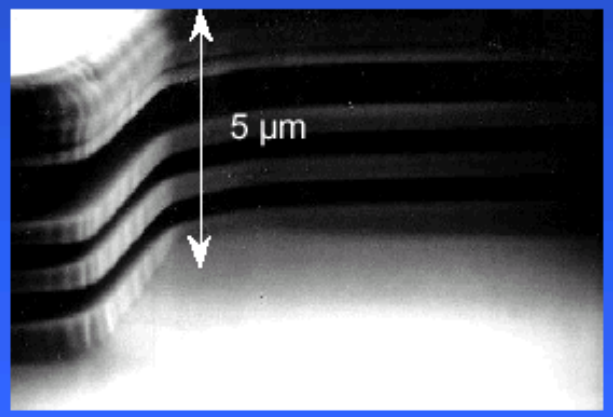

Contraintes résiduelles

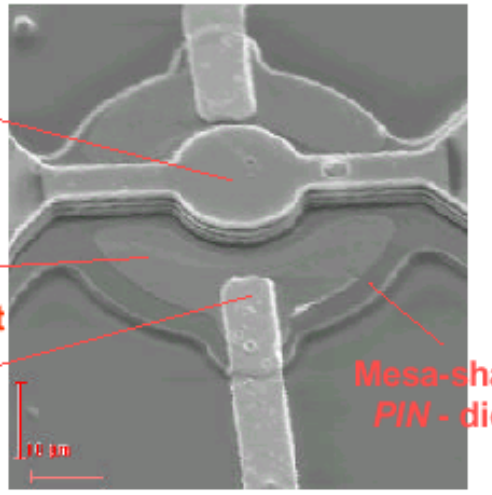

Tunable disk-laser

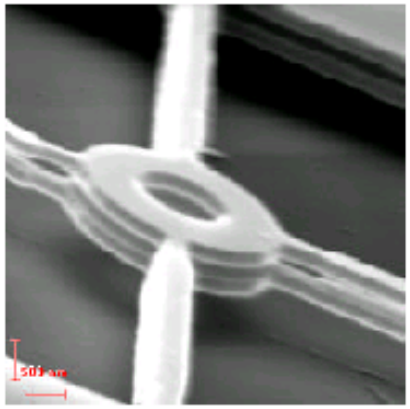

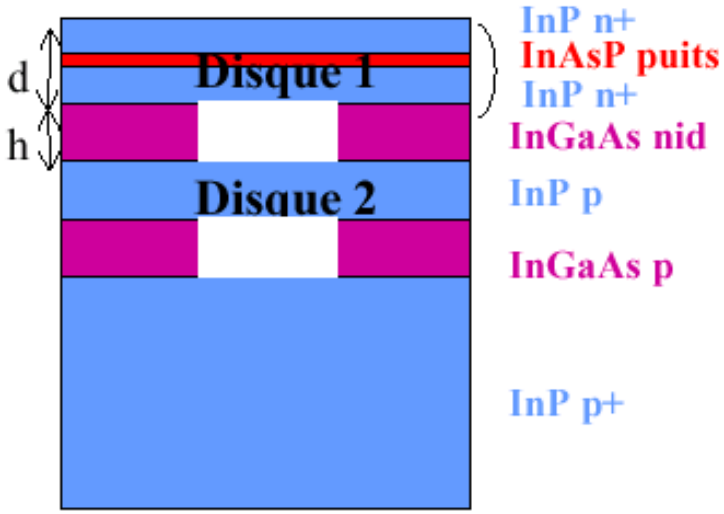

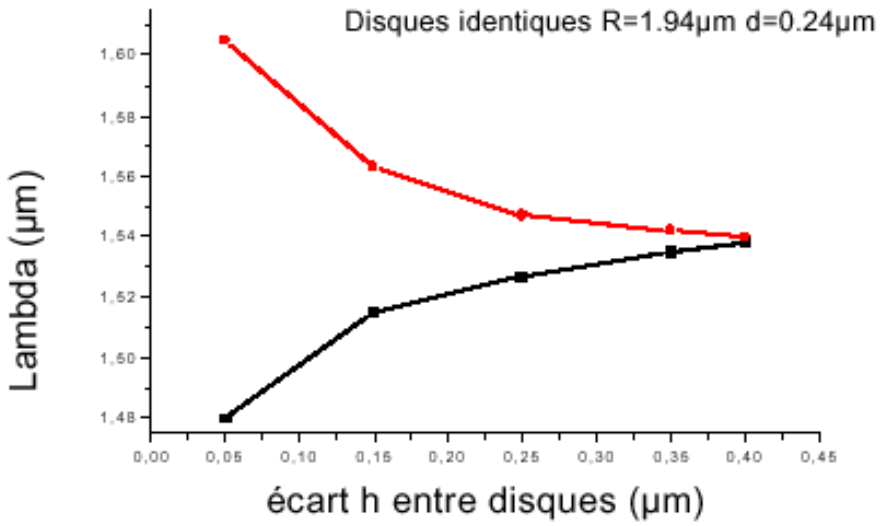

h_o ~ 200 nm ➔ Accordabilité 20 nm

(INL-LEOM)

Tunable VCSEL

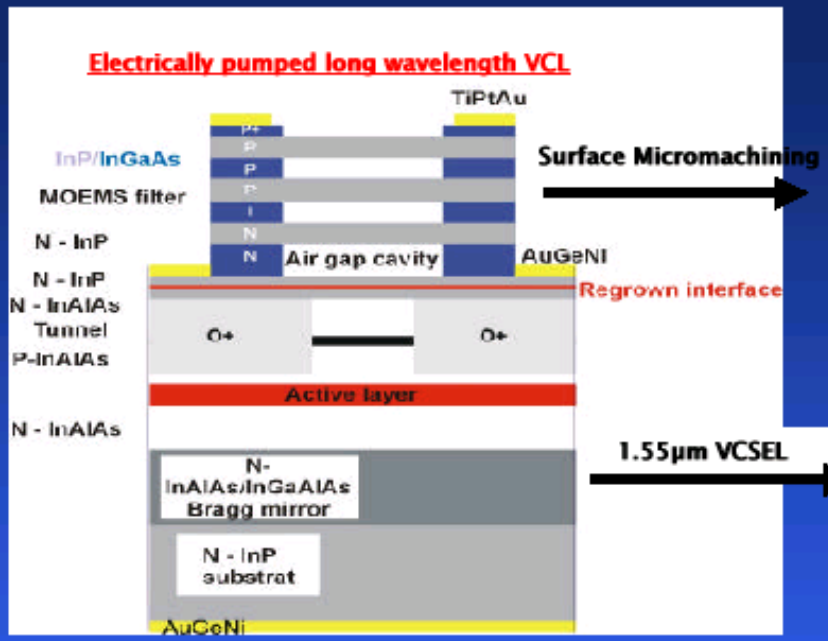

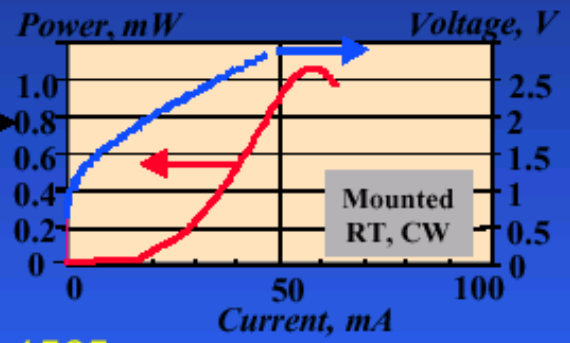

- Transmission band 1530 - 1565 nm
- Tuning speed < 100 µs
- Tuning voltage < 15 V
- WDM system 100 GHz channel spacing
- Output Power > -3 dBm, CW, RT
- Side mode suppression > 25 dB

▪ In conclusion :

PBG-devices allow to develop the engineering dispersion of photon particle (ultimate control of the dispersion curves)

➔ Ultra-strong integration (sub-λ nanophotonic devices)
➔ Control of the localization of the light in spatial and spectral domains (trapping the light in PBG regime)
➔ Control of the density of states D(ω) of the optical modes (for example control the spontaneous emission proportional to ω.D(ω) in laser applications).
➔ Control of respectively the group celerity and the τ-time of life of an optical mode on a proper area of the PC (resonance phenomena Q $\propto$ $\omega\tau$, slowing down of photons), increase of such τ-time so as to maximize the interaction between the light and matter (nano-probe and sensors applications).
➔ And so on … concerning sub-λ physic and new concepts and functions.

- **IV.3 : Biomimetic and auto-assembled molecular nano-materials for photonics; nano-tubes and ridges; nano-connexions and networks; bio-nanophotonic.**

IV.3.1 Silica and nanophotonics : nano-tubular-structures

- **Inspiration from physical and chemical bio-mineralization of sea-organism**

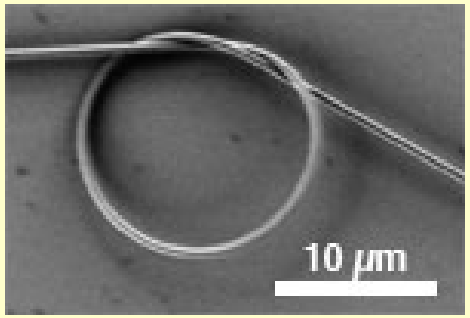

Harvard. 2006

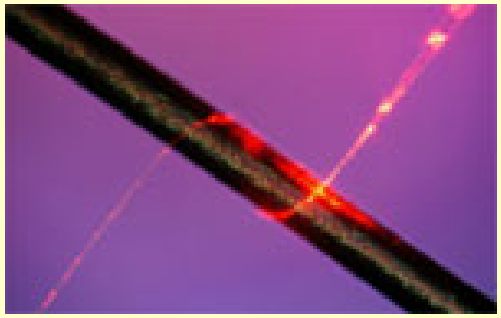

Lucent Tech. 2003➔ Harvard

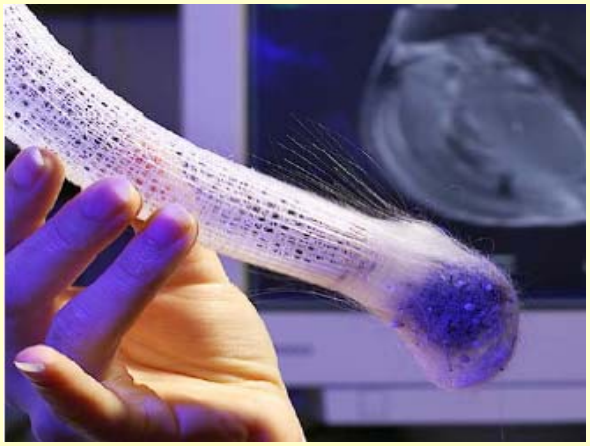

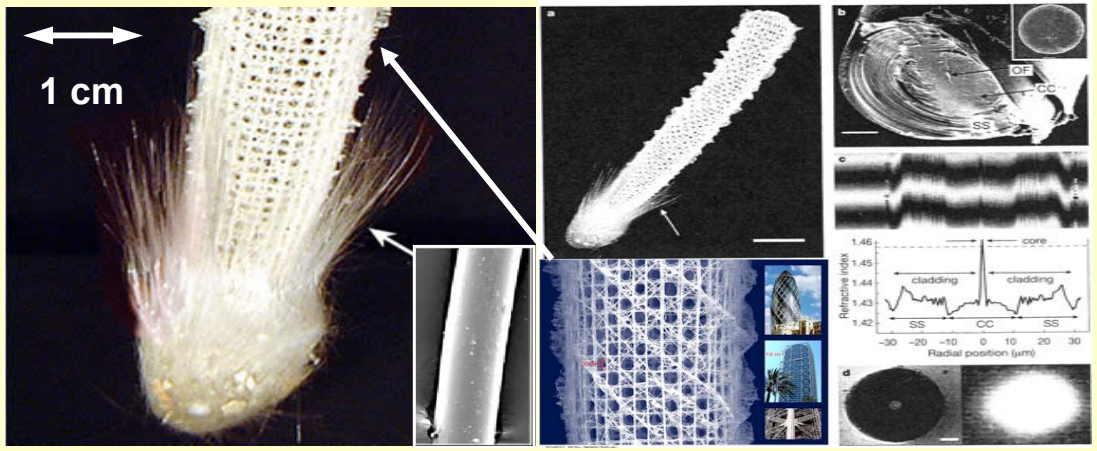

Transfer of technology and functionnality of such living organism

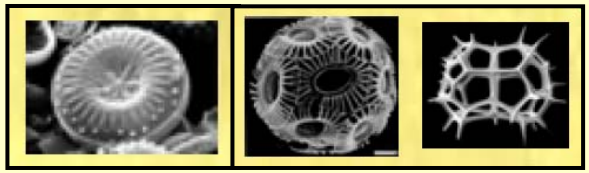

▪ **Lanreotide : medicine & peptidic gel**

▪ **IPSEN-drug that block the hormone-growth (Acromegaly disease). Peptidic gel (carbon chain) shape an hydrophylic 'U'-form (but aromatic and aliphatic elements are hydrophobic):**

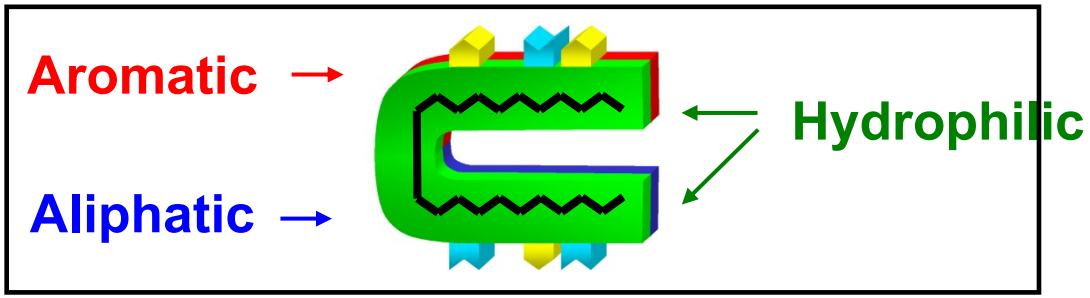

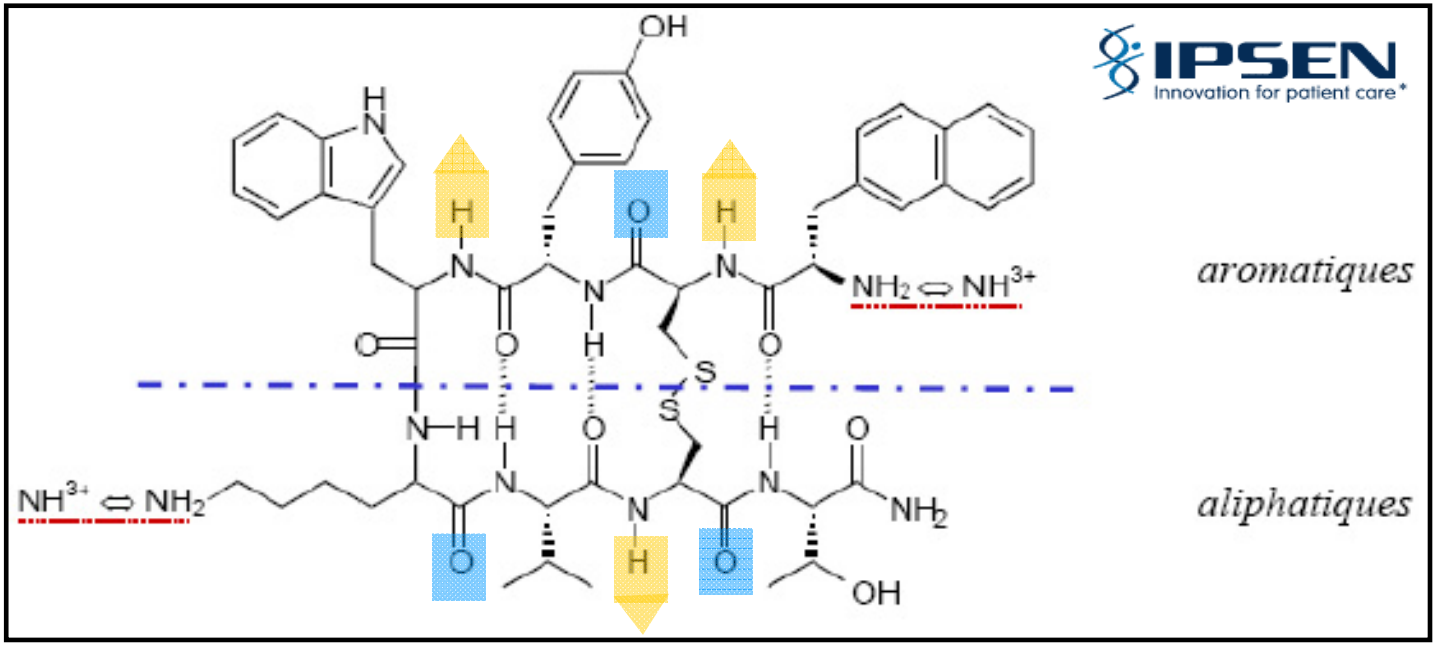

▪ **'U'-cycle is closed by disulfure covalence connection(+ electrostatic O, H)**

▪ **Lanreotide self-assembled processus**

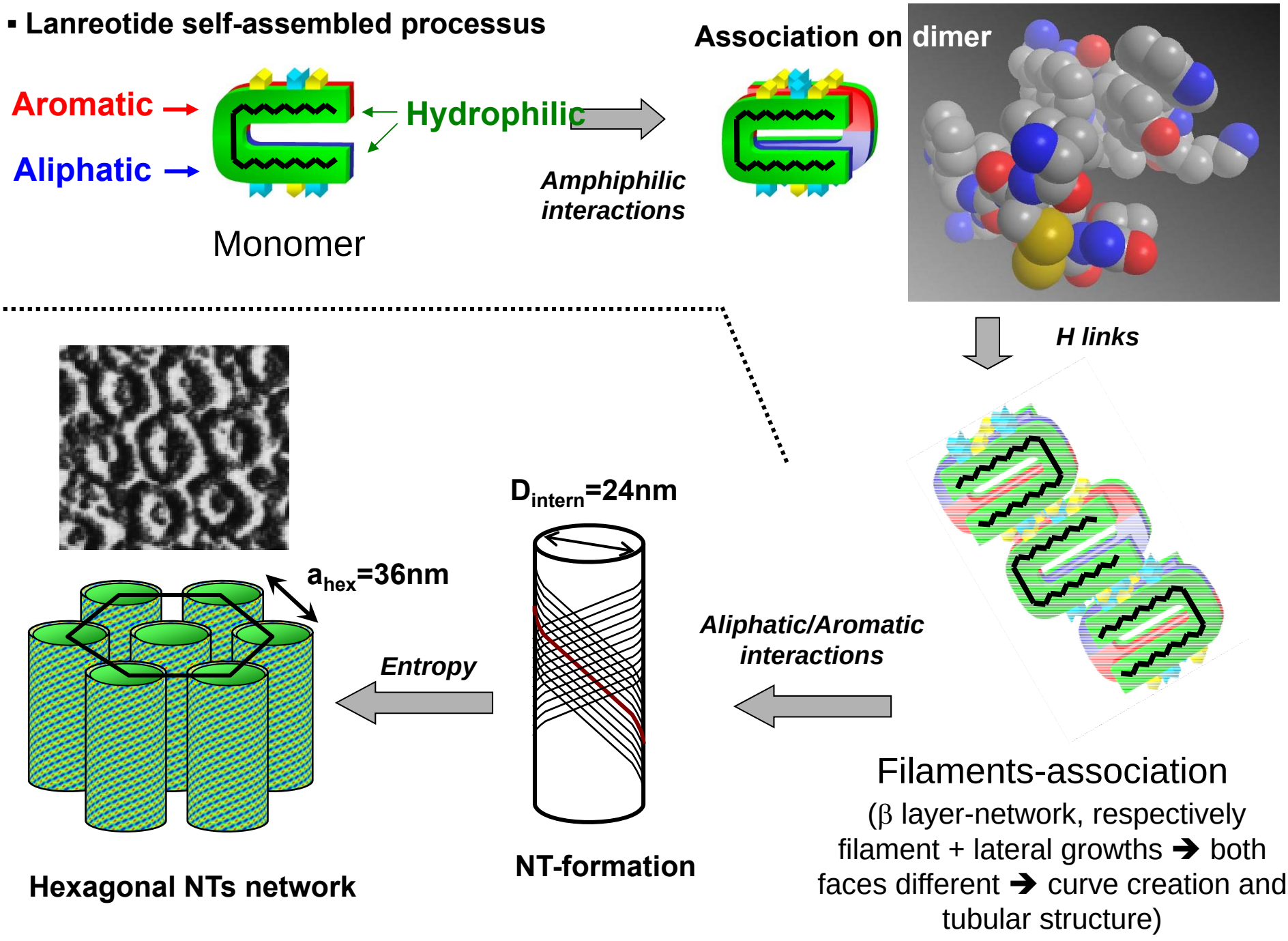

▪ **Characterization of NTs (FTIR, XPS, X-ray, SAXS, AFM, SEM & transmission, …)**

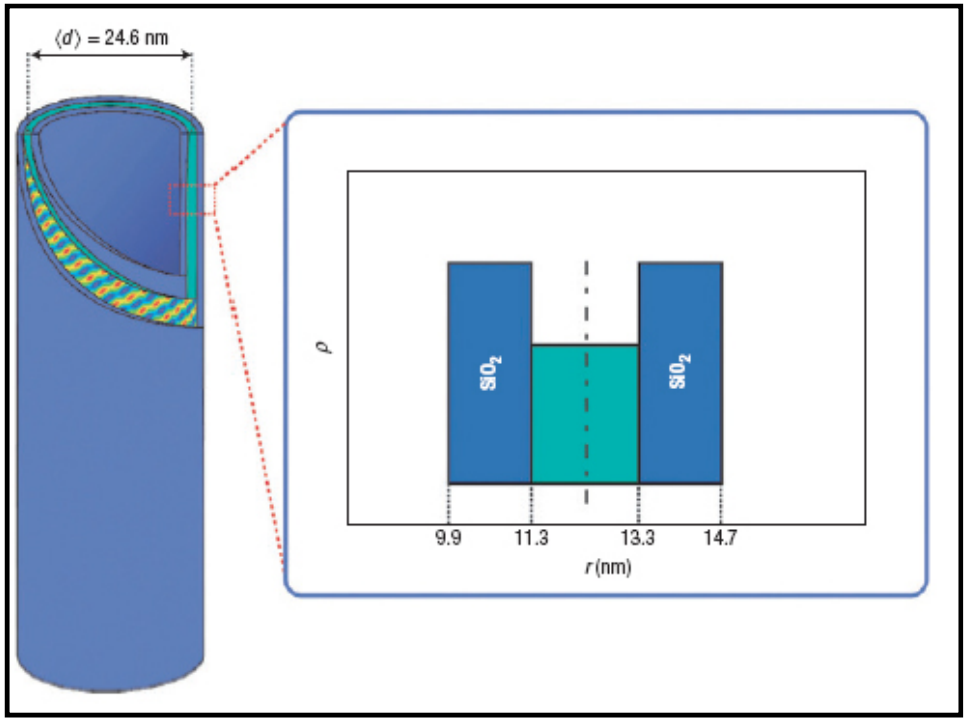

Hybrid bi-layers NT SiO_2
Extern diameter : 29 nm
Silica layers : 1.4 nm
Peptidic layer : 2 nm

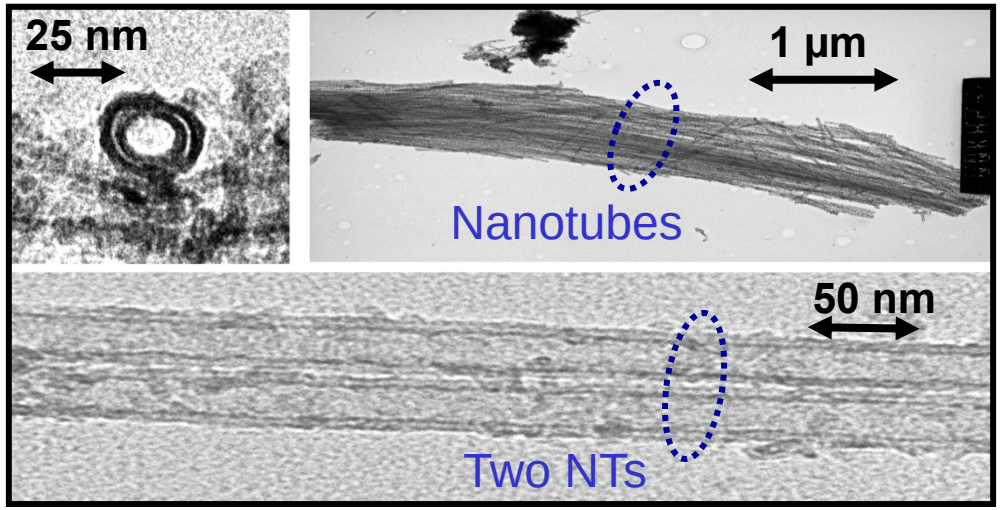

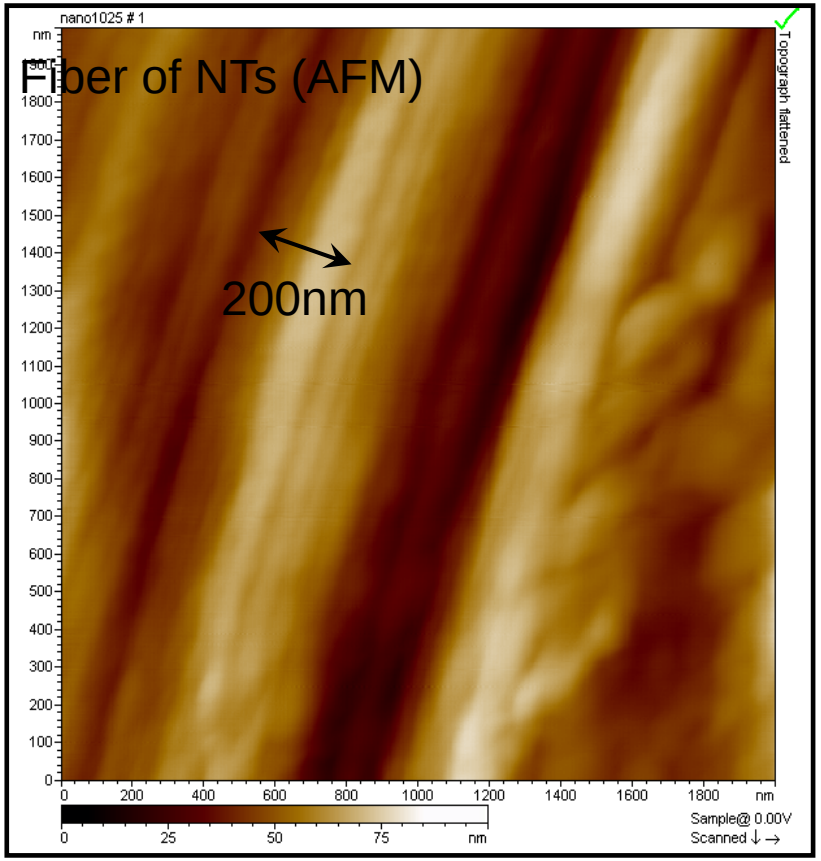

▪ **Obtention of optical coupling and propagation at the reservoir-disk ➔ insertion of NTs into the organic matrix**

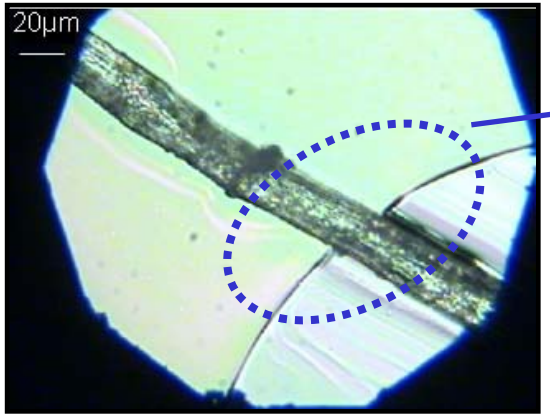

Insertion of NTs-fiber into disk SU8 area

➔ Propagation on the cm and optical losses measurements ➔ 1 à 3 dB/cm.

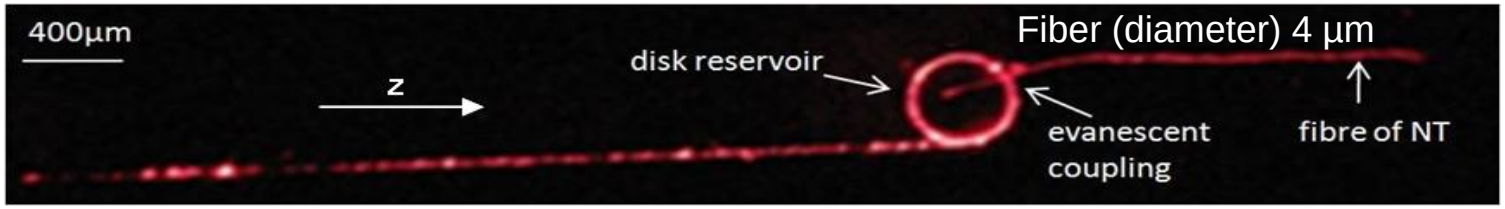

▪ IV.3.2 Silica and nanophotonics : nano-ridges structures

▪ **We report a practical concept based on reproducible fluidic mechanisms coupled with silica nano-particles for the development of nano-optical-connections directly on organic integrated photonic chips. Silica nano-ridges waveguides have been shaped with various widths ranging between 50 nm and 300 nm and about a hundred µm in length respectively.**

The effective nano-photonic coupling has been demonstrated and a sub-wavelength propagation regime obtained between two organic rib waveguides. The specific silica nano-ridge-waveguides structures show off optical losses propagation ranging around [37-68] dB/mm at visible and infra-red (IR) wavelengths. Such flexible devices offer a versatile and reproducible fabrication control by changing respectively nano-particles and surfactant concentrations. Thus, they present great potential regarding future applications for shaping nano-connections and high-density network integrations between original optical segmented circuits such as plots, lines, tapers or any pre-formed photonics structures.

- Chemical and fluidic technologies

Solution of nanoparticles of silica

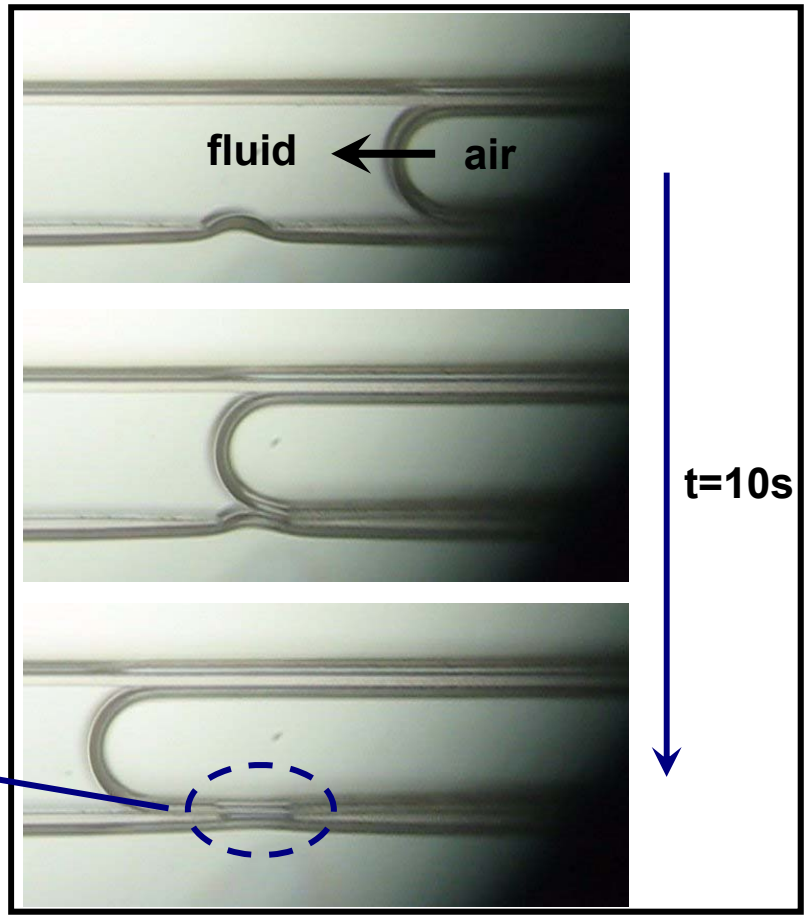

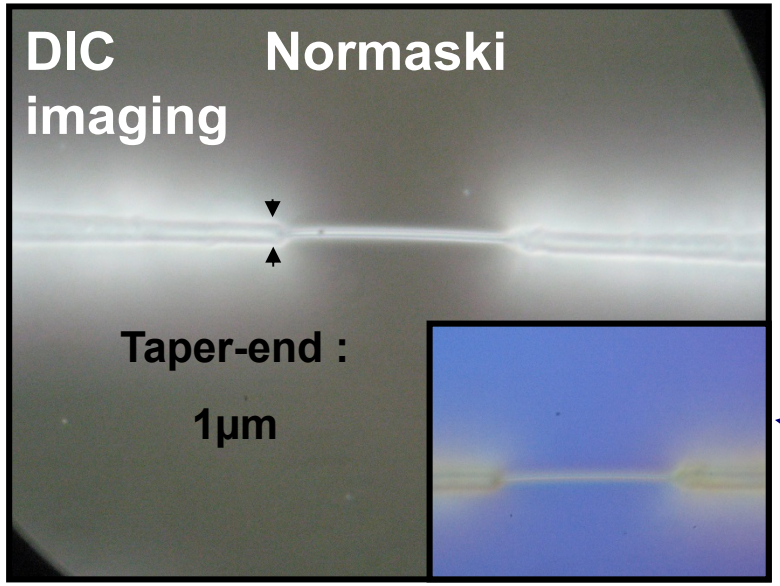

- **SEM & optical injection : taper➔ sub-λ ridge waveguides**

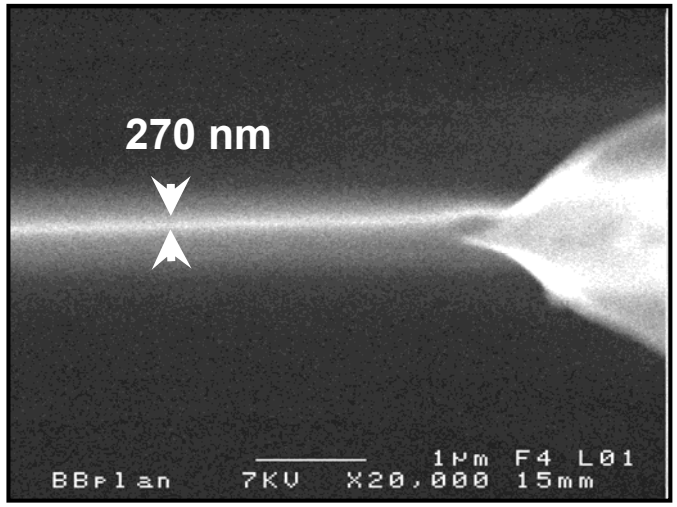

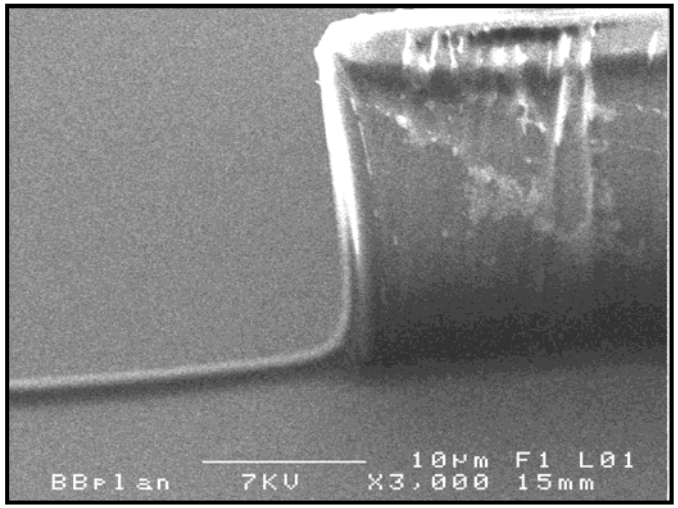

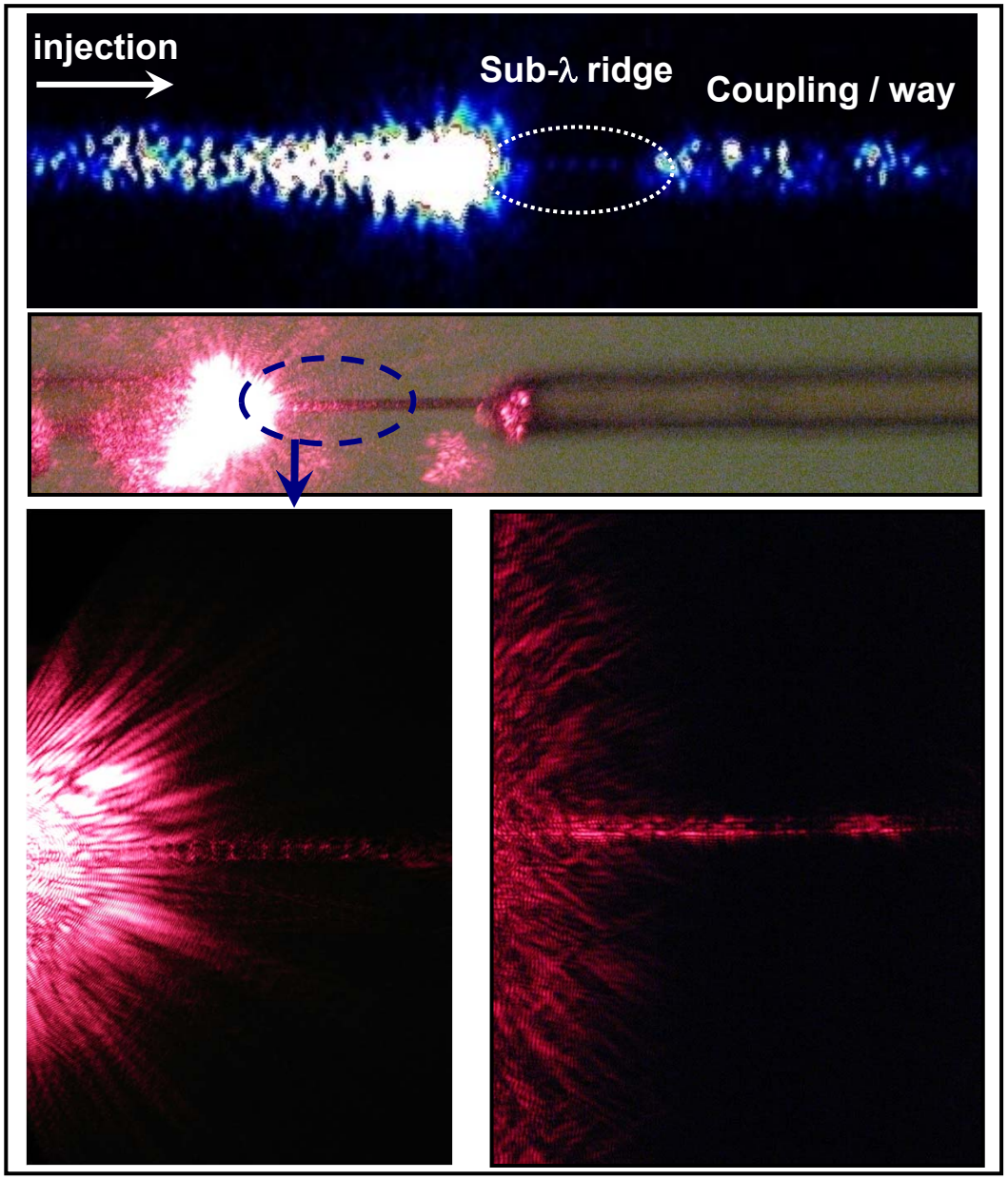

➔ Validation of sub-λ photonic propagation on 100 µm in distance

▪ **Waveguide/waveguide photonic coupling by a sub-λ nanoridges structures**

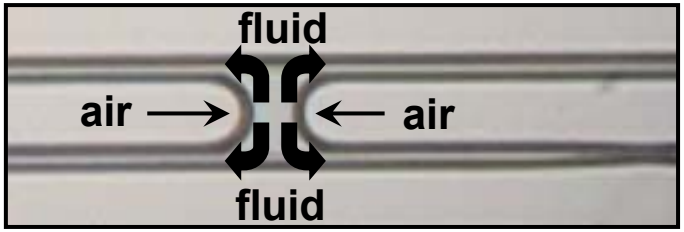

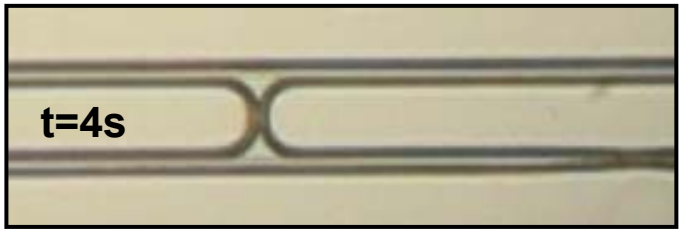

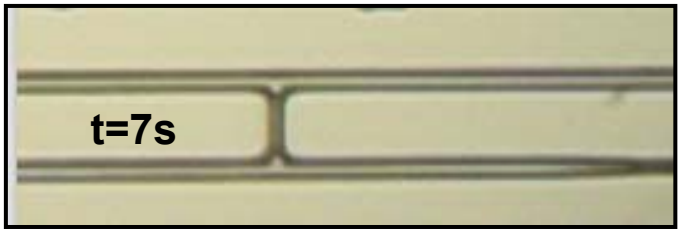

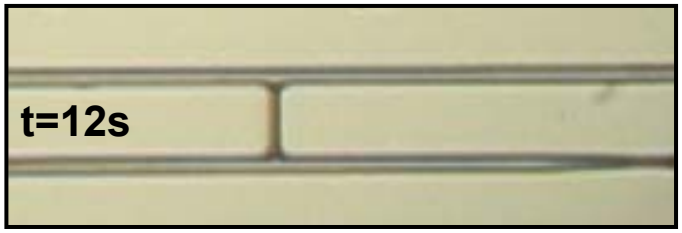

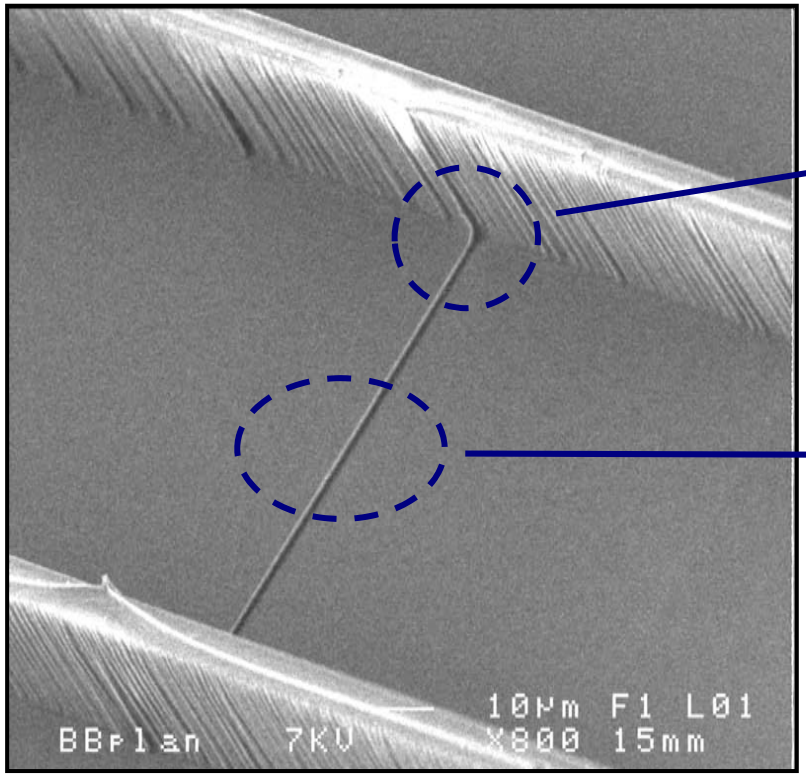

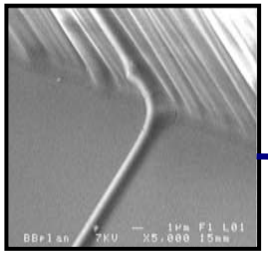

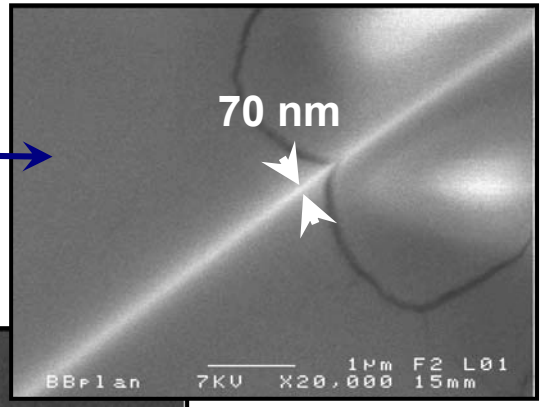

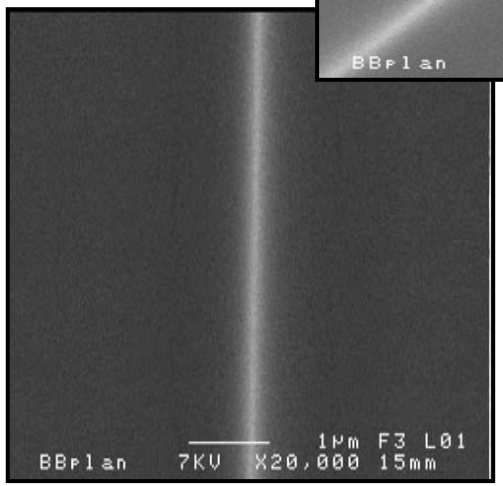

▪ λ=670 nm

CCD+monitor

Optical detection by waveguide section

Optical field section

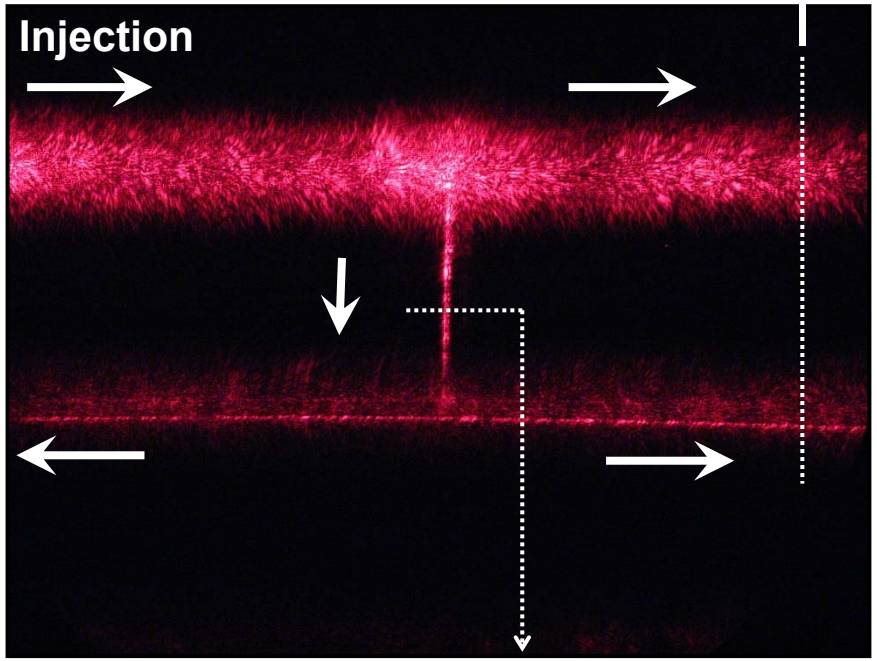

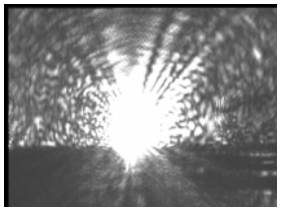

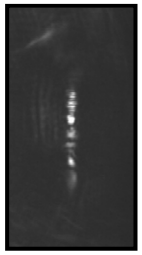

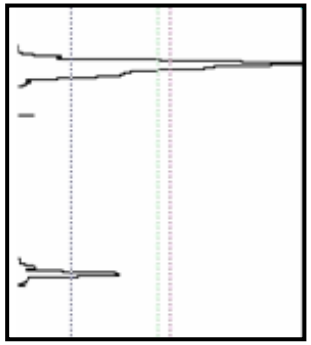

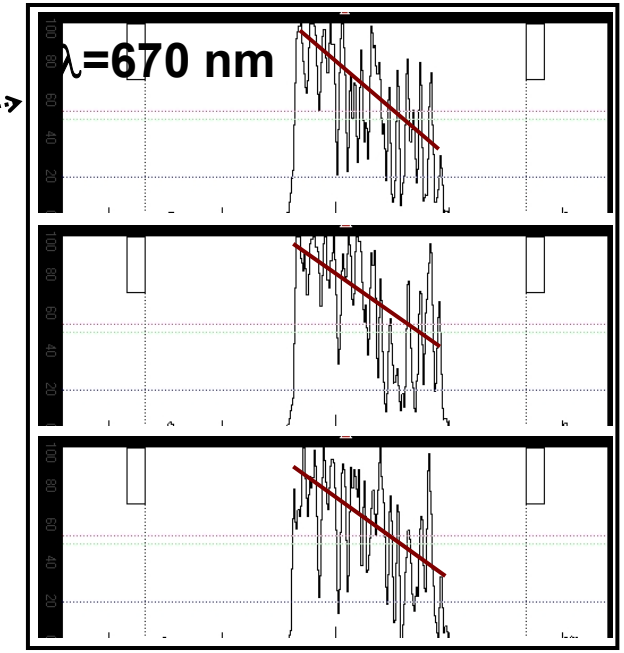

Upper-view propagation into the silica nano-ridge

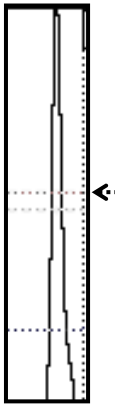

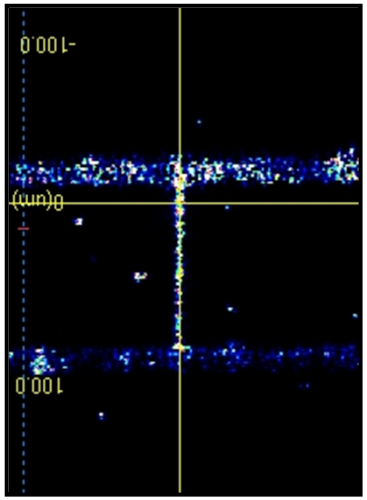

➔ Optical coupling and propagation on 100 µm with 30 dB/mm optical losses value

IEEE pub :

A GUIDING LIGHT

PAGE 356. As photonic devices get smaller and smaller, one of the challenges facing the community is to connect the nanoscale components. Researchers from the Institute of Physics of Rennes and The University of Le Mans, France, have demonstrated a low-cost approach for manufacturing connections between polymer waveguides. Using a solution of silica nanoparticles, the organic waveguides are connected at sub-wavelength scales for infrared and visible light.

Larger polymer waveguides are connected via nanoscale waveguides for integration in optical circuits

Phys. Status Solidi C, 1–4 (2011) / DOI 10.1002/pssc.201084033

physica status solidi c
www.pss-c.com
current topics in solid state physics

Nano-photonics devices on organics and silica materials obtained with various thin layer processes

Bruno Bêche[*,1,2] **and Daphné Duval**[**,1]

[1] Institut de Physique de Rennes, Université Rennes 1, Campus Beaulieu, 35042 Rennes, France
[2] Institut Universitaire de France, 103 bd Saint-Michel, 75005 Paris, France

Received 3 October 2010, accepted 4 February 2011
Published online 28 April 2011

Keywords integrated photonics, nano-connections, silica nano-rib waveguides, silica nanoparticles, fluidic mechanisms

* Corresponding author: e-mail bruno.beche@univ-rennes1.fr, Phone: +33 223 235 257
** e-mail daphne.duval@univ-rennes1.fr, Phone: +33 223 236 438

We report a practical and novel concept based on reproducible fluidic mechanisms coupled with silica nanoparticles for the development of nano-optical-connections directly on organic integrated photonic chips. Silica nano-rib waveguides have been shaped with various widths ranging between 50 nm and 300 nm and about a hundred µm in length respectively. An effective nano-photonic coupling mechanism has been demonstrated and a sub-wavelength propagation regime obtained between two organic rib tapers and waveguides with a perpendicular and a parallel configuration respectively. The specific silica nano-rib-waveguides structures show off optical losses propagation ranging around [37-68] dB/mm at visible and infra-red (IR) wavelengths. Such flexible devices offer a versatile fabrication control by changing respectively nano-particles and surfactant concentrations. Thus, they present great potential regarding future applications for shaping nano-connections and high-density network integrations between original optical segmented circuits such as plots, lines or any preformed photonics structures.

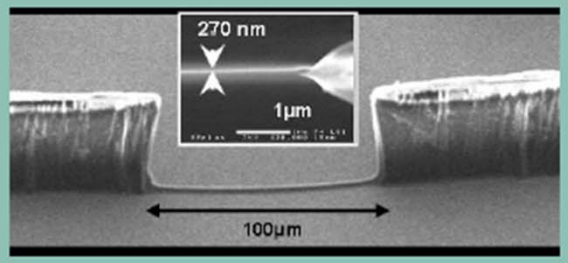

© 2011 WILEY-VCH Verlag GmbH & Co. KGaA, Weinheim

Optics and Photonics Journal, 2011, 1, 11-14
doi:10.4236/opj.2011.11003 Published Online March 2011 (http://www.SciRP.org/journal/opj)

Silica Nano-Networks as Stretches on Segmented SU8 Rods for Sub-Wavelength Photonics

Francois Doré[1], Bruno Bêche[1], Nolwenn Huby[1], F. Artzner[1], Lionel Camberlein[2], Etienne Gaviot[2]
[1]*Institute of Physics of Rennes, UMR CNRS* 6251, *University of Rennes* 1, *Rennes, France*
[2]*Laboratory of Acoustics, UMR CNRS* 6613, *University of Maine, Le Mans, France*
E-mail: bruno.beche@univ-rennes1.fr, francois.dore@univ-rennes1.fr
Received January 20, 2011; *revised March* 4, 2011; *accepted March* 8, 2011

Abstract

We report an original approach based on a fluidic mechanism involving silica nano-particules that allowed us to design a elaborate set of segmented-optical structures such as arranged clusters of pillars and cross-tapered-waveguides. We show that the association of such complex segmented pre-formed structures can be specifically shaped, by way of coupling nano-fluidics and drying mechanisms. The formation of specific silica nano-patterns or organized networks of silica nano-ridges may be predictable and in perfect agreement with the theory of minimal surfaces dealt with physics of fluids. The interest of such nano-photonic coupling mechanisms has been clearly highlighted thanks to their abilities to build original nano-silica-networks and the specific development of new filters based on resonant tunnelling effects between multi-nano-ridges.

Keywords: Integrated Photonics, Nano-Connections, Silica Nano-Rib Waveguides, Nano-Optical Coupling, Nano-Network, Fluidic Mechanisms

- **IV.4 : Near field optical; introduction to the main concepts; presentation of specific probes, and near optical field microscopy (STOM, SNOM).**

IV.4.1 Brief historic of microscopy, resolution notion and Raleigh's criteria

- **1690 (Van Leuvenhook) : birth of microscopy ; simple aspect (object carrier + sample + lens).**
- **19th century : composed microcopy (objective + ocular).**

Limit of resolution : Raleigh and Abbe criteria

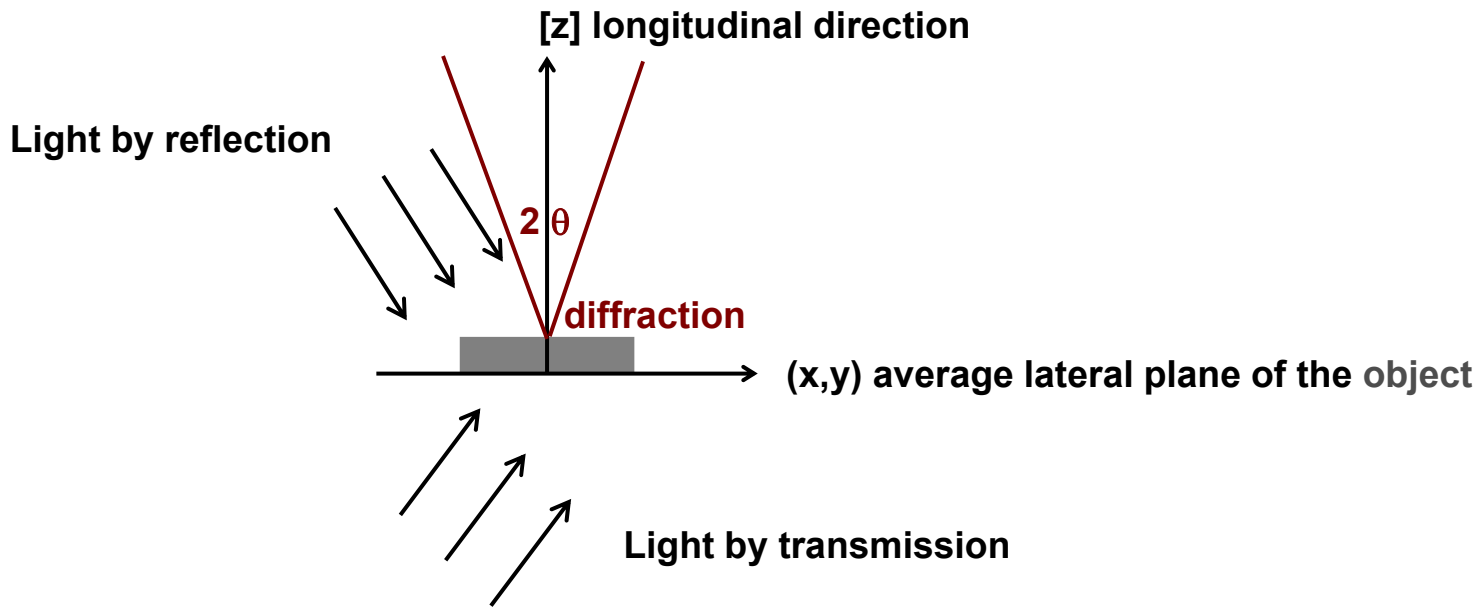

- **Lateral resolution (x,y)** ➔ limited by Raleigh, Abbe criteria (Δx resolution limit distinction into the sample or the space-object, *n* index of the embedded-object-medium)

$$\Delta x \geq \frac{0.6\lambda}{n.\sin\theta} \quad \text{[IV-23]}$$

Possibilities to increase such a lateral resolution (Δx decreasing) : $-1<\sin\theta<1$ is fixed and $\sin(\theta) \rightarrow 1$ is the maximum ! Imaging can be done into high index (*n*=2). Then for visible wavelength $\Delta x>0.25\mu m$.

- Theoretically, the **longitudinal resolution** seems to have no limit ! As an example, with a heterodyne interferometer detection $\Delta z<0.1nm$.

▪ 1923 (De Broglie) : electron-wave aspect $\lambda_{e^-} = \frac{h}{mv} = \frac{h}{\sqrt{2eUm}}$ [IV-24], with tension U.

▪ 1934 (Rusto) : electronic microscopy, deviation of the electrons with fields (no divergent lens with magnetic field, aberration correction not possible). Microscopy in Gauss condition $\sin(\theta) \approx \theta$. High U-tension (100kV).

▪ 1980 : First imaging of atoms.

Idea : Information is losses between the sample (or object) and the objective ➔ notion of local information and probe in near field microscopy so as to obtain a resolution below the Rayleigh's limit

▪ 1981 (Binnig and Roher) : new family of microscopy with local probe, working-tension 5V with atomic resolution (Nobel price in 1986).

➔Various type of probe :

- STM (or STEM) : Scanning Tunneling (Electronic); microscope based on the measurement of a I-current (probe and sample conductors!) ; piezoelectric displacements, when *z*=d(sample-probe) is nanometric (tunnel effect) :

$$\boxed{I = I_0 \cdot e^{-z/\delta}}$$ [IV-25], with δ metal-characteristic.

and, ΔI highlights Δz-relief.

- AFM : Atomic Force Microscopy; microscope based on a atomic force measurement (molecular resolution).

▪ IV.4.2 Optical near field microscopy

▪ 1928 (Singe) : Theoretical description of the device of such optical near field microscopy (so as to overcome the Rayleigh's criteria, idea to take the local information by a nanometric-hole (➔ diffraction theory and notion of near optical field!), typically Δz=10nm.

▪ 1984 (Pohl and Betzig) : various configurations ; as an example SNOM configuration (light in near optical field with a probe and imaging and detection in far field, notion of nano-source) and STOM configuration (T=tunneling, that is light in far field over the l_{limit} and detection in near optical field with a probe). No contact with the samples (optic) and possibility of spectroscopy measurements with the detected light.

- Various functionalities on the SNOM measurements : *z* can be fixed and intensity $I(x,y, z_{fixed})$ detected ; Intensity *I* is constant (enslavement) and *z*(x,y) ($/I_{constant}$) is deduced.

▪ IV.4.3 Return on diffraction theory - applications to SNOM

▪ **Principle :**

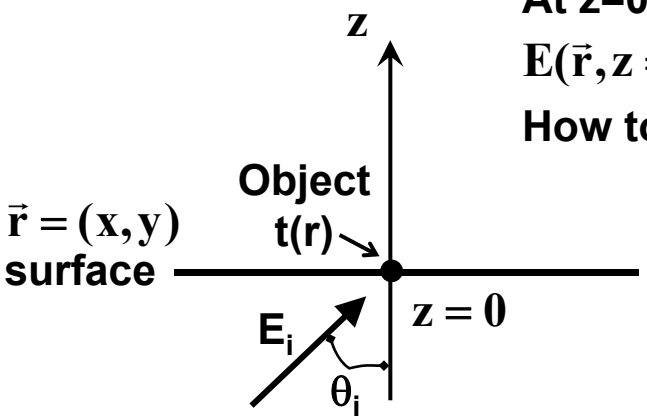

At z=0, $E(\vec{r}, z=0)$ is known (=incident field x transmission function),

$$E(\vec{r}, z=0) = t(\vec{r}).E_i(\vec{r}, z=0)$$

How to determinate $E(\vec{r}, z \neq 0)$?

Waves packet (*h.w.* plus *e.w.*)

Spatial spectral aspect of the object

Filter term

[IV-26]

$$\boxed{E(\vec{r}, z \neq 0) = \frac{1}{4\pi^2}\iint F(\vec{q}, z=0).e^{j\vec{q}.\vec{r}}.d\vec{q}.e^{jw.z} = \frac{1}{4\pi^2}\iint F(\vec{q}, z=0).e^{j\vec{k}.\vec{R}}.d\vec{q}}$$

with,

$$\vec{R}(x,y,z) = (\vec{r}, z)\,;\,\vec{k} = (\vec{q}, w) = (u, v, w)\,;\,w = \sqrt{\left(\frac{\omega}{c}\right)^2 - \vec{q}^{\,2}} = \sqrt{\left(\frac{\omega}{c}\right)^2 - u^2 - v^2}$$

$$k^2 = \left(\frac{\omega}{c}n\right)^2\,;\,\vec{q}\left(\frac{\omega}{c}n\sin(\theta_i), 0\right)$$

▪ **Physical meaning :**

Δx lower => Δu higher ; u (or q)<ω/c (homogeneous waves, *h.w.*), q>ω/c that is high frequencies [evanescent waves *e.w.*, w=jβ and exp(jwz)=exp(-βz), q higher => spatial frequencies w higher => β lower) attenuation of high frequencies = low-pass filter]

▪ **Application to SNOM modelization (detection in far field) - calculus:**

$\boxed{E(\vec{r},z=0)=t(\vec{r}).E_i(\vec{r},z=0)}$, with t(r) transmission (transparence) function of the object,

and by definition (TF, TF^{-1}): $t(\vec{r})=\frac{1}{4\pi^2}\iint e^{j\vec{q}.\vec{r}}T(\vec{q})d\vec{q}$ and $T(\vec{q})=\iint e^{-j\vec{q}.\vec{r}}T(\vec{r})d\vec{r}$

Due to $E_i(\vec{R})=E_0e^{j\vec{k}_i.\vec{R}}$, and $\vec{k}_i=(q_i,w_i)$ with $q_i\left(\frac{\omega}{c}n\sin\theta_i,0\right)$, $k_i^2=\left(\frac{\omega}{c}n\right)^2$

we can write:

$E(\vec{r},z=0)=t(\vec{r}).E_i(\vec{r},z=0)=t(r).E_0.e^{j\vec{q}_i.\vec{r}}$ = incident wave (z=0 case) through the object

TF to obtain $F(\vec{q},z=0)$ the spatial spectral aspect of the incident wave after (z=0) the object

$$F(\vec{q},z=0)=\frac{1}{4\pi^2}\iint e^{-j\vec{q}.\vec{r}}.\left[t(r).E_0.e^{j\vec{q}_i.\vec{r}}\right].d\vec{r}$$

$$=E_0.T(\vec{q}-\vec{q}_i)$$

[IV-26]

Diffraction at $z\neq 0$

$$\boxed{E(\vec{r},z\neq 0)=\frac{E_0}{4\pi^2}\iint T(\vec{q}-\vec{q}_i).e^{j\vec{q}.\vec{r}}.d\vec{q}.e^{jw.z}}$$ [IV-27]

➔ Difficulties to estimate such integral

▪ **Physical meaning : Such previous expression, in the case of normal incident wave excitation (q_i=0 and z=0) leads to the object = E_0.t(r) !**